Cascaded partial core resonant transformers

Yanosh Irani

A thesis presented for the degree of
Doctor of Philosophy
in
Electrical and Computer Engineering
at the
University of Canterbury,
Christchurch, New Zealand.

18 July 2017

ABSTRACT

High voltage field testing of electrical insulation can necessitate the use of bulky test equipment and large power supplies. This is due to the significant insulation capacitance presented by some types of high voltage machinery. For these applications, test equipment should be portable and have some way of compensating for the load capacitance. Partial core resonant transformers (PCRTXs) were developed as a solution to this problem. These are light weight transformers with a core consisting of a single limb which can be inductively tuned to resonate with the load capacitance at power frequency. These transformers have been designed for medium voltage applications such as high potential testing of generator stators. This thesis explores the concept of connecting multiple PCRTXs in cascade to generate higher voltages to enable portable field testing of high voltage cables and gas insulated switchgear.

An existing two winding model is extended to predict the performance of three winding PCRTXs. A new equivalent circuit model is developed to represent multiple PCRTXs connected in cascade and validated by measurements conducted on existing prototypes. New challenges presented by the cascaded arrangement are explored including a method for tuning multiple stages, primary winding current distribution and load voltage distribution across stages. The limitations of cascaded PCRTXs are investigated and it is concluded that designs with more than three stages become impractical due to increased losses and a reduction in the resonant load capacitance.

A suite of flexible software design tools is developed to make the design process user friendly. A constrained particle swarm optimisation algorithm is applied to compare the relative benefits of cascaded and single PCRTXs. Simulated cascaded test kits with varying numbers of stages are optimised for weight to meet the same design specification. The relationship between the number of stages and the optimal stage weight is presented.

A new two stage cascaded PCRTX test kit is designed and built to generate a 66 kV test voltage. New construction methods are trialled and evaluated including radially laminated core sections to reduce losses and fibreglass inter-layer winding insulation with vacuum resin infusion. The transformer is thoroughly tested and numerous design strengths and areas for improvement are identified. An existing PCRTX is added as a third stage to energise a 343 nF load to 100 kV whilst drawing 60.6 A from the supply.

UNIVERSITY OF CANTERBURY
Te Whare Wānanga o Waitaha
CHRISTCHURCH NEW ZEALAND

Deputy Vice-Chancellor's Office
Postgraduate Office

Co-Authorship Form

This form is to accompany the submission of any thesis that contains research reported in co-authored work that has been published, accepted for publication, or submitted for publication. A copy of this form should be included for each co-authored work that is included in the thesis. Completed forms should be included at the front (after the thesis abstract) of each copy of the thesis submitted for examination and library deposit.

Please indicate the chapter/section/pages of this thesis that are extracted from co-authored work and provide details of the publication or submission from the extract comes:

Chapter 4 includes material published in:

Equivalent Circuit Model of Cascade Connected Partial Core Resonant Transformers, Australian Universities Power Engineering Conference, Hobart, Tasmania

Please detail the nature and extent (%) of contribution by the candidate:

Data collection processing, model development, paper writing and oral presentation. 99%

Certification by Co-authors:

If there is more than one co-author then a single co-author can sign on behalf of all

The undersigned certifys that:

- The above statement correctly reflects the nature and extent of the PhD candidate's contribution to this co-authored work
- In cases where the candidate was the lead author of the co-authored work he or she wrote the text

Name: *Yanosh Irani* Signature: Date: *05/04/2017*

Name: *Andrew Lapthorn* Signature: Date: *05/04/2017*

PUBLICATIONS

1. Irani, Y., Lapthorn, A. and Bodger, P. (2013) A comparison of VLF and 50 Hz Field Testing of Medium Voltage Cables, *Electricity Engineers Association Conference*, Auckland, New Zealand, 19 to 21 June

2. Irani, Y., Lapthorn, A. and Bodger, P. (2013) Equivalent Circuit Model of Cascade Connected Partial Core Resonant Transformers, *Australian Universities Power Engineering Conference*, Hobart, Tasmania, Australia, 29 September to 3 October 2013

3. Irani, Y. (2014) High Voltage Testing with Partial Core Resonant Transformers, *Annual Power Engineering Exchange (APEX) Summit*, Wellington, New Zealand, 16 September

4. Lapthorn, A., Irani, Y., Enright, W., Race, P., Schicker, K. and McDonald, C. (2016) Three Phase Partial Discharge Investigation of a 108 MW Hydro Stator, *Electricity Engineers Association Conference*, Wellington, New Zealand, 22 to 24 June

ACKNOWLEDGEMENTS

This thesis was made possible by the excellent foundation of research built by Simon Colin Bell. Simon went missing near Mt Earnslaw while attempting his 68th ascent from a list of New Zealand's 100 most challenging peaks. I owe him my gratitude and hope my contributions do justice to his work.

I could not have asked for a better combination of supervisors. Thank you to Andrew Lapthorn for being a positive, motivating force throughout my research, I am proud to be your first PhD student. Sincere thanks to Pat Bodger for your guidance and the example you have set for young engineers throughout your career, I am proud to be your last PhD student.

I owe a huge thank you to Wade Enright, Rowan Sinton, Kerry Tunstall and Ryan Van Herel for being great mentors and partners in crime. The weekends spent building impulse generators in a plasma laboratory at Koukourarata were unforgettable. The best is yet to come.

Thanks to the technicians involved in bringing my project to life, especially Paul Agger for winding the transformers and providing hours of entertaining discussion in the lab. Thank you also to Dave Healy, Matua Ken Smart, Jac Woudberg, Edsel Villa, Florin Predan and Mike Shurety for help in my many hours of need. Special thanks to Andrew Berry for his assistance with transformer testing. Since you have decided to ignore my advice and continue with your PhD I wish you best of luck with your journey.

Thank-you to the other post graduate students in the department for the fun times including Lance Frater, Hae Geun, Diwakar Bhujel, Abdulrahman Peimankar, Zhiyang Jin, Mike Frampton, John Morris and Blair Bonnet. Thanks to Allan McInnes, David Santos-Martin, Allan Miller, Neville Watson, Martin Allen and all the ECE department staff and researchers who have shared their time, experience and sage advice through the years.

I would like to show my sincere appreciation to all the industry contributors that assisted with this work in different ways. Thank you to Hugh Reynolds, Christopher Boyle and Matthew Dimock at Fabrum solutions for your time and efforts in building the prototype transformers. Thanks to all the asset owners around New Zealand brave

enough to use new high voltage test equipment straight out of the university. Thanks also to the Electric Power Engineering Centre, the Power Engineering Excellence Trust and all its members for the financial support.

Thanks to all the staff and students at College House hall of residence for making my time there as a resident tutor so memorable. Thanks to my former flatmates Mathew Falloon, Rory Horne and Tristan Read for making our damp, mouldy, and freezing flat a great place to come home to. Thanks to all my rock climbing partners through the years for dragging me away from my thesis at literally every hour of the day from 6am sessions at The Cave to midnight missions to Flock Hill.

The final year of my work was made especially difficult by simultaneously working a full time job. Thanks to the Upper Waitaki maintenance team, contractors and colleagues at Meridian Energy. Special thanks to Mike Brownlie, Mike Webb, Steve Dolan and Paul Churton. You made going to work each day something to look forward to you.

My family have provided unwavering support right from the beginning of this undertaking. Thanks to my grandmother Khorshed Irani who taught me to read and sparked my thirst for knowledge. Thanks to Mum and Dad, Yasmin and Farahad Irani for their love and support through this unique and challenging process. Thanks to my brother Shirzad for being a consistent source of entertainment and reminding me that life is meant to be enjoyed.

Finally and most importantly of all, none of this would have happened without the support of my beautiful partner and best friend Laura King who recently completed her own PhD thesis. Your love and encouragement got me here even though it seemed like this day would never arrive. I look forward to exciting new adventures ahead.

There is one more thing...
It's been emotional.
-Big Chris, Lock Stock and Two Smoking Barrels, 1998

CONTENTS

LIST OF FIGURES

LIST OF TABLES

GLOSSARY

This glossary contains a list of symbols and abbreviations found throughout this thesis.

NOTATION

a	Nominal turns ratio
$\lceil x \rceil$	Ceiling of x
$\lfloor x \rfloor$	Floor of x
$\|\|x\|\|$	Magnitude of x
$\angle x$	Angle of x
l_x	Length of x
R_x	Resistance of x
X_x	Reactance of x
V_x	Voltage of x
I_x	Current of x
L_{xk}	Self inductance of winding x on k'th stage.
M_{xyk}	Mutual inductance between windings x and y on k'th stage.
m_x	Mass of x
P_{xy}	Permeance between windings x and y
r_x	Radius of x
d_x	Diameter of x
t_x	Thickness of x
T_x	Temperature of x
Y_x	Admittance of x
Z_x	Impedance of x

ABBREVIATIONS

AC	Alternating current
AT	Ampere turns
DAC	Damped alternating current
DC	Direct current
emf	Electromotive force

FEA	Finite element analysis
GIS	Gas insulated switchgear
HV	High voltage
IPB	Isolated phase busbar
lb	Local best
LV	Low voltage
mmf	Magnetomotive force
PCRTX	Partial core resonant transformer
pb	Personal best
PD	Partial discharge
PSO	Particle swarm optimisation
VLF	Very low frequency
VT	Voltage transformer
XLPE	Cross linked polyethylene

Chapter 1

INTRODUCTION

1.1 GENERAL OVERVIEW

Partial core resonant transformers (PCRTXs) were developed to perform high voltage testing on hydro generators. This kind of test normally requires a significant amount of power to energise the capacitive load of a hydro stator. A PCRTX can be inductively tuned to resonate with the insulation capacitance thus reducing the current drawn from the power supply. The transformers themselves are lighter than equivalent full core transformers because the steel core consists of a single limb. They were built using solid insulation to make them easy to transport to the test location.

The next stage of development for PCRTXs involves generating higher voltages and/or resonating with larger capacitive loads. This would expand potential applications to testing underground cables, gas insulated switchgear and power transformers. One way of doing this could be further development of the insulation and cooling system.

Another way of producing higher voltages with the existing insulation system would be to connect multiple PCRTX units in a cascade arrangement. In this configuration each unit is designed with one high voltage (HV) winding and two low voltage (LV) windings. Both LV windings are wound with a unity turns ratio. The neutral end of the second LV winding is connected to the live end of the HV winding and energises the LV winding of another stage. The HV windings of all stages are connected in series. The LV is thus the sum of all stage voltages.

The advantage of this concept would be the ability to generate high voltages with smaller modular transformers using a simpler insulation system. Building a practical cascaded PCRTX test kit requires a mathematical model to enable design to a given specification. The method for tuning multiple cascaded PCRTX stages needs investigation. Finally the relative merits and limitations of the cascade arrangement needs to be compared to single PCRTXs.

1.2 THESIS OBJECTIVES

The first objective of this thesis was to prove the feasibility of connecting partial core resonant transformers in cascade. The next step was to develop a design process for cascaded PCRTXs. Subsequently the intent was to determine the limitations of cascading PCRTXs and their relative cost and performance compared to using a single stage. The final objective was to design, build and test a high voltage cascaded PCRTX test kit.

To achieve these goals a mathematical model of cascaded PCRTXs was developed. This model was embedded within a set of software design tools incorporating finite element analysis. An optimisation routine based on the particle swarm algorithm was implemented to produce optimal single and cascaded PCRTX designs within a set of constraints. The design capability was demonstrated by designing and constructing a two stage 66 kV prototype PCRTX. During the manufacture of the final prototypes, a new composite insulation system and core lamination method was trialled and evaluated.

1.3 THESIS OUTLINE

Chapter 2: Introduces the concept of high voltage testing and summarises current practices, standards and methods. Commonly used test equipment and diagnostic tools in laboratory and field testing applications are presented along with new developments. Work on partial core transformers is presented. Potential applications for a portable high voltage resonant test system are outlined. The concept for a cascaded partial core resonant test system is detailed.

Chapter 3: Existing models for partial core resonant transformers are reviewed. A new model for three winding partial core resonant transformers is developed. An equivalent circuit and its derivation using the finite element model is detailed. Results are presented from tests conducted on a prototype three winding partial core resonant transformer.

Chapter 4: Existing models for cascaded transformers are reviewed and a new equivalent circuit model for cascaded partial core resonant transformers is presented. An analytical solution for this model is outlined and used to investigate the electrical performance of the cascade. The current and voltage distribution between stages is investigated along with the behaviour under resonant conditions. Different tuning methods are investigated to identify their strengths and limitations.

Chapter 5: The design of a custom software tool for modelling cascaded partial core resonant transformers is presented. The object oriented structure and composition

of the program is outlined. Key functions are described along with the graphical user interface.

Chapter 6: The application of an optimisation routine for single and cascaded partial core resonant transformers is presented. The particle swarm algorithm is outlined and its implementation on partial core resonant transformers is detailed. The algorithm incorporates a constraint handling mechanism to ensure designs meet user defined specifications before optimising weight. The results for an example specification are presented and a comparison is performed between optimal designs for single and cascaded partial core resonant transformers.

Chapter 7: The design and construction of a prototype two stage cascaded PCRTX test kit is outlined. Construction methods are presented for radially laminated core sections and a new resin infused insulation system.

Chapter 8: Results are given for extensive tests conducted on single and cascaded PCRTXs to validate the model and determine device performance.

Chapter 9: Discusses a range of avenues for further research associated with this thesis. Preliminary investigations into some of the ideas are discussed.

Chapter 10: Presents the contributions and main conclusions of this thesis.

Chapter 2

BACKGROUND

2.1 INTRODUCTION

Electric machines designed to create high voltages have been studied and engineered for centuries. Their applications have ranged from purely academic exploration of high voltage phenomena to practical testing of electric power equipment. The increasingly challenging requirements for these machines have been matched by progressively powerful tools and techniques developed to analyse their behaviour and push the limits of their performance.

This chapter is a review of concepts and applications in the field of high voltage testing that provide a clear foundation and context for the rest of this thesis. These include different types of high voltage testing and the associated equipment that enables the tests. The concept of cascaded transformers is introduced along with their early applications in laboratories and x-ray imaging. Historical and recent developments in the area of resonant testing are detailed. Previous research conducted into partial core transformers and their applications in high voltage resonant testing is summarised.

2.2 HIGH VOLTAGE TESTING

The insulation on high voltage electrical equipment is tested repeatedly over its lifetime. Examples of such equipment include power transformers, generators, motors and gas insulated switchgear (GIS). The insulation that separates their live components is required to continue to function under normal and sometimes abnormal conditions. The extent to which this ability is tested depends on the relative cost of testing compared to the consequences of in service failure.

2.2.1 Reasons for testing

The motivations for conducting a high voltage test depend on the equipment age and the stage of development. Samples of single parts such as generator stator coils or whole assemblies like transformers undergo *type testing* to provide confidence in the design. After manufacturing has begun, *routine testing* provides further verification of production quality. Once produced, equipment often undergoes *factory acceptance testing* (FAT) to verify it meets the requirements of the purchaser. Equipment is usually tested in the field after transportation and installation to ensure no damage has occurred during the process. Once in service, *on-line testing* is used to monitor the health of insulation. With the equipment removed from service *off-line* testing can be conducted to assess insulation health or find faults. Results obtained from *maintenance testing* are an important input into strategic decisions about major equipment refurbishment and determining end of life.

2.2.2 Types of testing

Different types of high voltage tests are conducted to test different aspects of the insulation performance. Detailed requirements and specifications are given by international standards but most fall into the following categories.

2.2.2.1 Withstand

Withstand testing is conducted with the aim of establishing if insulation can continue to function at a certain voltage. The waveforms of the applied test voltage can vary in frequency from DC to high frequency impulses depending on the application. The outcome of these types of test are a simple pass or fail.

The simplest form of high voltage withstand testing is the short duration high potential withstand test, or "hi-pot". During this procedure a large voltage is applied across the insulation on the equipment under test, otherwise referred to as the test article. This is sustained for a fixed period of time and if the insulation survives without being compromised it is deemed to have passed the test. This type of test usually subjects the insulation to a voltage much higher than its rating to represent the effects of abnormal system conditions and service ageing. If U_0 is the rated voltage one international standard for rotating machines [IEC 60034-1 2010] specifies $2U_0+1$ kV as an appropriate test voltage for new insulation.

The induced voltage test on transformers is another example of a withstand test [IEC 60076-3 2003]. This test involves applying a three phase voltage to the LV winding/s of a transformer with the HV winding/s open circuited. The test voltage is raised in

stages and can be close to twice the rated HV winding voltage. The test is considered successful if there is no collapse of the test voltage for 60 seconds.

2.2.2.2 Breakdown

Breakdown testing deliberately pushes the insulation to failure. This type of testing is usually conducted as a type test because it can irreparably damage the insulation under test. An example of breakdown testing is a flash-over test on high voltage insulators as shown in Figure 2.1a. During this test the voltage across a string of insulators is increased beyond its rating until breakdown across the insulator surface is achieved. Breakdown testing can also be applied as a maintenance test when checking the breakdown strength of a sample of transformer oil. Test kits like the one shown in Figure 2.1b apply measured voltages of up to 100 kV across oil samples until breakdown occurs.

(a) Flashover testing [Wardman 2013]

(b) Oil dielectric strength tester [Megger 2017]

Figure 2.1 Examples of dielectric breakdown testing

2.2.2.3 Impulse

High voltage insulation in the field can be subject to large voltages exceeding ratings for short time intervals. These voltage surges can occur due to lightning strikes or switching operations. Impulse testing replicates these conditions by applying a simulated lightning or switching impulse voltage.

Impulse testing can also be used as a method to locate weak inter-turn insulation within machine coils. A fast impulse applied across a coil sends a travelling voltage wave across the insulation. Changes in the frequency of the resulting voltage oscillation are indicative of inter-turn insulation failure.

2.2.2.4 Diagnostic testing

High voltage testing is often conducted with the aim of collecting diagnostic information about insulation condition. This data can be collected on-line whilst the equipment is running or off-line requiring the equipment to be taken out of service. Diagnostic testing can provide information on insulation condition without exceeding the rated voltage, although tests conducted above the rated voltage can reveal more information about insulation health.

2.2.3 Diagnostic measurements

Each type of insulation diagnostic measurement is based on detecting deviations from an ideal model of healthy insulation. Different types of instruments are used to collect and process signals that could indicate the condition of insulation.

2.2.3.1 Tan delta and insulation capacitance

Tan delta testing relies on a fundamental concept that ideal insulation can be modelled as a capacitor where the voltage and current are phase shifted by 90° [Arora and Mosch 2011] as shown in Figure 2.2. The applied electric field acts to polarise the dielectric. In reality, defects in the insulation result in a resistive current flow. The dissipation factor or tan δ is the ratio of resistive to reactive current and indicates the level of resistive loss within the insulation. It can be expressed as [IEEE Std 286 2000]:

$$\tan\delta = \frac{X_C}{R} = \frac{1}{\omega RC} = \frac{I_{loss}}{I_C} \tag{2.1}$$

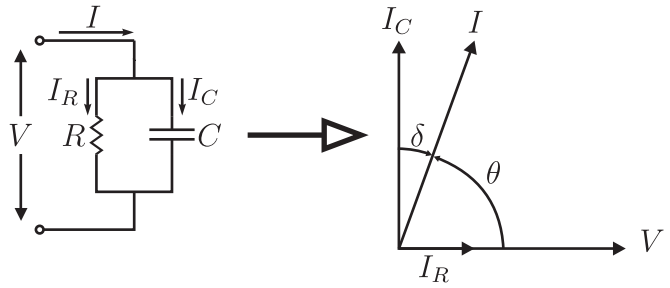

Figure 2.2 Insulation model and tan δ representation

Significant insulation defects such as water ingress [Tanaka et al. 1976], contamination [Pinto 1991] and ageing [van Bolhuis et al. 2002] can be quantified with a tan δ measurement. Another critical aspect of tan δ is its voltage dependence otherwise known as the differential tan δ or "tip-up". In a new cable tan δ readings should be

voltage independent whereas an aged cable will show an increasing trend as illustrated in Figure 2.3.

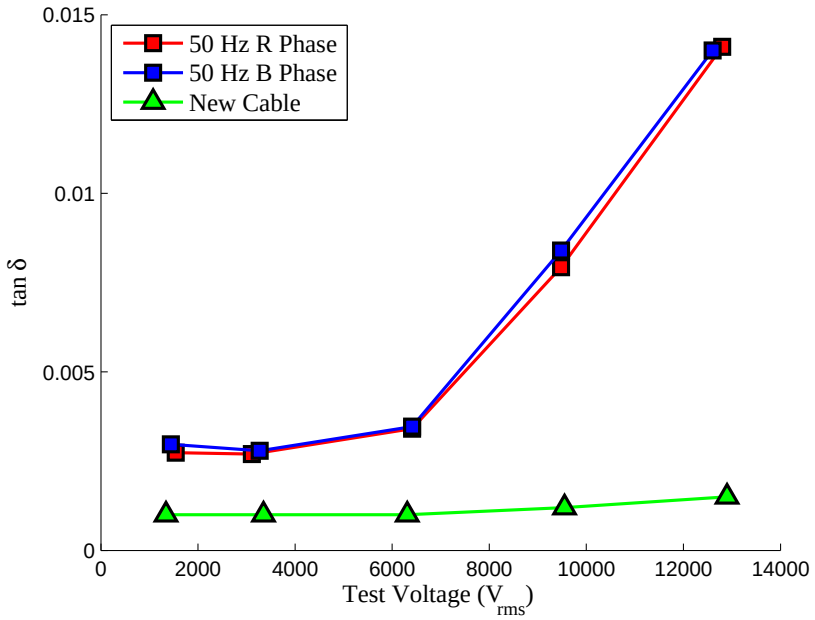

Figure 2.3 tan δ tip up characteristic showing aged cables (red and blue squares) against a new cable (green triangles)[Irani et al. 2013]

2.2.3.2 Partial discharge

High voltage applied across a piece of insulation can trigger localised breakdown of parts of the material. This phenomenon is known as partial discharge (PD) and occurs within voids in the insulation [Dawes and Hoover 1926]. The relative permittivity of the gas in the void is less than that of the surrounding material. As a result a large electric field is distributed across the void which can lead to PD if it exceeds the dielectric strength of the gas in the void.

A common model for partial discharge is the three capacitor equivalent circuit shown in Figure 2.4 [Gemant and Philippoff 1932]. The insulation is represented by a parallel capacitance C_P and the void is represented by the capacitance C_V in series with the total capacitance between the void and the electrodes C_S. An arc within the void causes C_V to discharge through a resistance R_V. Because this discharge current cannot be directly measured, a coupling capacitor C_C is connected in parallel with the cable under test. This stabilises the voltage during the PD pulse and supplies the current drawn by the discharge within the void. By integrating this current over time, a numerical value is obtained for the apparent charge released during a PD pulse.

The apparent charge quantifies the extent of dielectric polarisation causing a change in

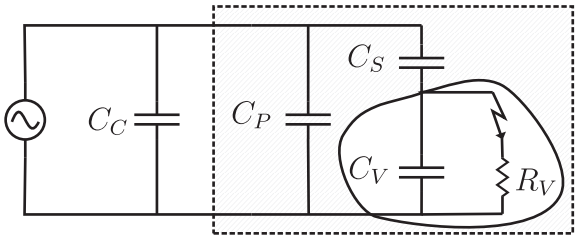

Figure 2.4 Equivalent circuit model of PD detection circuit

the cable capacitance and not the number of charges released. Partial discharge can also be detected acoustically or with a tuned directional antenna.

2.2.4 Factory and laboratory testing equipment

Large fixed high voltage sources are used in situations where the test article can be transported to the location of the test apparatus. These could be located at a laboratory or a test bay within a factory. Laboratory tests are often performed during product development, where prototype insulation systems are repeatedly tested to develop and validate mathematical models.

2.2.4.1 High voltage testing transformers

Without size as a constraint, laboratory test equipment can be large and highly rated. The most common means of achieving high alternating current (AC) voltages in the lab is using a testing transformer. These are large single phase, oil insulated high voltage transformers designed specifically for producing voltages and available with voltage ratings up to 800 kV. Compared to a single phase power transformer they are designed to have a smaller core flux density to mitigate harmonics produced by high magnetising currents [Kuffel et al. 2000]. The high voltage winding is well insulated and designed to handle the large short circuit mechanical forces produced by insulation failure within the test article.

High voltage windings of testing transformers often have large capacitances due to their large number of turns. They can even present a leading power factor under open circuit conditions [Olivier et al. 1984]. The winding cross section is trapezoidal to ensure a similar interlayer capacitance is obtained with each winding layer. This creates a more even voltage gradient across the high voltage winding.

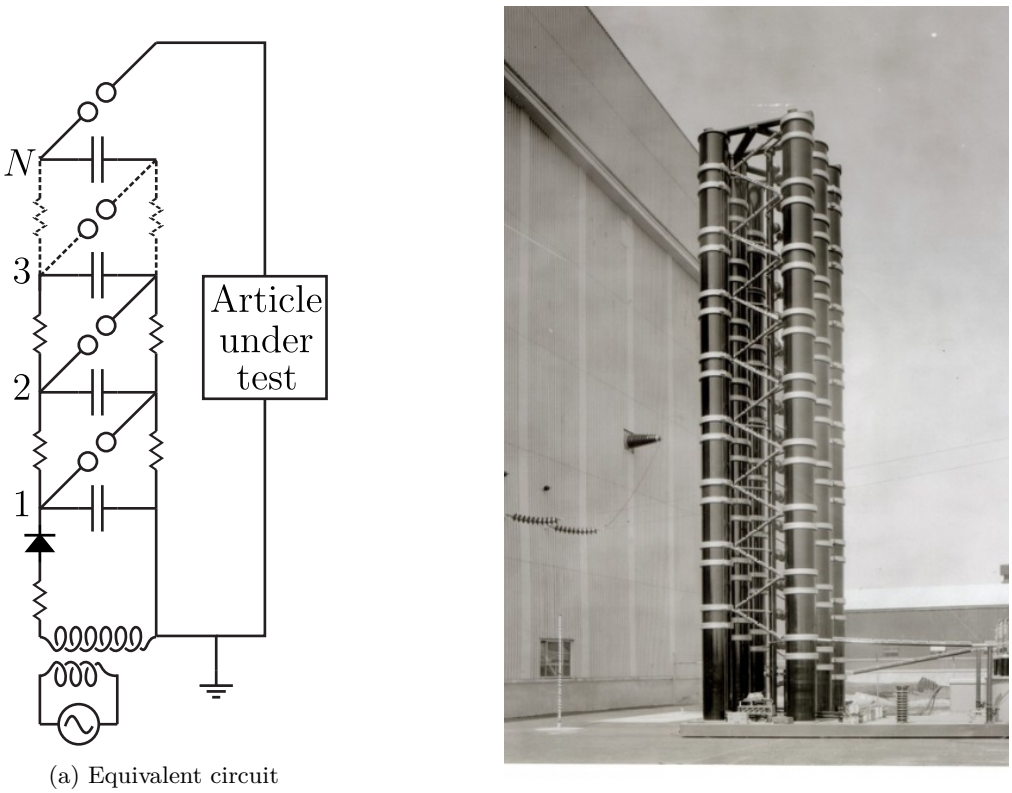

(a) Equivalent circuit

(b) Photo [Blalock 1997]

Figure 2.5 Marx generator

2.2.4.2 Impulse generators

An impulse generator can produce extremely high voltages and currents in a short burst. The most commonly used impulse generator is the Marx generator. This device slowly charges multiple capacitors in parallel and discharges them in series through spark gaps as shown in Figure 2.5. The impulse voltage or current waveform must conform to a pre-defined standard. One common industry standard waveform is defined as 1.2/50 µs [IEC 60060-1 2010] where the waveform must rise from 10% to 90% of its peak value in 1.2 µs and decay to 50% in 50 µs. In this case the waveform parameters were derived from actual measurements of lightning surges [Okabe et al. 2013].

2.2.5 Field testing equipment

Field testing equipment is far more constrained when it comes to size and input power requirements. The test equipment has to be able to reach remote locations. A transformer is often adequate for high voltage testing where the test article has a negligible capacitance such as an insulator or isolated phase bus duct (IPB). If it is designed for this purpose the HV winding and hence the whole transformer can be kept small to minimise the size due to the low load. However when the test article has a

large capacitance a testing transformer is often impractical. A range of testing methods have been used by the industry to overcome this challenge.

2.2.5.1 Direct current

Testing with DC voltages was common practice until recently because of its portability and low power requirements. A small DC test kit can slowly charge insulation capacitance to the required test voltage. This method has fallen out of favour with asset owners due to reports of reduction in life of XLPE cables after testing or failures of otherwise healthy insulation during testing [Srinivas 1993]. DC voltages can lead to accumulation of space charges within extruded insulation which can cause insulation failure promptly after return to service [IEEE Std 400 2012]. Test voltages are required to be much higher than what is required for power frequency.

2.2.5.2 Damped alternating current

As an alternative to DC testing a new method was developed for providing an alternating test voltage using portable equipment. Damped alternating current (DAC) involves slowly charging up the insulation capacitance to a given voltage level and discharging it through an inductor [IEEE Std 400.4 2015]. During discharge the insulation is subject to a damped alternating voltage with a frequency dependent on the resonant circuit formed by the insulation capacitance and external inductance.

DAC presents an alternative to DC testing however concurrent diagnostic measurements (PD, tan δ) are not representative of in service conditions. Measurements are not comparable with data gathered using other types of high voltage sources.

2.2.5.3 Very low frequency

The most popular method of testing medium voltage cables is very low frequency (VLF). A VLF test kit applies a 0.01 to 0.1 Hz sine wave across the cable insulation, significantly reducing both the supply power requirements and reactive power drawn by the cable insulation. Just like DC testing, this method enables both a small and low power test kit but does not harm healthy insulation [Eager et al. 1997]. The disadvantage of using VLF is that it does not stress insulation in a manner the cable will experience whilst in-service [Cavallini and Montanari 2006]. Hence, all test data collected regarding insulation health cannot be compared to factory tests which are performed using power frequency. Another disadvantage is the required test times are greater to apply the same insulation stress and collect the same diagnostic information as a power frequency test [IEEE Std 400 2012].

2.2.5.4 Power frequency

Power frequency field testing is commonly performed using resonant test systems. These consist of a variable frequency supply, exciting transformer and compensating reactors to resonate in series or parallel with the load capacitance [Schikarski et al. 1999][Rickmann and Kremer 2012]. They can be frequency tuned by varying the supply frequency between 30 - 300 Hz, which is considered "near power frequency" [Schufft 1999][Gerlach et al. 1991]. They can also be inductively tuned by varying the inductance of an external inductor connected in series or parallel. The size of resonant test systems makes their use impractical and uneconomic in some cases. Commercially available units need to be mounted in trucks as shown in Figure 2.6 or shipping containers and can weigh 40 T.

Figure 2.6 Truck mounted variable frequency resonant test system [Phenix Technologies 2013]

Recent work has looked at tuning transformers using DC biased coils within the magnetic circuit to alter the resonant inductance [Yuan et al. 2015]. This device has been called a magnetically controlled resonant transformer (MCRT).

2.3 PARTIAL CORE TRANSFORMERS

One method developed to reduce equipment weight involves using partial or open core transformers. In this design the outer limbs and connecting yokes of a traditional transformer are discarded and a single limb core is used with air completing the magnetic circuit as shown in Figure 2.7. The concept can be traced back to a patent filed in 1890 [Gaulard 1886] but was superseded soon afterwards by full core designs [Asztalos 1985]. Partial core transformer models have been developed based on circuit theory [Liew 2001], finite element analysis [Bell and Bodger 2008a] and for designs using superconducting windings [Lapthorn 2012].

High voltage insulation testing has presented the most practical application of the partial core transformer. The inductance of the transformer can be altered by moving

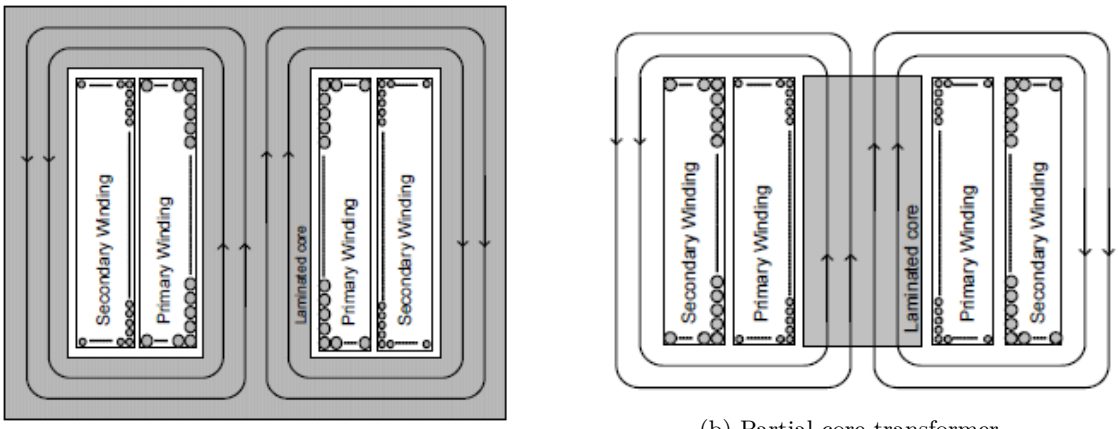

(a) Full core transformer

(b) Partial core transformer

Figure 2.7 Full core and partial core transformer cross section [Bendre et al. 2008]

Figure 2.8 Three versions of partial core resonant transformers at Clyde power stations [Lapthorn et al. 2016]

or inserting air-gaps within the core. In this application it behaves like a resonant test system where the exciting transformer and compensating reactor are combined into the same device. This design is known as a partial core resonant transformer (PCRTX) and has been used for high potential testing of generator and motor stators around New Zealand [Bodger and Enright 2004] as shown in Figure 2.8. A methodology for designing PCRTXs optimised for weight was the topic of a PhD thesis [Bell 2009]. Three PCRTXs shown in Figure 2.9 were constructed to be capable of testing a range of capacitive loads from open circuit to 1 µF, at voltages up to 40 kV.

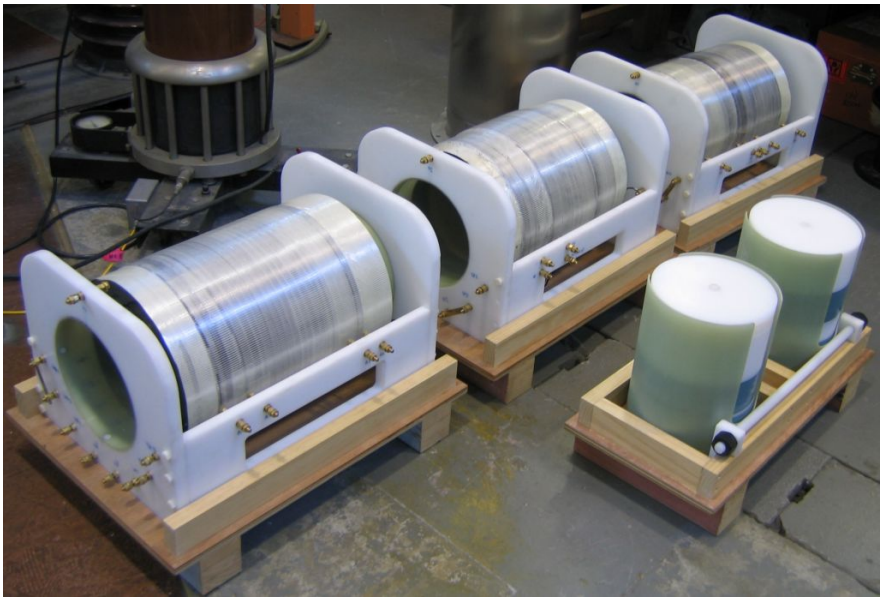

Figure 2.9 Partial core resonant transformer kitset [Bell 2009]

2.4 CASCADED TRANSFORMERS

Generating high voltages using cascaded transformers is a concept devised by Professor Friedrich Dessauer to produce X-rays [Norris and Taylor 1931]. The high voltage was used to excite a vacuum tube, forming a beam of high energy electrons that emit X-rays [Rogers 1955]. In this arrangement, shown in Figure 2.10, the primary winding of each transformer excites a HV secondary and a tertiary coupling winding which usually has the same number of turns as the primary. The primary of the next transformer is energised by the coupling winding of the previous transformer.

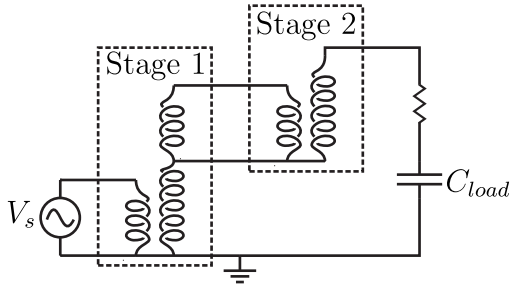

Figure 2.10 Dessauer cascade connection

The main advantage for cascading transformers is that each unit only has to be insulated to its own maximum secondary voltage, resulting in smaller and more transportable transformers. Each successive unit has to be appropriately insulated from ground. This can be accomplished by placing the transformers side by side on increasingly larger insulators, or stacking them on top of one another with each tank connected to the HV winding of the previous stage. The primary winding on the first stage carries the full

load current of subsequent stages and needs to be dimensioned accordingly. Cascade transformers are ubiquitous in high voltage test facilities worldwide. The worlds highest rated cascade transformers can produce AC voltages up to 3 MV [Kuffel et al. 2000]. An example of a cascade transformer installation in a high voltage laboratory is shown in Figure 2.11.

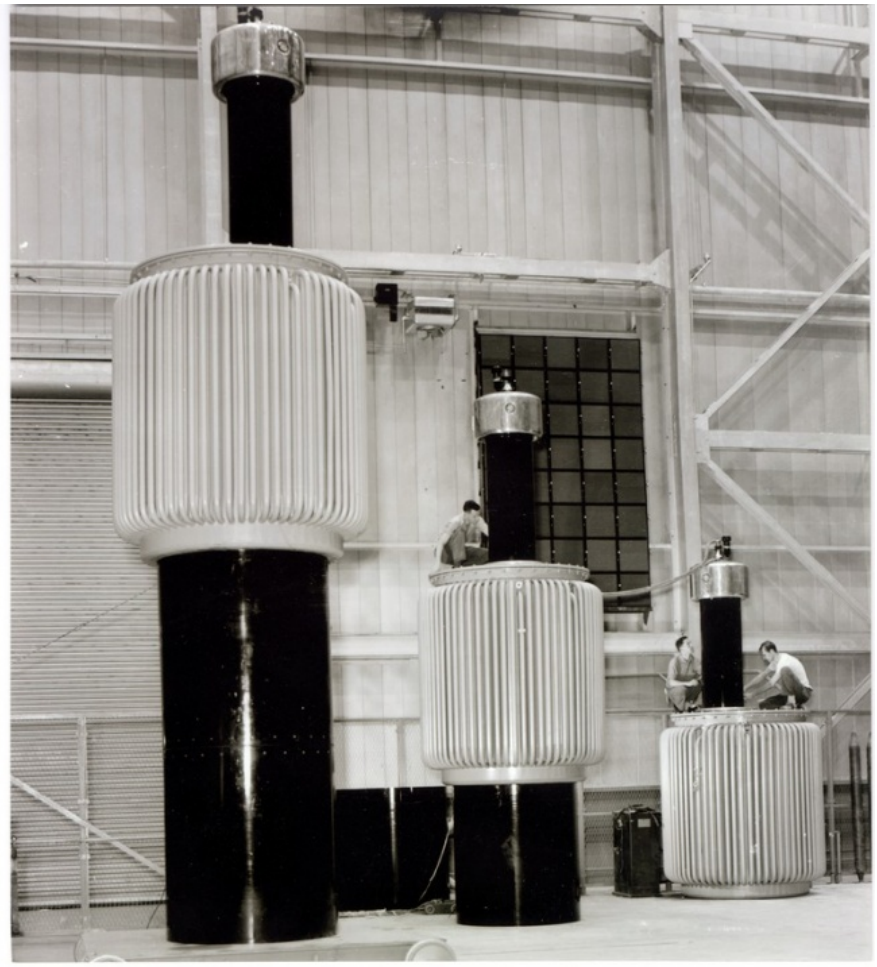

Figure 2.11 Photo of a cascaded transformer installation [Blalock 1997]

Efforts to model the effects of cascading transformers began with a simplified series equivalent circuit considering only winding resistances and leakage reactances [Goodlet 1937]. Circuit models including magnetising reactance and core losses were presented for two and three stage cascaded transformers [Jayaram 1958]. The models were advanced by including stray capacitances [Jayaram and Badkas 1960] and a method was described for predicting the output voltage by measuring only the input admittance [Jayaram and Badkas 1962]. The effect of adding external compensating reactors has also been investigated [Train and Vohl 1976]. Numerous researchers have observed that the voltage distribution between stages is not uniform and the final stage tends to develop the highest voltage.

The variation of voltage ratio with frequency has been modelled along with the resulting distortion on the output voltage wave shape [Olivier et al. 1980]. A modification in the circuit model to eliminate isolating transformers was presented enabling the same frequency response to be analysed using matrix algebra [Olivier et al. 1984]. All research conducted to date has focused on big cascaded testing transformers rated 100 kV or above. These transformers have a large number of secondary turns and a considerable equivalent winding capacitance. This causes the transformer to present a leading power factor under open circuit conditions [Jayaram and Badkas 1960] and necessitated the inclusion of tank and winding capacitances in circuit models.

2.5 APPLICATIONS

Portable high voltage sources are used wherever high voltage insulation needs to be energised in a controlled manner above its rated voltage, in situ. The nature of the load and the available power supply determine the level of inductive compensation required. The test voltage is defined by international standards.

2.5.1 Rotating machine stator testing

Partial core resonant transformers have been used for high potential testing of new and refurbished stators. The maximum test voltage V_{test}, as specified in the standard IEC 60034-1, is given below where U_0 is the rated operating voltage of the machine.

$$V_{test} = 2U_0 + 1 \tag{2.2}$$

Modern hydro generators are produced with rated line to line voltages up to 25 kV [Voith Hydro 2013]. The capacitive load of a single phase of the stator winding can vary from 90 nF for a small machine to 1.8 µF for a large salient pole synchronous generator [NengLing and Yan 2005].

The rating of available supplies at hydro power stations can be over 100 A when using welding outlets. For ease and speed of connection it is desirable for a test kit to use standard three phase socket outlets rated 32 A and below.

Off-line testing is usually accompanied by PD and tan δ measurements. To prevent disturbance from the source interfering with the PD signal from the test object, it is desirable that the source is PD free. A certain level of source PD can be effectively mitigated by the use of filters, directional sensors and gating which involves sampling and cancelling the source PD signature.

Portability is desirable on remote hydro sites where shipping weight can increase costs and space is constrained. It is not the most important factor on some sites due to the

Figure 2.12 Hydro generator stator under hi-pot test

presence of large station cranes, forklift access and large station doors. An example of the equipment set-up for a generator stator hi-pot at Tekapo A hydro power station is shown in Figure 2.12. Space can be more constrained when testing industrial motors and synchronous condensers.

2.5.2 Underground cable testing

Underground cables generally present large capacitive loads and higher voltages than rotating machine stators. Voltage ratings for underground cables in New Zealand vary from 1 kV to transmission voltages of 220 kV. There are naturally more medium voltage cable installations, however the economic case is stronger for testing high voltage cables due to their high capital cost and importance.

Presently the industry standard source for medium voltage cable testing is VLF. In New Zealand there are few cable installations at transmission level voltages above 66 kV. Where these have been installed truck mounted variable frequency resonant test systems have been used for commissioning testing. A portable HV source that could energise large cable capacitances to required test voltages would significantly reduce the testing cost. Such a system would also make power frequency testing economic for medium voltage cable installations.

Portability and size are important constraints for medium voltage cable testing. There can be limited space around cable terminals within indoor substations. A photo from a cable test conducted at Lancaster zone substation in Christchurch with an existing

PCRTX is shown in Figure 2.13 and shows how cramped the area can be [Irani et al. 2013]. High capacity power supplies are generally not easily available and the ability of the test kit to function from a standard three phase supply is desirable.

Figure 2.13 PCRTX being used for PD and tan δ testing on 11 kV distribution cables

2.5.3 Gas insulated switchgear testing

Gas insulated switchgear is used more often as a compact alternative to outdoor high voltage switchyards. The switching apparatus is encased in an insulating gas, most commonly sulfur hexafluoride (SF6). One of the benefits touted by GIS manufacturers is the low frequency of routine switchgear inspections required. These can be spaced at 25 year intervals due to the difficulty of safely removing the gas and opening the switchgear for inspection. An IEC standard [IEC 62271-203 2003] recommends routine high voltage withstand testing to verify the integrity of the insulation. The insulation capacitance of GIS is nominally in the order of 1 nF. However the test voltage for a short duration withstand test can exceed 460 kV.

Testing has been performed with large oil filled cascaded transformers with separate resonant inductors housed within the tank [Mohseni et al. 2008]. Another modern test system requires the installation of a special voltage transformer (VT) within the GIS during manufacturing [Omicron 2013]. When routine testing is required a variable frequency source with parallel compensating reactors is connected to the LV side as shown in Figure 2.14.

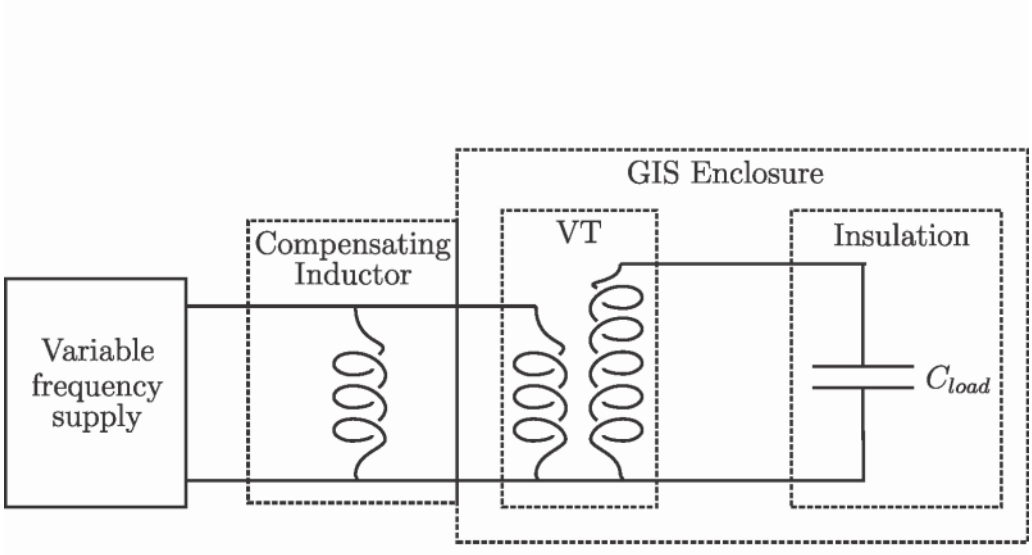

Figure 2.14 Modular GIS test kit with factory installed VT

2.5.4 Transformer testing

High voltage power transformers are routinely tested in the factory before being shipped to the location of installation. The shipping and installing of a transformer presents further risk of damage so extensive testing is completed on site before it enters service. Some tests conducted in the factory cannot be repeated on site due to the size of equipment required. These tests are outlined in [IEC 60076-3 2003] and include the separate source AC withstand voltage test to test the phase to earth insulation. For this test a voltage above the transformer rating is applied from an external high voltage source. Another test includes the long and short duration induced voltage tests described in Section 2.2.2.1.

A commercially available system exists for performing these tests on new installed transformers on site. This system is similar in appearance and size to the truck mounted kit shown in Figure 2.6. This system weighs nearly 40 T and requires a 750 kVA power supply [Horeth 2012].

2.6 CASCADED PARTIAL CORE TRANSFORMERS CONCEPT

The concept explored in this thesis combines cascaded transformers with partial core resonant transformers. This is a combination of systems used in the field and high voltage laboratories. Similar to laboratory based cascaded transformers, the goal is to achieve higher voltages than a single transformer without modifying the insulation system. Similar to existing resonant test systems, the inductance is tunable to compensate the reactive power drawn by a large capacitive load. The conceptual circuit diagram

of this arrangement is shown in Figure 2.15. The transformers use a solid insulation system similar to existing PCRTXs to reduce shipping weight and make them easily transportable.

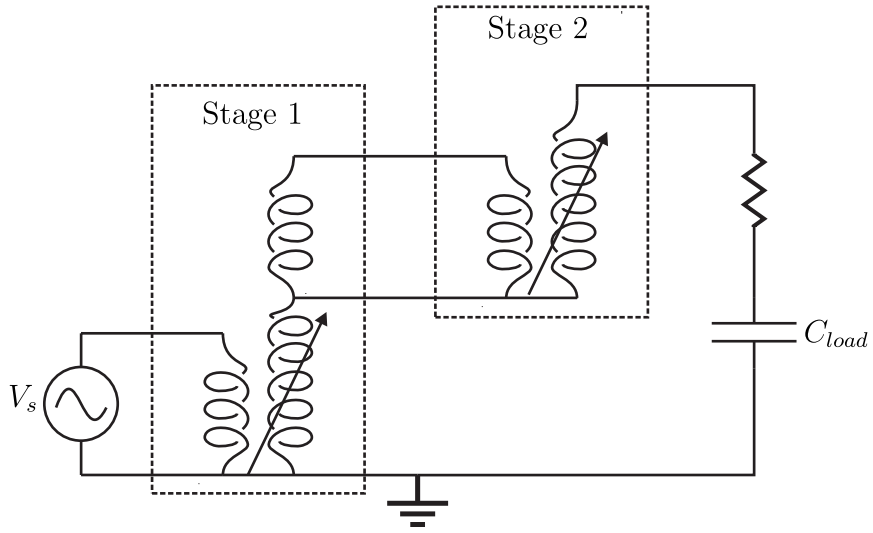

Figure 2.15 Cascaded partial core resonant transformer conceptual circuit

The success of this concept depends on the ability to increase portability compared to an equivalent single stage test kit. This is aimed at reducing the cost of field testing high voltage and high capacitance loads.

Chapter 3

SINGLE PARTIAL CORE RESONANT TRANSFORMER MODEL

3.1 OVERVIEW

This chapter presents the mathematical model for partial core resonant transformers (PCRTXs) with two and three windings. Two types of equivalent circuit models for two winding transformers are reviewed and expanded upon to model three winding transformers. The first equivalent circuit models the PCRTX as a multi winding coupled inductor and the second model is based on the Steinmetz 'exact' transformer equivalent circuit. The inductive components of the circuit are determined with a 2D magnetostatic finite element analysis (FEA) of the core and winding geometry. The peak flux density of PCRTXs with different aspect ratios is also estimated using FEA. A new method for estimating the core losses which involves the use of excess losses is presented along with an analysis of the sensitivity of the circuit model to core losses. A computationally efficient matrix formulation of both equivalent circuits is presented and used to predict the transformer's electrical performance. The model is validated by testing against two prototype transformers.

3.2 TWO WINDING CIRCUIT MODELS

The electrical performance of a transformer can be determined using an equivalent circuit model. Each element in the equivalent circuit is chosen to represent an electromagnetic phenomenon within the core, windings or surroundings that significantly impacts the electrical behaviour of the transformer. Extensive work has been performed on developing equivalent circuit models to aid in the design of partial core transformers [Bell 2009] [Liew 2001]. Using the reverse design process, equivalent circuit parameters are derived from the geometry and material properties of available components. Although mathematically identical, each equivalent circuit models the transformer in a different way with varying complexity. A coupled inductor model is useful for modelling terminal conditions and the Steinmetz 'exact' transformer equivalent circuit can be used to determine other

performance characteristics such as the energy stored in leakage reactance [Bell 2009] and phase shifts.

3.2.1 Dual winding coupled inductors

Inductance is a property assigned to a circuit element that produces a magnetic flux when a current is passed through it. The voltage produced at the terminals of a coil is proportional to the rate of change of magnetic flux. In a single coil this property is referred to as self inductance, L. If this flux is time varying and another coil is placed nearby, a voltage will be produced at the terminals of this second coil. This voltage is proportional to the time rate of change of current in the first coil with the proportionality constant termed the mutual inductance, M [Hayt et al. 2007]. The circuit symbol for two mutually coupled coils is shown in Figure 3.1.

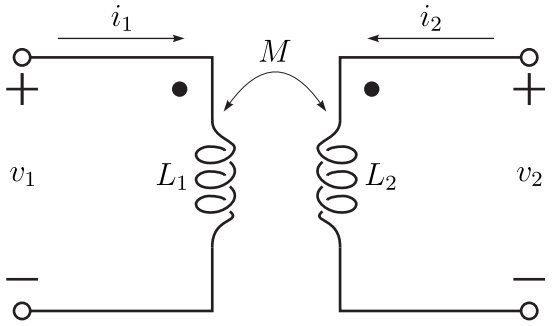

Figure 3.1 Dual winding mutual inductor

If a load is placed across the terminals of the second coil, a current will flow in this coil producing its own magnetic flux. Therefore, a mutual voltage is produced in each coil due to the magnetic flux produced by the other. This mutual voltage is independent of the voltage produced due to the self inductance. Therefore, the terminal voltages of two mutually coupled inductors are the sum of the voltages induced by the winding self inductances and the voltages induced by the mutual inductances between the windings. For a two winding inductor this relationship is defined by

$$v_1 = L_1 \frac{di_1}{dt} + M \frac{di_2}{dt} \tag{3.1}$$

$$v_2 = L_2 \frac{di_2}{dt} + M \frac{di_1}{dt} \tag{3.2}$$

The value of M is bound by the inequality

$$M \leq \sqrt{L_1 L_2} \tag{3.3}$$

The maximum value of M represents maximum coupling between the coils. The level of coupling between the coils is quantified by the coupling coefficient k,

$$k = \frac{M}{\sqrt{L_1 L_2}} \tag{3.4}$$

where

$$0 \leq k \leq 1 \tag{3.5}$$

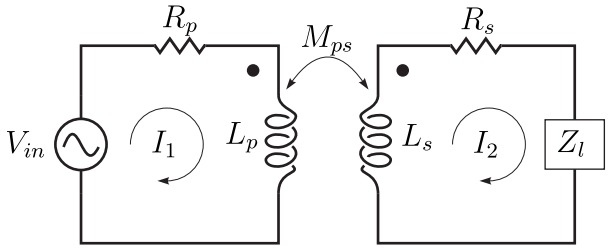

Figure 3.2 Loaded dual winding coupled inductor

The circuit for a pair of coupled coils transferring power to a load is shown in Figure 3.2, where R_p and R_s are the primary and secondary winding resistances respectively and Z_l is the load impedance. M_{ps} is the mutual inductance between the primary and secondary. The input impedance can be expressed analytically by considering the mesh equations of the circuit.

$$V_{in} = Z_p I_1 - j\omega M_{ps} I_2 \tag{3.6}$$

$$0 = -j\omega M_{ps} I_1 + Z_s I_2 \tag{3.7}$$

where $Z_p = R_p + j\omega L_p$ and $Z_s = R_s + j\omega L_s + Z_l$.

Rearranging Equation (3.7) gives

$$I_2 = \frac{j\omega M_{ps} I_1}{Z_s} \tag{3.8}$$

By substituting this into Equation (3.6), an expression can be found for the input impedance of a dual winding coupled inductor.

$$Z_{in} = \frac{V_{in}}{I_{in}} = Z_p + \frac{\omega^2 M_{ps}^2}{Z_s} \tag{3.9}$$

Using this expression, allowable ranges of equivalent circuit parameters can be derived from design specifications. The model is limited to predicting the terminal conditions

of the PCRTX such as input impedance and winding current but not the voltage ratio because there are no secondary terminals [Bell 2009]. The energy stored in the leakage reactances is not modelled separately, so the exact voltage drop due to leakage flux cannot be calculated using this model [El-Hamamsy and Chang 1989]. Losses within the transformer core are also not taken into account.

3.2.2 Two winding T and Steinmetz 'exact' equivalent circuits

The T-equivalent circuit can be derived from the mutually coupled inductor model as shown in Figure 3.3 by recognising that both windings share a common parallel inductance M_{ps}. The total inductance around the left hand mesh is L_p, so a series inductance of $L_p - M_{ps}$ must be inserted in the left hand mesh and $L_s - M_{ps}$ into the right hand mesh to construct an identical equivalent circuit [Hayt et al. 2007].

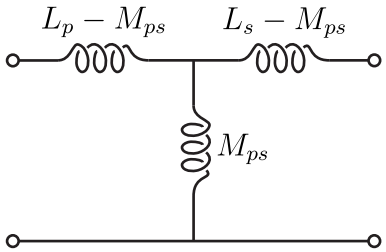

Figure 3.3 T-equivalent circuit in terms of coupled inductor parameters

With the addition of core and winding losses, the T-equivalent circuit becomes the Steinmetz 'exact' transformer equivalent circuit [Steinmetz 1895] shown in Figure 3.4. The magnetising current drawn by the primary winding when the secondary is open circuited is represented by a shunt inductance L_m. In addition, some of the flux generated by the primary and secondary winding currents bypasses the core and flows through the voids around the windings. This unwanted flux is termed leakage flux and induces an opposing electromotive force (emf) e in each winding. This effect is accounted for with the leakage inductances L_{lp} and L_{ls}. An ideal transformer is connected to the end of the circuit with a voltage ratio a defined as

$$a = \frac{N_p}{N_s} \tag{3.10}$$

where N_p is the number of turns on the primary winding and N_s is the number of turns on the secondary winding.

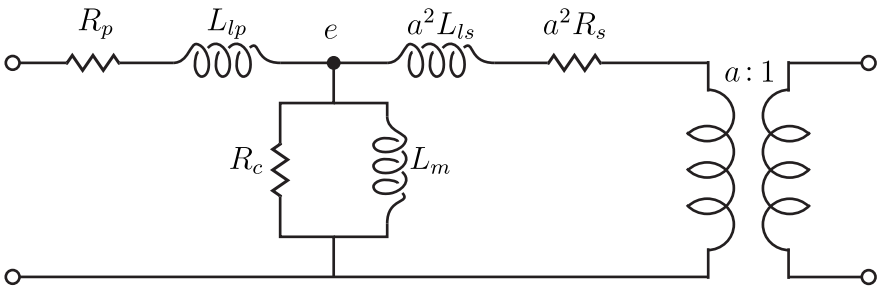

Figure 3.4 Steinmetz 'exact' transformer equivalent circuit

The Steinmetz equivalent circuit emphasises the unity of the exciting current drawn by both windings and separates the individual winding leakage reactances. Resolving the leakage reactance into primary and secondary components is an indeterminate problem [Boyajian 1925]. Therefore it is normally assumed that the leakage reactances are the same when referred to the primary because the same terminal conditions are obtained. This assumption is not valid for transformers with different winding lengths and incomplete magnetic cores [Margueron and Keradec 2007]. If M_{ps} is greater than any of the winding self inductances it is possible that one of the inductances could be negative. This does not make sense practically but is necessary to represent the terminal conditions accurately.

3.3 THREE WINDING EQUIVALENT CIRCUIT MODELS

Two, three winding transformer models have been used to predict the performance of the PCRTX. The first is an extension of the coupled inductor model and the second is the T-equivalent circuit.

3.3.1 Three winding coupled inductors

The two winding model can be extended to three winding transformers, however, the complexity is increased as it is necessary to account for three mutual inductances and three self inductances. The matrix formulation of the winding terminal voltages is

$$\Big[V\Big] = \Big[L\Big]\,\frac{d}{dt}\,\Big[I\Big] \tag{3.11}$$

where L is the inductance matrix

$$\Big[\mathbf{L}\Big] = \begin{bmatrix} L_{11} & M_{12} & M_{13} \\ M_{21} & L_{22} & M_{23} \\ M_{31} & M_{32} & L_{33} \end{bmatrix} \tag{3.12}$$

and L_{ii} is the self inductance of the i^{th} coil and M_{ij} is the mutual inductance between coils i and j. The inductance matrix is symmetric due to the reciprocity theorem and is necessary for conservation of energy [Hayt et al. 2007]. This can be mathematically expressed as

$$M_{12} = M_{21} \tag{3.13}$$

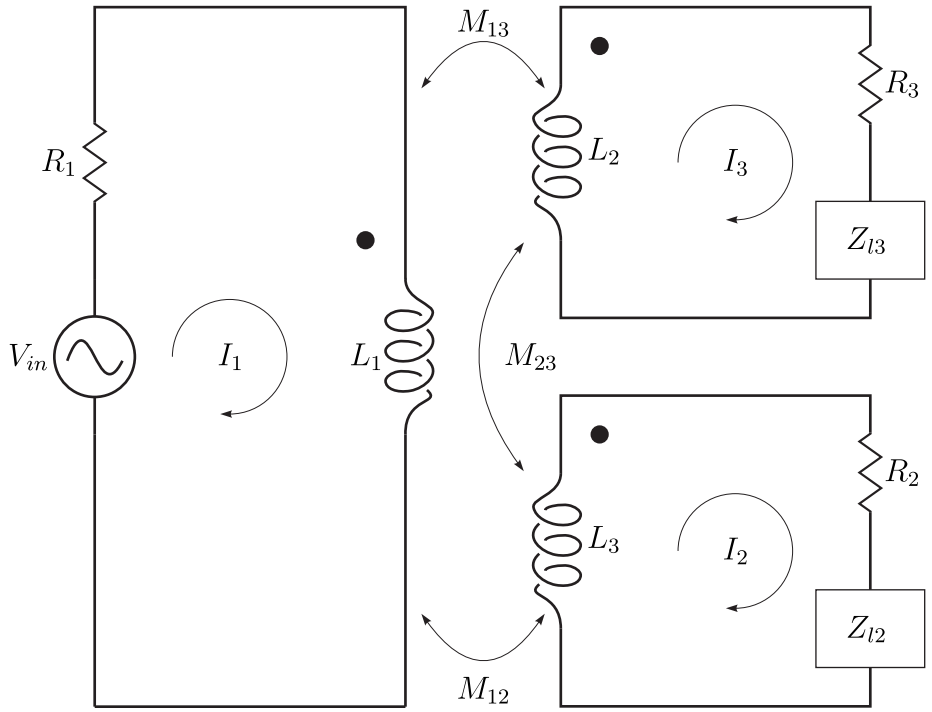

Figure 3.5 Three winding PCRTX coupled inductor model

Consider a three winding coupled inductor with both secondary and tertiary windings loaded as shown in Figure 3.5. Analysis of the mesh equations for this circuit yields the frequency domain matrix formula

$$\begin{bmatrix} V_s \\ 0 \\ 0 \end{bmatrix} = \begin{bmatrix} Z_{11} & -j\omega M_{12} & -j\omega M_{13} \\ -j\omega M_{21} & Z_{22} & -j\omega M_{23} \\ -j\omega M_{31} & -j\omega M_{32} & Z_{33} \end{bmatrix} \begin{bmatrix} I_1 \\ I_2 \\ I_3 \end{bmatrix} \tag{3.14}$$

where Z_{jj} is the sum of the j^{th} winding's losses R_j, the impedance due to self inductance L_j and the load impedance Z_{lj} defined by

$$Z_{jj} = R_j + L_j + Z_{lj} \tag{3.15}$$

Back substitution gives the input impedance of a three winding inductor with a loaded

secondary and tertiary winding as

$$Z_{in} = Z_{11} + \frac{\omega^2(M_{12}^2 Z_{33} + M_{13}^2 Z_{22}) + j2\omega^3 M_{12} M_{13} M_{23}}{Z_{22} Z_{33} + (\omega M_{23})^2} \tag{3.16}$$

When referring to transformers the subscript notation is changed to have p, s and t denote the primary, secondary and tertiary windings. To include core losses in the circuit it is proposed that a resistance R_c is connected across the primary winding self inductance as shown in Figure 3.6. This loss is dependent on the flux density within the core under resonant conditions. This parameter should be included in the circuit only when the loaded circuit performance of the PCRTX is being modelled.

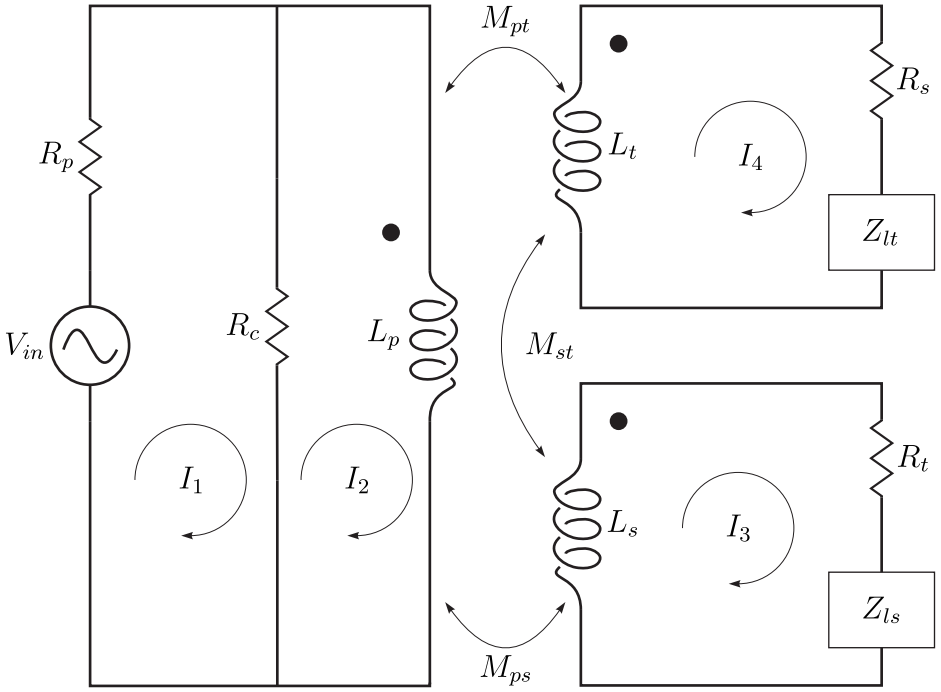

Figure 3.6 Three winding PCRTX coupled inductor model including core losses

The matrix formula for this circuit now becomes

$$\begin{bmatrix} V_{in} \\ 0 \\ 0 \\ 0 \end{bmatrix} = \begin{bmatrix} R_p + R_c & -R_c & 0 & 0 \\ -R_c & j\omega L_p + R_c & -j\omega M_{pt} & -j\omega M_{ps} \\ 0 & -j\omega M_{pt} & j\omega L_t + R_t + Z_{lt} & -j\omega M_{st} \\ 0 & -j\omega M_{ps} & -j\omega M_{st} & j\omega L_s + R_s + Z_{ls} \end{bmatrix} \begin{bmatrix} I_1 \\ I_2 \\ I_3 \\ I_4 \end{bmatrix} \tag{3.17}$$

3.3.2 Three winding T-equivalent circuit

Existing models of high voltage three winding transformers are based on the T-equivalent circuit [Olivier et al. 1984] [Olivier et al. 1980] [Jayaram and Badkas 1962]. These

models have accurately predicted the voltage ratio and distribution between stages of large HV testing transformers. The circuit shown in Figure 3.7 can be used to model the voltage ratios between windings and phase shifts across leakage components.

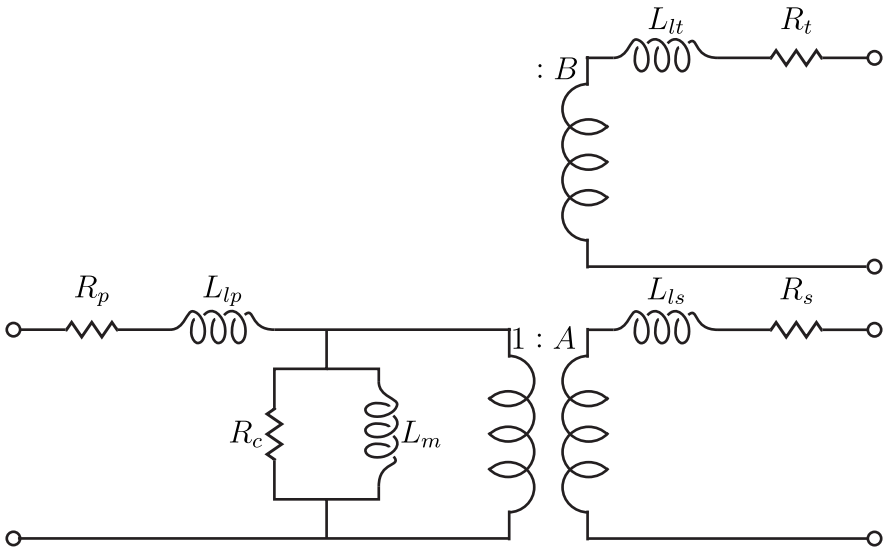

Figure 3.7 Three winding transformer model

The parameters are the same as the Steinmetz model except there is a third set of winding resistances and leakage reactances. A three winding ideal transformer is employed with ratios $1 : A : B$ where

$$A = \frac{M_{st}}{M_{pt}}$$

$$B = \frac{M_{st}}{M_{ps}}$$

These may differ slightly from the turns ratios the transformer was wound with [Ludwig and El-Hamamsy 1991]. Unlike the coupled inductor model which does not have any secondary terminals, the T-equivalent circuit can be used to calculate the voltage ratios of a three winding transformer.

3.4 CIRCUIT PARAMETER CALCULATIONS

3.4.1 Inductive reactance components

The inductive components of the equivalent circuit model shown in Section 3.2 and 3.3 were derived from the transformer geometry using a finite element analysis (FEA) model. The model was built using *Infolytica MagNet Version 7.4*, a commercially available

FEA software package. The drawing of the model and processing of the results was controlled by a *Python* script, the details of which are outlined in a later chapter.

To calculate self and mutual winding inductances it is not necessary to consider losses or saturation characteristics within the FEA model. It is also assumed that the magnetised state of the core is below saturation and within the linear region of the B-H curve. For these reasons the windings are modelled as blocks of perfectly conductive material and the core is modelled as a non conducting homogeneous block with a linear relative permeability of 3000. Only a quarter of the transformer needs to be modelled due to symmetry, which saves computation time. These simplifications are adequate for predicting PCRTX inductances [Bell 2009].

Within the program, a series of open circuit tests were simulated by exciting each winding with unit current. The corresponding permeance matrix was defined using the relationship

$$P_{ij} = \frac{\lambda_{i'}}{i_{j'}} \tag{3.18}$$

where $\lambda_{i'}$ is the flux linkage due to winding j' being excited by a current i'_j. Windings i' and j' have a unity number of turns but occupy the same space as windings i and j. The permeance matrix P is defined as

$$\Big[\mathbf{P}\Big] = \begin{bmatrix} P_{11} & P_{12} & \cdots & P_{1n} \\ P_{21} & P_{22} & \cdots & P_{2n} \\ \vdots & \vdots & \ddots & \vdots \\ P_{n1} & \cdots & \cdots & P_{nn} \end{bmatrix} \tag{3.19}$$

where n refers to the number of coils being modelled. These could be n windings or n winding sections with separate taps. The inductance matrix can be found using

$$L_{ij} = N_i N_j P_{ij} \tag{3.20}$$

where N_i and N_j are the number of turns on winding i and j. With all the self and mutual inductance components defined, the inductive reactance components of the T-equivalent circuit can be found using the transformation equations derived in Ludwig and El-Hamamsy [1991] and presented below. The size of the inductance matrix corresponds to the number of windings and the rows and columns are arranged so the primary, secondary and tertiary windings correspond to row/column $1, 2$ and 3. For a two winding transformer the magnetising and leakage inductances referred to the

primary winding are given by

$$L_m = \frac{N_p}{N_s} M_{ps} \tag{3.21}$$

$$L_{lp} = L_p - \frac{N_p}{N_s} M_{ps} \tag{3.22}$$

$$L_{ls} = L_s - \frac{N_s}{N_p} M_{ps} \tag{3.23}$$

For a three winding transformer the inductances are given by

$$L_m = \left(\frac{M_{ps} M_{pt}}{M_{st}} \right) \tag{3.24}$$

$$L_{lp} = \left(L_p - M_{ps} \frac{M_{pt}}{M_{st}} \right) \tag{3.25}$$

$$L_{ls} = \left(L_s - M_{ps} \frac{M_{st}}{M_{pt}} \right) \tag{3.26}$$

$$L_{lt} = \left(L_t - M_{pt} \frac{M_{st}}{M_{ps}} \right) \tag{3.27}$$

3.4.2 Flux density

A common approximation of the peak flux density B_{pk} inside a transformer is the 'transformer equation' given as

$$B_{pk} = \frac{\sqrt{2} V_{in,pk}}{\omega N_p A_c} \tag{3.28}$$

where $V_{in,pk}$ is the peak primary peak voltage and A_c is the effective core cross-sectional area. This formula is used to design full-core transformers where the approximation of a uniform core flux density is more valid than in partial core transformers [Bell and Bodger 2008b]. FEA can give a detailed picture of the spatial flux density distribution within the core. A comparison of flux density distribution on two transformers with different aspect ratios is shown in Figure 3.8.

The point of highest flux density within the core depends on the aspect ratio of the transformer. It is important to note that finite element approximations reach singularities at corners and sharp points. When the point of highest flux density is located in the corners, this is usually limited to a very small region. To account for this

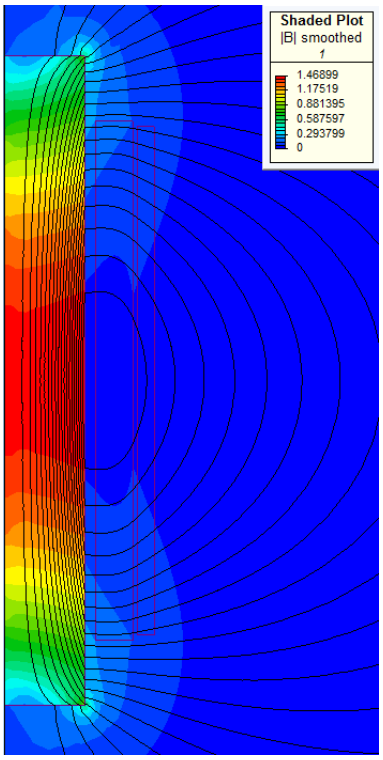

(a) Finite element flux density plot for a long thin core

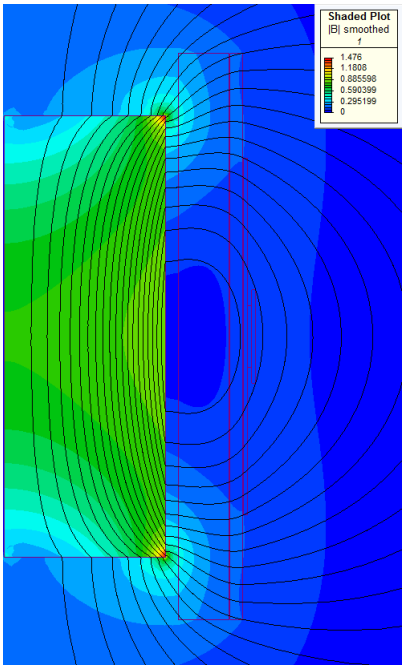

(b) Finite element flux density plot for a short fat core

Figure 3.8 Finite element flux density distribution

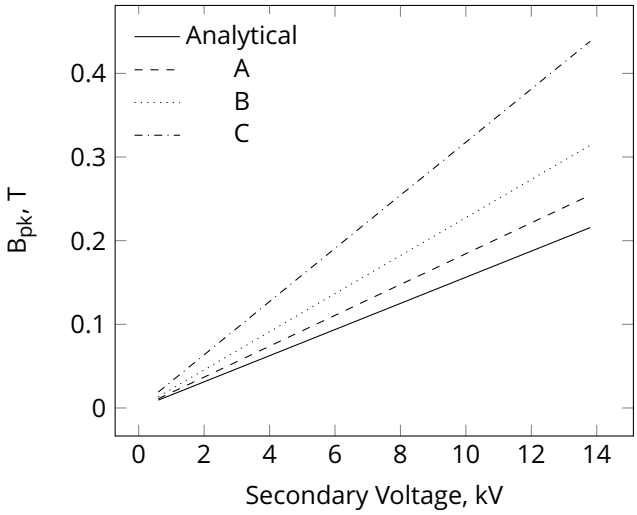

(a) Comparison of FEA B_{pk} with analytical estimation

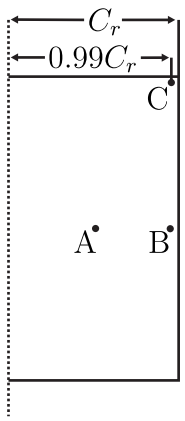

(b) Locations of sampling B_{pk}

Figure 3.9 Finite element flux density distribution

the flux density is sampled at 99 % of the core outer radius near the core outer edges. A loaded circuit test involving a fat core was conducted. B_{pk} was estimated analytically using Equation (3.28) and the applied voltage. This was compared to an FEA estimate of the same situation. The flux density was sampled at the points shown in Figure 3.9b.

Figure 3.9a compares the validity of the analytically estimated B_{pk} according to Equation (3.28) compared to the FEA flux density estimate for a short fat core. The equation underestimates the flux density at all sampled points.

3.4.3 Winding losses

In any transformer the two main sources of real power losses occur within the windings and the core. Equivalent circuit models represent them with a series or parallel resistance. All losses generate heat which can thermally degrade the insulation and lower the efficiency of the transformer. In PCRTXs, losses lower the maximum input impedance achievable at resonance and increase the current drawn from the supply. High parallel resistances are desirable but high series resistances are not.

The resistivity ρ of metals for small variations around ambient temperature $20°C$ is calculated as [Liew 2001]

$$\rho = (1 + \Delta\rho(T - 20))\rho_{20°C} \tag{3.29}$$

where $\Delta\rho$ is the thermal resistivity coefficient, T is the temperature in °C and $\rho_{20°C}$ is the material resistivity at ambient temperature, $20°C$. The resistance of winding i is

calculated as [Bell 2009]

$$R_i = \frac{\rho_i l_i}{A_i} \tag{3.30}$$

where l_i is the winding length and A_i is the effective current carrying cross sectional area of the conductor once the winding skin depth is taken into account.

3.4.4 Core loss resistance

When a time varying magnetic field is applied to a conductive material, voltages are induced in any closed conductive paths. These voltages drive currents through the material that cause Joule heating [Bertotti et al. 1992]. Qualitatively this is the bulk of real power loss under open circuit conditions and is represented by the parallel resistance R_c in equivalent circuit models (Figure 3.4 and 3.6).

No universally reliable core loss model for partial core transformers has been developed. The existing model found in [Liew 2001] has proved adequate for a small number of cases. A complete model requires detailed information about the electromagnetic properties of the core steel which is often unavailable. Otherwise a sample set of steel laminations can be tested using an Epstein frame to obtain the magnetodynamic properties [IEC 60404-2 2008]. Without material information and the necessary measurement apparatus the losses must be estimated to an acceptable degree of accuracy.

Under resonant conditions most of the current drawn by the PCRTX powers the losses in the windings, the load and the core. Collectively these losses represent damping within the system that limits the maximum achievable input impedance. Therefore the necessary accuracy of the core loss model is determined by its real value relative to other losses in the circuit. For a sample transformer the sensitivity of the calculated input impedance to changes in the core loss resistance value is shown in Figure 3.10.

For design purposes this indicates that after a certain threshold, increases in core loss resistance have negligible impact on the input impedance, in the case of Figure 3.10 about $150\,\Omega$. Below this threshold the input impedance significantly drops off even if the transformer is operating at resonance. A sensitivity analysis like this can be performed at design time to calculate a minimum value for core loss resistance. With lower core losses there is less gain from an increasingly accurate model of core losses.

Any method for calculating R_c must first determine the total real power loss in the core P_c. In partial core transformers the voltage drop across the leakage reactance is not

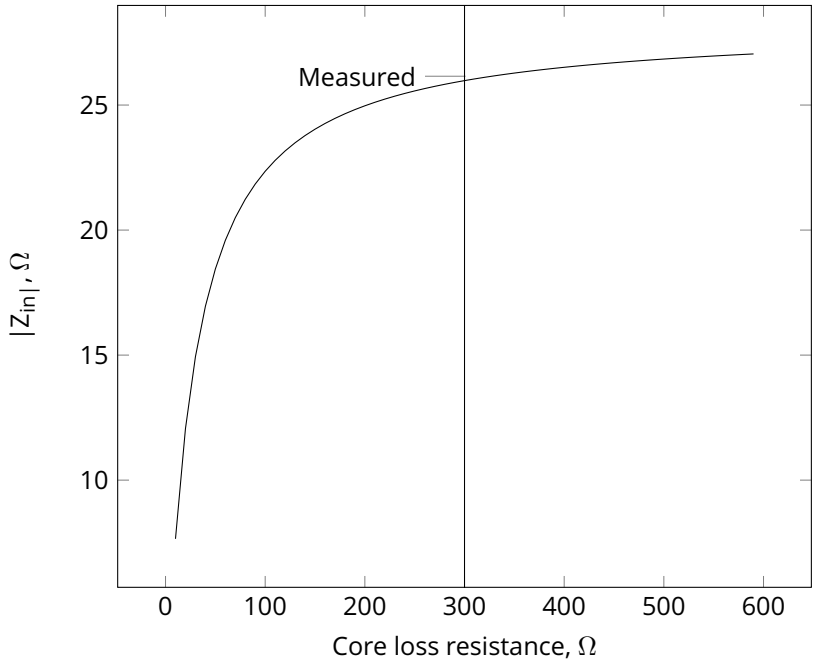

Figure 3.10 Sensitivity of modelled input impedance at resonance to core loss resistance, for an example transformer

negligible, so the voltage driving the loss is the induced emf e giving

$$R_c = \frac{e^2}{P_c} \tag{3.31}$$

To understand the physical origin of this loss it must be realised that magnetisation does not apply uniformly to a material. It is confined to localised domains which are saturated regions of identical magnetic orientations separated by domain walls [Pry and Bean 1958]. Under an externally applied magnetic field, domains with the same magnetic orientation as the applied field grow at the expense of other domains. The movement of a growing domain wall can be slowed by imperfections in the crystal structure of the material and cause rapid movements of the wall boundary known as Barkhausen noise [Graham 1982]. Magnetisation changes at the region swept by moving domain walls generate localised eddy current losses. Additionally there is a loss associated with the motion of the domain wall called spin relaxation loss [Reinert et al. 2001].

There is no practical way of knowing the temporal and spatial distribution of magnetic domains. Hence engineers resort to using macroscopic and empirical techniques. The classical empirical loss calculation P_{class} involves separating core losses into hysteresis losses P_h and eddy current losses P_{ec} by

$$P_{class} = P_h + P_{ec} \tag{3.32}$$

Hysteresis losses occur during the rotation and growth of magnetic domains within a material that is exposed to a time-varying magnetic field. Some of the published literature disputes the physical basis for separating losses. It is argued that all losses are due to eddy current losses from domain wall movement and spin relaxation loss [Graham 1982].

The steady state hysteresis power loss in a transformer core can be empirically estimated by

$$P_h = k_h f B_{pk}^x \tag{3.33}$$

where P_h is the hysteresis loss per unit weight of the core, k_h is the hysteresis loss constant, f is the supply frequency and B_{pk} the maximum flux density. x is an experimentally derived parameter known as the Steinmetz coefficient. It depends on the material properties of the core steel and is typically given as a value between 1.5 and 2.5.

According to the classical theory, a time-varying magnetic field applied to a transformer core induces a voltage within it. This voltage drives a current in a closed loop known as an eddy current. This loss is reduced by using core materials with a high resistivity and making the core from alternating laminations of steel and insulation. A general expression for steady state eddy current losses in $\mathrm{W\,kg^{-1}}$ is given by

$$P_{ec} = k_{ec} f^2 B_{pk}^2 \tag{3.34}$$

where k_{ec} is an empirically derived constant.

A more specific expression for the instantaneous value of eddy current losses per unit volume is given by

$$P_{ec}(t) = \frac{t_{lam}^2}{12\rho_c} \left(\frac{dB(t)}{dt} \right)^2 A_c l_c \tag{3.35}$$

where A_c is the cross sectional area of the core, ρ_c is the core resistivity, l_c is the length of the core and t_{lam} is the lamination thickness. The induced voltage in the primary winding is

$$e = N_p \frac{d\phi}{dt} = N_p A_c \frac{dB}{dt} \tag{3.36}$$

and since

$$P_{ec} = \frac{e^2}{R_{ec}} \tag{3.37}$$

this loss can be expressed as a resistance [Slemon 1966]

$$R_{ec} = \frac{N_1^2 A_c 12 \rho_c}{l_c t_{lam}^2} \tag{3.38}$$

where N_1^2 is the number of turns on the primary winding.

The problem with this formula is that it assumes a uniform flux density within the core and that the flux density vector points parallel to the core laminations. In partial core transformers the flux density is not uniform throughout the core and there is a significant radial component to the flux that points perpendicularly to the laminations [Huo 2009]. This generates significantly more eddy current losses than predicted by Equation (3.38).

Through experimentation with similar partial core transformers a simple empirical correction factor of 10 is suggested [Lapthorn et al. 2013]. This changes Equation (3.38) to

$$R_{ec} = \frac{N_1^2 A_c 120 \rho_c}{l_c t_{lam}^2} \tag{3.39}$$

The classical empirical approach presented above does not consider losses that occur at a domain level. It also excludes Barkhaussen noise. These are combined into a third component called excess losses. Numerous methods are presented for calculating P_{exc} from the Pry and Bean model [Pry and Bean 1958] to a statistical consideration of all domain effects [Bertotti 1988]. A simplified approximation of excess losses can be performed by [Boglietti et al. 2003]

$$P_{exc} = k_{exc} f^{1.5} B^{1.5} \tag{3.40}$$

where k_{exc} is an empirically derived constant. As an example, a small sample of PCRTXs with the same steel core were tested. For this particular case the fitted values for the loss constants are given in Table 3.1

The total core loss resistance can be expressed as the parallel combination of R_{ec}, the hysteresis loss resistance R_h and the excess loss resistance R_{exc} as shown in Figure 3.11. Two core loss components P_h and P_{exc} are initially calculated as power losses and one as a resistance R_{ec}. To measure the electrical performance of a transformer, the sum

Table 3.1 Core loss constants

Constant	Value
k_h	0.11
x	1.84
k_{exc}	0.015

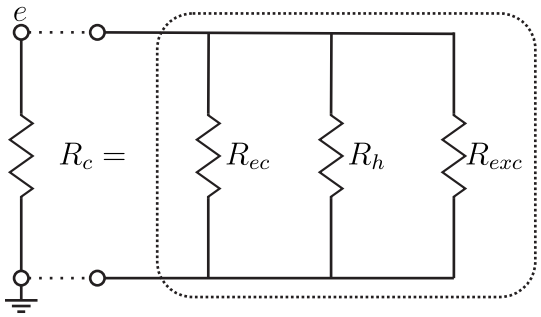

Figure 3.11 Core loss equivalent resistance components

of P_h and P_{exc} is converted into a corresponding resistance with Equation (3.31). The resistance has to be chosen so that it dissipates the calculated power and satisfies the complete circuit when combined in parallel with the eddy current resistance. This is done iteratively by simulating an open circuit test at rated input voltage. Different estimates for e are used to calculate R_c and the circuit is solved for a better approximation of e until a given tolerance is reached.

3.5 MODEL VALIDATION

3.5.1 Prototype geometry

Two partial core resonant transformers were used to verify the mathematical models. They are referred to as PC-Sarah [Velluppillai 2010] which has two windings and PC-Reuben [Meder 2011] which has three. They are both tuned by axial offsetting the core. The windings were wound with the highest voltage winding closest to the core and the lowest voltage winding on the outside. The physical parameters for both transformers are given in Table 3.2 and the arrangement of windings for PC-Reuben is shown in Figure 3.12.

The tertiary coupling winding was wound first on the inner most layer using 5 x 2.5 mm rectangular aluminium conductor. One end of this winding was connected to the HV end of the secondary winding, wound using a 0.33 mm circular conductor. The 5-10-5 grade of Nomex-Mylar-Nomex^{TM} was used as the interlayer insulation on the HV winding. A primary winding was wound on the outside using the same conductor size and the same number of turns as the tertiary.

Table 3.2 Transformer prototype construction details and dimensions

	PC-Sarah	PC-Reuben
Core Length, mm	300	300
Core Radius, mm	37	37
Lamination Thickness, mm	0.5	0.5
Primary winding		
Voltage Rating, V	230	230
Shape	Rectangular	Rectangular
Dimensions, mm	2.5 x 5	2.5 x 5
Axial length, mm	239	239
Turns	141	141
Layers	3	3
Layer insulation thickness, mm	0	0
Material	Aluminium	Aluminium
Secondary winding		
Voltage Rating, V	20	20
Shape	Circular	Circular
Diameter, mm	0.33	0.33
Axial length, mm	240	240
Turns	12640	12640
Layers	20	20
Layer insulation thickness, mm	0.5	0.5
Material	Copper	Copper
Tertiary winding		
Shape	-	Rectangular
Dimensions, mm	-	2.5 x 5
Axial length, mm	-	239
Turns	-	141
Layers	-	3
Layer insulation thickness, mm	-	0
Material	-	Aluminium

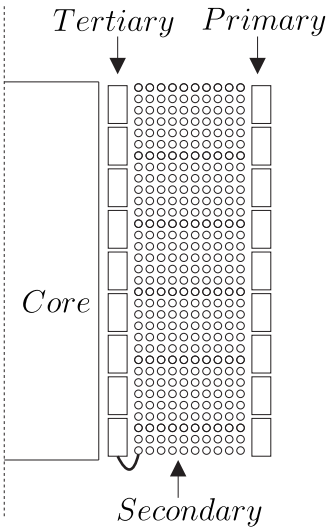

Figure 3.12 Winding arrangement of three winding PCRTX

3.5.2 Parameter measurement

The resonant tuning test was developed to measure the inductive parameters of a two winding PCRTX [Bell and Bodger 2008b]. This test is performed with a variable frequency sine wave generator exciting the primary and a known load capacitance C_l connected across the secondary. Due to the losses in the windings and primary self inductance there are two resonant frequencies defined by unity power factor $\omega_{0,u}$ and maximum impedance $\omega_{0,z}$. Usually there is negligible difference between the two frequencies and a maximum and minimum value of the secondary inductance is given by

$$L_s = \frac{1}{\omega_0^2 C_l} \tag{3.41}$$

where $\omega_0 = 2\pi f_0$ is the measured angular resonant frequency. The difference between the two resonant frequencies is usually negligible but indicates the uncertainty in the measurement of L_s. This uncertainty is given by

$$\pm \mid 1 - \frac{{\omega_{0,u}}^2}{{\omega_{0,z}}^2} \mid 100\% \tag{3.42}$$

The mutual inductance M_{ps} is measured simultaneously at the same resonant frequency [Bell 2009]

$$M_{ps} = \frac{\sqrt{(\Re\{Z_{in}\} - R_p)R_s}}{\omega_0} \tag{3.43}$$

The winding resistances R_p and R_s are measured directly with a micro-ohmmeter. The

self inductances of the primary and tertiary windings L_p and L_t are usually much smaller than the secondary inductance L_s. Therefore, the resonant tuning test was not performed on these windings due to the difficulty in sourcing large enough capacitors and a high voltage variable frequency supply. The self inductances of these windings were measured with an open circuit test

$$L_p = \frac{\sqrt{\left(\frac{V_{oc}}{I_{oc}}\right)^2 - R_p^2}}{\omega_0} \tag{3.44}$$

where V_{oc} is the open circuit voltage with the primary energised and I_{oc} is the open circuit current. The same test can be repeated for L_t. The accuracy of this test depends on the measurement of R_p.

For three winding PCRTXs a simple test for the mutual coupling between tertiary and secondary M_{st} is a short circuit test where the secondary is energised and the primary is short circuited. This test can be conducted when the LV end of the tertiary winding is connected to the HV end of the secondary. In this situation the M in Equation (3.9) is replaced with $-M$ to take into account the series aiding connection. Equation (3.9) can then be re-arranged to isolate the mutual inductance

$$M_{st} = \sqrt{\frac{(|Z_s| - |Z_{in}|)|Z_t|}{\omega^2}} \tag{3.45}$$

where $|Z_j| = \sqrt{R_j^2 + (\omega L_j)^2}$ for the winding j

The mutual inductance between the primary and tertiary winding was measured using the series connection method [Hayes et al. 2003]. When the primary and tertiary windings are connected in series with the windings oriented in an aiding configuration as shown in Figure 3.13a the total inductance measured L_{aid} is

$$L_{aid} = L_p + 2M_{pt} + L_t \tag{3.46}$$

When the same test is repeated with the windings oriented in an opposing configuration as shown in Figure 3.13b the total inductance L_{opp} is

$$L_{opp} = L_p - 2M_{pt} + L_t \tag{3.47}$$

By subtracting the two inductances the mutual inductance between the primary and tertiary winding is given by

$$M_{pt} = \frac{L_{aid} - L_{opp}}{4} \tag{3.48}$$

The inductances L_{aid} and L_{opp} can be measured by finding the resonant frequency

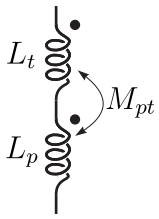

(a) Series aiding connection

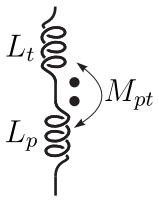

(b) Series opposing connection

Figure 3.13 Connections for measuring M_{pt}

when the windings are connected in series with a variable frequency supply and a large capacitor, using Equation (3.41) where the resonant frequency ω_0 corresponds to the minimum impedance. Alternatively the inductance can be measured with a network analyser or an open circuit test.

Core losses are normally measured with an open circuit test. With PCRTXs this method is ineffective because under open circuit conditions the transformer usually cannot generate the required ampere turns to achieve rated flux densities without overloading most power supplies. It is therefore necessary to measure the core losses under loaded circuit conditions at close to resonance. The real power loss at resonance P_{in} was measured along with the current I_j in each j winding. These losses are assumed to be a combination of the two winding losses $I_p^2 R_p$, $I_s^2 R_s$ and the core losses P_c. By taking the difference between these losses the core loss is estimated as

$$P_c = P_{in} - I_p^2 R_p - I_s^2 R_s \tag{3.49}$$

Using the measured primary current, a value for the induced emf e is estimated by subtracting the voltage drop across the primary resistance and leakage reactance from the supply voltage. The total core loss resistance is then estimated as

$$R_c = \frac{e^2}{P_c} \tag{3.50}$$

This model is an empirical approximation that combines the eddy current losses in the end turns of the windings with the core losses.

3.5.3 Test results

The transformers were tested to obtain the equivalent circuit parameters.

3.5.3.1 Inductive components

The resonant tuning test was used to calculate L_s and M_{ps}. An open circuit test was conducted to find the primary winding self inductance L_p. For the three winding transformer a short circuit test was conducted with the secondary energised and the tertiary shorted to find M_{ts}. The series resonance test was conducted on the primary and tertiary winding to find M_{pt}.

The results for the inductive components presented in Table 3.3 and Figure 3.14, show that the tertiary self inductance on PC-Reuben is higher than the primary. This is because it is wound closer to the core. PC-Sarah has a slightly higher secondary self inductance than PC-Reuben even though the secondary winding wire dimensions and number of turns are identical. This is due to the extra tertiary winding in PC-Reuben increasing the distance between the secondary winding and the core. There is a good agreement between the measured and modelled parameters with a maximum error of 6.1%.

Table 3.3 Three winding PCRTX measured and modelled inductances

	PC-Reuben		PC-Sarah	
Parameter	Measured	Modelled	Measured	Modelled
L_p,mH	5.60	5.67	5.84	5.86
L_s, H	47.0	47.1	47.8	48.0
L_t, mH	6.02	5.95	-	-
M_{ps}, mH	469	498	485	514
M_{pt}, mH	5.21	5.38	-	-
M_{st}, mH	496	517	-	-

A further analysis was conducted to see the effect of core displacement on the inductance values. As shown in Figure 3.14, the FEA model gives an accurate prediction of the secondary winding self inductance. This is the inductance value used when tuning to a capacitive load. Again both transformers show similar characteristics with PC-Sarah having a slightly higher self inductance across the tuning range. This shows that the addition of an interior tertiary winding did not cause a significant difference to the self inductance.

3.5.3.2 Resistive components

Comparisons between modelled and measured winding resistances, shown in Table 3.4, indicate that the model is adequate for design purposes. The primary and tertiary

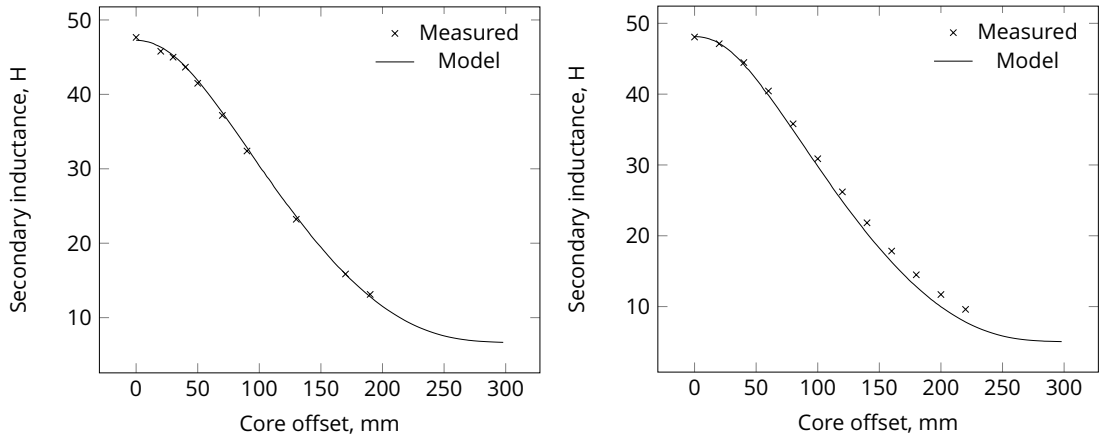

(a) PC-Reuben (b) PC-Sarah

Figure 3.14 Inductance variation diagram

windings have the same cross sectional area but because the primary is wound on the outside it is longer and hence has a larger resistance.

Table 3.4 Three winding PCRTX measured and modelled resistances

	PC-Reuben		PC-Sarah	
Parameter	Measured	Modelled	Measured	Modelled
R_p, mΩ	171	158	156	144
R_s, Ω	941	958	741	786
R_t, mΩ	75.1	91.7	-	-
R_c, Ω	95	84	87	87

All measurements and simulations were conducted assuming room temperature conditions. The models achieve good agreement with the measurements. The input power loss of a loaded circuit under resonant conditions was modelled and experimentally tested for each transformer. The results are presented in Figure 3.15 and 3.16.

Most of the input losses can be attributed to the resistive losses in the secondary winding. The core losses make up approximately 15% of the total input power losses and the primary winding losses are negligible. This is because the secondary winding cross sectional area is 146 times smaller than the primary windings and hence has a much larger current density as shown in Figure 3.17. The transformers studied are designed for withstand testing and are rated for very short duty cycles. A transformer with a larger secondary winding cross sectional area will have a lower operating current density and make a smaller contribution to the total losses.

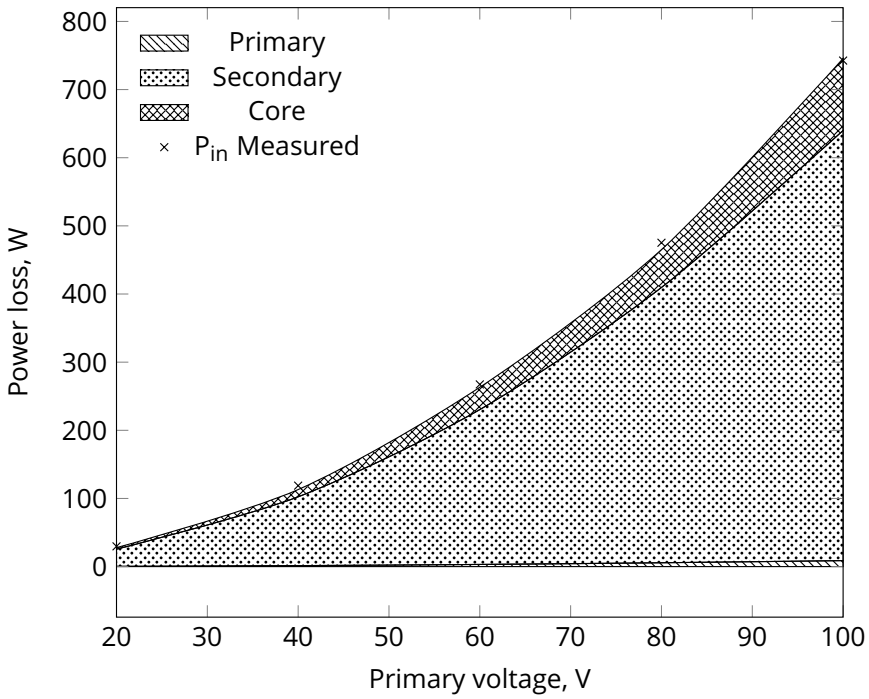

Figure 3.15 Power losses for PC-Reuben under resonant operation

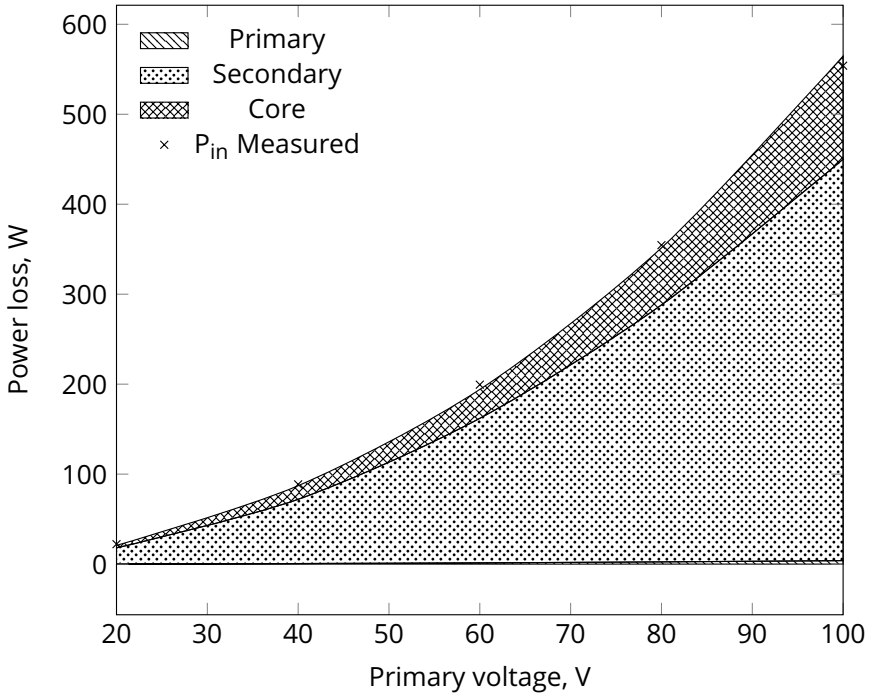

Figure 3.16 Power losses for PC-Sarah under resonant operation

3.5.3.3 Tuned circuit response

The frequency response of PC-Sarah was measured using a variable frequency source. The input impedance was determined from voltage and current measurements at the

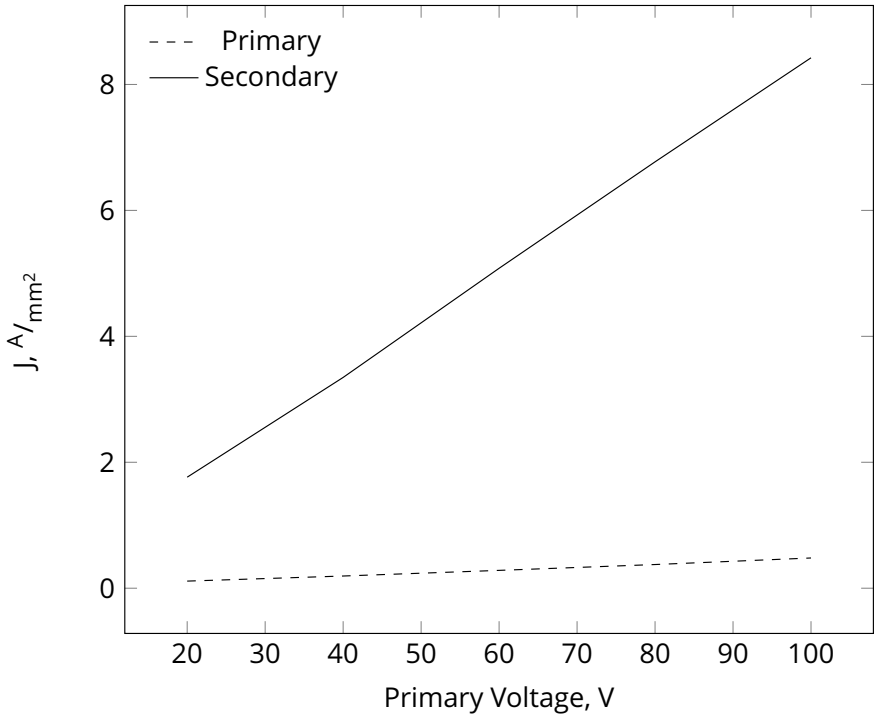

Figure 3.17 Current densities of primary and secondary winding under loaded circuit operation for PC-Reuben

primary winding. The test was conducted at very low voltages in the order of 10 V on the primary side to remain within the current rating of the source. The model is a good predictor of input impedance for small variations around the designed frequency as shown in Figures 3.18 and 3.19.

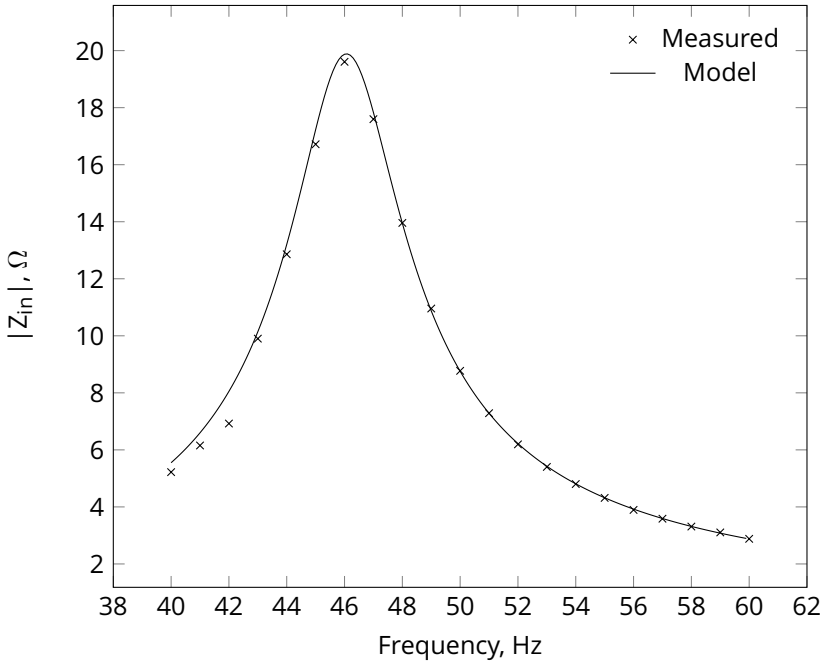

Figure 3.18 Input impedance magnitude frequency response for PC-Sarah. Core offset = 0, C_l = 250 nF

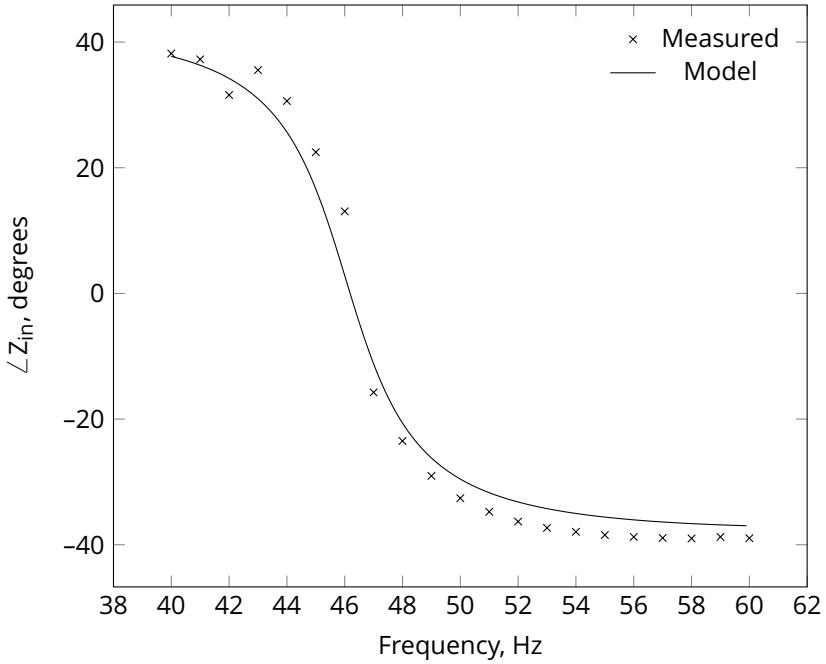

Figure 3.19 Input impedance phase angle frequency response for PC-Sarah. Core offset = 0, $C_l = 250\ nF$

3.6 CONCLUSION

A model for predicting the behaviour of two and three winding partial core resonant transformers has been presented and experimentally verified. Analytical expressions

for the input impedance were derived by treating the PCRTX as mutually coupled inductors. The voltage ratio calculations were performed using a T-equivalent circuit with ideal transformers. The inductance matrix and inductance variation with core displacement was derived using a FEA model of the core and windings. The input power losses were modelled and found to consist mostly of the secondary winding loss. Measurements conducted on a prototype PCRTX generally showed good agreement with the modelled equivalent circuit parameters.

Chapter 4

CASCADED PARTIAL CORE RESONANT TRANSFORMER MODEL

4.1 INTRODUCTION

In this chapter an equivalent circuit model of PCRTXs connected in cascade is developed and verified with experimental results. Existing cascade transformer models are reviewed along with methods to calculate voltage and current distributions between stages. The phase shifts between stages and voltage imbalance is explained using phasor analysis along with the input impedance and resonant characteristics of the entire arrangement. Different tuning methods are investigated and it was found that simultaneously tuning each stage was the simplest way of achieving a high input impedance along with a balanced voltage distribution. Approximations of the resonant load capacitance are compared against an iteratively calculated model. The factors limiting the addition of more stages to achieve higher voltages are discussed and modelled.

4.2 BACKGROUND

The earliest known cascaded transformer circuit model is the simplified series equivalent circuit shown in Figure 4.1 [Goodlet 1937]. This model ignored the magnetising reactance of each stage and the load impedance to produce an expression for the short circuit impedance.

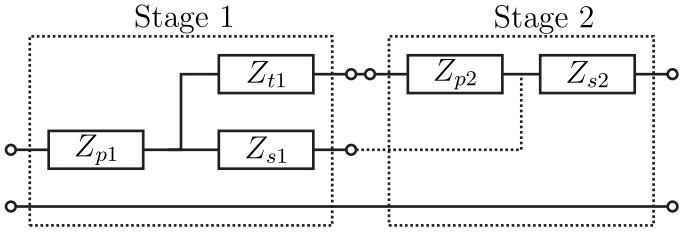

Figure 4.1 Series equivalent cascade transformer model

When stating his assumptions Goodlet mentions that the above model may be seriously

in error if the magnetising current is appreciable. Therefore this simplification is inadequate for modelling partial core transformers which are known to have non-negligible magnetising currents [Liew 2001]. A circuit analysis including the effects of magnetising currents was conducted by Jayaram [1958]. The model consisted of multiple three winding transformer equivalent circuits connected in series as shown in Figure 4.2. The voltage and current relationships between stages are preserved using a unity turns ratio transformer.

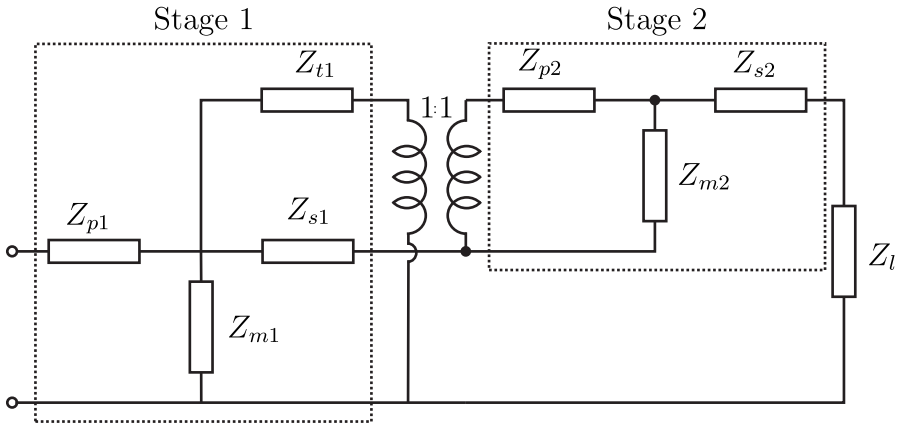

Figure 4.2 Extended Stienmetz model for cascaded transformers

The same authors also presented an experimental validation of the above models using a three stage set of cascaded high voltage testing transformers rated at 350 kV [Jayaram and Badkas 1960]. A significant challenge at the time was measuring the high AC voltages produced by these test kits without resorting to expensive capacitive voltage dividers. It was found that the output voltage ratio was a linear function of the measured input admittance [Jayaram and Badkas 1962]. This admittance method allows the final output voltage of a cascaded set to be determined by measuring the input admittance and voltage ratio of a cascaded set at two different loads. Voltage ratios for other loads can now be determined using a straight line extrapolation of the voltage ratio as a function of measured input admittance.

The admittance method was expanded to include the effects of compensating reactors which are used to reduce the reactive power drawn from the supply [Train and Vohl 1976]. Additionally it was found that the voltage distribution across cascade connected transformers is usually non uniform with the final stage developing the highest voltage. Therefore a major limitation on these test kits was the voltage across the final stage transformer exceeding its rated value. These effects were verified using a set of six cascaded HV testing transformers with each rated at 550 kV.

Further studies have been conducted on the frequency response of cascaded HV test transformers and the corresponding resonant frequencies that amplify higher order harmonics [Olivier et al. 1980]. All research conducted to date has focused on large HV

testing transformers rated 100 kV or above. These transformers have a large number of secondary turns and a considerable equivalent winding capacitance. This causes the transformer to present a leading power factor under open circuit conditions [Jayaram and Badkas 1960] and necessitates the inclusion of tank and winding capacitances in the model. As tank and winding capacitance are negligible for most practical partial core transformer designs they can be ignored.

4.3 EQUIVALENT CIRCUITS

The purpose of the equivalent circuit is to predict the electrical performance of a cascaded set of partial core resonant transformers. Two different equivalent circuit models for cascaded transformers are presented below. Both consist of multiple three winding transformer equivalent circuits connected together. The first model is commonly used and consists of two 'Steinmetz' transformer equivalent circuits connected together using a transformer with a unity turns ratio. The second is a new model where each stage transformer is represented as a set of mutually coupled coils with losses.

4.3.1 Existing cascade model

The circuit model for a two stage cascaded transformer unit is constructed from a distributed set of shunt and series admittances as shown in Figure 4.3.

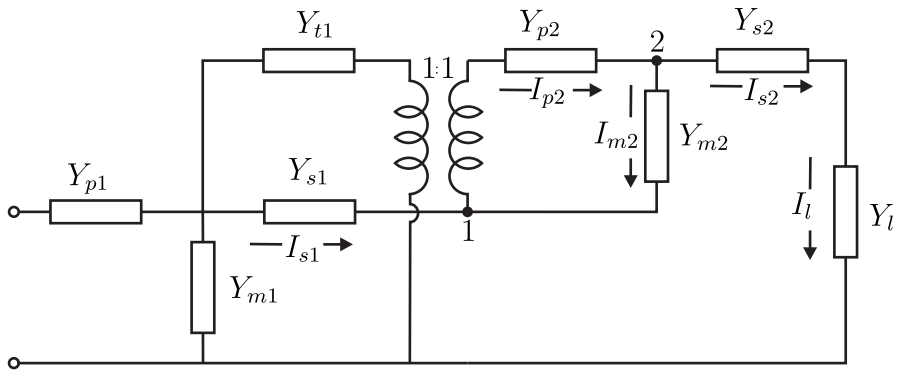

Figure 4.3 Equivalent circuit for a two stage cascade transformer

If i represents the stage number of the transformer when connected in cascade, the shunt admittances Y_{mi} correspond to the parallel combination of the transformer magnetising reactance and core loss resistance as expressed in Equation (4.1). The series admittances Y_{pi}, Y_{si} and Y_{ti} correspond to the series combination of the primary, secondary and tertiary winding resistances and leakage reactances as expressed in Equations (4.2) to (4.4). These values are referred to their own stage's primary winding which is denoted as the i'th stage. An ideal transformer with a unity turns ratio preserves the voltage

and current relationships between the stages. The load admittance Y_l is connected between the high voltage terminal of the final stage transformer and ground.

$$Y_{mi} = \frac{R_{ci} + (j\omega L_{mi})}{R_{ci}(j\omega L_{mi})} \tag{4.1}$$

$$Y_{pi} = \frac{1}{R_{pi} + (j\omega L_{pi})} \tag{4.2}$$

$$Y_{si} = \frac{1}{R_{si} + (j\omega L_{si})} \tag{4.3}$$

$$Y_{ti} = \frac{1}{R_{ti} + (j\omega L_{ti})} \tag{4.4}$$

To simplify the circuit analysis, the unity turns ratio transformer has to be replaced. This circuit reduction is outlined in Olivier et al. [1984] and can be accomplished by recognising that the load current flows through all secondary windings. Kirchhoff's current law is applied to the nodes numbered one and two in Figure 4.3 by

$$I_{s1} = I_{p2} - I_{m2} = I_{s2} = I_l \tag{4.5}$$

Conceptually this illustrates that the secondary windings of all stage transformers are connected in series and carry the load current. Each secondary winding can now be connected to a current source representing the load current as shown in Figure 4.4.

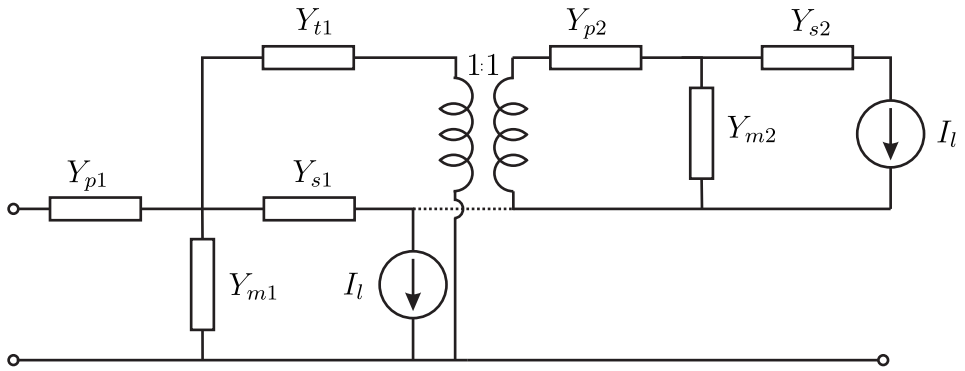

Figure 4.4 Current sources inserted carrying load current

With the current flowing through the secondary winding represented by the current sources there is no need for the isolating transformer as shown in Figure 4.5. The load voltage is now the sum of the voltages across each current source.

$$V_l = V_{s1} + V_{s2} \tag{4.6}$$

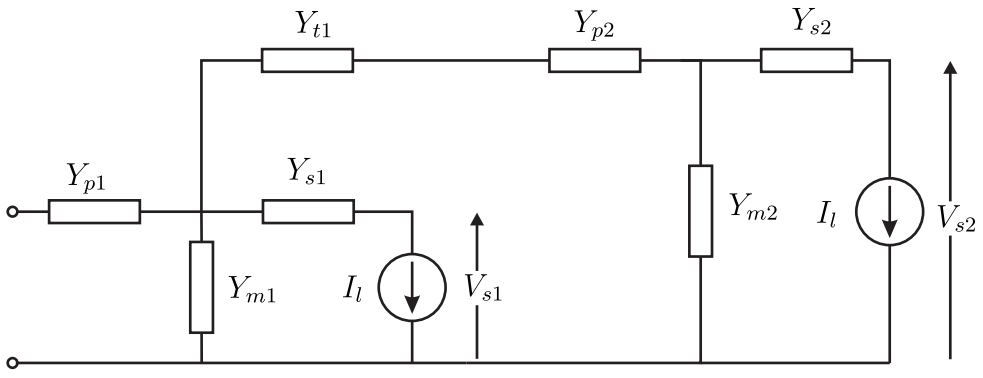

Figure 4.5 Equivalent circuit without unity turns ratio transformer

The load current is given by

$$I_l = V_l Y_l \tag{4.7}$$

This circuit has been used extensively to model existing cascaded high voltage testing transformers where each stage is built almost identically. Thus when the load admittance is referred to the primary winding the scaling factor is the square of the primary secondary turns ratio common to each stage. Referring a given load admittance to the primary is not as simple when non-identical transformers are used, with different turns ratios. This difficulty is not addressed by any of the present models.

4.3.2 Coupled inductor model

A new circuit model has been developed where each stage except the final stage is modelled as a three winding coupled inductor, as shown in Figure 4.6.

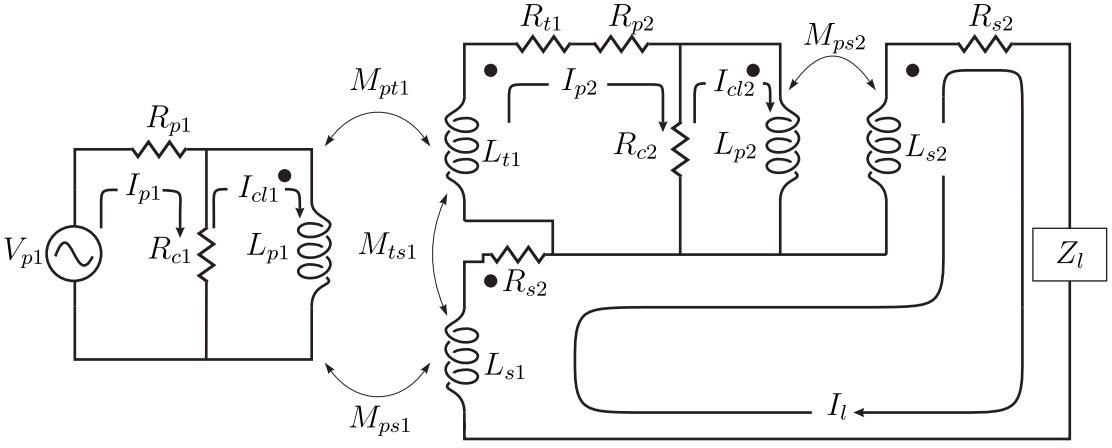

Figure 4.6 Coupled inductor model of cascaded partial core resonant transformers

The inductive circuit parameters are directly calculated from the FEA model as described

in Chapter 3. Unlike the existing model there is no extra conversion involved. This also means there are no negative inductances which are often needed to represent three winding transformers using the existing model. There are no unity turns ratio transformers between stages so the tertiary winding of one stage can be directly connected to the tertiary winding of the next stage. Ideal transformers on the secondary windings of each stage are unnecessary so the load does not need to be referred to any winding. The magnitude of the load is represented as it would be in the real world and is insensitive to changes in the individual stage turns ratios.

4.4 MATRIX FOMULATION

Both equivalent circuits can be solved using circuit simulation software but this is time consuming when trying to find an optimised design. When multiple combinations of circuit parameters need to be simulated, an analytical solution is faster. The simplest method that is scalable to multiple cascaded transformer stages is a matrix formulation of the voltage and current relationships.

4.4.1 Existing cascade model

The existing cascaded circuit model can be solved by nodal analysis using the linear system of equations expressed as

$$\boldsymbol{I} = \boldsymbol{Y}\boldsymbol{V} \tag{4.8}$$

where $\boldsymbol{I}$ and $\boldsymbol{V}$ are voltage and current vectors with a length of $3n$ and $\boldsymbol{Y}$ is the $3n \times 3n$ nodal admittance matrix of the circuit.

The equivalent circuit is easily scalable to n stages. The matrix formulation for the three stage cascade example shown in Figure 4.7 is given by Equation (4.9). To simplify the calculation of input impedance, the nodes are systematically ordered from the final stage secondary winding, to the input node.

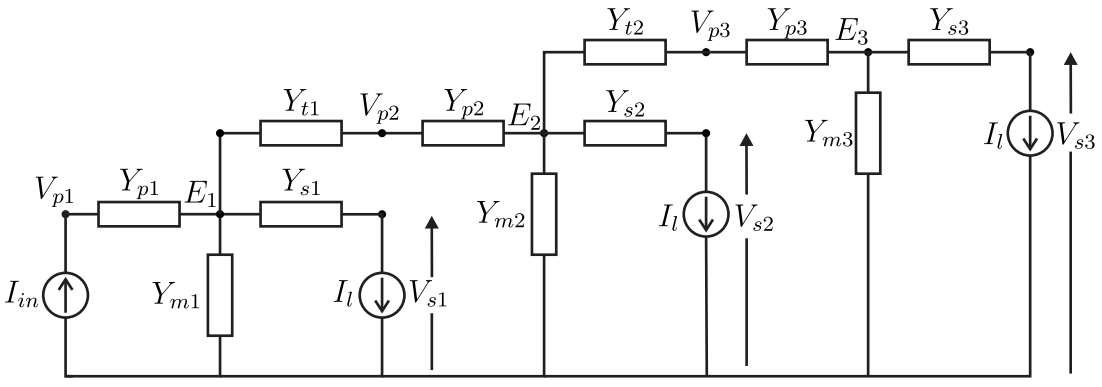

Figure 4.7 Three stage equivalent circuit with node labels

The sum of the self admittances at each node is written along the main diagonal, with the mutual admittances between nodes occupying the off-diagonal entries. The current source carrying the load current is represented by a mutual load impedance Y_l shared across each secondary winding node. This ensures the secondary windings carry the same current regardless of the voltage distribution across their terminals. Equation (4.8) can be rewritten as

$$\left[\begin{array}{ccc|ccc|ccc} A_3 & Y_l & Y_l & -Y_{s3} & 0 & 0 & 0 & 0 & 0 \\ Y_l & A_2 & Y_l & 0 & -Y_{s2} & 0 & 0 & 0 & 0 \\ Y_l & Y_l & A_1 & 0 & 0 & -Y_{s1} & 0 & 0 & 0 \\ \hline -Y_{s3} & 0 & 0 & B_3 & 0 & 0 & -Y_{p3} & 0 & 0 \\ 0 & -Y_{s2} & 0 & 0 & B_2 & 0 & -Y_{t2} & -Y_{p2} & 0 \\ 0 & 0 & -Y_{s1} & 0 & 0 & B_1 & 0 & -Y_{t1} & -Y_{p1} \\ \hline 0 & 0 & 0 & -Y_{p3} & -Y_{t2} & 0 & C_3 & 0 & 0 \\ 0 & 0 & 0 & 0 & -Y_{p2} & -Y_{t1} & 0 & C_2 & 0 \\ 0 & 0 & 0 & 0 & 0 & -Y_{p1} & 0 & 0 & C_1 \end{array}\right] \begin{bmatrix} V_{s3} \\ V_{s2} \\ V_{s1} \\ E_3 \\ E_2 \\ E_1 \\ V_{p3} \\ V_{p2} \\ V_{p1} \end{bmatrix} = \begin{bmatrix} 0 \\ 0 \\ 0 \\ 0 \\ 0 \\ 0 \\ 0 \\ 0 \\ I_{in} \end{bmatrix} \tag{4.9}$$

where

$$\begin{aligned} A_i &= Y_{si} + Y_l \\ B_i &= Y_{pi} + Y_{si} + Y_{ti} + Y_{mi} \\ C_i &= Y_{pi} + Y_{t(i-1)} \end{aligned}$$

and i denotes the number of the stage. With reference to C_1 the tertiary winding admittance of the previous stage $Y_{t(i-1)}$ is non-existent and hence excluded from this term. Similarly B_n will not include a Y_{tn} term because the n'th stage does not need a tertiary winding.

In general, for an n stage cascaded transformer, the load voltage is the sum of the voltage across each current source

$$V_l = V_{s1} + V_{s2} + ... + V_{sn} \tag{4.10}$$

All these voltages are referred to the primary side of their stage transformer. To get

the real secondary voltage, the values are divided by the transformer turns ratio.

$$V'_{si} = \frac{V_{si}}{a_i} \tag{4.11}$$

where a_i is the primary-secondary turns ratio for the i_{th} stage

4.4.2 Coupled inductor model

The coupled inductor model for cascade connected transformers can be solved via a mesh analysis. The circuit for a three stage cascade including core losses is shown in Figure 4.8.

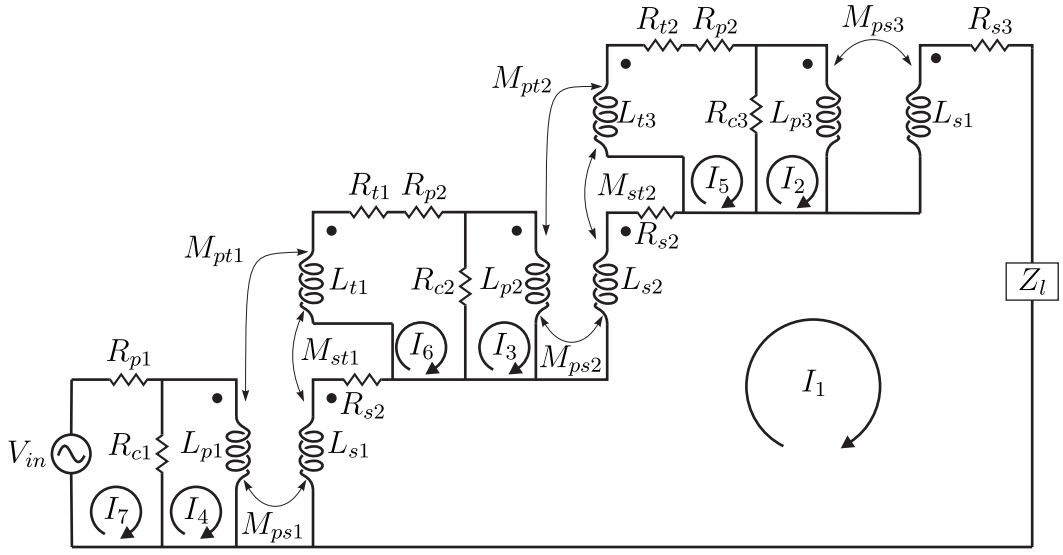

Figure 4.8 Three stage equivalent circuit with node labels

The mesh current loops I_j are numbered backwards from the load mesh I_1 to the input mesh I_7. For an n stage cascade there will be $2n + 1$ meshes which is one smaller than the $3n$ nodes required to solve the existing model. The linear system of equations that describes this circuit is given by

$$\boldsymbol{V} = \boldsymbol{Z}\boldsymbol{I} \tag{4.12}$$

where $\boldsymbol{V}$ is a vector of external voltage sources, $\boldsymbol{Z}$ is the mesh impedance matrix and $\boldsymbol{I}$ is a vector of current sources.

For a three stage cascade Equation (4.12) can now be expressed as

$$\begin{bmatrix} 0 \\ 0 \\ 0 \\ 0 \\ 0 \\ 0 \\ V_{in} \end{bmatrix} = \begin{bmatrix} Z_{sl} & -X_{ps3} & -X_{ps2} & -X_{ps1} & X_{st2} & X_{st1} & 0 \\ -X_{ps3} & Z_{cl3} & 0 & 0 & -R_{c3} & 0 & 0 \\ -X_{ps2} & 0 & Z_{cl2} & 0 & -X_{pt2} & -R_{c2} & 0 \\ -X_{ps1} & 0 & 0 & Z_{cl1} & 0 & -X_{pt1} & -R_{c1} \\ X_{st2} & -R_{c3} & -X_{pt2} & 0 & Z_{pc3} & 0 & 0 \\ X_{st1} & 0 & -R_{c2} & -X_{pt1} & 0 & Z_{pc2} & 0 \\ 0 & 0 & 0 & -R_{c1} & 0 & 0 & Z_{pc1} \end{bmatrix} \begin{bmatrix} I_1 \\ I_2 \\ I_3 \\ I_4 \\ I_5 \\ I_6 \\ I_7 \end{bmatrix} \tag{4.13}$$

where i is the number of the stage and n is the total number of stages

$$\begin{aligned} Z_{sl} &= Z_L + j\omega L_{s1} + R_{s1} + ... + j\omega L_{sn} + R_{sn} \\ X_{psi} &= j\omega M_{psi} \\ X_{pti} &= j\omega M_{pti} \\ X_{sti} &= j\omega M_{sti} \\ Z_{cli} &= j\omega L_{pi} + R_{ci} \\ Z_{pci} &= R_{ci} + R_{pi} + R_{p(i-1)} + j\omega L_{t(i-1)} \end{aligned}$$

The coupling reactance between the secondary and the tertiary X_{st} is positive in Equation (4.13) because the secondary and tertiary inductors are connected in a series mutually aiding configuration. This means they are wound in the same direction.

4.5 INPUT IMPEDANCE

Calculating the input impedance at resonance is important for determining if the design will reduce the input current required during testing below the supply's rating.

4.5.1 Calculations

The calculation of Z_{in} can be performed by reducing the mesh impedance matrix $\boldsymbol{Z}$ to upper triangular form using Gaussian elimination. The resulting matrix has the form,

$$\boldsymbol{Z} = \begin{pmatrix} z_{1,1} & z_{1,2} & \cdots & z_{1,n} \\ 0 & z_{2,2} & \cdots & z_{2,n} \\ \vdots & \vdots & \ddots & \vdots \\ 0 & 0 & \cdots & z_{n,n} \end{pmatrix} \tag{4.14}$$

The only entry on the bottom row, $z_{n,n}$ is now independent and represents the ratio between the voltage and current at the input node. Thus,

$$Z_{in} = z_{n,n} \tag{4.15}$$

Most computational mathematics tools such as Matlab® have an in-built function to perform this transformation, but their algorithm usually involves pivoting. This is a step in the matrix decomposition where rows and columns are swapped for computational efficiency. This results in an incorrect upper triangular matrix where the entries do not correspond to nodes in the equivalent circuit. A custom function was created that performs the necessary row operations without pivoting rows. A pseudocode representation of this algorithm is

Algorithm 4.1 Gaussian elimination algorithm without row swapping

```
function upperTriangular(Z)
    for i ← 0 to N do
        pivot ← Z[i][i]
        for j ← i+1 to N do
            Z[k][i] ← Z[k][i]/pivot
            Z[k, i + 1 : N] ← Z[k, i + 1 : N] − Z[k][i] ∗ Z[i, i + 1 : N]
        end for
    end for
    return Z
end function
```

The same calculation can be performed for the existing model by reducing the nodal admittance matrix to upper triangular form. The resulting matrix $\boldsymbol{Y}$ has the form

$$\boldsymbol{Y} = \begin{pmatrix} y_{1,1} & y_{1,2} & \cdots & y_{1,n} \\ 0 & y_{2,2} & \cdots & y_{2,n} \\ \vdots & \vdots & \ddots & \vdots \\ 0 & 0 & \cdots & y_{n,n} \end{pmatrix} \tag{4.16}$$

The only entry on the bottom row, $y_{n,n}$ is now independent and represents the ratio between the voltage and current at the input node. Thus the input impedance is

$$Z_{in} = \frac{1}{y_{n,n}} \tag{4.17}$$

4.5.2 Optimal tuning method

An important problem in designing cascaded PCRTXs that needs solving is that of selecting a tuning method to achieve resonance with a capacitive load. Each stage has

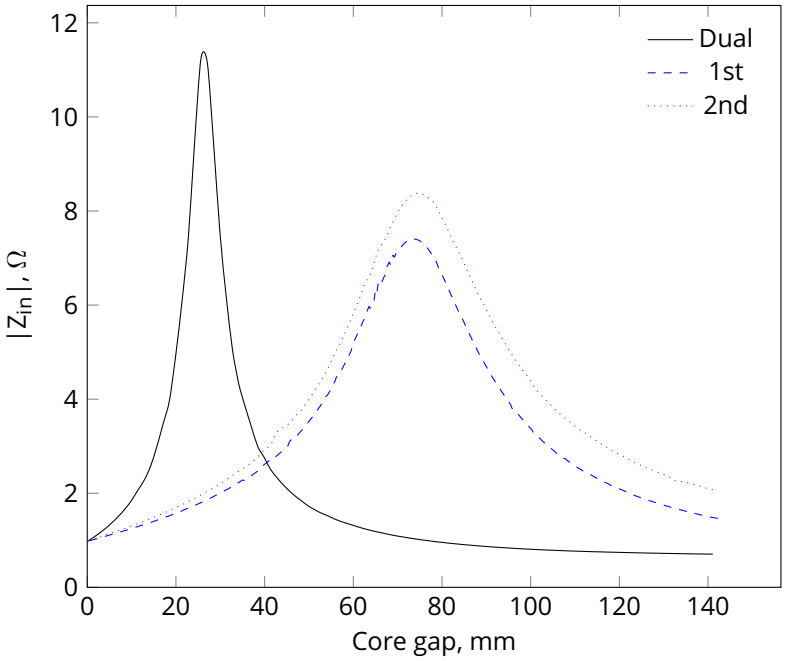

Figure 4.9 Input impedance variation with core gap for different tuning methods

its own core gap setting which covers a range of positions r. The number of possible core gap settings is therefore r^n where n is the number of stages. To deal with this apparent increase in tuning complexity, two simple tuning methods are considered first. One method involves tuning only one of the stages, be refereed to as separate tuning. The other method involves tuning both stages simultaneously, referred to as simultaneous tuning. These two methods are the easiest and most practical options for use in the field but to verify if they are optimal, a two dimensional simulation of the full range of possible core gap combinations is presented.

The tuning methods were simulated on a sample two stage PCRTX cascade with identical 33 kV stages energising a capacitive load and fed from a 400 V supply. The load was selected to give a leading input power factor when there is no core gap. The gap was then increased in small increments with the circuit parameters calculated by FEA at each step. This was intended to bring the cascade into resonance, then towards a lagging power factor. The calculated input impedance for each tuning method for the range of gap settings is presented in Figure 4.9, with the tabulated results presented in Table 4.1. The core gap necessary for resonance under separate tuning is approximately three times higher than simultaneous tuning. The highest maximum input impedance in this example is achieved by simultaneous tuning, followed by separate tuning of the second stage with the lowest impedance achieved by separate tuning of the first stage.

The magnitude of the input impedance resonant peak is inversely related to the power losses in the system. With larger core gaps the coupling between windings is reduced and a larger magnetising current is drawn from the supply, which in turn increases the

Table 4.1 Gap settings for maximum impedance for a sample two stage cascaded PCRTX

Parameter	Optimal	Simultaneous	Separate 1st Stage	Separate 2nd Stage
l_{cg1}, mm	27.6	25.6	73.5	0
l_{cg2}, mm	31.6	25.6	0	75.5
$\|Z_{in}\|$, Ω	11.4	11.1	7.40	8.37

losses in the primary winding [Bagheri et al. 2012]. This is why the magnitude of the resonant peak for separate tuning is much smaller than simultaneous tuning. Under separate tuning, the stage being tuned has to have a larger core air gap to achieve the same total resonant inductance as simultaneously tuned stages. The higher magnetising current and power losses associated with a large air gap in a single stage reduces the input impedance to a greater extent than having smaller, equal gaps in simultaneously tuned transformers. Separate tuning of the first stage has the lowest maximum resonant impedance due to the extra losses in its third winding.

It can also be seen in Table 4.1 and Figure 4.9 that under separate tuning the resonant air gap for the separately tuned second stage is slightly higher than the separately tuned first stage. This indicates that to achieve the correct inductance for resonance the second stage needs a larger air gap than the first stage. This is because the first stage tertiary winding is loaded and connected in a series aiding configuration to the secondary. Conversely the second stage tertiary winding operates on open circuit. The first stage gets help from the mmf generated by the tertiary winding so it does not need as large an air gap as the second stage to achieve the same net inductance.

To investigate if there is a maximum point for Z_{in} between the two methods another simulation was conducted over a range of possible center gap settings for both stages. The results are shown in Figure 4.10. At the point of maximum impedance the second stage core gap is approximately 4 mm higher than the first. Whilst for all practical purposes this point is the same as simultaneous tuning, the small difference illustrates the same difference in losses and inductance between the windings as explained above.

The input power factor variation for the same variation in core gaps is shown in Figure 4.11. Instead of a single point as in the case of impedance, there are a range of core gap combinations that give a unity power factor shown by the dark curved region. For single PCRTXs the unity power factor and maximum impedance resonant points are very similar [Bell 2009] but in a cascade arrangement a unity power factor does not necessarily indicate the maximum impedance point has been reached.

4.5.3 Model validation

A prototype two stage cascade test kit was tested for proof of concept and to validate the model parameters. The transformers tested in Chapter 3 were used with PC-Reuben

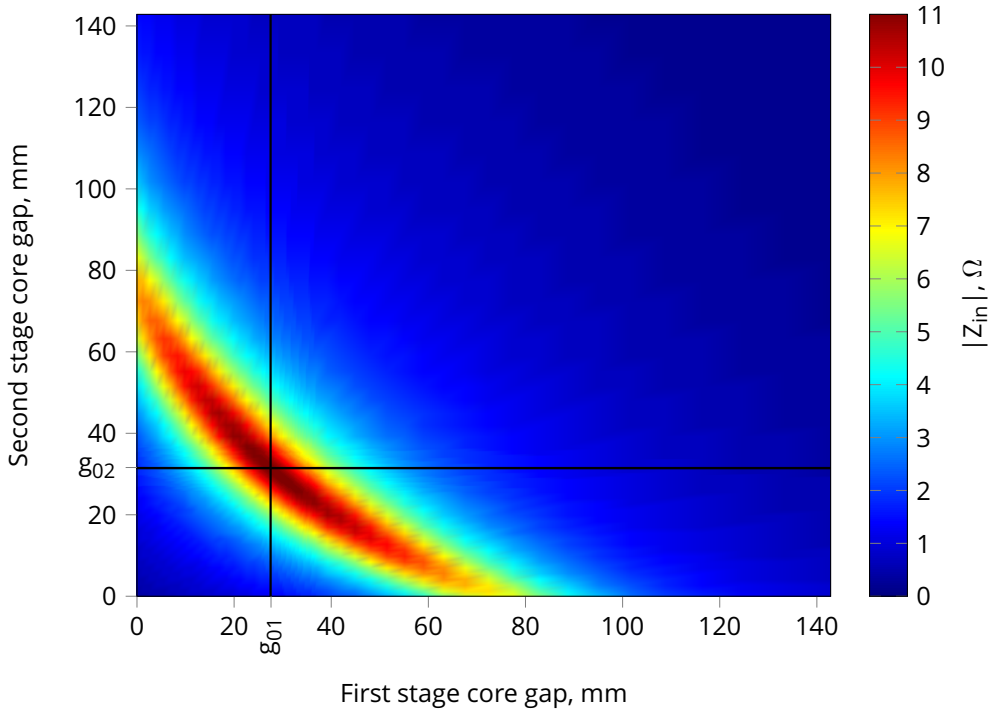

Figure 4.10 Input impedance variation with full range of core gap settings for a two stage PCRTX cascade

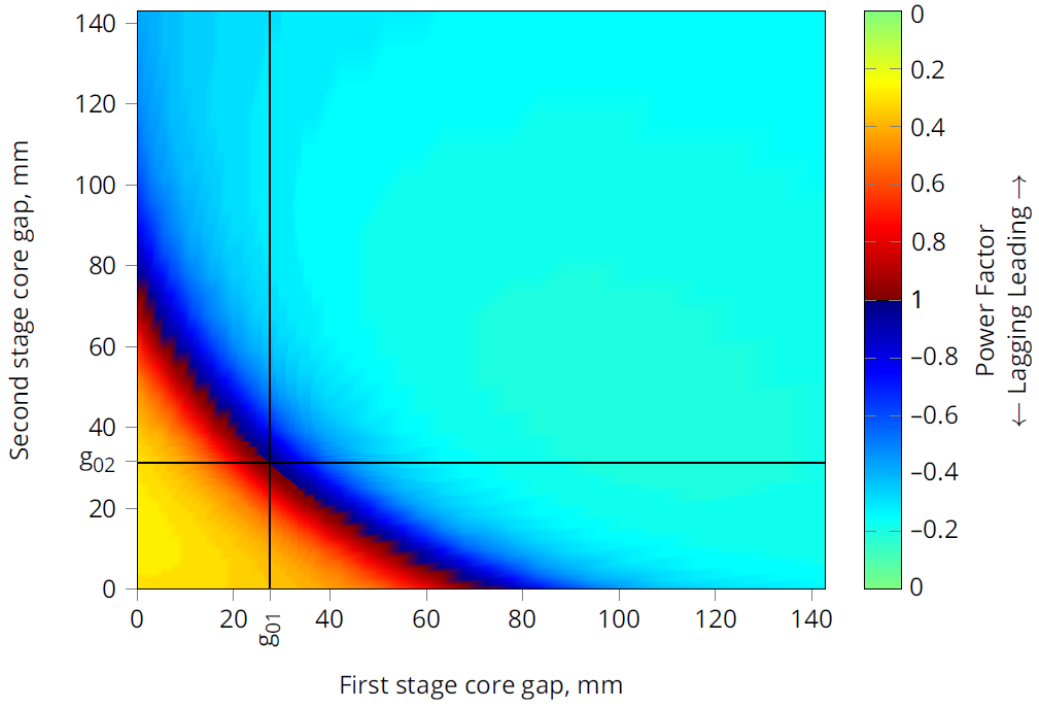

Figure 4.11 Input power factor variation with full range of core gap settings for a two stage PCRTX cascade

serving as the first stage and PC-Sarah as the second stage. A photo of the test set up is shown in Figure 4.12.

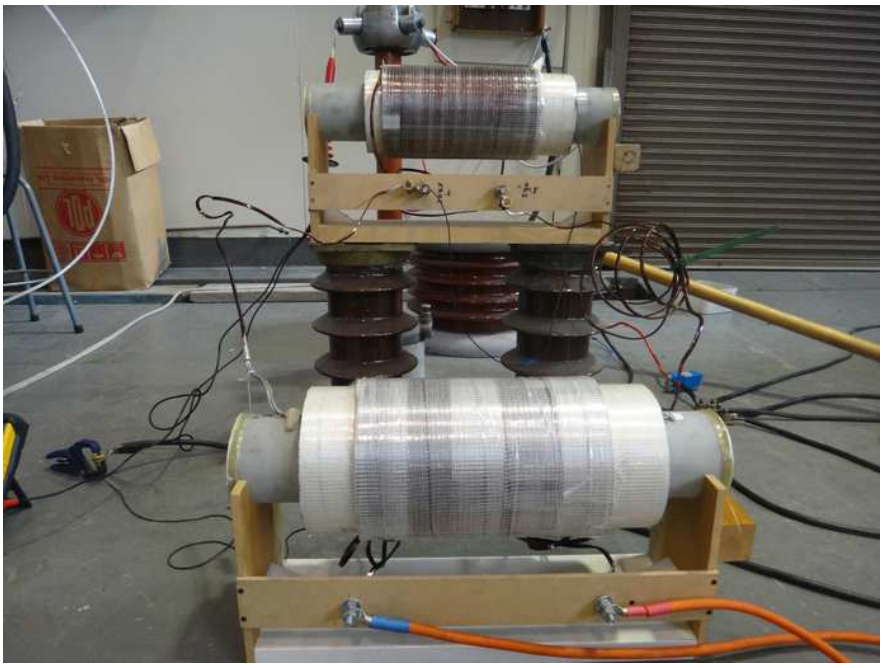

Figure 4.12 Test setup for cascade connection of PC-Reuben(bottom) and PC-Sarah(top)

The test kit was energised with a load of 100 nF to its rated voltage of 40 kV for one minute to confirm its electrical performance. Significant core vibration was noticed and the wooden supports holding the axially offset cores in place had to be reinforced after failing during early attempts. The core vibration was due to the design value of core peak flux density of 1.6 T. It has been recommended that future designs should a lower design value peak flux density of 1.2 T [Bell 2009]. The centering force on the offset core was due to imbalanced axial magnetic forces which is a known disadvantage of axial offset tuning.

The tuned circuit frequency response was measured at low voltages using a Chroma variable frequency power supply. The input impedance, voltage and current on each stage was measured using high voltage probes and current clamps. Initially the core losses were excluded from the circuit model. The results of this simulation and the measured results are shown in Figure 4.13. The model overestimates the measured peak input impedance magnitude at resonance by approximately 50 % whilst the phase angle calculation shows good agreement with the measured values.

A simulation with core losses included is shown in Figure 4.14. The model shows good agreement with the measured values. The circuit had a resonant frequency of 52 Hz which corresponded to a resonant inductance of 93.7 H. This value is approximately the sum of both transformer secondary self inductances. The effect of including core losses was more pronounced when simulating cascaded PCRTXs compared to single PCRTXs.

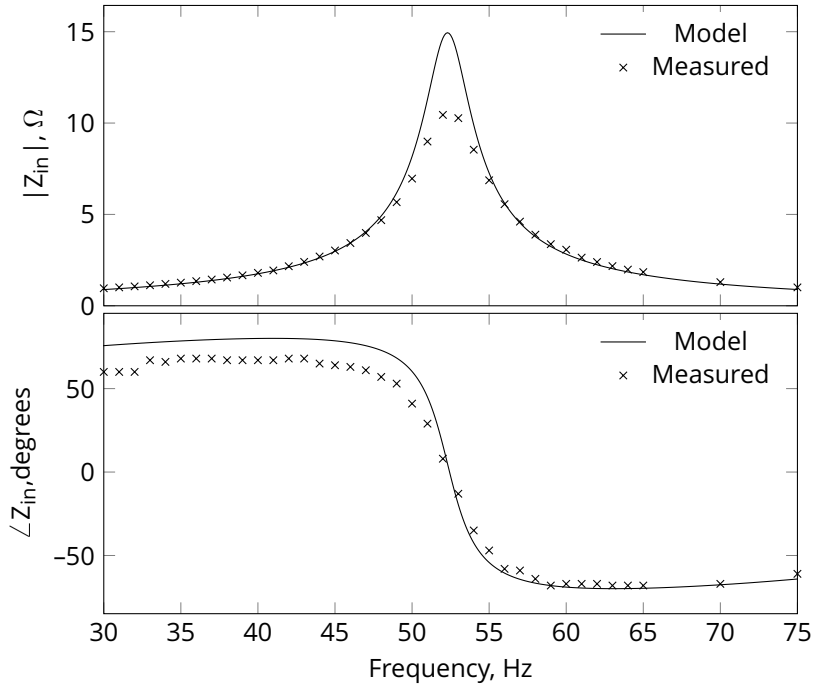

Figure 4.13 Input impedance frequency response, excluding core losses

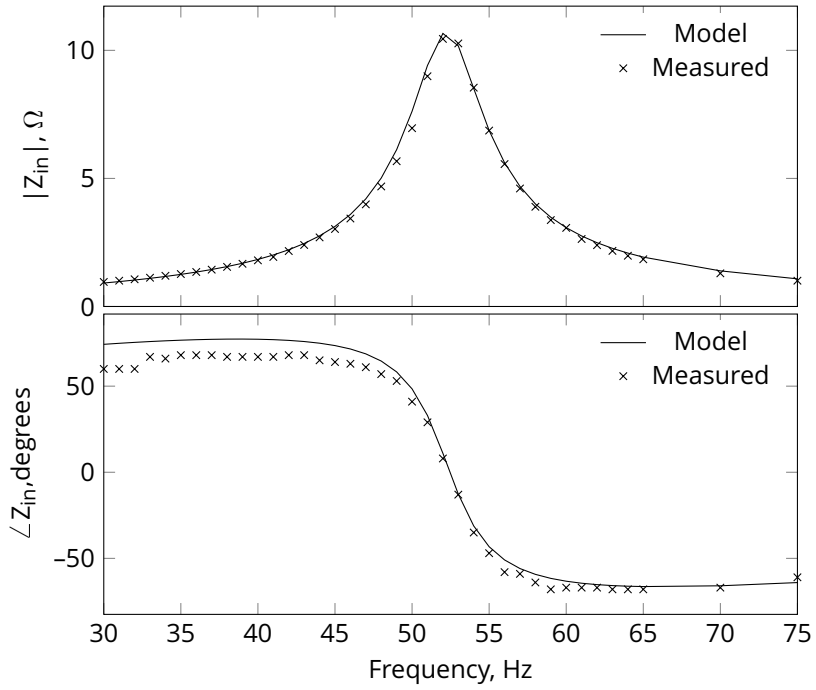

Figure 4.14 Input impedance frequency response, including core losses

4.6 CURRENT AND VOLTAGE DISTRIBUTION

The nature of the cascade circuit means the primary winding of each lower stage has to provide the cumulative exciting current of the higher stages above it. This means the

primary windings of lower stages carry more current then each subsequent stage. The primary windings on lower stages have to be dimensioned appropriately to carry this extra current [Kuffel et al. 2000].

It has also been observed that cascaded high voltage testing transformers do not share the load voltage equally amongst the secondary windings of each stage [Anis et al. 1975]. The final stage was found to develop the highest voltage across it [Train and Vohl 1976]. No explanation has been given for this uneven voltage distribution but manufacturers and designers of commercial cascaded transformers state the voltage distribution can be reduced with external compensating reactors [Booker et al. 1983, Haefely Hipotronics 2015]. For a cascade connection of tunable transformers that do not utilise external compensating reactors the effect of tuning on the voltage distribution is not known.

The voltage distribution across the secondary winding of each stage in a cascaded transformer circuit is closely related to the current distribution between each stage primary winding. Because earlier stages are loaded more heavily than later stages there is a larger voltage drop across the leakage reactances and winding resistances leading to a lower secondary voltage. Conversely, higher stages are lightly loaded with a smaller voltage drop across the leakage reactances and winding resistances.

4.6.1 Phasor analysis

A phasor diagram can illustrate the voltage distribution in a cascaded set and its relation to current distribution. Consider the equivalent circuit of a two winding single stage PCRTX shown in Figure 4.15.

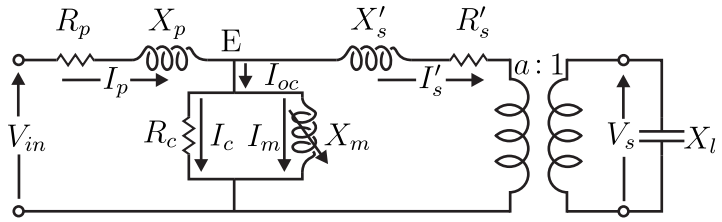

Figure 4.15 Equivalent circuit for a single partial core resonant transformer

The current drawn by the PCRTX under open circuit conditions is labelled I_{oc}. This value consists of the magnetising current I_m and the current drawn by the core loss resistance I_c. Under open circuit conditions there is a small but significant voltage drop across the primary winding resistance R_p and the leakage reactance X_p. This means the induced emf in the primary winding E is lower than the applied terminal voltage V_{in}. Since there is no current drawn from the secondary the terminal voltage V_s is the same as E which is illustrated in Figure 4.16.

By adjusting the magnitude of I_m the PCRTX can be tuned to a capacitive load with

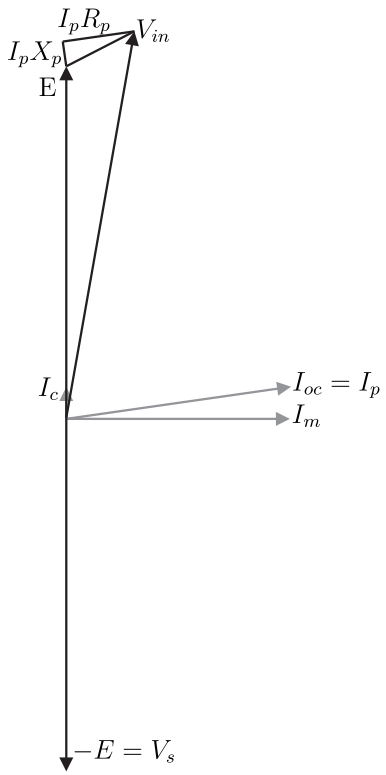

Figure 4.16 Phasor diagram for a single PCRTX operating on open circuit

leading power factor $\cos\theta$. The angle and magnitude of I_{oc} changes to oppose the load current referred to the primary I'_s. However there are two conditions for parallel resonance, unity power factor and maximum impedance [Lee 1933]. The phasor analysis in Figure 4.17a presents the unity power factor condition, which is used in the field, due to easy availability of power factor measurements. Figure 4.17b shows the same analysis with a slightly lower I_m to achieve the maximum impedance condition.

In both cases the magnitude of the primary current I_p is significantly reduced relative to open circuit operation. The results from both tuning methods are quite similar because for a typical PCRTX the series resistances are far smaller than the parallel magnetising reactance and the load capacitance. Also, due to the capacitive load, the secondary terminal voltage increases.

Two PCRTXs connected in cascade follow a similar principle. Under open circuit conditions, the terminal voltage for each secondary winding is equal to the induced emf in that winding. Under open circuit conditions, the secondary terminal voltages V_{s1} and V_{s2} are the same as E_1 and E_2 as shown in Figure 4.18. In a cascade connection of two transformers, the tertiary winding of the first stage is loaded with the open circuit current of the second stage.

The phasor diagram for this circuit is shown in Figure 4.19. It shows that the primary winding carries the load of the primary and secondary open circuit current. It shows

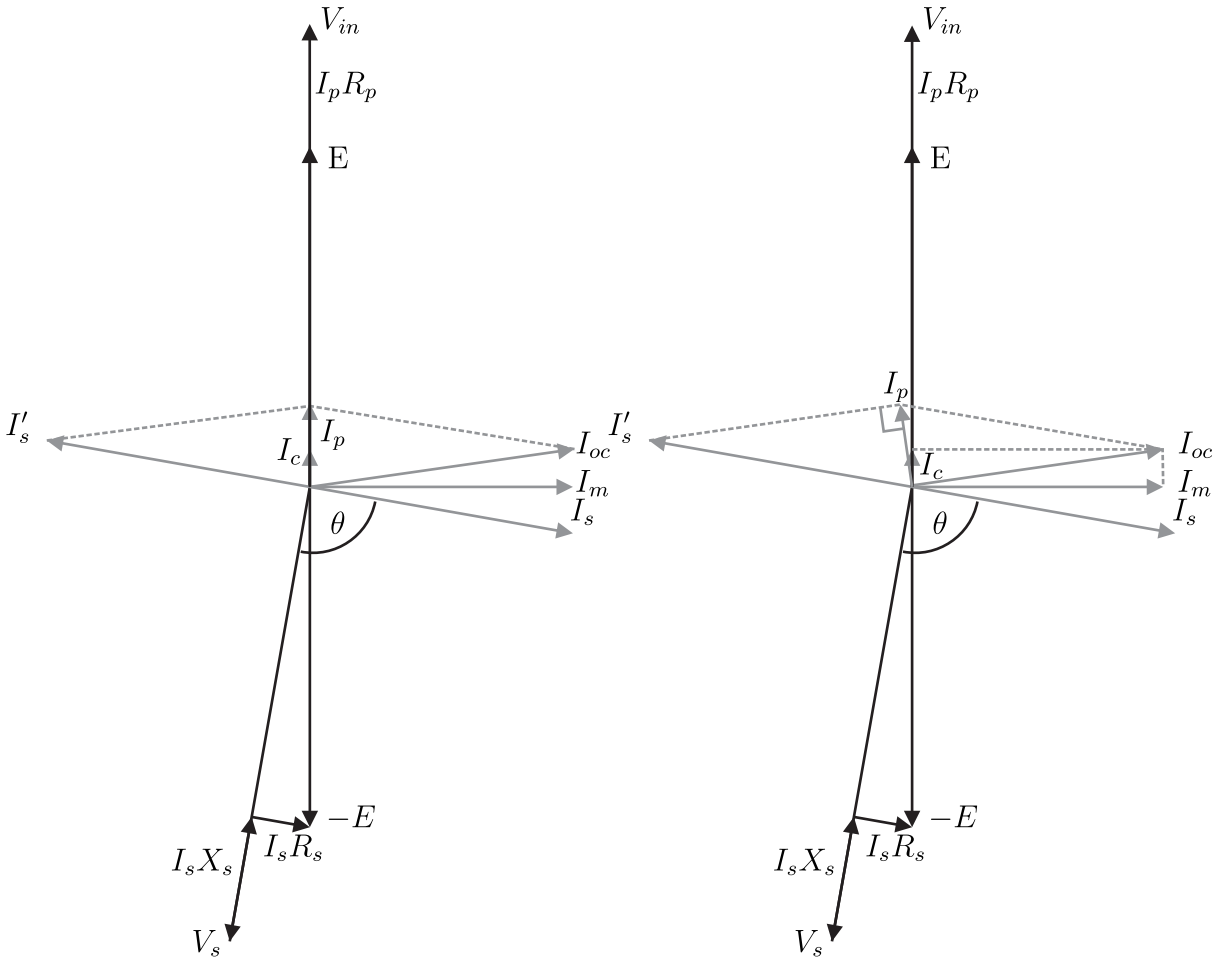

(a) Phasor diagram for a single PCRTX tuned to a capacitive load for unity power factor

(b) Phasor diagram for a single PCRTX tuned to a capacitive load for maximum impedance

Figure 4.17 Phasor analysis of PCRTX tuning conditions

that the secondary voltages are out of phase mostly due to the voltage drops of the leakage reactance and winding resistance. The resulting open circuit voltage is thus lower than the value achieved by having both secondary voltages adding in phase.

If both transformers are simultaneously tuned to a capacitive load, each stage's I_{oc} equally compensates the load current referred to the primary winding. The secondary winding currents of both transformers become far more significant than the primary currents. This means the voltage drops and resulting phase shifts across the primary and tertiary leakage reactances and winding resistances are negligible. Tuning the transformers has thus reduced the voltage imbalance between stages. This is shown in Figure 4.20.

On the second stage, the magnitude of the secondary winding terminal voltage increases from the induced emf due to the capacitive load. This is not true for the first stage due to the negative leakage inductance which acts to lower the secondary terminal voltage

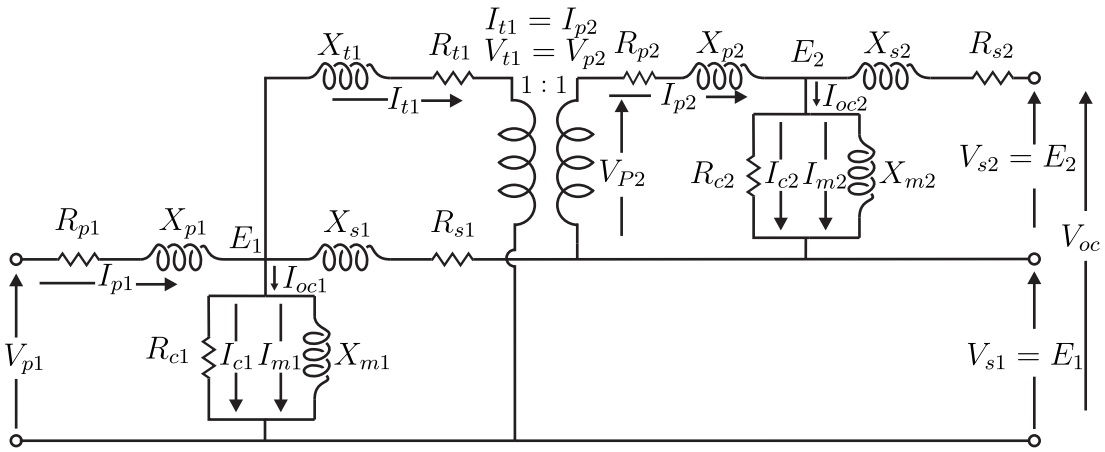

Figure 4.18 Phasor diagram for a two stage cascaded PCRTX under open circuit conditions

relative to the induced emf. It is important to note that the three winding transformer model used here adequately represents the terminal conditions of the unit. Internal parameters such as negative inductances and the induced *emfs* are not measurable in real life and are a consequence of the short circuit calculations.

4.6.2 Calculations

The current distribution through each primary winding can be solved using the coupled inductor model presented in Section 4.4.2. The supply voltage V_{in} is included in the voltage vector shown in Equation (4.13) and the current distribution is calculated by solving Equation (4.12).

$$\boldsymbol{I} = \boldsymbol{Z^{-1}V} \tag{4.18}$$

The coupled inductor model gives the most accurate calculation of the input impedance of cascaded PCRTXs and the current distribution but not the voltage distribution across the secondary windings as the secondary terminals of each stage are absent. The voltage distribution can be calculated by first calculating Z_{in} and I_{in} with a known V_{in} as outlined in Section 4.5.1, then solving Equation (4.8) as

$$\boldsymbol{V} = \boldsymbol{Y^{-1}I} \tag{4.19}$$

The first n entries in $\boldsymbol{V}$ are referred to the primary winding and need to be multiplied by the transformer ratio to get the true secondary voltage.

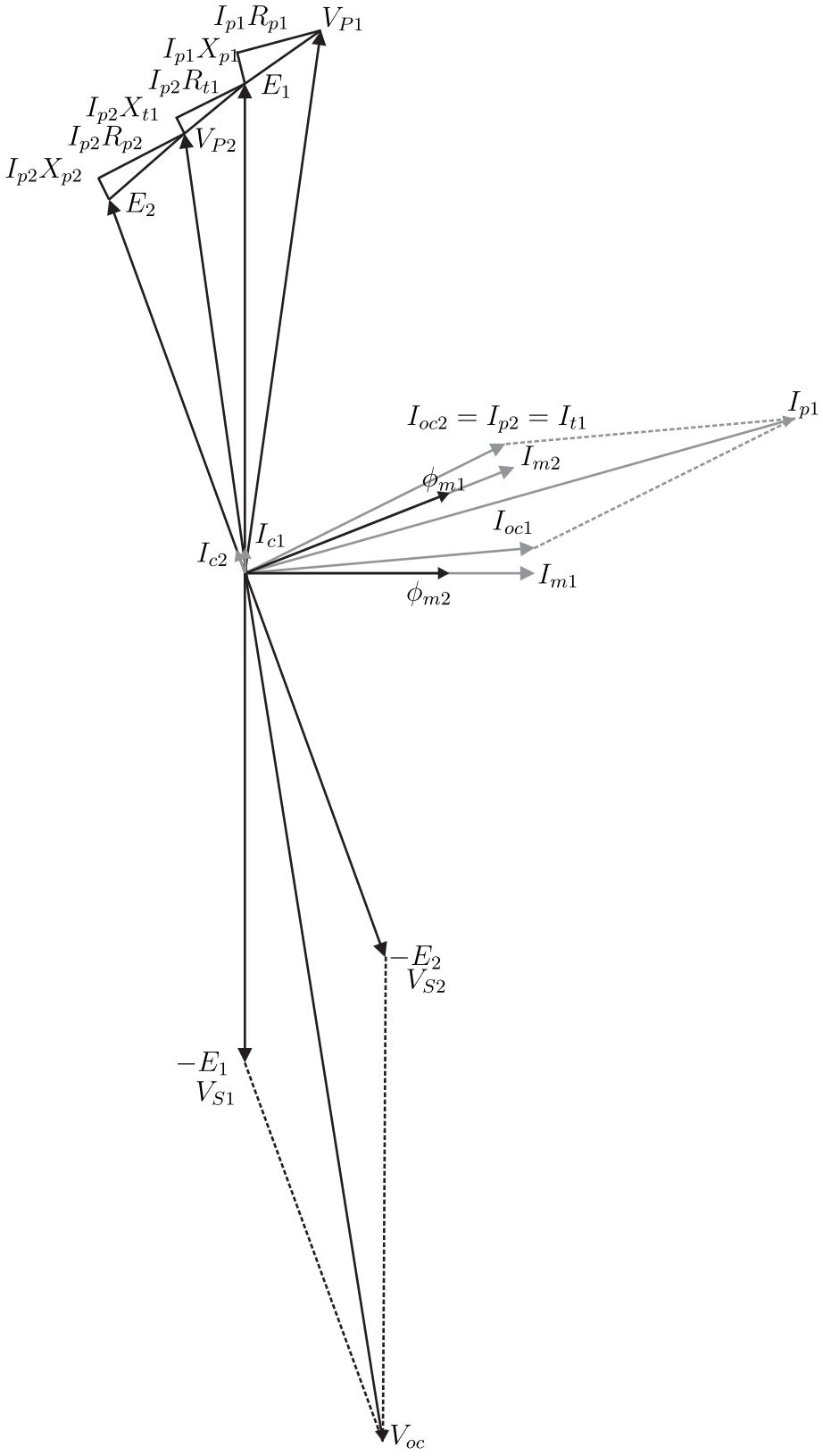

Figure 4.19 Phasor diagram for a two stage PCRTX cascade under open circuit conditions

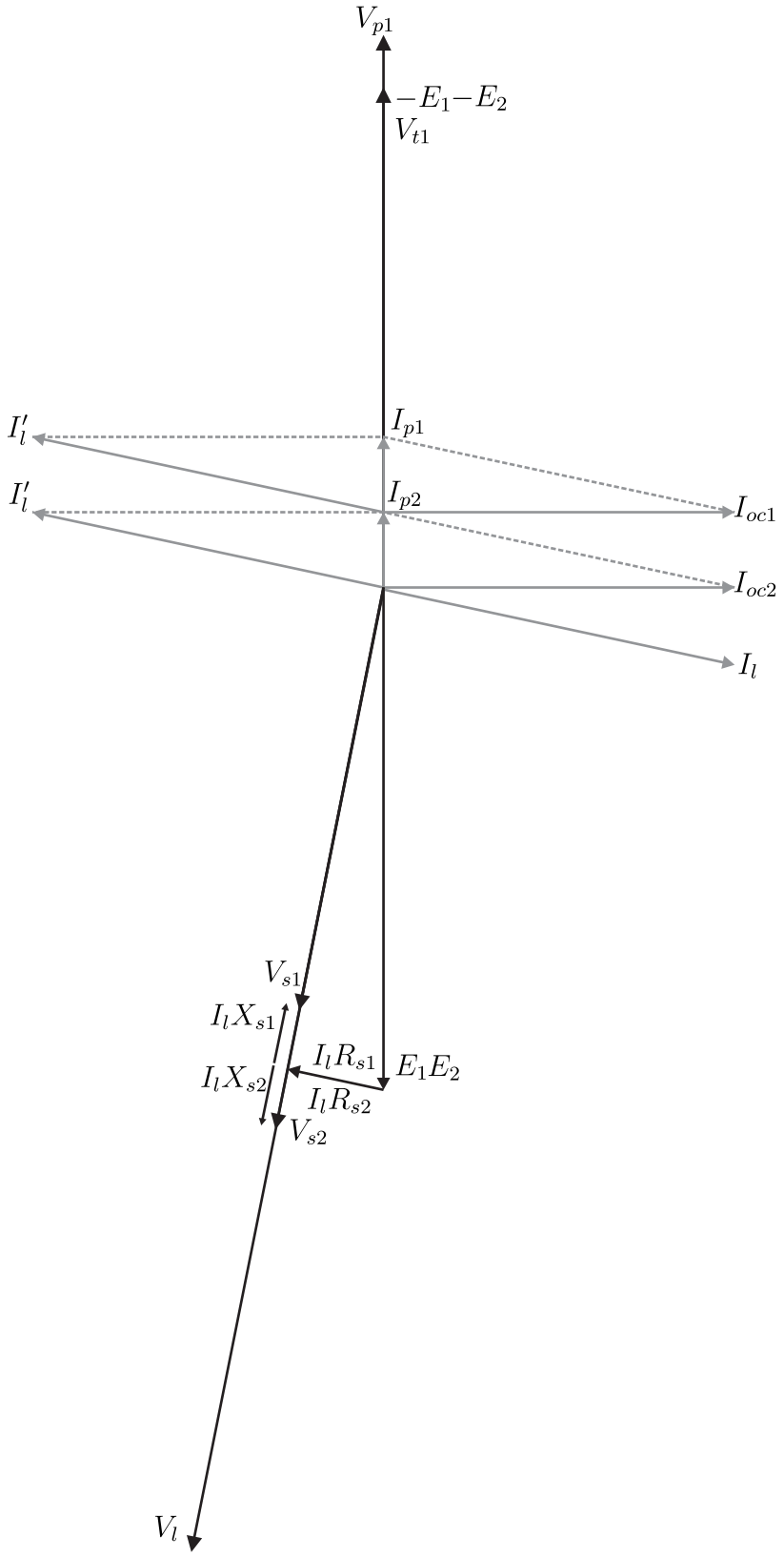

Figure 4.20 Phasor diagram for two cascaded PCRTXs tuned to a capacitive load

Table 4.2 Sample cascaded PCRTX parameters

Parameter	Value
C_l	524 nF
V_l	66 kV
V_{in}	400 V

4.6.3 Tuning effects

As the cascade set is tuned it is expected there will be an impact on the distribution of the load voltage across stage secondary windings and primary current between the stages. The extent of this relationship is unknown and is explored below by simulating the same two stage cascaded PCRTXs used in Section 4.5.2. Tests were conducted at a fixed inductance with variable frequency and with variable inductance at power frequency. The effects of simultaneous and separate tuning introduced in Section 4.5.2 are evaluated with reference to voltage and current distribution between stages.

4.6.3.1 Variable frequency analysis

When stages are tuned simultaneously they equally compensate the reactive power of the load capacitance. Under this condition all stages have the same or very similar resonant frequencies. To illustrate this, the same sample two stage PCRTX was modelled with each stage having a 10 mm gap. The load and input parameters are given in Table 4.2. The distribution of primary currents and the input impedance variation is shown in Figure 4.21. Additionally the variation in the ratio of the stage primary currents is shown in Figure 4.22.

The second stage has a slightly higher resonant frequency, indicating that it has a smaller net inductance than the first. This supports the earlier finding that the additive flux from the tertiary winding on the first stage gives it a higher net inductance than the second stage's tertiary, which is not loaded. The peak input impedance at 50 Hz is 13.5 Ω. Due to the difference in stage resonant frequencies the ratio of the stage primary currents varies significantly before and after the resonant point, but at resonance the first stage primary current I_{p1} is approximately double the magnitude of I_{p2}. This is expected at resonance because the first stage primary has to excite two identical transformers.

As the cascaded test set is brought to resonance and the primary current on both stages is reduced the magnetomotive force provided by the primary windings reduces significantly. As a result, less flux is driven through the core by the primary windings and less flux leaks through surrounding windings and air. This effect manifests itself as a reduction in the voltage drop across the primary winding leakage reactances and

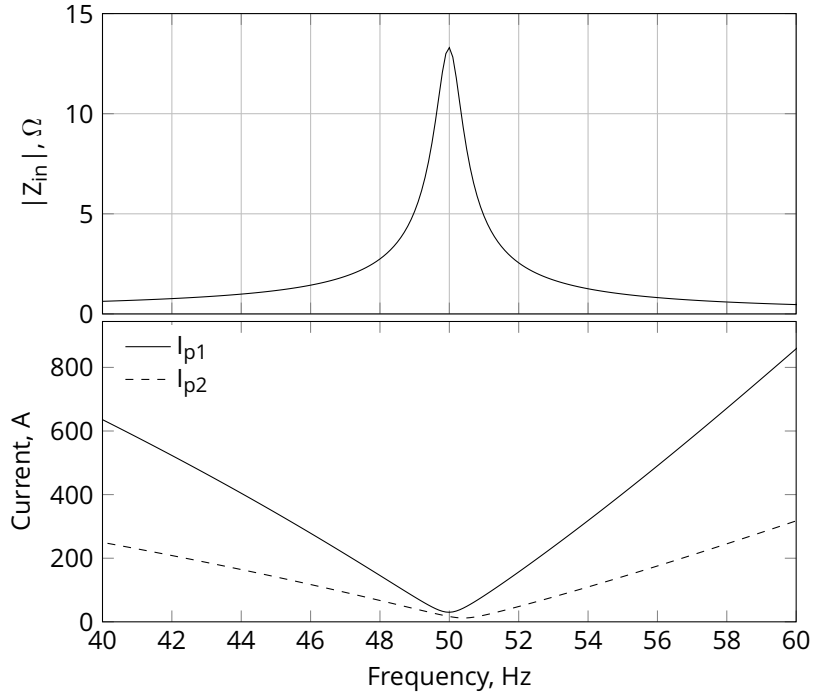

Figure 4.21 Input impedance and primary winding current distribution with simultaneous tuning. Both stages have a 10 mm gap

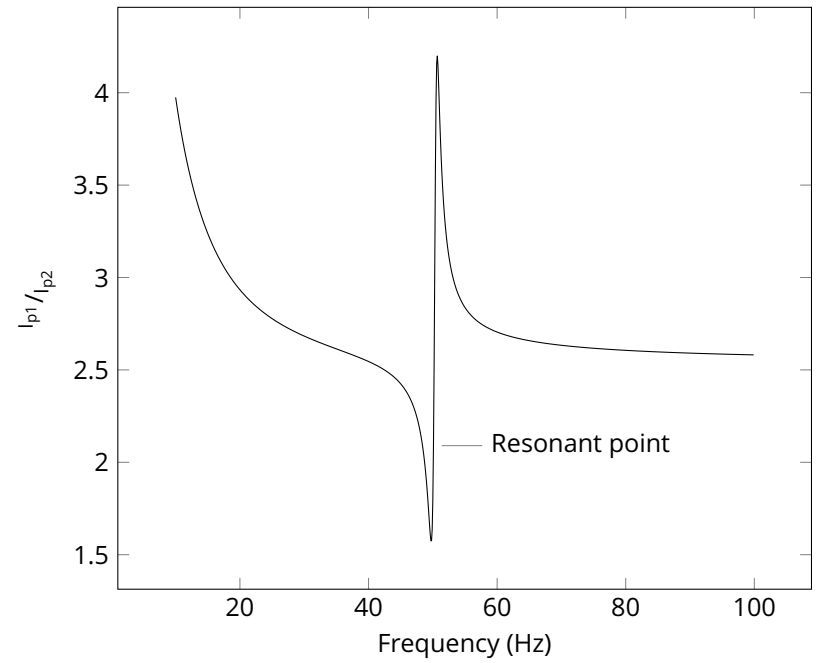

Figure 4.22 Ratio of first stage to second stage primary current with simultaneous tuning. Both stages have a 10 mm gap

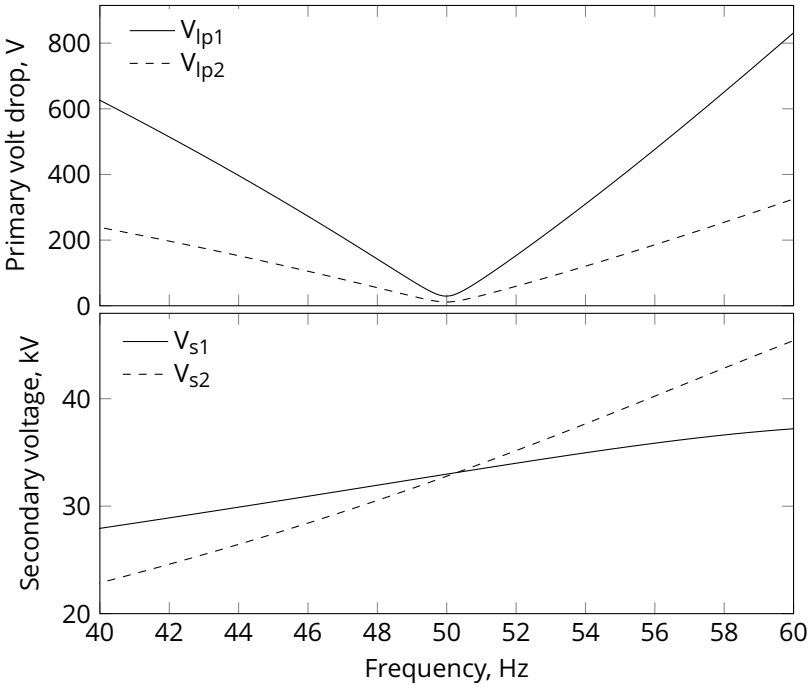

Figure 4.23 Primary winding voltage drop and secondary winding voltage distribution with simultaneous tuning. Both stages have a 10 mm gap

.

resistances V_{lp} as shown in Figure 4.23. Additionally the secondary voltages across both stages are brought more into balance with the reduction in exciting current for both stages, as shown in Figure 4.23.

The same simulation was repeated with the same load but this time only the second stage was tuned with a 23.2 mm core gap while the first stage core gap was kept at zero. From Figure 4.24 it can be seen that the resonant frequencies for each stage differ to a greater extent than for the simultaneous tuning case. Under these conditions, non-resonant stages will draw more current from the supply to correct this mismatch in reactive power. This leads to a reduction in the peak input impedance to 12 Ω which translates to a supply current increase from 29.6 A to 33.3 A at rated voltage. The different stage primary current minimum points are reflected in the calculated voltage drops across the primary leakage reactances for each stage as shown in Figure 4.25.

The stage secondary voltage distribution is also effected when only one stage is tuned. Balanced voltages were achieved at 52 Hz as shown in Figure 4.25 compared to slightly over 50 Hz for the simultaneous tuning case. Less of the load voltage is distributed over the second stage secondary winding at 50 Hz because it has a lower self inductance than the first stage. The voltages become balanced at a higher frequency due to the second stage secondary winding self impedance rising with frequency at a greater rate than the first stage.

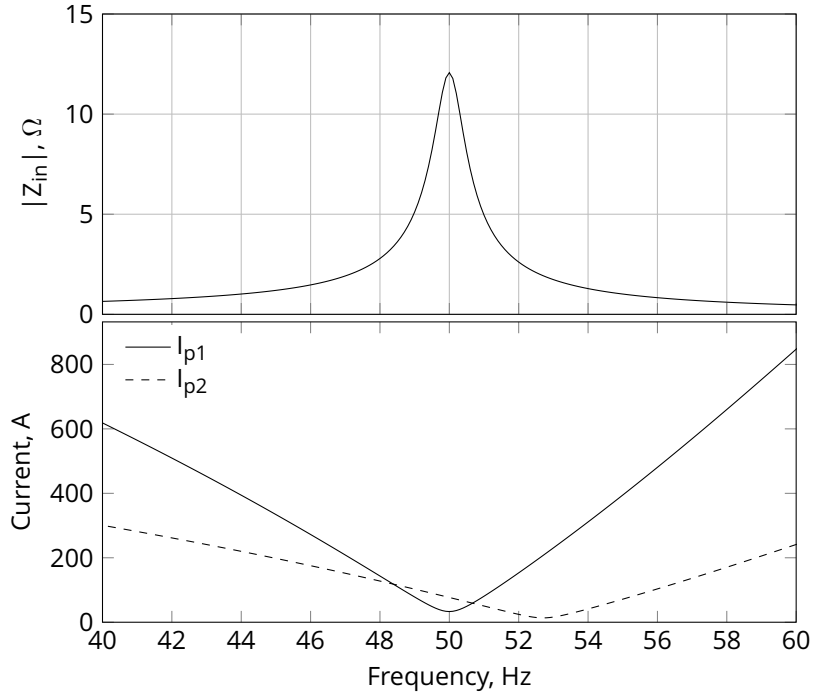

Figure 4.24 Input impedance and primary winding current distribution. The first stage has a 0 mm gap and the second stage has a 23.2 mm gap

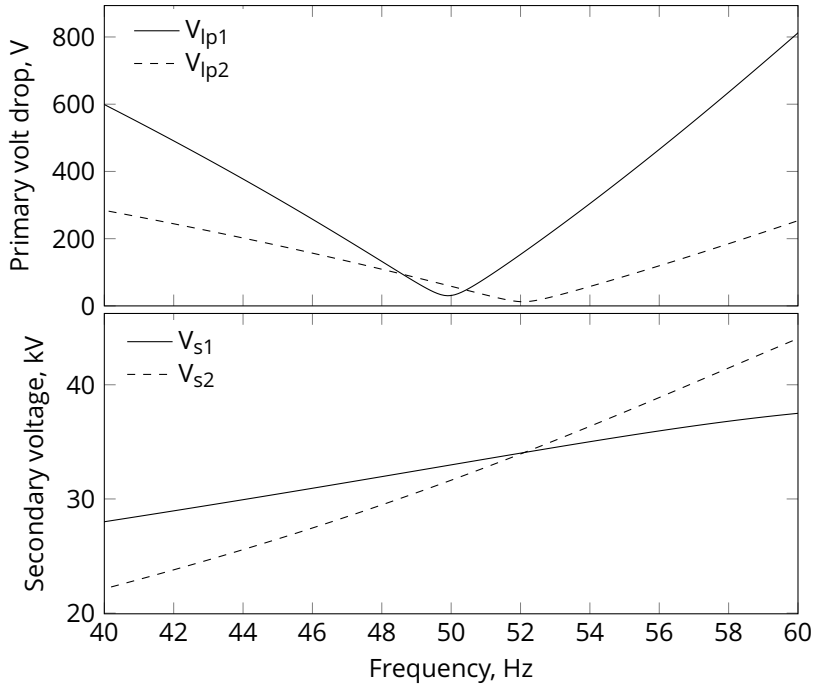

Figure 4.25 Primary winding voltage drop and secondary winding voltage distribution. The first stage has a 0 mm gap and the second stage has a 23.2 mm gap

4.6.3.2 Variable inductance analysis

The PCRTX is designed to operate at a fixed supply frequency with a variable inductance. Any choice of tuning method has to consider the variation in performance with the variation in core gap tuning. The simulations conducted to look at input impedance variation over all possible core gap settings in Section 4.5.2 were repeated to consider primary current and secondary voltage distribution. Again two methods of tuning are shown: simultaneous tuning where both PCRTXs are tuned with the same gap and single tuning where the transformers are tuned separately. In addition a two dimensional analysis of core gap settings was conducted.

The first consideration is the current distribution between the primary windings of each stage. When both stages are tuned simultaneously the primary current in both stages reaches a minimum at a very similar resonant core gap setting as shown in Figure 4.26. A coloured plot indicating the input power factor is given on the same graph to indicate the approximate resonant operating point when viewed from the supply.

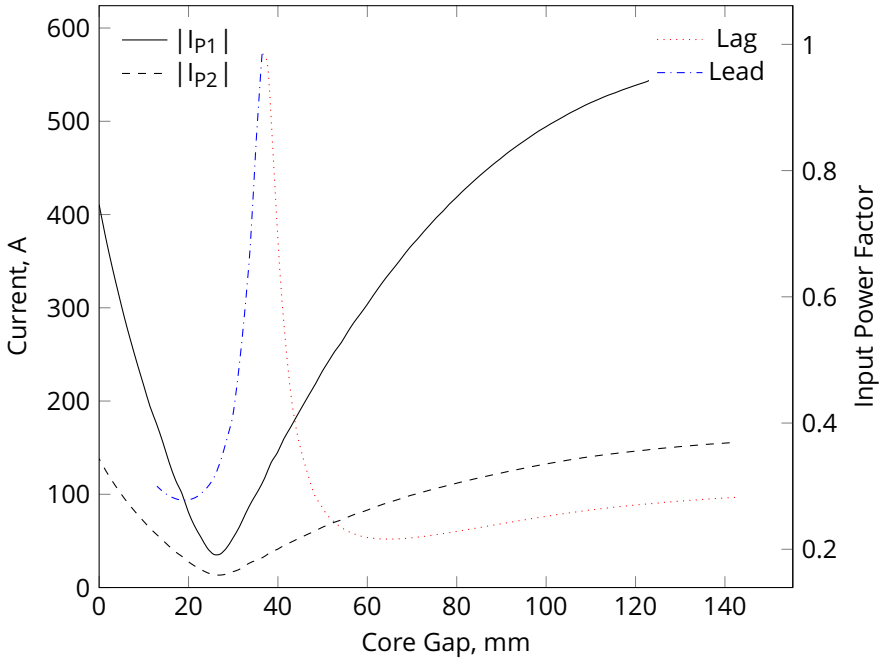

Figure 4.26 Primary current distribution and input power factor under simultaneous tuning with core gap variation

The same simulation was repeated with only the second stage tuned. In this case the second stage required a much larger air gap to bring the combined cascade into resonance as shown in Figure 4.27. The minimum primary winding current for each stage occurs at two different core gap settings. At resonance the second stage primary winding carries approximately 150 A compared to the first stage which carries approximately 50 A. In practical terms a phase to phase connection from a standard three phase power supply could power this circuit. However, there is a danger that the second stage primary will

exceed its thermal rating.

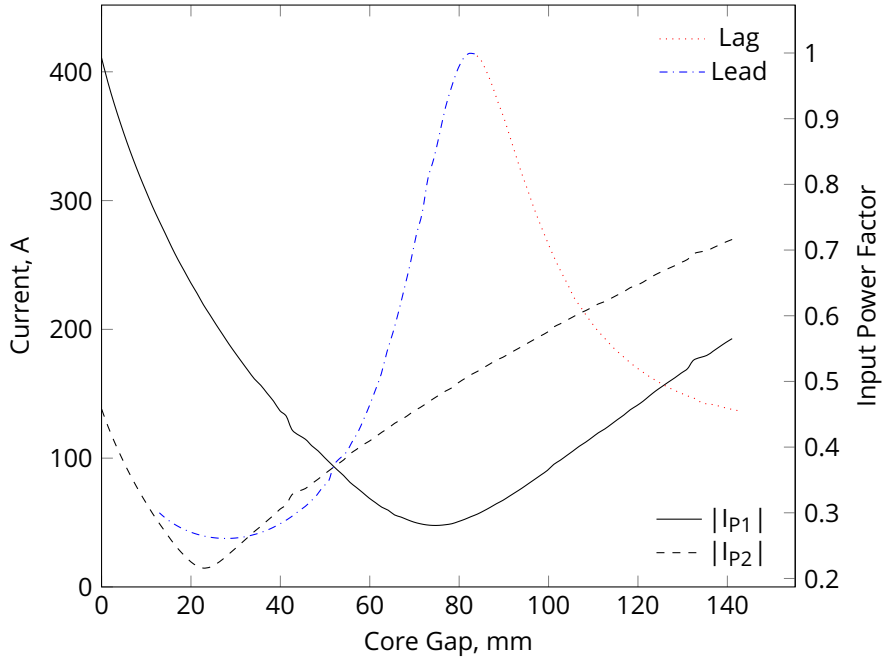

Figure 4.27 Primary current distribution with only the second stage tuned with core gap variation

With only the first stage is tuned, the primary current of the second stage stays relatively constant as the core gap on the first stage is increased as shown in Figure 4.28. This is expected because only the circuit inductances of the first stage are varied. Again at resonance the magnitude of the primary current on the second stage is considerably higher than the first stage and might exceed the winding's current rating.

The same tuning mechanisms also have an impact on the voltage distribution between each stage secondary winding. As Figure 4.29 shows, tuning both stages together produces an almost balanced secondary voltage distribution between stages. The result is that at resonance both stages carry a similar percentage of the load voltage even though the division is not exactly equal.

With only the second stage tuned, its inductance is much lower than the first so the load voltage distributes itself mostly on the first stage at resonance as shown in Figure 4.30. The first stage secondary voltage sits closer to its 33 kV rating at 32.6 kV which is approximately 10% higher than the second stage secondary voltage at 29.5 kV.

Under the opposite scenario with only the first stage tuned, most of the load voltage sits across the second stage secondary winding at resonance as shown in Figure 4.31. In this case the second stage secondary voltage sits at 35.3 kV which is approximately 9% higher than the first stage secondary voltage at 32.6 kV.

A range of possible core gap settings on both stages was simulated. The difference between stage secondary voltages V_{s1} and V_{s2} is shown in Figure 4.32. The relative

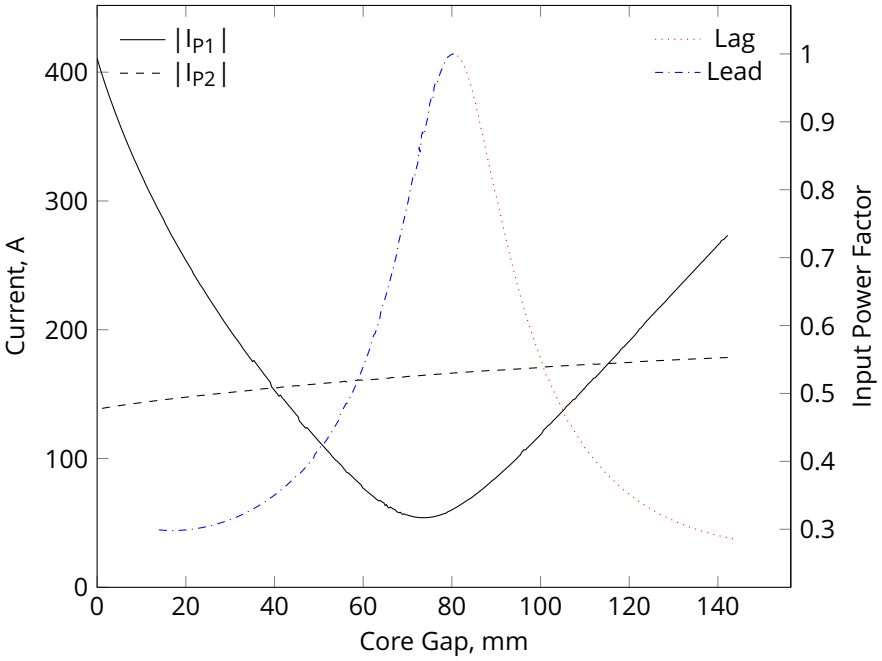

Figure 4.28 Primary current distribution with only the first stage is tuned with core gap variation

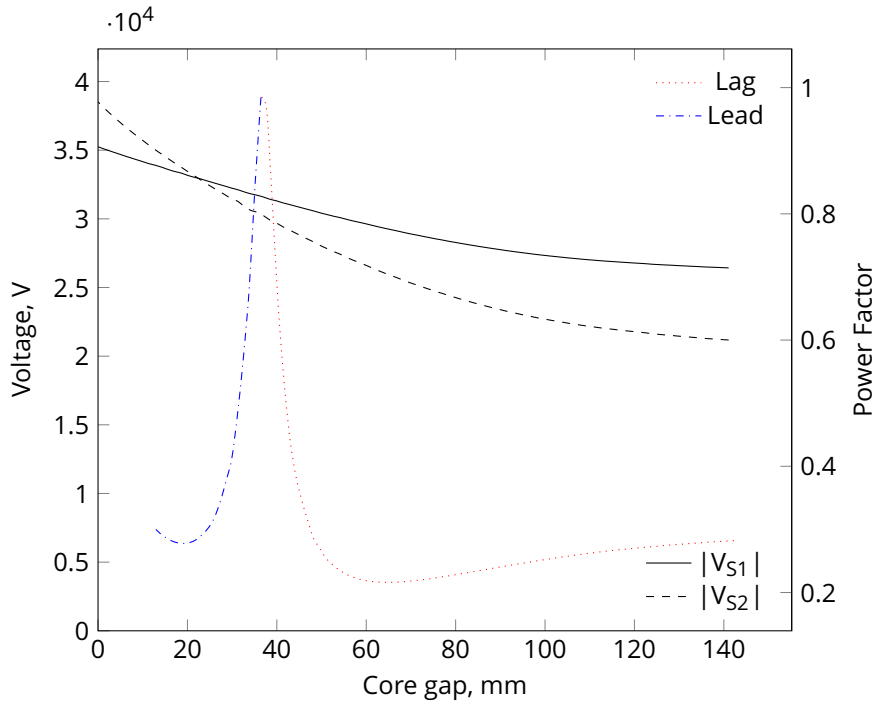

Figure 4.29 Secondary voltage distribution under simultaneous tuning with core gap variation

voltage difference between secondary windings is almost entirely determined by the gap setting of the second stage. The first stage core gap setting has a negligible effect on the difference between the stage secondary voltages. This confirms the results shown in Figure 4.31 that when the first stage is tuned both stage secondary voltages decrease

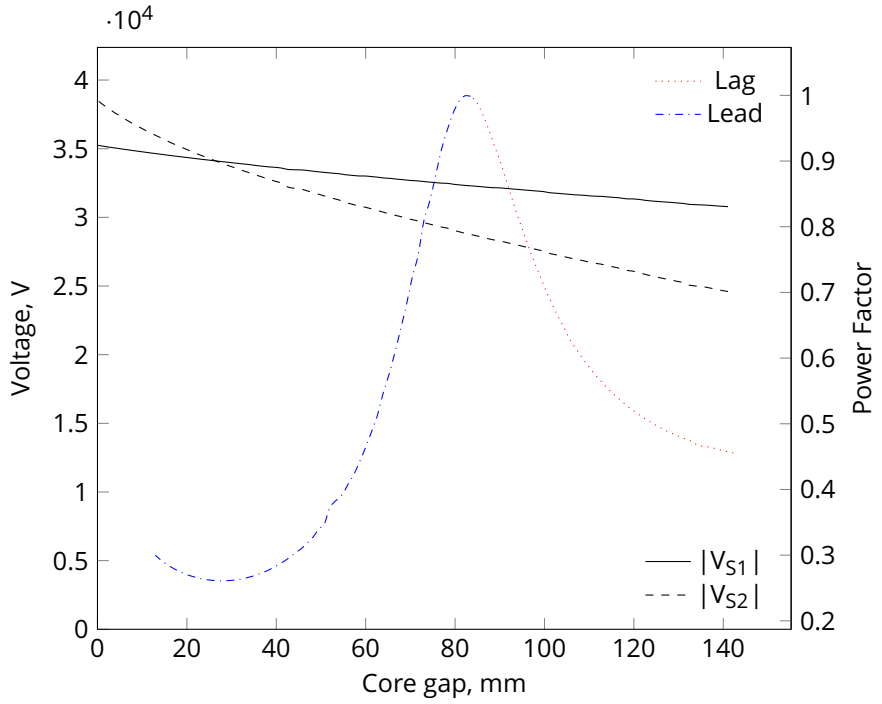

Figure 4.30 Secondary voltage distribution with only the second stage tuned with core gap variation

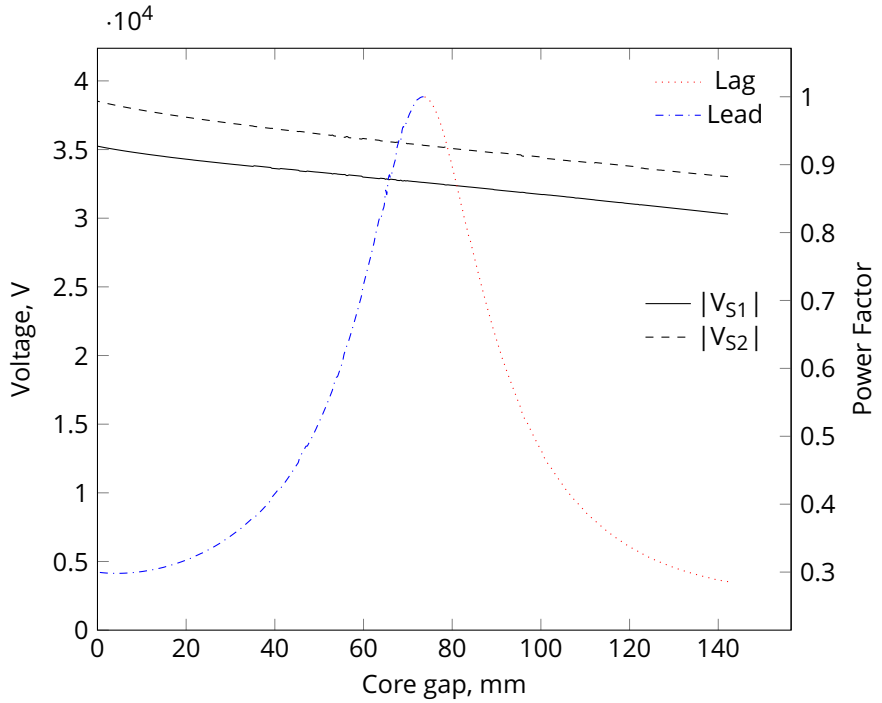

Figure 4.31 Secondary voltage distribution with only the first stage tuned with core gap variation

with the core gap at the same rate.

A similar plot is given in Figure 4.33 showing the ratio of the first stage primary current to the second stage primary current for a range of core gap settings. The dark blue

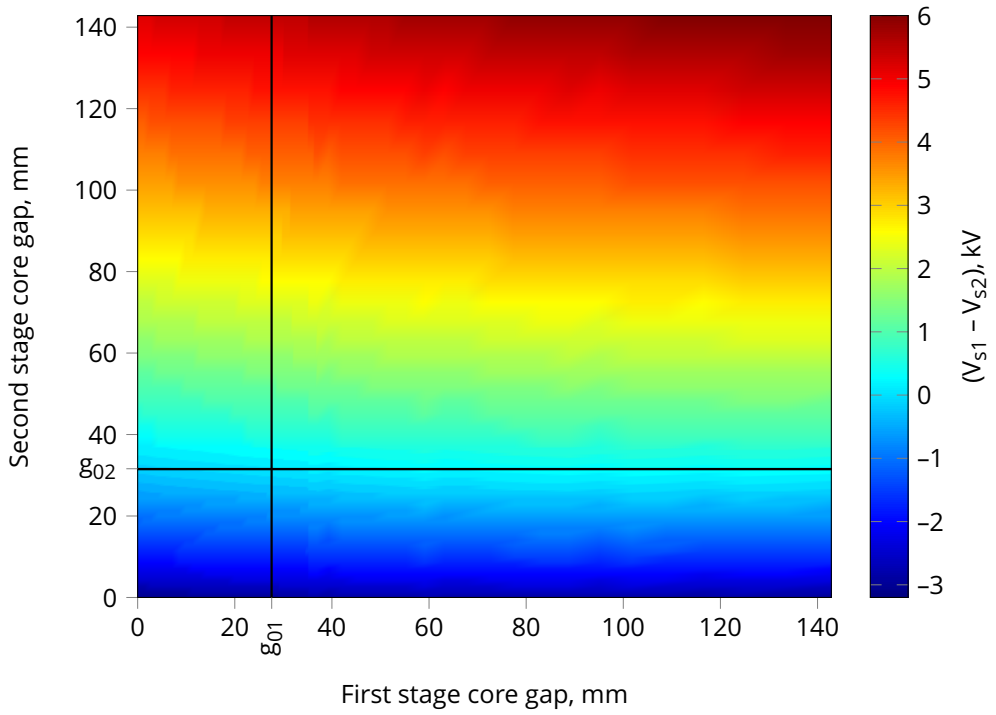

Figure 4.32 Difference in stage secondary voltages under different combinations of stage core gap settings

regions on the plot show operating areas where the second stage primary current exceeds the first stage. The light blue zones represent areas where the first stage primary current is approximately double the second stage. The resonant point sits in this zone. The graph also illustrates the dramatic changes in current balance between stages outside of the peak resonant point.

4.6.4 Model validation

The prototype cascaded PCRTXs used in Section 4.5.3 were tested to verify the current distribution models. Using the same variable frequency supply at a low voltage the current on both stage primary windings was measured. The results are shown in Figure 4.34.

The model shows good agreement with the measured results. The second stage resonant frequency is slightly higher than the first as the model predicted. At resonance the second stage primary winding carries approximately twice the current of the first stage primary winding.

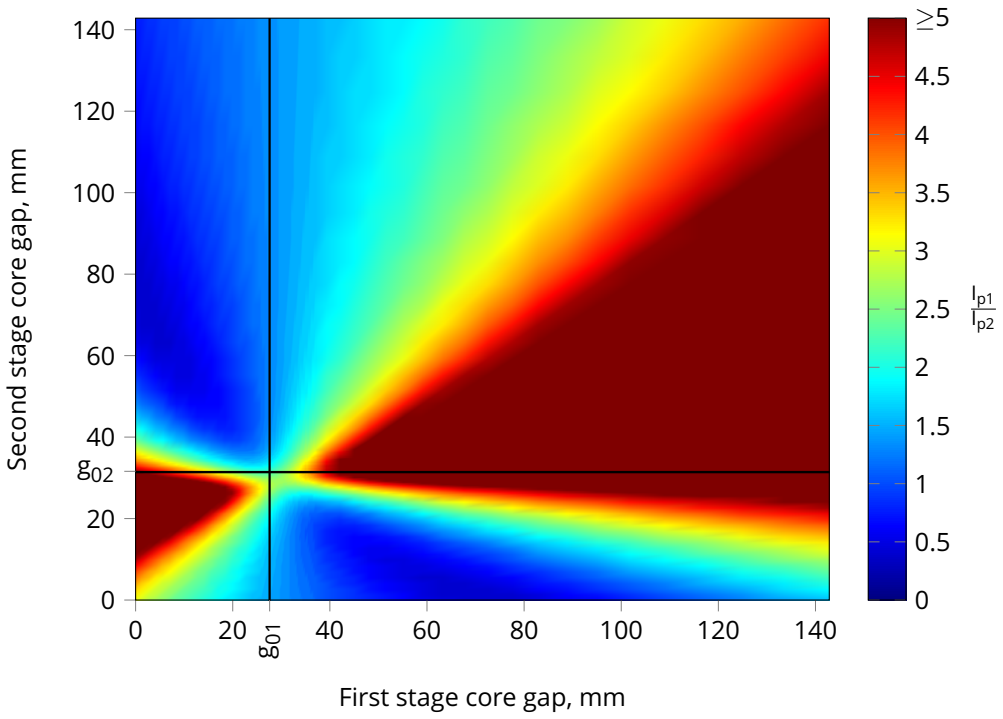

Figure 4.33 First stage primary current divided by second stage primary current under different combinations of stage core gap settings

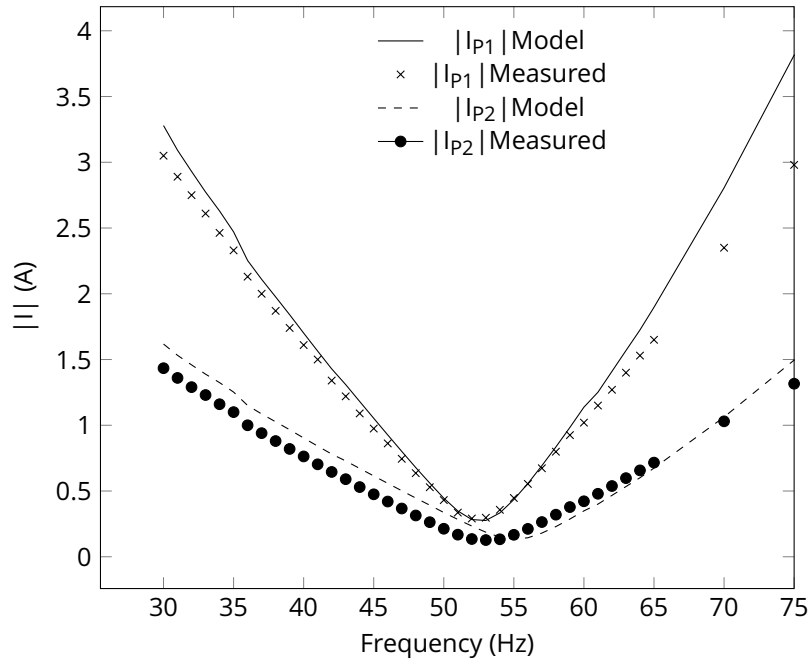

Figure 4.34 Current distribution variation with frequency for cascade prototype test

4.7 RESONANT CAPACITANCE

Calculating the exact resonant capacitance of a cascaded set of partial core resonant transformers is not trivial. With reference to the coupled inductor model, a simple approximation can be performed based on the assumption that the resonant inductance is the sum of the magnetising inductances of each stage

$$C_{res,approxM} = \frac{1}{\omega_0^2 \sum_{i=1}^{n} L_{mi}} \tag{4.20}$$

where L_{mi} is the magnetising inductance of the i'th transformer.

This calculation ignores any resonance from leakage inductances because these values are usually three orders of magnitude less than the magnetising inductance when there is no axial offset or air gap applied to the core. The coupled inductor model can give a different approximation to the resonant capacitance where the resonant inductance is the sum of the secondary self inductances L_s

$$C_{res,approxS} = \frac{1}{\omega_0^2 \sum_{i=1}^{n} L_{si}} \tag{4.21}$$

This calculation ignores the coupled primary winding inductance L_p and any mutual inductance because they are in the order of mH whilst for most practical load capacitances L_s is in the order of tens of H. The definition of the resonant frequency at which C_{res} is calculated can also have a small effect on the value as covered in Chapter 3. Forming an exact analytical expression for C_{res} that takes into account these factors would require complex manipulation of the impedance and admittance matrices $\boldsymbol{Z}$ and $\boldsymbol{Y}$. This is unnecessary as an iterative optimisation routine can then find the optimum C_{res} that maximises $|Z_{in}|$ or achieves a unity input power factor, otherwise expressed as $\angle Z_{in} = 0$. The results of different resonant capacitance approximations of a two stage cascade are compared to iterative calculations in Figure 4.35 for a range of core offsets. The first stage is PC-Reuben and the second stage is PC-Sarah, with both cores offset equally. The iterative resonant capacitance is calculated as $C_{res,zmax}$ under maximum impedance conditions and $C_{res,upf}$ at unity power factor.

The results show that all the different methods reach similar values for core offsets below 30 %. At higher core offsets $C_{res,upf}$ is approximately 20 nF greater than $C_{res,zmax}$. This is due to a decreasing coil coupling increasing the significance of the primary winding self inductance. The approximation using the sum of secondary self inductances $C_{res,approxS}$ sits between the two values and is an acceptable approximation for tuning in the field.

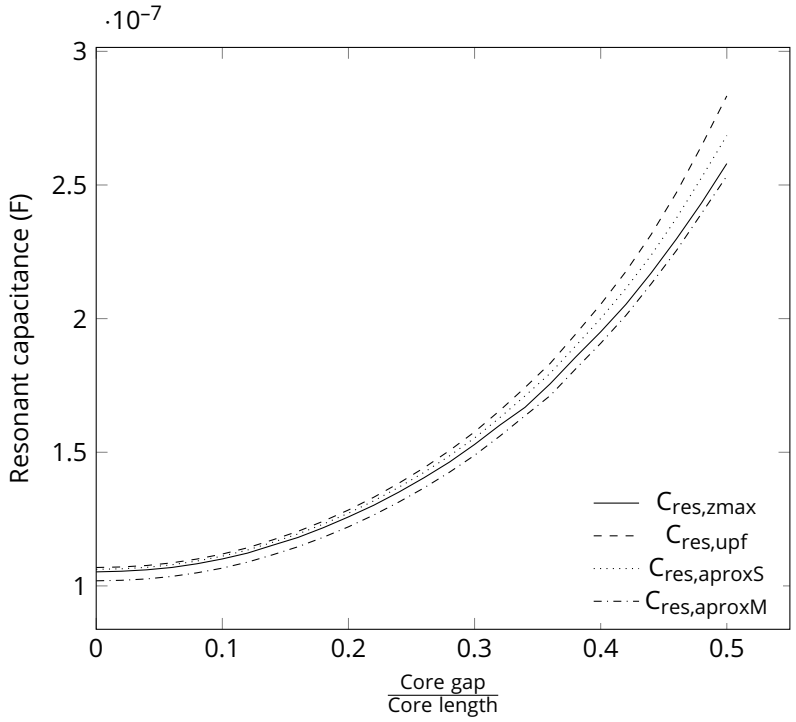

Figure 4.35 Accuracy of capacitance estimate

4.8 WINDING POLARITY

The cascaded transformer concept requires all stage secondary winding voltages to add in series and in phase. For this to occur the relative winding polarity of each stage must be correctly identified to enable the stage secondary windings to be connected in a series aiding configuration.

The simplest place to connect the tertiary and secondary windings together is on the side of the transformer where their lead-outs are closest. This removes the need to run a high voltage lead to the other end of the transformer. If both tertiary and secondary are wound in the same direction and connected at the same side of the transformer then the windings will be connected in a series opposing configuration. This is illustrated in Figure 4.36a where the polarity is indicated by the winding voltage as measured on a differential oscilloscope.

As a result the combined voltage magnitude across the primary and tertiary will be slightly less than the voltage across the secondary as shown in Figure 4.36b. For identical stages connected in cascade, the polarity of the windings between stages will have to be transposed as shown in Figure 4.37. This is required to give the second stage secondary winding the correct voltage polarity to add in phase with the first stage.

The transposition shown in Figure 4.37 can be seen in cascaded transformer circuit diagrams presented by other authors [Schaffer 1960][Goodlet 1937], although the reason

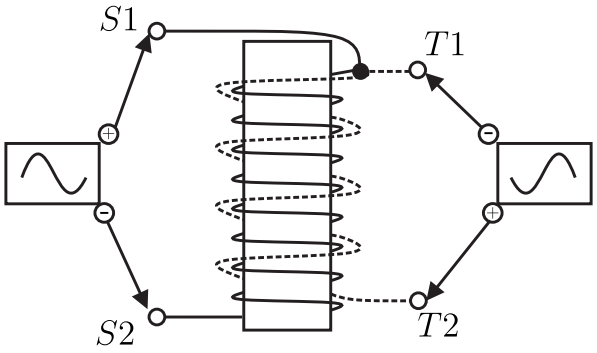

(a) Wound polarity for secondary (solid line) and tertiary winding(dotted line)

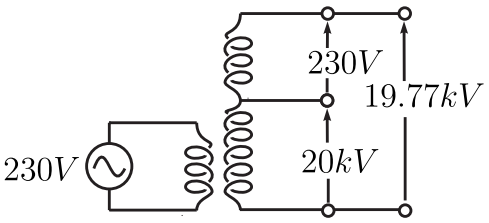

(b) Three winding PCRTX equivalent circuit showing rated winding voltages

Figure 4.36 Tertiary secondary relative winding polarity

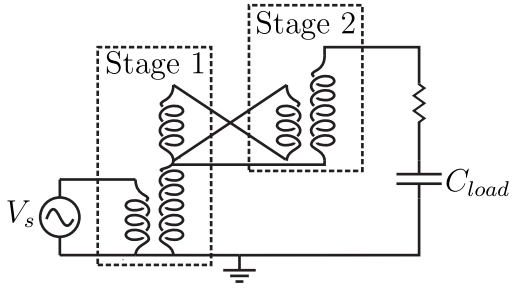

Figure 4.37 Two stage cascade transformer connection showing inter-stage polarity transposition

behind it is not directly addressed. For PCRTXs, alternatives to physically transposing the conductors include rotating subsequent stage transformers 180 degrees and winding the tertiary winding in the opposite direction to the secondary winding.

4.9 LIMITATIONS

The advantage of testing with cascaded PCRTXs compared to an equivalent single unit is that a higher load voltage can be generated without increasing the transformer insulation requirements. This concept is limited by the losses within the circuit and an increasing inductance which lowers the resonant capacitance. Generating higher voltages by adding additional stages to a PCRTX cascade only works until the penalty imposed by these limiting factors becomes greater than the benefit gained from using smaller units.

The first factor considered here is the losses. Whilst the load capacitance and magnetising inductance are mutually compensated, the losses always draws current from the supply. With each additional cascaded stage, more winding and core losses are added to the circuit. These losses lower the maximum input impedance achievable at resonance. This was tested by simulating multiple identical cascaded stages of a sample PCRTX operating with no core gap. For each simulation the resonant load capacitance was

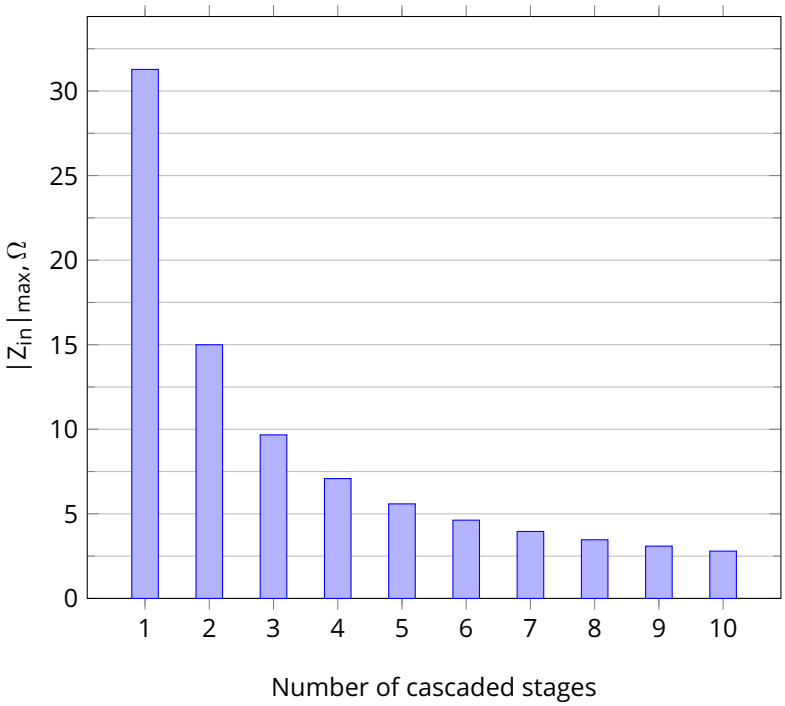

Figure 4.38 Maximum input impedance achieved at resonance for a different number of cascaded stages

calculated using the unity power factor and maximum impedance definition. There is a dramatic decrease in input impedance with the addition of stages as shown in Figure 4.38. The power losses also increase significantly with winding losses being a main contributor as shown in Figure 4.39. Winding losses can be reduced with lower current densities using thicker wire or a cooling system. However as long as the maximum input impedance and hence the supply current can meet the constraints of the intended power supply this is an acceptable trade-off.

Adding more stages increases the resonant inductance of the cascaded test set because the secondary windings are all connected in series. This lowers the achievable resonant load capacitance as illustrated in Figure 4.40. This means cascaded stages need to be designed together for a given load. Merely adding extra stages onto an existing test kit rapidly reduces the resonant capacitance for testing. To maintain the same tuning range whilst increasing the number of stages, individual stages need to be designed with lower secondary self inductances.

4.10 DISCUSSION

The best practical way to tune cascaded PCRTXs is simultaneously where the inductance is equally modified for each stage. With this method all stages in the cascaded circuit have the same resonant frequency. For design purposes there is no significant benefit to

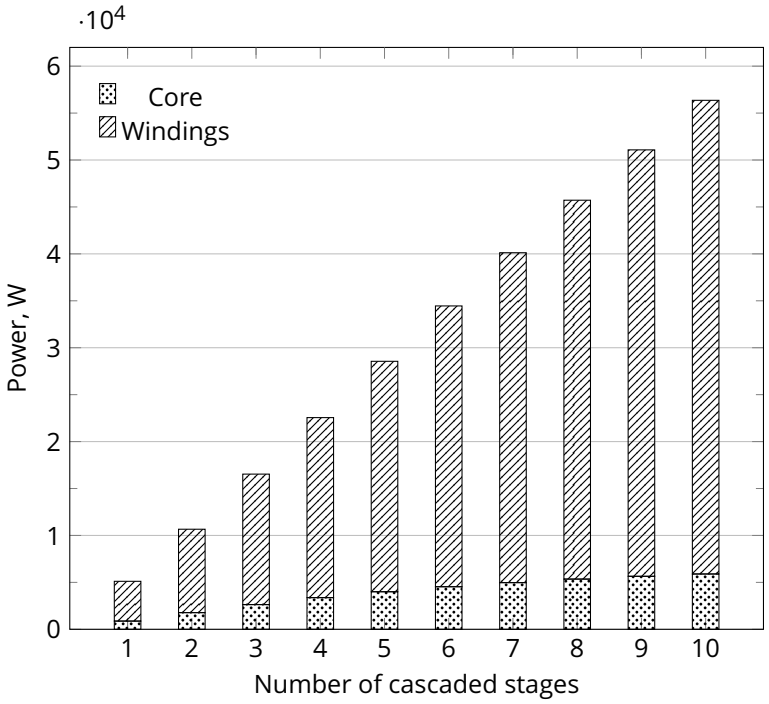

Figure 4.39 Total core and winding power losses for a different number of cascaded stages

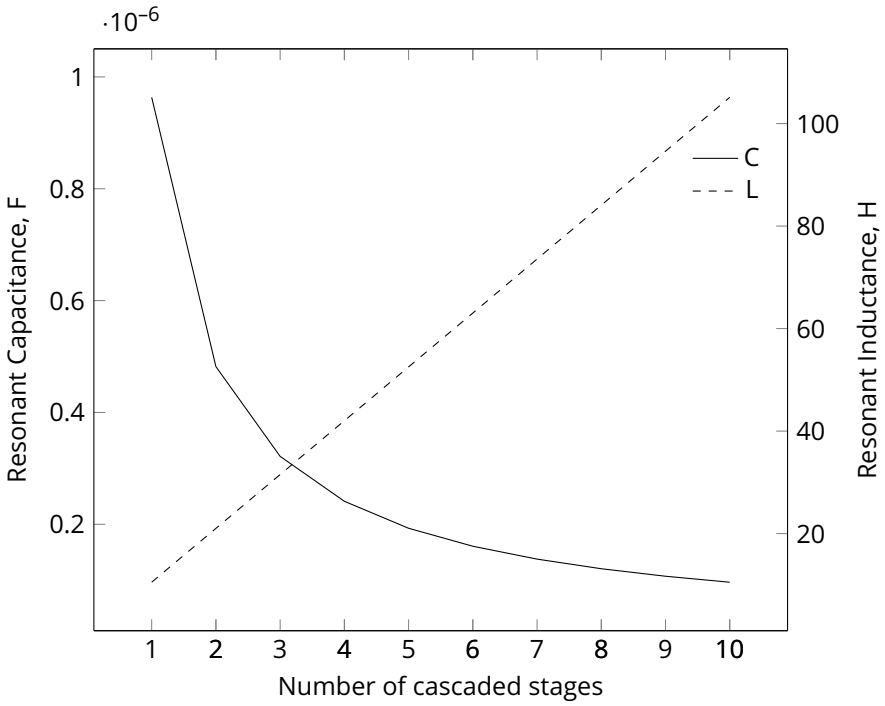

Figure 4.40 Resonant inductance and capacitance relative to the number of cascaded stages

be had from designing stages with different specifications. One area where the design could be modified is in smaller dimensions of the primary and tertiary windings of higher stages because they do not carry the same current as the first stage primary.

This is unlikely to significantly reduce transformer weight and cost because PCRTXs tend not to have a large number of primary turns and the purchase of multiple wire sizes may increase material costs.

4.11 CONCLUSION

Two equivalent circuit models for cascaded partial core resonant transformers were presented in this chapter. The existing equivalent circuit based on the Steinmetz model was reviewed and a new model based on mutually coupled inductors was described along with the matrix formulation to solve these circuits. The models were used to calculate the input impedance, primary current distribution and secondary voltage distribution over a range of inductive and frequency tuning variations. Assuming identically designed stages, the optimal tuning point was found to occur when all stages had a similar air gap with higher stages needing a slightly larger air gap than lower stages. This was due to the additive magnetomotive force from each stage's tertiary windings increasing the resonant inductance of lower stages for the same core gap. Thus it was concluded the most practical method for tuning in the field would be simultaneously varying the air gap of each stage transformer. The limiting factors to adding more cascaded stages were found to be a decrease in resonant load capacitance and a decrease in maximum input impedance at resonance, mostly due to an increase in losses. The models were validated by performing experiments on a sample set of cascaded partial core resonant transformers.

Chapter 5

MODELLING AND DESIGN TOOLS

5.1 OVERVIEW

This chapter details the software tools developed to design cascaded partial core resonant transformers. These consist of a flexible, modular library of functions, classes and simulation routines written in the open source programming language *Python*. Users interact with the library through a purpose built graphical interface or through custom written scripts. The structure of the program is presented along with a functional description of its features.

5.2 INTRODUCTION

The purpose of the modelling program is to simulate a partial core resonant transformer (PCRTX) using the geometric details and material properties of the windings, core and other components. The program simulates electrical performance characteristics and calculates the physical dimensions of the transformer. It also simulates the performance of multiple PCRTXs connected in cascade. The program is designed to allow users to vary any combination of transformer design parameters to see the effect on the final system.

Existing software tools developed to model partial core transformers used imperative programming to automate the modelling process. This style of programming involves sequentially calculating every transformer parameter and storing the results in discrete variables. These programs were developed using the languages *Fortran* [Liew 2001] and *Visual Basic for Applications* (VBA) [Bell 2009]. This method proved adequate for modelling single transformers but does not scale efficiently to modelling cascaded transformers. This is due to repetition of the same modelling parameters for multiple stages and the difficulty in keeping track of them. Additionally, this process lacks the modularity to enable easy inclusion of new features and allow changes to certain functions without affecting the rest of the program.

For this thesis the software is required for research and design purposes, hence it requires a high degree of flexibility to accommodate additional features and models as the requirements evolve. This flexibility can be achieved by breaking down the model into sets of low level components that can be used by higher level processes. This is easier to achieve with an object orientated model. A transformer model lends itself to such a structure because classes can be based on the physical components that make up a transformer.

5.3 PROGRAM ARCHITECTURE

The software design aims to decouple as many elements of the modelling process as practical to achieve a robust system where faults can be isolated and new features can be seamlessly integrated. Accordingly, the program was designed with the three layers of abstraction shown in Figure 5.1. The back end of the design consists of two libraries. The first library contains common materials used in transformer construction along with their properties. The second library contains classes of components required to conduct a full transformer simulation. The control layer performs the actual modelling work using a simulation controller to coordinate the creation and exchange of objects between the front end and back end. This layer also contains a library of commonly used simulation functions to perform finite element analysis, frequency response analysis and calculation of tuning characteristics. The top layer is the interface which includes a purpose built graphical user interface or a script file that sends commands to the simulation controller.

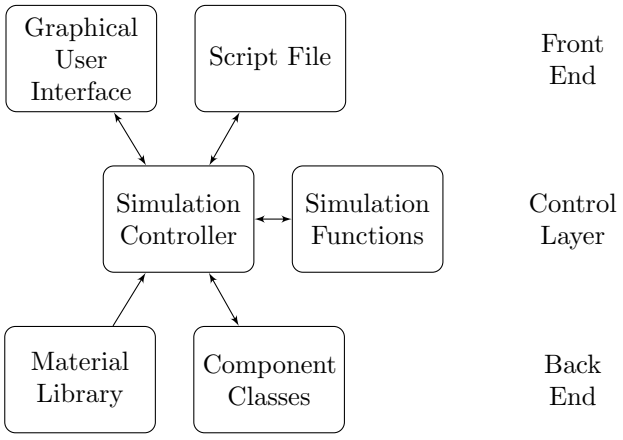

Figure 5.1 Functional overview of transformer simulation program

5.4 CLASS STRUCTURE

The transformer classes are arranged hierarchically, starting with material definitions at the bottom and cascaded transformers at the top. Higher class objects such as the core have arrays of lower class objects like core sections passed to them. Figure 5.2 shows the class hierarchy for the transformer design program.

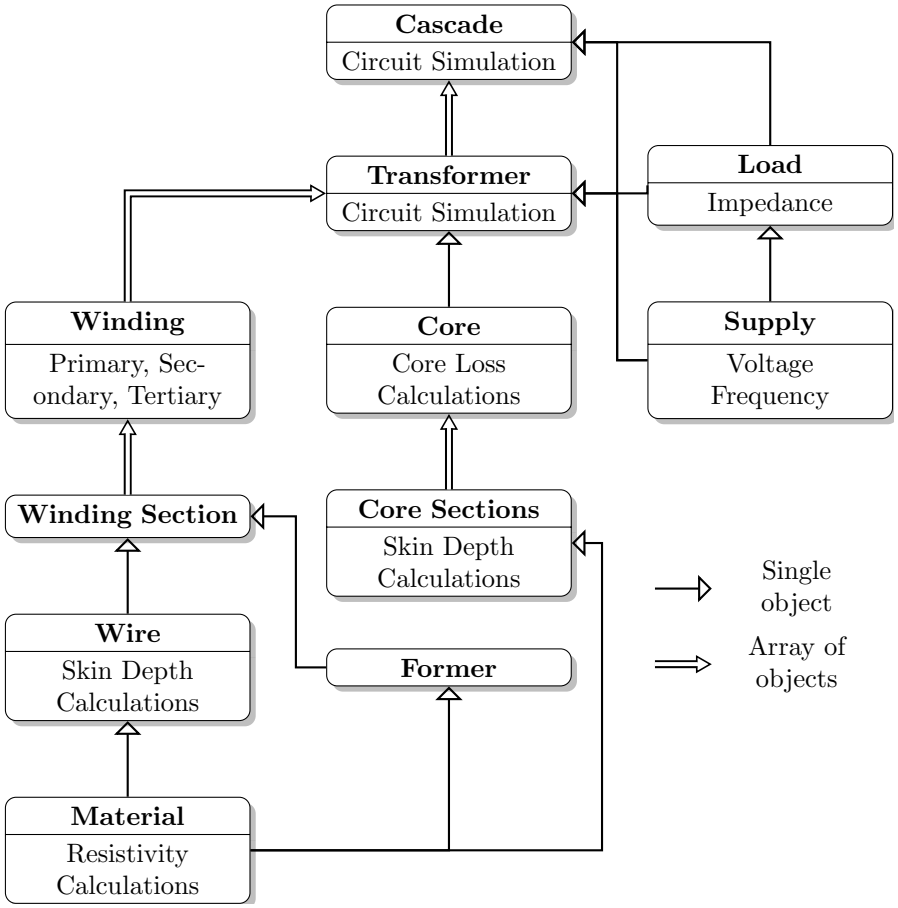

Figure 5.2 Class hierarchy of transformer design program

Each class can contain class methods which are procedures associated with that class. A method does not need to be passed variables, attributes and properties associated with its class. The methods only require additional inputs if the information is contained outside of the class. Methods provide a useful overriding ability by allowing multiple classes to have the same method with the same name but remain decoupled. For example, the core section and winding section classes contain methods to calculate the skin depth. These do not need to be passed resistivity or magnetic permeability values because these values are already contained in the class. The methods do however require the supply frequency as an additional input because it is contained elsewhere in the program.

5.4.1 Materials

Available materials and their properties are the first quantities defined in the modelling process. This class applies to the winding material, transformer steel and insulation. A range of commonly used materials are stored in a material library. Input arguments required to define a material object are given in Table 5.1.

Table 5.1 Material class input arguments

Symbol	Units	Description
-	-	Name
ρ_{20}	$\Omega\,\mathrm{m}$	Resistivity at $20°C$
μ_r	H/m	Relative magnetic permeability
B_{sat}	T	Saturation flux density
Δ_ρ	K^{-1}	Thermal resistivity coefficient
C_γ	$\mathrm{J/(m^3\,K)}$	Volume specific heat capacity
D	$\mathrm{kg/m^3}$	Material density
ϵ	\$/kg	Material cost

The room temperature resistivity value ρ_{20} is used later in the modelling process to calculate material resistivity once the operating temperature is known. The core steel is modelled as a solid block with a linear isotropic relative permeability nominally set to 3000. For copper and aluminium winding materials μ_r is set to 1. The assumption of a linear relative permeability is not valid around the saturation flux density B_{sat} which is approximately 1.6 T for most commercially available transformer steel sheets. The design value B_{max} is usually set lower to reduce excessive noise, vibrations and heat. The thermal resistivity coefficient Δ_ρ is a proportionality constant used to calculate the material resistivity ρ at operating temperatures. The volume specific heat capacity C_γ is used when determining acceptable thresholds for current density.

Table 5.2 Material class methods

Name	Additional inputs	Description
calculateResistivity	Supply Frequency (f)	Calculates material resistivity (ρ) at operating temperatures

The class has a method for calculating the material resistivity at operating temperatures as outlined in Table 5.2 using equations Equations (3.29) and (3.30). The method is called once the operating temperature of the component made from the material is specified by the user.

5.4.2 Core

A PCRTX core can be split into multiple sections to enable centre gap tuning and make it more portable. Each section is defined as a different instance of the core section class. This structure provides a systematic way to define and simulate cores made from non identical sections. Input arguments required to model a core are given in Table 5.3.

Table 5.3 Class input arguments

Class	Symbol	Units	Description
Core section	l_{cs}	mm	Axial length
	r_{cs1}	mm	Outer radius
	r_{cs2}	mm	Inner radius
	t_l	mm	Lamination thickness
	sf_c	-	Stacking factor
	T_c	°C	Operating temperature
Core	[coreSections]	-	Array of core sections
	l_{cg}	mm	Central gap
	l_{csg}	mm	Inter section gap
	σ_c	mm	Axial offset

The core section class input arguments are illustrated in Figure 5.3. The inner radius variable r_{cs2} is included to account for designs where a non conductive rod is used to clamp the core sections together to minimise vibration.

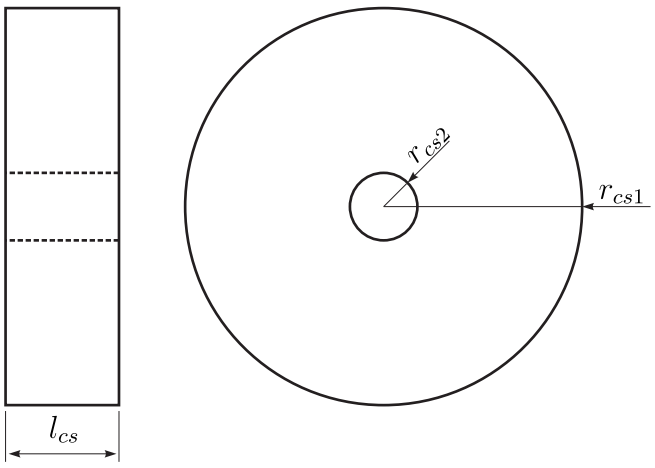

Figure 5.3 Schematic of a typical core section

Usually the thinnest available laminations with a thickness t_l of 0.23 mm are used to minimise eddy current losses. The stacking factor is nominally set to 0.96. The operating temperature of the core T_c is needed for resistivity calculations. This value is estimated based on expected duty, load and previous experience with similar designs. As outlined in Table 5.4 this class possesses a method to calculate the skin depth and the associated effective cross sectional area of the core laminations. This method requires the supply

frequency as an additional input.

Table 5.4 Core class methods

Class	Method name	Additional inputs	Description
Core section	calculateSkinDepth	Supply Frequency (f)	Calculates lamination skin depth (δ)
Core	calculateBpk	Excited Winding Excitation Current	Calculates peak fluxdensity (B_{pk})
	calculateCoreLoss	Supply, Equivalent circuit component values	Calculates core loss resistance

The next class is the core class and it requires an array of core section objects as input arguments (Table 5.3). This class calculates the overall properties of the core such as weight, cost, flux density and losses.

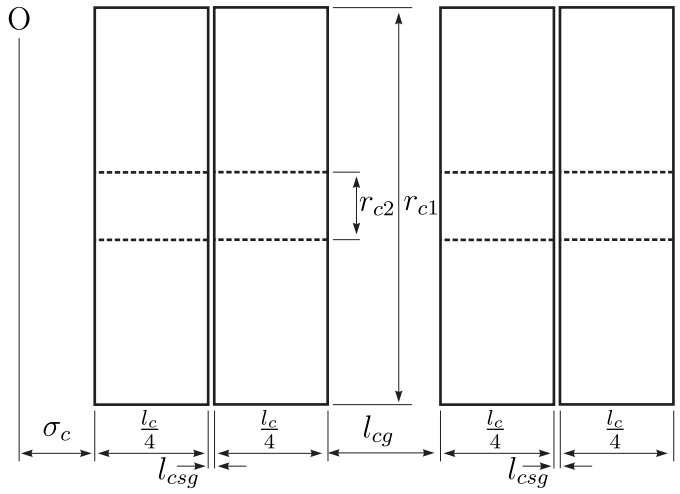

Figure 5.4 Schematic of a core with length l_c centre gap l_gc and axial offset σ_c

The total length of the core is defined as the sum of the axial length of its core sections as shown in Figure 5.4. The core sections are kept separate during FEA simulations so an extra factor l_{csg} is added to account for the thickness of any insulation between core sections resulting from the manufacturing process.

There are two methods contained within the core class which are detailed in Table 5.4. The first method calculates B_{pk} using the process outlined in Section 3.4.2. To do this the simulation controller opens an FEA model, excites the secondary winding with rated ampere-turns and returns the flux density near the center of the core. The second method calculates the core losses, using the model defined in Section 3.4.4. This method is called after determining the rest of the equivalent circuit.

5.4.3 Windings

A winding class object is made from an array of winding section class objects which are each passed a wire class object. The input arguments needed to create this class are outlined in Table 5.5. The wire class defines the dimensions, shape and insulation thickness of the winding wire. The cross sectional area, weight per metre and cost per metre are calculated within this class. Two variables defining the dimensions (dim_1, dim_2) are assigned as either a diameter or as a thickness and width depending on the shape. The insulation thickness t_{wi} shown in Figure 5.5 refers to the wire insulation which is usually made from polyester-imide. The wire class can be created each time or chosen from a predefined library of available wire sizes.

Table 5.5 Input arguments for classes used to make windings

Class	Argument name	Units	Description
Wire	**material**	-	Winding wire material
	Shape		Rectangular or Circular
	dim_1	mm	Diameter/radial thickness
	dim_2	mm	Width if rectangular
	t_{wi}	mm	Insulation thickness
	T_w	°C	Operating temperature
Winding Section	**wire**	-	Winding wire object
	previous section	-	Previous winding section
	Designation	Primary, Secondary, Tertiary	Group into windings
	$l_{w,est}$	mm	Estimated length
	N_{lw}	-	Number of layers
	t_{il}	mm	Inter-layer insulation thickness
	t_{is}	mm	Inter-section insulation thickness
Winding	[winding sections]	-	Array of winding sections with same designation

The wire class has a method which calculates the skin depth of the wire δ. This method uses the material properties already defined when creating the wire class and requires the frequency of the power supply as an additional input. The wire object is passed as an input argument to the winding section class. A winding section is defined as any continuous coil wound with the same sized winding wire. The input arguments needed to create this object are shown in Table 5.5. It is treated as a separate class to allow the use of secondary winding taps for tuning, and primary winding taps for voltage ratio control. This class defines all the the physical and electrical parameters of a given winding section.

An object containing the previous winding section is needed to calculate the radius of

Table 5.6 Class methods used to simulate a winding

Class	Name	Additional inputs	Description
Wire	calcSkinDepth	Supply Frequency (f)	Calculate skin depth (δ) for winding wire
Winding Section	calcCurrentDensity	Winding section current	Calculates current density (J) within winding section

the winding. The section has to be designated as part of the primary, secondary or tertiary winding. The number of turns is determined by fitting an integer number of turns per layer within the estimated axial length $l_{w,est}$. The designer has to define the interlayer insulation thickness t_{il} and the insulation between the current section and the previous winding section t_{is} shown in Figure 5.5. If there are no taps on the transformer the number of winding sections will be the same as the number of windings.

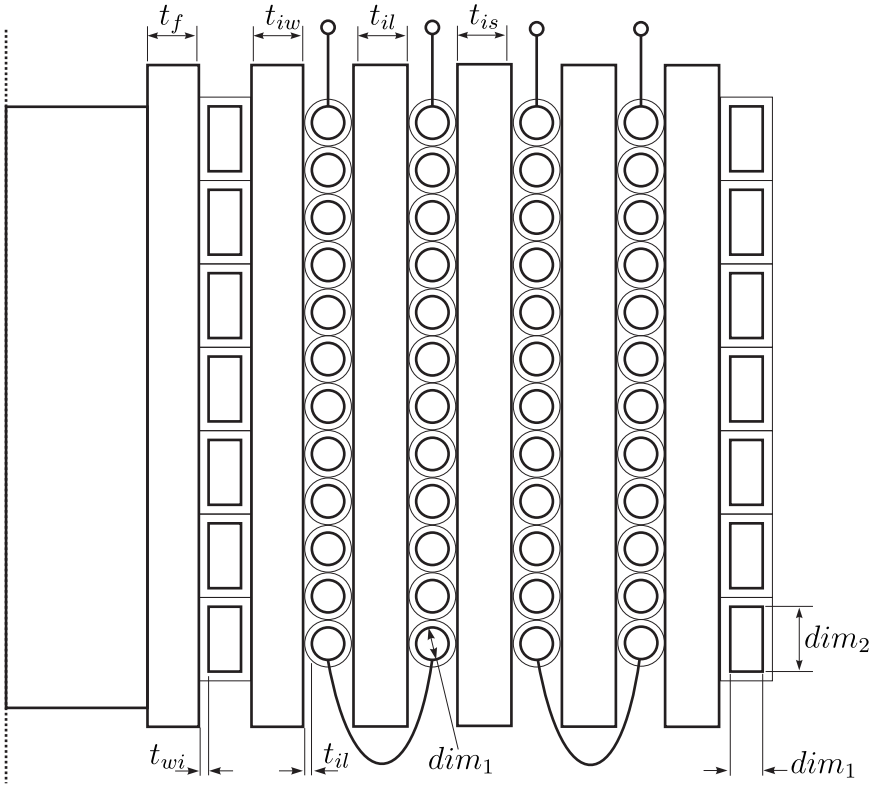

Figure 5.5 Inter winding, inter section and inter layer insulation on a PCRTX

Calculations performed within the winding section class include wire length, resistance, weight and cost. The class method shown in Table 5.6 calculates the current density of the winding once the winding section current value is determined using a circuit model. At this point all the information necessary to perform a finite element simulation is available. The simulation controller passes an array of all winding sections and core sections to the finite element simulation class which calculates and assigns the self inductance to each winding section. The permeance matrix is passed to the transformer

class to calculate mutual inductances between windings.

An array of winding sections is combined into a winding object. The simulation controller performs this task by grouping together arrays of winding sections with the same designation and passing them as an input argument to the winding class. The winding class sums parameters from its component winding sections such as resistance, self inductance, wire length, weight, number of layers and thickness.

5.4.4 Transformer

The windings and core are passed to the transformer class along with the permeance matrix produced by the finite element simulation as detailed in Table 5.7. This class calculates turns ratios between all windings and winding sections along with the total weight of the windings, core and insulation. Inductance and coil coupling matrices are calculated to determine the mutual inductances between windings and winding sections. Equivalent circuit model component values are determined for both the Steinmetz and coupled inductor models.

Table 5.7 Transformer class input arguments

Name	Description
[windings]	Winding sections with the same designation
core	Core object
Permeance matrix	Permeance matrix produced by FEA

As shown in Table 5.7 a class method belonging to the transformer class performs a circuit simulation of a single transformer. This method requires the load and power supply as inputs and solves both equivalent circuits (Steinmetz and coupled inductor), storing the results within the transformer class object. Another class method shown in Table 5.8 finds the resonant capacitance of the transformer. The tuning options determine which definition of resonance is used, such as unity power factor or maximum impedance. This value is calculated iteratively using a simplex algorithm available within the *Python* programming library. This algorithm chooses a capacitance that either maximises the magnitude of the input impedance or achieves a unity input power factor at power frequency.

Table 5.8 Transformer class methods

Name	Additional inputs	Description
simCircuit	**load**,**supply**	Simulates equivalent circuit model
findResCapacitance	Tuning options	Calculates resonant capacitance

5.4.5 Cascade

The cascade class is used to model multiple transformers connected in cascade. The class requires an array of transformer objects as an input argument as shown in Table 5.9. All transformers passed to this class except the final stage must be three winding transformers. The equivalent circuit components of all stage transformers are used to create the circuit model impedance and admittance matrices presented in Section 4.4. Total values for material weight and cost are also calculated.

Table 5.9 Cascade class input arguments

Name	Description
[transformers]	Array of transformers

As with the transformer class there are class methods to perform a circuit simulation and calculate the resonant capacitance for a fixed inductance, as shown in Table 5.10.

Table 5.10 Cascade class methods

Name	Additional inputs	Description
simCircuit	**load**,**supply**	Simulates equivalent circuit model
findResCapacitance	Tuning options	Calculates resonant capacitance for cascade

5.5 SIMULATION FUNCTIONS

Combining and co-coordinating these classes and methods requires another layer of abstraction called the simulation controller. This class contains a series of methods to create class objects, pass them to simulation functions and present the results to the user. Peripheral functions are also provided to assist with loading and saving design data. The functions described in this section are listed in Table 5.11 along with their inputs and outputs.

5.5.1 Loading and saving

The load and save functions handle loading and saving simulation files. As shown in Table 5.11 these files can be either design files or object files. Design files contain information on material properties and component geometry for a transformer design. Object files contain a complete transformer or cascade object with all its equivalent circuit parameters. The save function creates an object or design file depending on the type of input it receives. Loading an object file eliminates the need to perform another finite element analysis when reviewing previous simulations. Transformer objects are

Table 5.11 Simulation functions

Function	Inputs	Outputs
Load	Filename File type	Design file or Object file
Save	Transformer/Cascade Object Design parameters	-
Finite Element Analysis	Winding sections Core Deleted items	Permeance matrix
Frequency Response Analysis	Transformer or cascade Frequency range Load	Frequency response plot
Tuning	Transformer or cascade Core gap or offset range	Inductance variation plot Data file Resonant core gap

loaded into an array each time the load function is called. This array can be passed to the cascade simulation function to simulate the transformers connected in cascade.

5.5.2 Finite element analysis

The simulation controller co-ordinates the interface with a commercial FEA software package called *MagNet*. Previous design tools for this purpose have used Microsoft Excel with *Visual Basic For Applications* (VBA) scripts as a user interface for controlling the modelling software [Bell and Bodger 2008a, Lapthorn 2012]. Whilst the interface is familiar to most users, VBA is not as efficient and flexible as many scientific programming languages. A *Python* interface was used for this work due to the increased computational intensity required to model and optimise cascaded PCRTXs. A *Python* package called *pywin32* was used by an FEA simulation function to send scripted commands to *MagNet* for all modelling tasks.

The modelling begins with initialising the software and setting up the simulation options. A significant contributor to simulation time involves the opening and closing of *MagNet* between successive simulations. To minimise this delay it is left open and the components in the deleted items input argument mentioned in Table 5.11 are deleted at the start of every new simulation. The materials library is loaded into *MagNet* in advance so new materials do not need to be defined before every simulation.

The next step involves drawing the components, starting with the core and finishing with the outermost winding. Only a quarter of the transformer is modelled as shown in Figure 5.6 due to symmetry. This further reduces the simulation time for each design. An air box is drawn around the model to define the boundary of the simulation. The final step involves simulating the model. Each winding is modelled as a single turn

and excited with 1 A. A 2D magnetostatic analysis is conducted and the flux linkage between the windings is used to calculate the permeance matrix. This is then returned to the simulation controller.

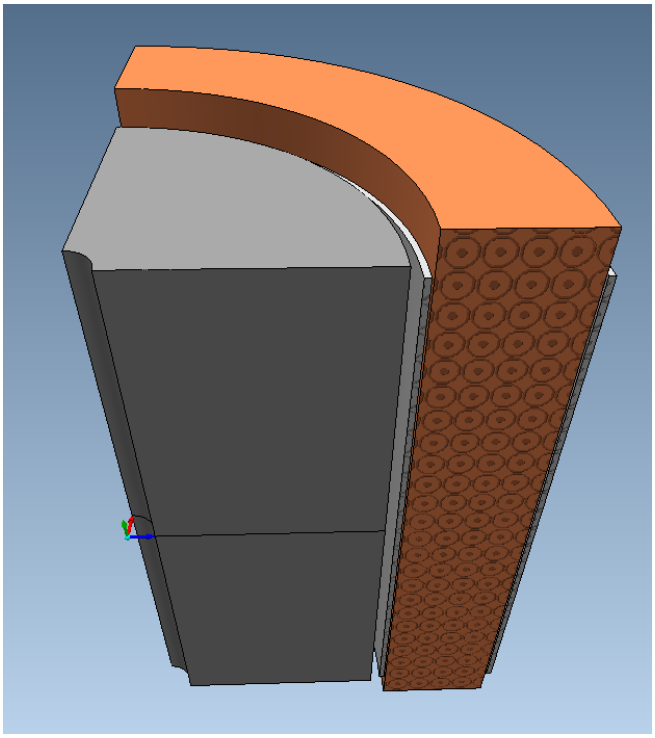

Figure 5.6 FEA model of transformer

5.5.3 Frequency response analysis

A frequency sweep of the test circuit is a useful way to establish if the circuit is tuned correctly to the load and the value of the maximum input impedance. This function varies the supply frequency exciting the equivalent circuit model across a given range as listed in Table 5.11. The output is presented to the user as a graph within the graphical user interface or is exported as a data file. The finite element simulation is conducted with a low frequency approximation and is valid for frequencies below an upper limit defined as

$$f_{max} = \frac{\rho x^2}{\pi \mu_0 \mu_r d^2} \tag{5.1}$$

where d is the conductor thickness and x is a constant set to (1.6 or 2.0) [Bell and Bodger 2008a]. In most practical designs the core has the lowest value of f_{max} with a worst case value of 300 Hz, assuming the laminations are 0.5 mm thick. This is well beyond the operating point and will not affect any analysis conducted for small variations around 50 Hz.

5.5.4 Tuning

The tuning function varies the central core gap spacing or axial offset for a simulated PCRTX test kit. It can do this for single and cascade connected transformers. The function returns a plot of the inductance variation over a range of core gaps or offsets along with the exact value at which resonance is achieved. For single transformers the tuning options input argument mentioned in Table 5.11 specifies the definition of resonance; unity power factor or maximum impedance. For cascaded transformers the tuning options also specify which stage or stages are tuned or if they are tuned simultaneously. Another option simulates optimal tuning described in Section 4.5.2 where a greater input impedance is achieved with one stage having a slightly larger core gap.

For single transformer simulations the function outputs include a tuning characteristic as shown in Figure 5.8, a datafile and the resonant core gap or offset values. For cascaded simulations that do not involve simultaneous tuning it is difficult to show a plot so only a datafile is exported along with the core gap settings at resonance.

5.6 INTERFACE

A simple graphical user interface (GUI) was developed to allow easy interaction with the design program. This is useful for quick design checks, however, detailed simulations and optimisation routines are better controlled with a script file. The interface contains a range of tabbed screens to access different functions.

The opening screen is the *Data Entry* tab, shown in Figure 5.7, which allows the user to enter material properties and sizes for the core and winding sections. Materials can be selected from a drop down list to save time but values can also be entered manually. The number of columns shown on the screen increases as the user adds more winding sections. The available designations for windings are limited based on the number of windings. Buttons are included to call the load and save functions in the simulation controller. Both functions open a file dialog menu allowing design information to be stored for later use or loaded onto the screen.

Once a simulation is completed the *Results* tab displays a table of all the results from the simulation process. This included physical characteristics, equivalent circuit components and electrical performance test results. A save button is included on this page to store the transformer object files.

The *Cascade* tab has a load button to take multiple previously saved transformer object files, compile them into an array and pass it to a cascade class object. The cascade arrangement is simulated and the equivalent circuit simulation results are displayed.

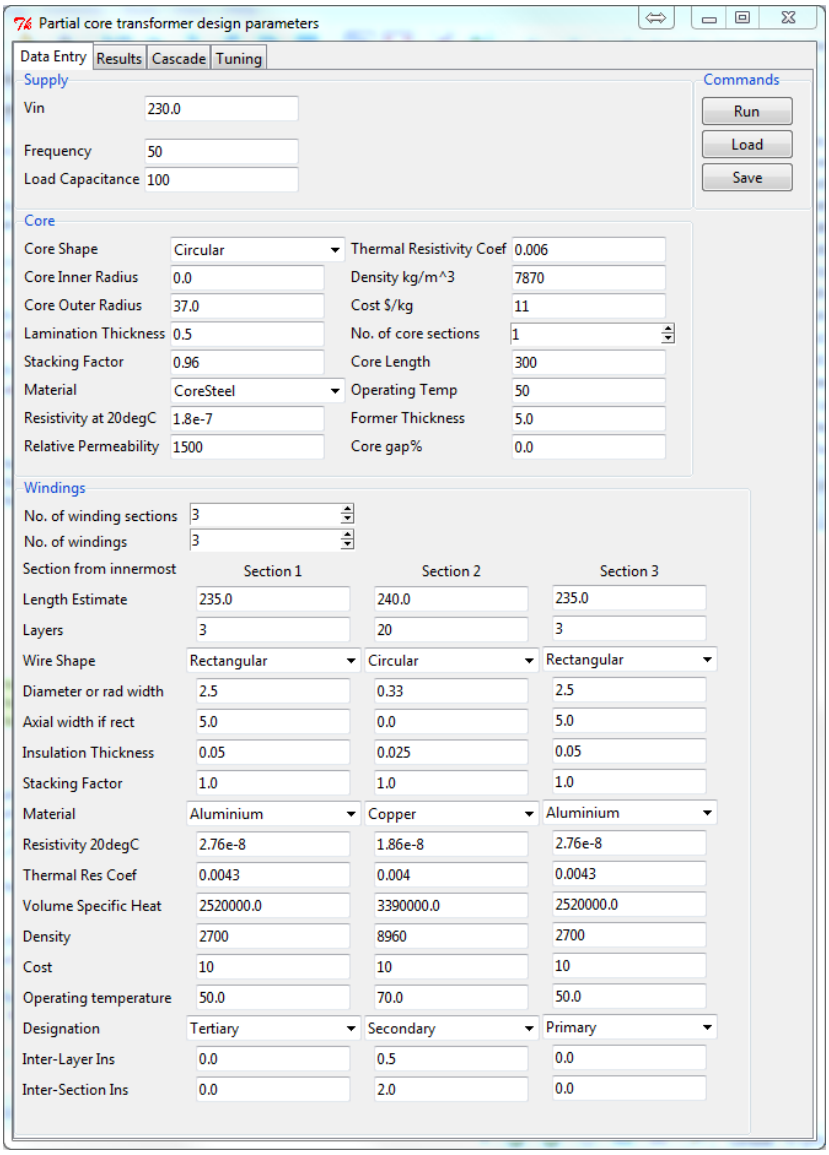

Figure 5.7 Graphical user interface

The user can save the results as a cascade object. An additional tuning tab has input fields where a range of core gaps or offsets can be entered. The program then performs a finite element simulation for each gap setting and returns the inductance variation characteristic as shown in Figure 5.8.

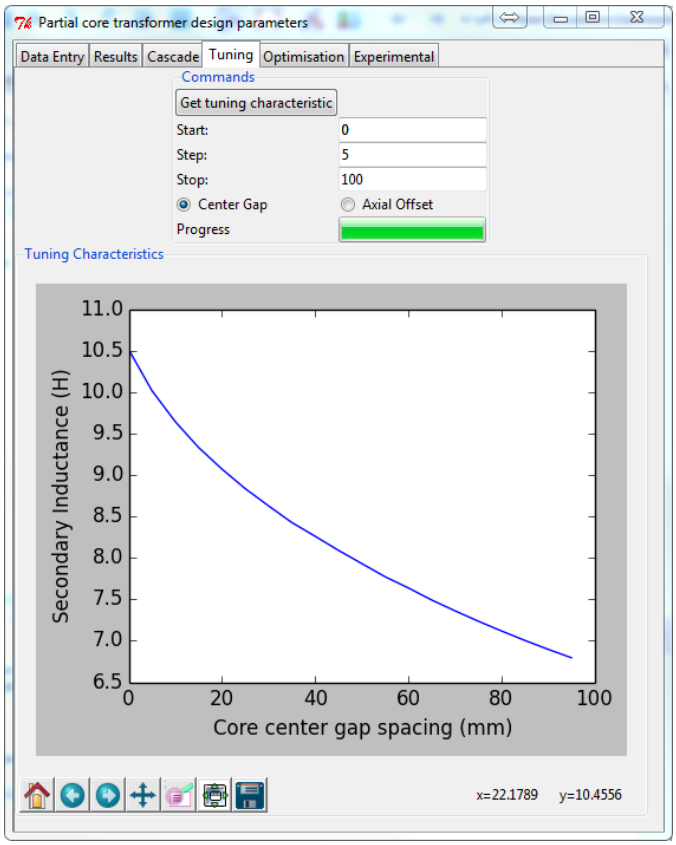

Figure 5.8 Tuning characteristic results in interface

5.7 CONCLUSION

An object oriented design program was created to simulate single and cascaded partial core resonant transformers. The software program was written in *Python* and was designed to be scalable, flexible and user friendly. A systematic class structure based on the assembly of transformer components was designed from scratch enabling future users to easily change and modify the code. A flexible simulation controller capable of creating all the necessary class objects was produced. The *Python* software was designed to interact with a commercial finite element simulation software *MagNet* to determine inductive equivalent circuit components. A user interface was produced to enable easy interaction with the simulation controller for normal operation. The tools were also designed with the ability to be easily controllable by scripted commands for more complicated simulation and optimisation tasks.

Chapter 6

OPTIMISATION

6.1 OVERVIEW

This chapter describes a new method for optimising the design of cascaded partial core resonant transformers (PCTRXs). The aim is to compare the cascade concept to the existing single transformer system and determine the limitations of cascaded PCRTXs as the number of stages increases. The definition of the problem is outlined along with preliminary investigations into the nature of PCRTXs. The transformer design is solved using a version of constrained particle swarm optimisation (PSO) for a real world design specification. The optimisation is conducted for single and multi stage cascaded designs and the relative merits of each arrangement are compared.

6.2 OPTIMISATION OVERVIEW

Optimisation problems can be expressed as a cost function that needs to be minimised

$$f(\vec{x}) \tag{6.1}$$

The cost function is subject to inequality constraints

$$g(\vec{x}) \leq 0 \tag{6.2}$$

and equality constraints

$$h(\vec{x}) = 0 \tag{6.3}$$

where $\vec{x}$ is a vector containing each degree of freedom of the problem [Preis et al. 1991]. Designing PCRTXs requires numerous parameters representing material properties and component geometries to adequately simulate a design. However, many of the parameters are constrained by available materials and others can be derived to satisfy a specification such as the turns ratio. The goal of the optimisation process is to

quickly produce the smallest PCRTX design that meets a certain high voltage testing specification. If the outcome is an acceptably sized PCRTX, the result can be used to inform a more detailed design process.

6.2.1 Cost function

The cost function $f(\vec{x})$, which is sometimes referred to as the objective function, represents the specific value the optimisation process is trying to minimise. Single PCRTXs have been optimised to reduce mass [Bell 2009] with $f(\vec{x})$ expressed as a combination of the masses of the windings m_w, core m_c and insulation m_{ins}.

$$f(\vec{x}) = m_w + m_c + m_{ins} \tag{6.4}$$

When dealing with cascaded transformers the cost function is defined as the mass of each stage transformer instead of the total mass of all stages. This is because the manoeuvrability of test equipment can be a decisive factor in a test technician's ability to set it up in the required location. For high voltage cable testing this could be in an indoor switch-yard where access is through fire-stop doorways and space is at a premium. These locations tend not to have traversing cranes like power stations. By optimising for the unit weight, a fairer comparison is obtained between the usability of cascaded and single stage resonant test kits. If however the total weight and cost of all the stages is the primary concern, a single transformer is the better design choice.

Two other candidates for the cost function are the material and manufacturing cost of the transformer. A combination of these figures would be used if the design was intended for commercial production. However this measure varies with commodity prices and labour costs which can be significant for low volume production. This is beyond the scope of this research so minimising weight is a suitable goal.

6.2.2 Degrees of freedom

The design tools and processes covered in Chapter 5 involve many different parameters defining the properties and geometry of the core and windings. The number of parameters required to design a PCRTX test kit are reduced significantly in two ways. Firstly material properties of the core and windings are fixed at the start of the optimisation process based on what is available. Secondly the geometric parameters of each winding are derived from the neighbouring components and electrical performance requirements.

There are two main sources of mass in a PCRTX, the core and the secondary winding. An existing optimisation method uses four degrees of freedom to optimise their masses [Bell 2009]. The core mass is optimised by including the core axial length l_c and core

outside radius r_{c1}. The core is the radially innermost component so once its dimensions are known the radial position of the windings and insulation can be derived once their thickness is calculated. The secondary winding mass is optimised by including the number of layers on the secondary N_{ls} and the secondary winding current density J_s.

To simplify the design process the secondary winding is constrained to an integer number of layers. The secondary winding wire diameter is derived from J_s. This is an indirect approach that often yields unavailable wire diameters and the optimised value has to be rounded to the nearest standard size.

Two changes are made to the degrees of freedom of the existing optimisation method. The secondary winding wire diameter d_{ws} is used directly as a degree of freedom instead of J_s. This allows the search space to be constrained to available wire sizes. Current density limits are used to define the boundaries of the search space.

The existing method has no way of checking all constraints are met over the transformer tuning range. This is because the maximum core air gap is assumed to be 80%, while experiments and simulations conducted on a range of different PCRTXs show that often the input impedance is too low at large core gap spacings. The new method adds the maximum core gap $l_{cg,max}$ as a degree of freedom to allow constraints to be checked over the entire transformer tuning range.

$$\vec{x} = [l_c, r_{c1}, N_{ls}, d_{ws}, l_{cg,max}] \tag{6.5}$$

The degrees of freedom are defined by the vector given in Equation (6.5). A unique partial core resonant transformer can be designed and evaluated with just these five parameters.

6.2.3 Constraints

There are four constraints that determine if a given $\vec{x}$ leads to a feasible solution. All constraints are expressed so that a feasible solution at $\vec{x}$ returns a value ≤ 0. For equality constraints a percentage tolerance h_{tol} is added to the equation. The first constraint is on the secondary winding self inductance with no core gap spacing $L_{sn,g0}$. This value should match the required maximum secondary winding self inductance $L_{sn,max}$ within the tolerance h_{tol}. At this setting, the test kit is tuned to resonate with the minimum design value of load capacitance.

$$h_1(\vec{x}) = \mid L_{sn,g0} - L_{sn,max} \mid - \frac{h_{tol}}{100} \leq 0 \tag{6.6}$$

If it is possible to achieve the target $L_{sn,max}$ by modifying l_s the binary search process

ensures this constraint is met. If not it sets l_s at the maximum or minimum allowable length and the resulting value of $L_{sn,g0}$ is as close as possible to $L_{sn,max}$ without exceeding the winding length limitations.

The second constraint states that the secondary winding self inductance at the maximum core gap spacing $L_{sn,gmax}$ should be less than the required minimum secondary winding self inductance setting $L_{sn,min}$. At this setting the test kit is tuned to resonate with the maximum load capacitance.

$$g_1(\vec{x}) = L_{sn,gmax} - L_{sn,min} \leq 0 \tag{6.7}$$

The third constraint is on the maximum core flux density. This is simulated using a finite element model, by exciting the secondary winding with the maximum number of ampere turns at maximum load and full voltage. The core flux density is sampled on the outside corner of the axial middle of the core as described in Chapter 3. For any value of peak flux density exceeding the saturation flux density B_{sat}, the solution is deemed infeasible by the following constraint,

$$g_2(\vec{x}) = B_{max} - B_{sat} \leq 0 \tag{6.8}$$

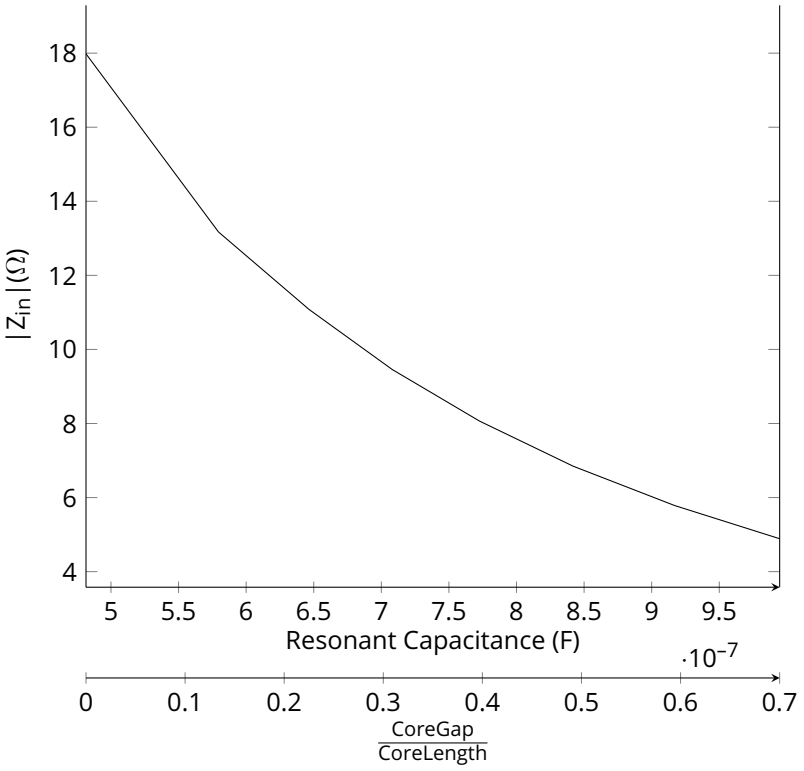

Figure 6.1 Variation of input impedance with resonant capacitance for a simulated PCRTX

The final constraint is on the minimum input impedance at resonance. The smallest allowable value $Z_{in,min}$ depends on the expected current and voltage rating of the power supply. The maximum input impedance at resonance reduces as the test kit is tuned to higher capacitive loads as shown in Figure 6.1. The impedance $Z_{in,gmax}$ is evaluated for a PCRTX test kit energising the maximum capacitive load at rated voltage with the maximum core gap spacing. This is the operating point with the lowest input impedance due to extra losses associated with the large secondary current and transformer flux density. The constraint is therefore defined as

$$g_3(\vec{x}) = Z_{in,min} - Z_{in,gmax} \leq 0 \tag{6.9}$$

6.2.4 Design Inputs

A list of transformer design inputs necessary to start the optimisation routine is given in Table 6.1. The starting specifications for a cascaded transformer design are the number of stages n, supply voltage V_{in}, maximum supply current rating $I_{in,max}$ and the load voltage V_l. This can be used to derive the minimum resonant input impedance $Z_{in,min}$ necessary to excite the transformer to rated voltage without exceeding the supply's current rating.

$$Z_{in,min} = \frac{V_{in}}{I_{in,max}} \tag{6.10}$$

Table 6.1 Optimisation design inputs

Symbol	Description
n	Number of stages
V_{in}	Supply voltage
$I_{in,max}$	Supply current rating
Ω	Supply frequency
V_l	Load voltage
$C_{l,min}$	Minimum load capacitance
$C_{l,max}$	Maximum load capacitance
t_f	Former thickness
t_il	Interlayer insulation thickness
V/L	Maximum interlayer voltage
w_{wp}, w_{wt}	Primary and tertiary wire width
t_{wp}, t_{wt}	Primary and tertiary wire thickness
-	Primary and tertiary wire material

It was shown in Chapter 4 that at resonance, the secondary voltages across each stage are practically equal. Additionally, it was shown that there is no distinct performance advantage to having non-identical stages. Based on this, the design value secondary

voltage for each stage transformer V_{sn} is calculated by dividing the load voltage V_l by the number of stages n. In practise the secondary voltage will vary slightly between stages depending on the relative core gap positions.

$$V_{sn} = \frac{V_l}{n} \tag{6.11}$$

The winding insulation system needs to be chosen before beginning the optimisation process. The system used in PCRTXs so far involves sheets of Nomex-Mylar-Nomex placed between winding layers and encapsulated in Sylgard [Velluppillai 2010]. Another method involves using slatted sheets of G10 fibreglass infused with an insulating resin under an alternating vacuum and high pressure cycle. Either of these two methods constrain the gap between layers to the standard dimensions of available insulating materials. Once a particular thickness is available, the maximum voltage between secondary winding layers $(V/L)_{max}$ can be calculated as a function of the dielectric strength of the insulating material and the thickness of the interlayer insulation. Once this is known the minimum number of layers necessary to prevent breakdown is given by

$$Nl_{s,min} = \frac{2V_{sn}}{(V/L)_{max}} \tag{6.12}$$

It is assumed that the windings are helically wound which has the advantage of being simple to construct. However this method can create high interlayer voltage stresses at the ends of layers.

6.2.4.1 Tuning range

The load capacitance C_l resonates with the total sum of secondary winding self inductances on all stages L_{st}. This is based on the assumption of identical stages and that each stage is tuned with a similar core center gap.

$$L_{st} = \sum_{i=1}^{n} L_{si} \tag{6.13}$$

The maximum and minimum total resonant inductances $L_{st,max}$ and $L_{st,min}$ are calculated from the minimum and maximum load capacitances $C_{l,min}$ and $C_{l,max}$.

$$L_{st,min} = \frac{1}{\omega^2 C_{l,max}} \tag{6.14}$$

$$L_{st,max} = \frac{1}{\omega^2 C_{l,min}} \tag{6.15}$$

The design is for identical stages so the design value secondary self inductance of each stage L_{sn} is expressed as

$$L_{sn,min} = L_{st,min}/n \tag{6.16}$$

$$L_{sn,max} = L_{st,max}/n \tag{6.17}$$

By re-arranging and substituting Equations (6.14) and (6.15) into Equations (6.16) and (6.17) gives

$$L_{sn,min} = \frac{1}{\omega^2 C_{l,max} n} \tag{6.18}$$

$$L_{sn,max} = \frac{1}{\omega^2 C_{l,min} n} \tag{6.19}$$

The ratio between $L_{sn,max}$ and $L_{sn,min}$ is the tuning ratio and existing work has found limitations for this value. PCRTXs have been designed successfully with tuning ratios of two [Bell 2009]. Greater tuning ratios can be achieved by adding tapping winding sections and using a variable frequency source [Rickmann and Kremer 2012]. Both these methods increase the complexity of the tuning procedure and the test equipment.

6.2.4.2 Minimum wire size

The maximum allowable current density of the secondary winding $J_{s,max}$ is an important factor in PCRTX design. If this value is too high the winding resistance will be high, severely limiting the maximum input impedance achievable at resonance. Additionally the wire and interlayer insulation could exceed their thermal rating if operated for too long at high load. A low current density specification can mean an oversized secondary wire which would significantly increase the weight of the transformer.

A simple conduction heating formula can be used to approximate the maximum acceptable current density $J_{s,max}$ for a given operating time [Davies 1990].

$$J_{s,max} = \sqrt{\frac{\theta_m}{t_{on}} \left(\frac{C\gamma}{\rho} \right)} \tag{6.20}$$

where t_{on} is the operating time of the transformer, θ_m is the maximum allowable

temperature rise, $C\gamma$ is the volume specific heat capacity and ρ is the material resistivity. This is a conservative estimate as the equation does not take into account radiation, convection or conduction losses. However heat from the core and eddy currents within the end winding are not considered and neither are variations in ρ and $C\gamma$ with temperature. For this reason a further safety factor T_{sf} is included when calculating θ_m given a worst case ambient temperature of $T_{ambient}$. This is calculated as

$$\theta_m = T_{max} - T_{ambient} - T_{sf} \tag{6.21}$$

where the thermal rating of the insulation is given by T_{max}.

An estimate of the secondary winding current is needed to determine the minimum diameter of the secondary winding wire. In a cascaded test set the load current flows through all the stage secondary windings. For test loads like XLPE cables, the Q factor is high meaning that the load resistance is negligible. Assuming a circular secondary winding wire the minimum secondary wire diameter $d_{s,min}$ for a given $J_{s,max}$ is calculated as

$$d_{s,min} = \frac{C_{l,max}\omega V_l}{J_{s,max}\pi} \tag{6.22}$$

This value is rounded to the nearest available wire size and used as a lower limit when defining the optimisation search space. Following the optimisation process the design is checked with a full circuit simulation to ensure that the current density is below the limit. The primary and tertiary windings use substantially less material than the secondary, therefore they can be safely oversized with a readily available wire size without adding any significant weight.

6.2.5 Design evaluation

A complete transformer design needs to be simulated at each iteration of the optimisation process. The design is developed using only the results from preliminary calculations and the parameters within a vector $\vec{x}$ located within the solution space. In other words a transformer is designed using only the pre-defined parameters described in Section 6.2.4 and the five variables being optimised: core length l_c, core radius r_{c1}, secondary winding layers N_{ls}, secondary winding diameter d_{ws} and the maximum core gap $l_{cg,max}$.

6.2.5.1 Inductance matching

Initially the design program attempts to determine whether the maximum stage inductance $L_{sn,max}$ can be achieved at the core dimensions and number of secondary winding

layers given in $\vec{x}$. The axial length of the secondary winding l_s is not optimised for and can be varied to achieve $L_{sn,max}$. The value of l_s can be shortened or lengthened to do this but at a certain point it is better to declare the design infeasible and try again during the next iteration with different values of r_{c1} and l_c. These thresholds for this are set by limiting the ratio of l_s to l_c to between 0.7 and 1.3%.

At this point the model is treated as an inductor consisting of only the secondary winding of length l_s with N_{ls} layers wound around a gap-less core with dimensions l_c and r_{c1}. The binary search algorithm described in Figure 6.2 is used to find the value of l_s that achieves the transformer target $L_{s,max}$. Initially the extremes of the thresholds described above are simulated. If the required inductance can be met, the algorithm continues searching between an upper bound UB and a lower bound LB until the change in l_s is less than the secondary winding diameter.

$$\left(\frac{l_s}{l_c}\right)_{min} = 0.7 \tag{6.23}$$

$$\left(\frac{l_s}{l_c}\right)_{max} = 1.3 \tag{6.24}$$

6.2.5.2 Turns ratio

The inductor is now used as the secondary winding for the transformer. A primary winding is wound on the exterior and if the design is for a cascaded set a tertiary winding is wound on the interior near the core. The axial length of both primary and tertiary windings is chosen so they meet the desired turns ratio. PCRTX designs have large turns ratios and the number of turns required on the primary and secondary is small. In most practical designs only one to three primary layers are required. This small modification to the geometry decreases the secondary winding inductance from the value calculated in the previous step but not enough to significantly impact the resonant load capacitance.

6.2.5.3 Peak flux density

The peak flux density within the core B_{pk} has a significant impact on several operational characteristics of the PCRTX. The core losses are higher at large flux densities which increases the current drawn from the supply. High flux densities also generate high magnetic forces within the core and hence produce greater audible noise and vibrations. Most transformer steel reaches saturation at approximately 1.6 T but to reduce noise and losses the maximum design value B_{sat} is set at 1.2 T.

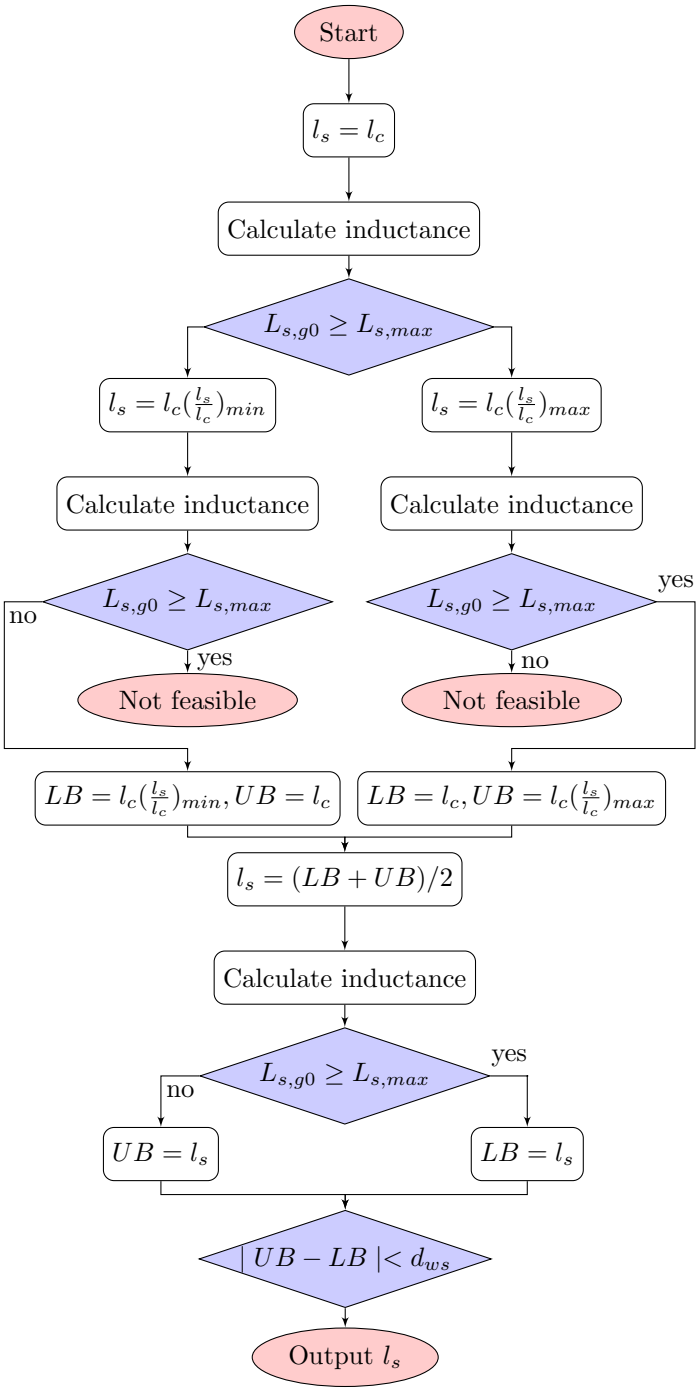

Figure 6.2 Binary search process for secondary winding length

The worst case operating point for B_{pk} occurs when the maximum load capacitance is excited to rated voltage and the core gap is at its maximum. Under these conditions the primary and tertiary winding ampere turns are negligible therefore only the peak

secondary winding ampere turns mmf_{spk} are considered. This value is calculated as

$$mmf_{spk} = \frac{\sqrt{2V_{sn}}}{R_s + \omega L_s} \tag{6.25}$$

The secondary winding within the FEA model is excited with this value. The peak core flux density is sampled at the outer radius on the axial center as described in Section 3.4.2. This value is strongly influenced by the core radius and through experience it was found to be the key constraint defining this parameter.

6.3 PARTICLE SWARM OPTIMISATION

The only technique used so far to optimise the design of PCRTXs is the multiple design or Monte-Carlo technique [Bell 2009]. This method evaluates every possible combination of each degree of freedom within the solution space. Feasible solutions are recorded and the one with the lowest cost function is selected. Whilst this method is simple it is computationally inefficient and depends on multiple attempts with the user refining the resolution of the search space. For PCRTX design, zones of feasible solutions within the search space are small and easily missed.

To overcome these difficulties an algorithm called particle swarm optimisation (PSO) is used. This population based method was modelled on flocking or swarm behaviour in biological systems [Kennedy and Eberhart 1995]. Each member of the swarm is called a particle and moves around a multi-dimensional solution space R in search of an optimum. Each particle is assigned a position within the solution space $\vec{x}$ and a velocity $\vec{v}$. At every generation, numbered i, each particle evaluates its cost function or fitness value $f(\vec{x_i})$ at its current position x_i. The nature of each particle's movement is informed by the position where it achieved its personal best fitness value $\vec{pb}$ and the global best location amongst other particles within the swarm $\vec{gb}$. Mathematically this is expressed as

$$\vec{v}_{i+1} = w_1\vec{v}_i + c_1r_1(\vec{pb} - \vec{x}_i) + c_2r_1(\vec{gb} - \vec{x}_i) \tag{6.26}$$

where w_1, r_1 and r_2 are randomly generated constants between 0 and 1. These serve the purpose of adding more diversity into the movement of particles by changing the relative influence of the existing velocity, global best and local best.

At every generation the new position of each particle is calculated as

$$\vec{x}_{i+1} = \vec{x}_i + \vec{v}_{i+1} \tag{6.27}$$

This can be visualised as shown in Figure 6.3

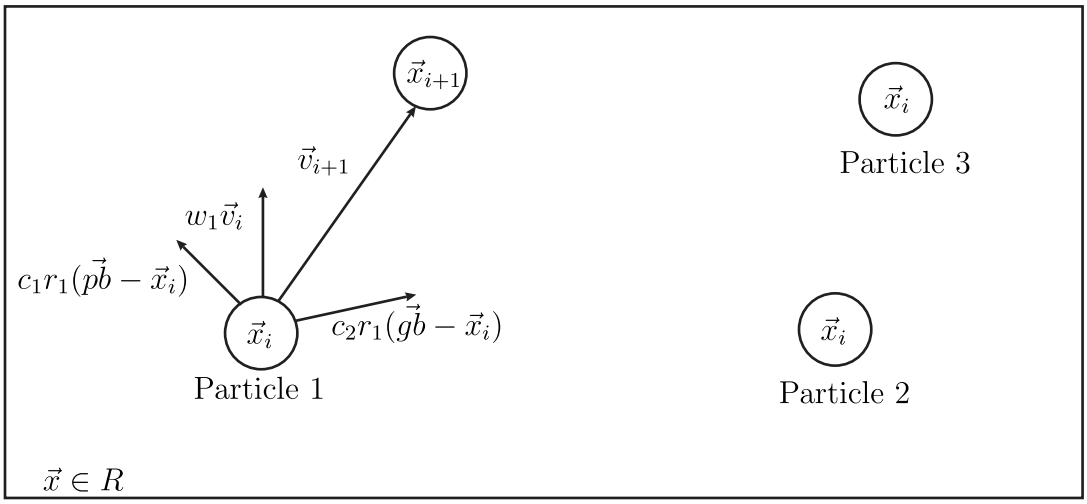

Figure 6.3 Visualisation of a small particle swarm

6.3.1 Swarm topology

One problem present in the traditional form of PSO is the premature convergence of particles to a local optimum [Bratton and Kennedy 2007]. One source of this problem is the swarm topology. This defines the way the global best $\vec{gb}$ is calculated. The simplest solution shown in Figure 6.4a is called the *gbest* topology, where the fitness values of all the particles in the swarm are compared to find the global best. Another possible solution is the *lbest* topology shown in Figure 6.4b where each particle only considers a pre-defined number of neighbouring particles k when determining the $\vec{gb}$ [Kennedy and Mendes 2002].

There are other more complex topologies that encourage different levels of exploration amongst the swarm [Mendes et al. 2004]. The method used here is the *lbest* or ring topology with each particle looking at its neighbour on either side to calculate its *gb*. By reducing the scope of the global best influence to localised regions around each particle the speed of information travelling through the swarm is slowed down. This leads to more exploratory behaviour by the particles. Eventually particles on the boundary between neighbourhoods start to pull the swarm towards the highest of the local best positions.

6.3.2 Re-initialisation

Another modification involves re-initialising particles with low fitness values. This makes it more viable to use a smaller population size due to the mix between evolved and

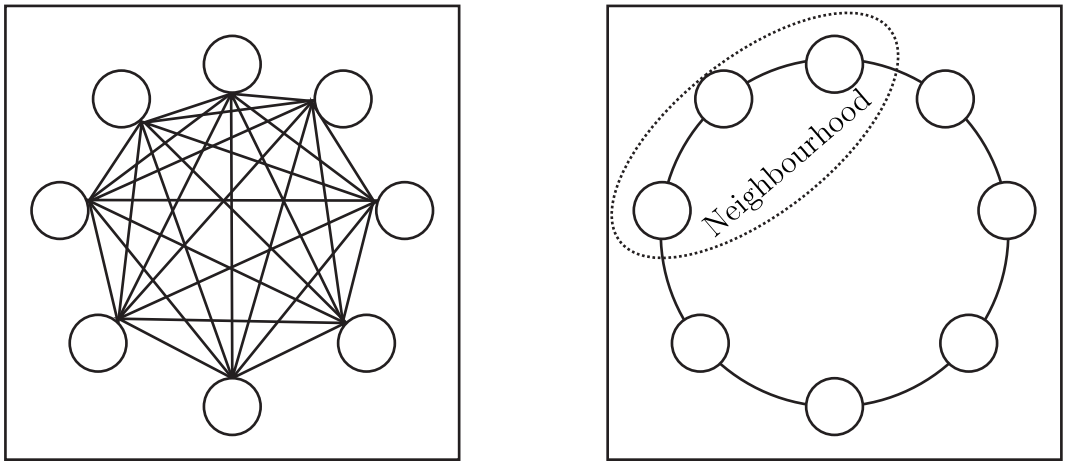

(a) Star or *gbest* topology

(b) Ring or *lbest* topology with neighbours

Figure 6.4 PSO topologies

randomly re-generated particles [Coello and Pulido 2005]. After a certain number of generations the solutions are ranked in order of fitness and the lowest ranking particles are reset to a random point within the solution space. The reset particles are allowed to retain their memory of their personal best and local best. This encourages exploration of the solution space by reset particles on their way back to the best positions they can remember from before the re-initialisation.

6.3.3 Velocity clamping

The speed at which a particle moves can also be detrimental to finding a global optimum. Without a constrained velocity, particles can oscillate wildly between extremes [Bratton and Kennedy 2007]. This risk is minimised by clamping the velocity of each degree of freedom to pre-set maximum or minimum values. There are formulas that can set velocity limits based on a definition of a solution space [Shahzad et al. 2009] but for this particular problem the limits are set manually based on knowledge of the specific engineering design problem. Table 6.5 shows a sample set of maximum and minimum velocities for each degree of freedom. For example the core length velocity is limited to 100 mm and the number of secondary layers can only change by 2. Velocities any higher than these values are likely to dramatically vary the constraint inputs such as $L_s, g0$, ignoring any feasible zones. These settings are chosen to allow fast convergence but ensure a particle thoroughly explores any path it travels on its way to an optimum.

6.3.4 Constraint handling

There are different ways to handle constraints within a PSO algorithm. The most commonly used method is the use of penalty functions to transform a constrained

optimisation problem to an unconstrained one [Parsopoulos and Vrahatis 2011]. This is done by adding a penalty to the fitness value of an infeasible solution that is proportional to the constraint violation. It has been shown that penalty functions do not perform well when the search space is highly constrained [Coello 2002] as is the case with optimising the PCRTX design.

The method used in this thesis has been used to solve optimisation problems with low population counts as demonstrated by Pulido and Coello [2004] and Fuentes Cabrera and Coello Coello [2007]. This is particularly important because the design process for PCRTXs used in this thesis requires repeated FEA simulations. The computational cost of using large swarm populations would be too high for a practical design solution. The constraints are included in the PSO process by changing how the fitness function is defined depending on the feasibility of the solution. The feasibility value of a particular inequality constraint $g_j(\vec{x})$ for a particle p is termed $g_{jp,feas}(\vec{x_p})$. This is a Boolean function defined as

$$g_{jp,feas}(\vec{x_p}) = \begin{cases} \text{True} & g_{jp}(\vec{x_p}) \leq 0 \\ \text{False} & g_{jp}(\vec{x_p}) > 0 \end{cases} \tag{6.28}$$

Likewise for the k'th constraint equation

$$h_{jp,feas}(\vec{x_p}) = \begin{cases} \text{True} & h_{kp}(\vec{x_p}) \leq 0 \\ \text{False} & h_{kp}(\vec{x_p}) > 0 \end{cases} \tag{6.29}$$

Both constraint values are set to zero if the constraint is not violated and remain the same if the constraint is violated, giving

$$g_{jp}(\vec{x_p}) = \begin{cases} 0 & g_{jp,feas}(\vec{x_p}) = \text{True} \\ g_{jp}(\vec{x_p}) & g_{jp,feas}(\vec{x_p}) = \text{False} \end{cases} \tag{6.30}$$

$$h_{kp}(\vec{x_p}) = \begin{cases} 0 & h_{kp,feas}(\vec{x_p}) = \text{True} \\ h_{kp}(\vec{x_p}) & h_{kp,feas}(\vec{x_p}) = \text{False} \end{cases} \tag{6.31}$$

The feasibility value of each particle $feas_p$ is true if and only if all constraints are met and all their feasibility values are true:

$$feas_p = \begin{cases} \text{True}, & g_{jp,feas}(\vec{x_p}) \ \& \ h_{kp,feas}(\vec{x_p}) = \text{True} \ \forall j,k \\ \text{False}, & \text{Otherwise} \end{cases} \tag{6.32}$$

The largest violation of a constraint across all n particles is referred to as G_j and H_k for inequality and equality constraints respectively. They are defined as

$$G_j = \max_{p \in \kappa^n} g_{jp}(\vec{x_p}) \tag{6.33}$$

$$H_j = \max_{p \in \kappa^n} h_{kp}(\vec{x_p}) \tag{6.34}$$

where κ^n is the space containing n particles. At every generation G and H are calculated to determine the maximum violation of each constraint across all particles in the swarm if their corresponding feasibility value is false. The fitness value or cost function of a particle $f_p(\vec{x_p})$ is calculated differently depending on its feasibility. If the particle meets all constraints and produces a feasible solution ($feas_p = \text{True}$) then its fitness value is simply the cost function defined in Section 6.2.1 as the total transformer mass. If one or more constraints are violated the fitness value is the sum of all the constraint violations normalised to the maximum population violations G_j and H_j.

$$f_p(\vec{x_p}) = \begin{cases} \text{Transformer Mass}, & feas_p = \text{True} \\ \sum_{j=1}^{b} \frac{g_j(\vec{x_p})}{G_j} + \sum_{k=1}^{c} \frac{|h_k(\vec{x_p})|}{H_j}, & \text{otherwise} \end{cases} \tag{6.35}$$

When a feasible solution is compared with a non-feasible solution the feasible solution is chosen. If two non-feasible solutions or two feasible solutions are compared the one with the lowest fitness value is chosen. This is a form of multi-objective optimisation which prioritises the feasibility of a solution before minimising a cost function. This results in the particles searching out feasible transformer designs that meet the specifications before searching out a solution that minimises transformer weight. An example of the three different scenarios for comparing two particles is given in Table 6.2.

Table 6.2 Constraint example

	Particle 1	Particle 2
Feasible	True	True
Fitness Value	500	300
Winner		√
Feasible	False	False
Fitness Value	0.5	1.8
Winner	√	
Feasible	True	False
Winner	√	

6.3.5 Algorithm

The PSO process is illustrated in Figure 6.5 and begins by randomly initialising a number of particles within the solution space. A unique transformer design is created from each particle's position and evaluated against the constraints. If the particle satisfies the constraints it is deemed feasible and its fitness value is the total transformer mass. If the design does not satisfy the constraints its fitness value is proportional to the amount by which it violated the constraints, normalised to the maximum constraint violation during that generation. The personal and local best values are determined and used to calculate particle velocities using Equation (6.26). Finally the velocities are added to the particle positions to determine their next position. This system encourages particles to look for feasible solutions before optimising the cost function. Particle velocities tend to start at large values and slow down as they converge to an optimal solution.

There is no theoretically proven definition of convergence for a PSO algorithm and methods that evaluate a convergence condition to halt the algorithm are highly empirical and subject to many assumptions [Ping Tian 2013]. Some simple methods involve stopping when particle velocities or the variance between their fitness values fall below a threshold [Clerc and Kennedy 2002]. There is no guarantee these methods will work for optimising PCRTX designs especially due to the highly constrained nature of the solution space. For the purposes of this thesis the PSO routine is set to run for a specified number of generations. The optimal solution is chosen based on the highest fitness value achieved by any particle during the routine.

6.4 EXAMPLE DESIGN

An example design is given for a practical use case. The design is for a PCRTX that can energise loads between 500 nF and 1 µF to 66 kV for 30 minute tests. Such a test kit would be used for performing PD testing on medium voltage cables. The available power supply is assumed to be a 400 V phase to phase connection with a nominal current rating of 40 A. This gives a minimum input impedance requirement of $Z_{in,min} = 10\ \Omega$. The specifications are given in Table 6.3.

The primary and tertiary windings do not contribute significantly to the total final mass of the transformer. Hence their dimensions are pre-defined based on availability instead of optimising. The primary is wound on the outside of the secondary which can increase its length significantly, so it is oversized by a large safety factor to prevent excessive losses. Both windings are wound using a 2.5 mm x 5 mm rectangular aluminium conductor. The insulation thickness between winding layers and the thickness of the former is set to match materials that are readily available. For this example, the interlayer insulation

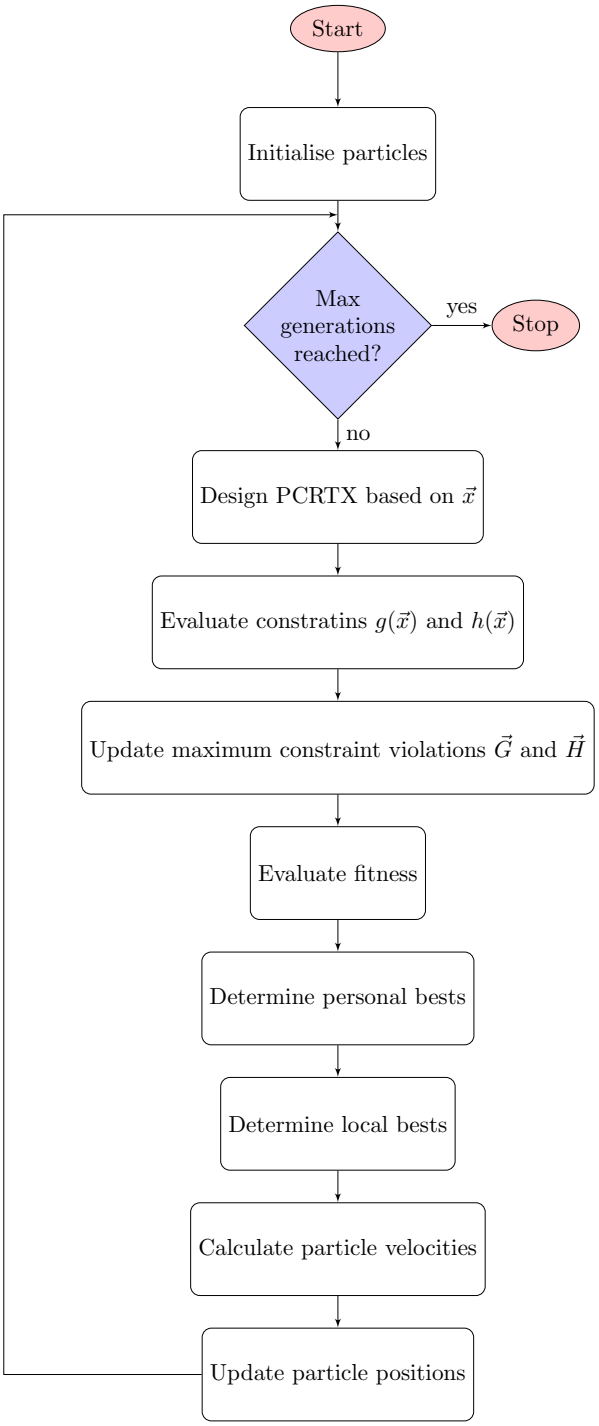

Figure 6.5 Particle swarm optimisation flowchart

thickness is set to 0.8 mm and the former thickness is 5 mm. The settings for the particle swarm optimisation are given in Table 6.4.

Velocity clamping is used to limit the speed of particle movement around the solution space. The settings are given in Table 6.5. Degrees of freedom that are sensitive to changes such as secondary wire diameter d_{ws} and the core maximum central gap ratio

Table 6.3 Design requirements

$C_{l,min}$	500 nF
$C_{l,max}$	1 µF
$Z_{in,min}$	10 Ω
V_{in}	400 V
V_l	66 kV
$I_{in,rated}$	40 A
t_{on}	30 mins

Table 6.4 PSO settings

Number of Particles	5
Number of particle neighbours	2
Re-initialisation generations	30
Number of particles re-initialised	2
Equality constraint tolerance	5%

$l_{cg,max}$ are given small limits to prevent wild oscillations in their movement.

The convergence behaviour of the algorithm was confirmed by comparing a sample set of different results with a brute force grid search conducted over the same solution space. Both methods produced the optimum solution but the PSO algorithm was generally able to reach this value in fewer iterations.

6.5 RESULTS

The PSO routine was applied to determine the change in optimum transformer weight as the number of stages in a cascade arrangement of PCRTXs is increased. Using the same load and supply specifications described above, a separate PSO routine was conducted for different numbers of cascaded PCRTX stages.

The first case considered was that of a single PCRTX test kit with two windings. The change in local best fitness value of each particle as the optimisation progresses is shown in Figure 6.6a. The plot shows the constraint handling process at work. At the beginning of the routine the values are close to zero because during this interval a feasible solution has not been found. As soon as a feasible solution is found the other particles move towards that location. After all particles have found a feasible solution

Table 6.5 Velocity clamping settings

x	l_c	r_{c1}	N_{ls}	$l_{cg,max}$	d_{ws}
v_{max}	100	10	1	0.09	0.5
v_{min}	-100	-10	-1	0.01	-0.5

the local best value will only change when a lighter transformer design is found. At any given generation there are three unique local best values. This is due to the ring topology where each of the five particles has $k = 2$ neighbours giving three unique neighbourhoods.

The same optimisation procedure was repeated while changing only the number of stages connected in cascade from two to four stages and using the same specifications. After initially searching for a feasible solution, good convergence of the three neighbourhood local best values was observed as shown in Figure 6.6.

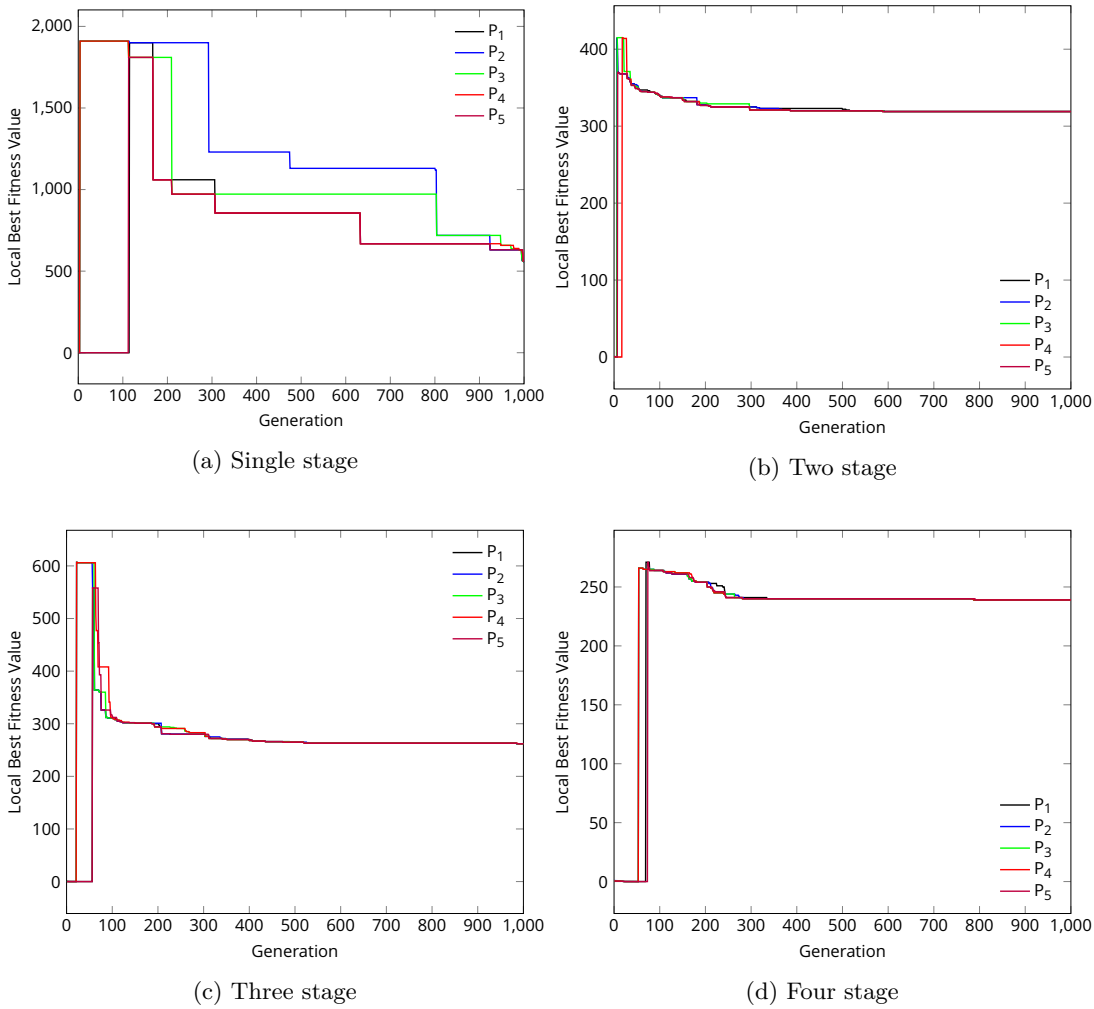

(a) Single stage

(b) Two stage

(c) Three stage

(d) Four stage

Figure 6.6 PSO local best fitness value for cascaded PCRTX optimisation

Detailed results for the four different stage numbers are tabulated in Table 6.6. For all stage configurations the values of the B_{max} and $|Z_{in,gmax}|$ settled at close to their minimum constrained value of 1.2 T and 10 Ω. This indicates that the optimisation process was successful in pushing the design to its limits. A lower secondary voltage on each stage corresponds to a lower peak flux density. This has been exploited by the PSO routine to reduce weight by reducing the radius of the core until the value of B_{max}

is just acceptable.

The value of $Z_{in,g0}$ reduces as more stages are added. This is because each new stage adds another set of transformer losses that dampen the resonant peak of the tuned circuit. The optimisation routine has maintained a value of $Z_{in,gmax}$ just above the specified minimum while trading off reductions in $Z_{in,g0}$ to save weight. This is difficult to do manually with a trial and error process. This has been achieved via a steady reduction in the maximum core central gap as more stages are added.

Table 6.6 Single stage PSO optimum design outcome

Parameter	1 Stage	2 Stage	3 Stage	4 Stage
l_c, mm	477	479	528	507
r_{c1}, mm	145	115	102	93.1
N_{ls}	28	25	20	21
d_{ws}, mm	2.16	2.29	2.44	2.71
$l_{cg,max}$, mm, (%)	185, (38.9%))	107, (22.3%)	90.3, (17.1%)	83.6, (16.5%)
$L_{s,max}$, H	20.3	10.1	6.76	5.07
$L_{s,g0}$, H	20.1	10.1	6.73	5.01
$L_{s,min}$, H	10.01	5.01	3.38	2.53
$L_{s,gmax}$, H	9.12	5.10	3.63	2.53
l_{ws}, mm	389	342	381	362
B_{max}, T	1.16	1.19	1.20	1.20
$\|Z_{in,g0}\|$, Ω	50.14	36.6	35.2	29.83
$\|Z_{in,gmax}\|$, Ω	10.12	10.1	10.01	10.01
m_c, kg	238	150	130.4	104.3
m_w, kg	192	138	115.3	125.3
$f(\vec{x})$, kg	517	318	261.8	239.1

The required tuning ranges have been achieved by each stage within the specified tolerance of 5%. The secondary winding diameter shows a steady increase from 2.16 mm to 2.71 mm as more stages are added. This is above the minimum required diameter to operate under full rated conditions for the specified duty cycle. The optimisation process has done this to reduce the winding resistance as more stages are added to achieve the minimum $|Z_{in,gmax}|$. This indicates that when more stages are added to a cascaded connection, the total winding wire length traversed by the load current is longer. For example when moving from one to two stages the load voltage is shared amongst two secondary windings, this does not mean that they require half the number of turns as the single stage. In a PCRTX many secondary winding turns are still required to provide the necessary ampere turns and create the correct inductance for tuning to the load capacitance.

Optimal stage number

The question still remains as to what is the optimal number of stages to use for a cascaded PCRTX. A plot of stage weight reduction against the number of stages is presented in Figure 6.7. For this example there is a significant stage weight decrease of 43% between a single stage PCRTX and a two stage cascade. The unit weight reduction is less significant as more stages are added.

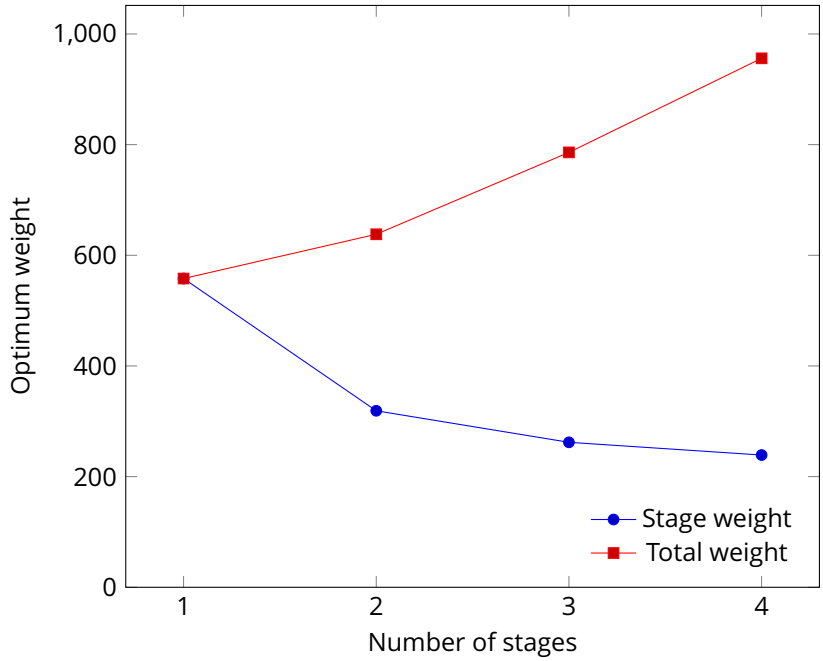

Figure 6.7 Lowest optimised stage weight for a different number of cascaded PCRTX stages

The total weight of a two stage cascade is 14% greater than a single stage PCRTX. Given the significant manufacturing costs associated with making multiple PCRTXs the material cost savings alone are not enough to justify using a cascaded system over a single stage. The benefits of cascaded transformers are only apparent when they are used to meet a specific voltage rating with transportability and modularity as important factors instead of cost and weight savings.

6.6 CONCLUSION

An optimisation routine was developed and used to design a cascaded partial core resonant transformer that met a set of constraints. The routine used particle swarm optimisation to optimise five design parameters from which a complete transformer or cascade can be simulated. These parameters were the core dimensions (length and radius) the secondary winding layers and wire diameter, and the maximum central core gap. The optimisation was limited by a set of constraints to ensure the design met the

required tuning range, maximum core flux density and minimum input impedance. The PSO routine included a constraint handling mechanism to guide the search towards feasible solutions before optimising for transformer weight. The algorithm was used to optimise PCRTX designs to meet a 66 kV load voltage and 500 nF to 1 µF tuning range. The number of cascaded stages specified was varied between 1 and 4 and the algorithm successfully converged within 300 and 1000 generations for each trial. It was found that the optimal stage weight reduces with every extra cascaded stage but this trend diminishes dramatically. The optimum unit weight for a single stage PCRTX was 517 kg compared with 262 kg for a three stage cascade.

Chapter 7

PROTOTYPE DESIGN AND CONSTRUCTION

7.1 OVERVIEW

A new prototype set of cascaded partial core resonant transformers was designed and built based on the results of the optimisation procedure presented in Chapter 6. This chapter details the design and construction of this set of transformers. The test kit consisted of two identical three winding 33 kV PCRTXs designed to be used in cascade. Design details are presented for hybrid cores using radial and parallel laminated sections to reduce core losses. The tuning system is described along with the winding method and lead out design. The design and construction of a new inter winding insulation system utilising vacuum resin infusion is outlined.

7.2 DESIGN PARAMETERS

The test kit was designed to perform two industry standard high voltage tests on medium voltage cables. The first is a voltage withstand test where the test voltage varies from between 1.5 U_0 to 3 U_0 [IEEE Std 400 2012]. The second is a partial discharge test where the voltage is raised only slightly above the rated voltage but test durations can be up to 30 mins [IEEE Std 400.3 2006]. A reasonable medium voltage cable capacitance was estimated at between 500 nF and 1 µF based on consultation with a local utility. A test voltage of 66 kV was chosen to comfortably perform phase to earth voltage withstand tests over 3 U_0 on 33 kV cables and PD tests up to 1.5 U_0 on 66 kV cables. The available power supply was assumed to be a 400 V three phase supply with a nominal current rating of 40 A.

7.3 CORE

Partial core transformers generally have higher magnetising currents than full core transformers due to the presence of the surrounding air in the flux path [Bell and Bodger

2008b]. They also have plenty of radial flux spilling from the end windings [Lapthorn et al. 2013] which cuts the usual parallel core laminations at steep angles producing planar eddy currents. The motivation to use radial cores for this design is due to the longer operating times desired for PD testing and to investigate the impact on the test kit's performance.

A single radial core section was built and trialled in an existing PCRTX [Bell 2009]. Thermal imagery of the core showed an approximately 30 °C difference in the operating temperature of a radial core section compared to a parallel core section. A copy of the image is shown in Figure 7.1 where the parallel laminated core in the fore ground is at a higher temperature compared to the radial core in the background which is cool enough to appear black.

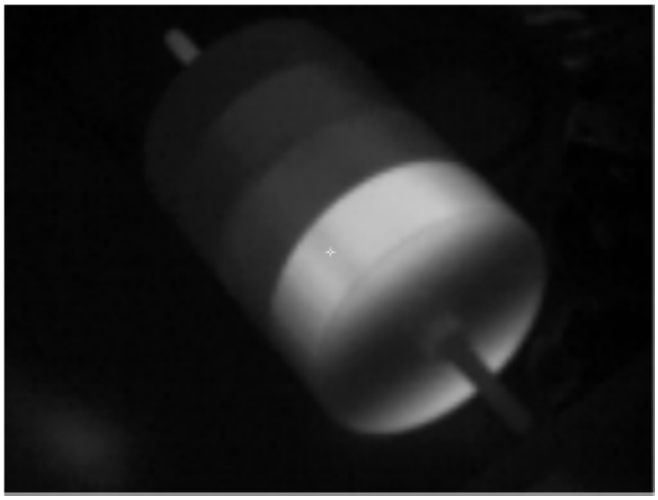

Figure 7.1 Thermal image of three parallel laminated and one radially laminated core section located towards the top of the photo after 12 minutes of operation [Bell 2009]

The partial cores built for this design were constructed in four sections for each stage transformer. Four of the sections were stacked using radial laminations and the other four were built using parallel laminations. A computer model was built to calculate the required sizes for both types of laminations. The specifications for the final design are given in Table 7.1. Two important factors in the viability of radially laminated cores were the available widths of core steel and the cost and time involved in cutting the steel.

7.3.1 Parallel laminated core

Parallel laminations are stacked in rectangular steps to approximate a circular shape. A larger number of steps means a better utilisation of the core cross section but this increases manufacturing cost and difficulty. The core was designed with a simple stacking

formation using 16 steps as shown in Figure 7.2. This arrangement achieved a stacking factor of 0.96.

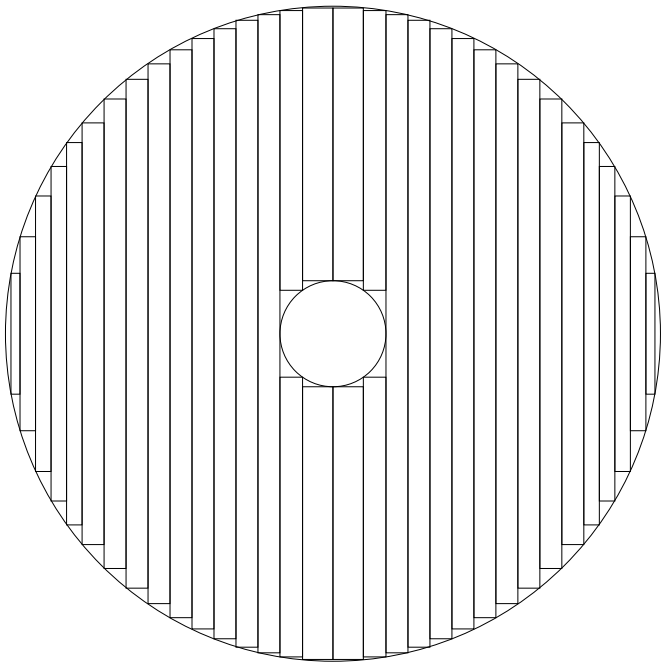

Figure 7.2 Parallel laminated core stacking arrangement

Table 7.1 Core design parameters

Material type	Grain oriented silicon steel grade 23080	
Parameter	Parallel laminations	Radial laminations
Core sections per stage	4	4
Core length	300 mm	300 mm
Core section length	75 mm	75 mm
Core outer radius	116.5 mm	116.5 mm
Core inner radius	10 mm	14.5 mm
Lamination thickness	0.23 mm	0.23 mm
Stacking factor	0.96	0.85
Number of blocks per section	36	382
Laminations per block	47x1, 34x10, 24x4, 14x1	7
Laminations per section	1156	2674
Total weight	100 kg	109 kg

7.3.2 Radially laminated core

Radial laminations are stacked in wedges that approximate a sector of the circle as shown in Figure 7.3. The exterior and interior wedge circumferences c'_{c1} and c'_{c2} are given by the corresponding core circumferences c_{c1} and c_{c2} divided by the number of

wedges N_{cw}.

$$c'_{c1} = \frac{c_{c1}}{N_{cw}}, c'_{c2} = \frac{c_{c2}}{N_{cw}} \tag{7.1}$$

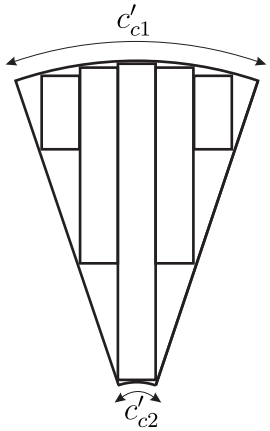

Figure 7.3 Radial lamination wedge

The interior circumference of this section c'_{c2} is approximately the lamination thickness l_t

$$c'_{c2} \approx l_t \tag{7.2}$$

It is assumed the wedges will be stacked with a wedge stacking factor of sf_w to account for manufacturing tolerances and lamination insulation. The number of wedges per core section is calculated as

$$N_{cw} = \lfloor \frac{c_{c2} sf_w}{l_t} \rfloor \tag{7.3}$$

By the same rationale, the number of laminations that can fit into a single wedge N_{lpw} is given by

$$N_{lpw} = \lceil \frac{c'_{c1}}{l_t} \rceil \tag{7.4}$$

By re-arranging and substituting the approximation for the inner radius in Equation (7.2) into Equation (7.4)

$$N_{lpw} = \lfloor \frac{c'_{c1}}{c'_{c2}} \rfloor \tag{7.5}$$

By substituting Equation (7.1) into Equation (7.5) and replacing the circumference measurements with the core radii the number of laminations per wedge is calculated as

$$N_{lpw} = \lfloor \frac{r_{c1}}{r_{c2}} \rfloor \tag{7.6}$$

A better utilisation of the core cross section can be achieved by making the wedge asymmetrical so that neighbouring wedges interlock. This involves reducing the length of laminations on one side of the wedge and increasing the length of laminations on the other side. This is illustrated in Figure 7.4 where the lamination thickness is exaggerated to show how adjacent wedges interlock with each other.

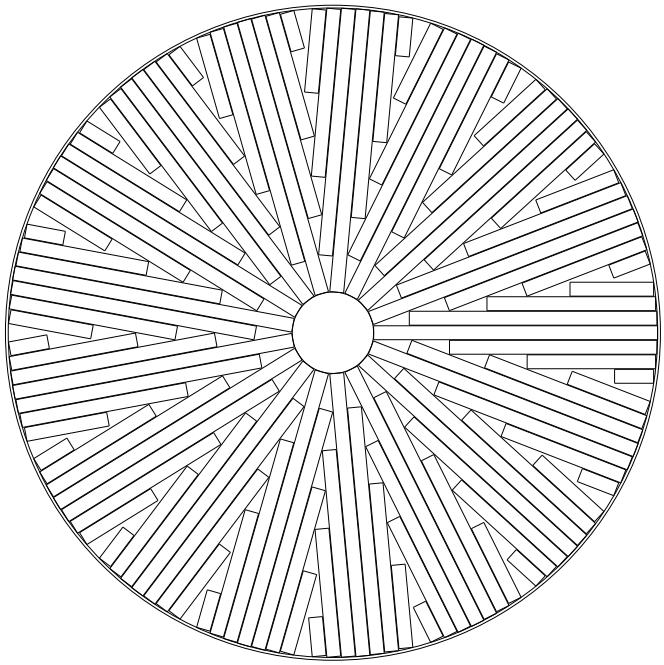

Figure 7.4 Example radially laminated core stacking arrangement with stacking factor of 0.84

The central lamination within a wedge has a length given by

$$l_{l0} = \sqrt{r_{c1}^2 - \left(\frac{l_t}{2}\right)^2} - r_{c2} \tag{7.7}$$

For each lamination either side of the central lamination the required length was calculated computationally using the pseudo code representation shown in Algorithm 7.1. The laminations are numbered from the longest to the shortest, starting from 0, where l_{li} is the length of the i'th lamination in the wedge. The angular size of each wedge is expressed as θ_w.

7.3.3 Construction

The laminations were cut at a local transformer manufacturing plant. First a 250 mm roll of steel was slit into smaller rolls of the required thickness of 75 mm. These were cut to different lengths using an automated steel cutting machine. There was a difference in cost, cutting time and construction time between the radial and parallel laminations. The parallel laminations require more lengths of laminations to approximate a circle.

Algorithm 7.1 Radial lamination length calculations

for i $\leftarrow$ 1 to N_{lpw} **do**
$\alpha \leftarrow \text{floor}((i+1)/2)$
$\beta \leftarrow \text{ceil}((i+1)/2)$
$x_1\ gets \frac{l_t((1/2+\alpha)+(-1/2+\beta)}{\cos(\theta_w))\tan(\theta_w)}$
$x_2 \leftarrow \sqrt{r_{c1}^2 - (l_t(-1/2+(1+\alpha))^2}$
$l_{li} \leftarrow x_2 - x_1$
end for

This translated to an added cutting cost due to the number of manual changeovers required on the cutting machine. The radial laminations only required seven different lengths of steel to be cut. The final lamination lengths and quantities required for a single core section are shown in Table 7.2.

Table 7.2 Lengths and quantities of laminations for parallel and radially laminated cores

Parallel Core		Radial Core	
Length	Quantity	Length	Quantity
97.0	188	102.0	382
99.5	136	87.5	382
227.0	68	73.0	382
223.0	68	58.0	382
217.0	68	43.5	382
210.0	68	29.0	382
202.0	68	14.5	382
192.0	68		
181.0	68		
167.0	68		
150.0	68		
136.0	48		
119.0	48		

For practical reasons the 250 mm wide roll of steel from the manufacturer was slit to the required width and cut to the required lengths as shown in Figure 7.5. This meant that the rolls were slit in the same direction as the grain and cut to the required lengths in a direction perpendicular to the grain.

As a result both types of core sections had their laminations stacked with the grain oriented perpendicularly to the direction of magnetic flux in the center of the core as shown in Figure 7.6. The radial flux at the ends of the core will flow parallel with the grain. This is not optimal for the two central core sections but proved to be the most practical method available due to the mechanism and constrained availability of the steel cutting machinery. An alternative would involve slitting the manufactured roll to the required lamination lengths and cutting to the required width. This would only be worthwhile for radial laminations as there are fewer changes in lamination length

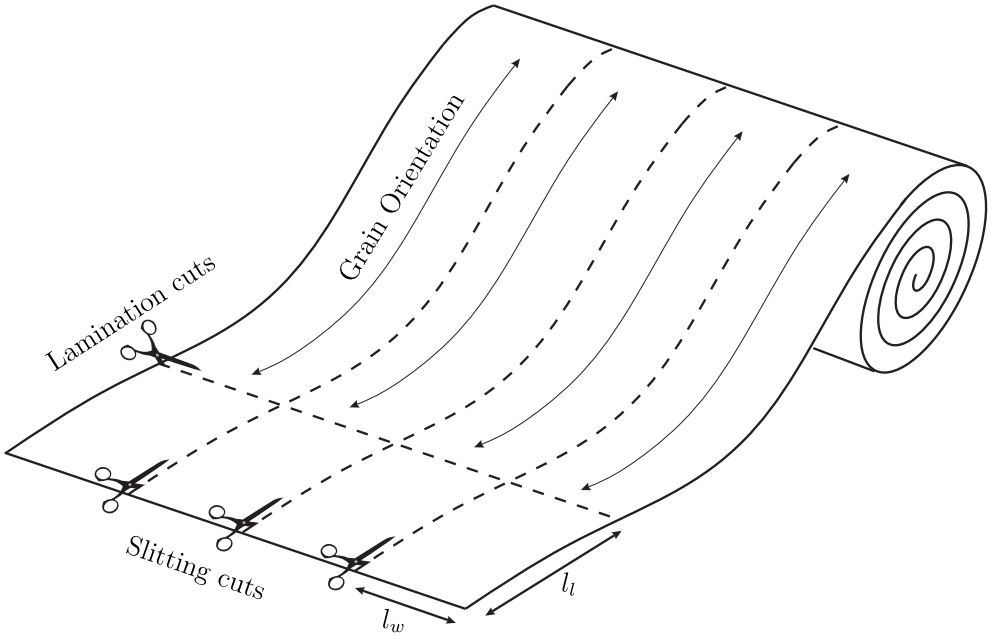

Figure 7.5 Cutting and slitting directions from steel roll

required.

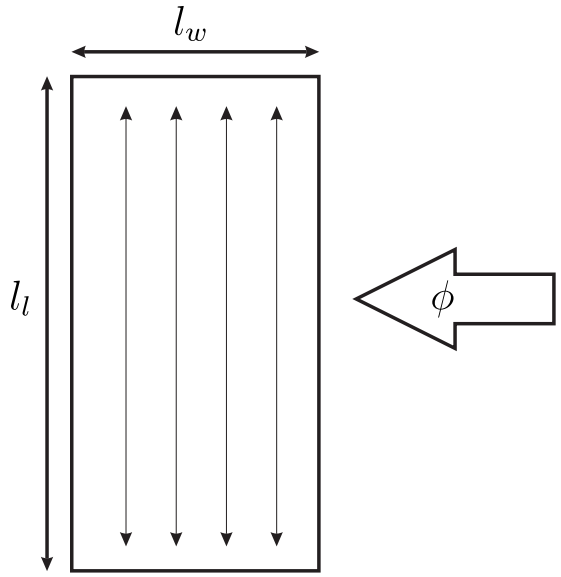

Figure 7.6 Grain orientation of the laminations relative to direction of magnetic flux ϕ in the center

All eight core sections were stacked manually within a nylon mould. Each radially laminated core section required a full working day for stacking. All four parallel laminated cores could be stacked in less than a working day. After stacking, the laminations were encased in a two part epoxy resin [West System 2014] and taped with impregnated fibreglass once they were removed from the mould. The completed cores and sections are shown in Figures 7.7 to 7.9.

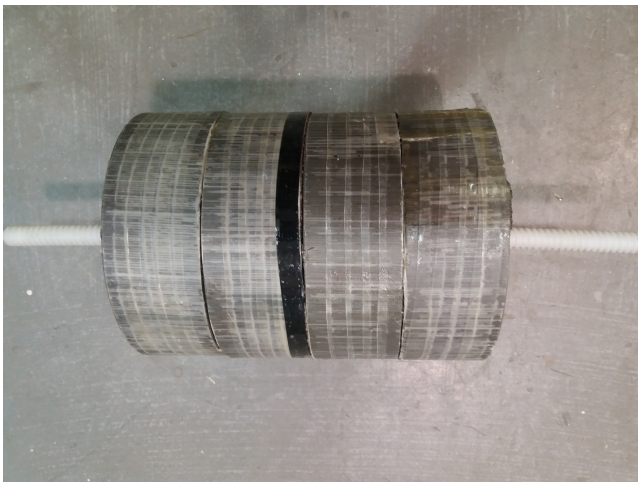

Figure 7.7 Completed core sections

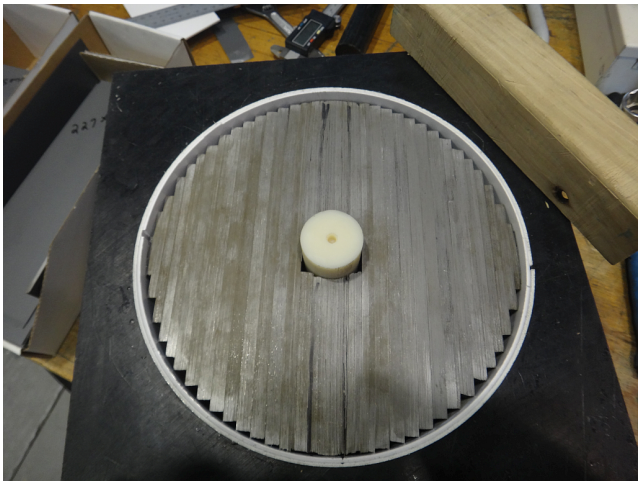

Figure 7.8 Parallel laminated sections

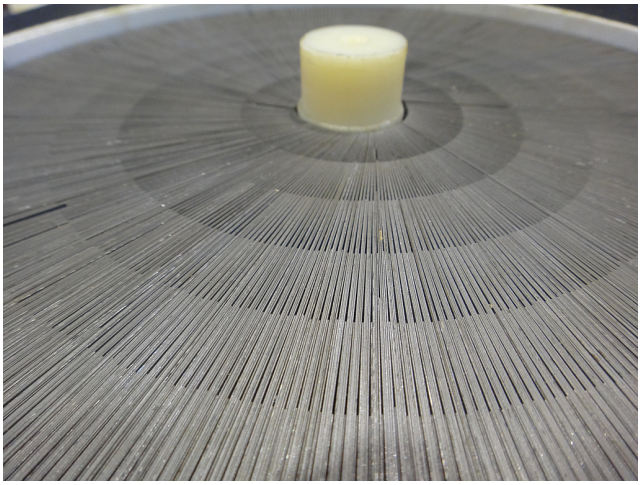

Figure 7.9 Radially laminated sections

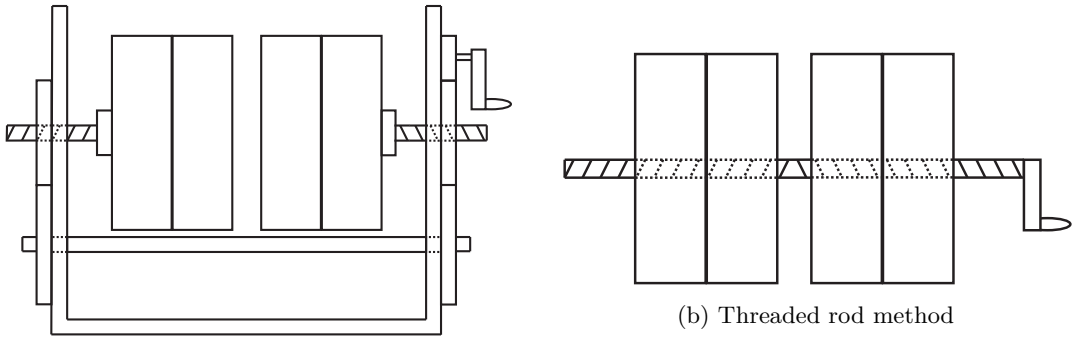

(a) Resin bonded method

(b) Threaded rod method

Figure 7.10 PCRTX tuning systems

7.4 TUNING SYSTEM

The tuning system employed for this transformer is central core gap variation. This allows for axially symmetrical magnetic forces within the core. This can be achieved in two ways.

A prototype transformer constructed for a commercial client used a resin bonded core gap separator. This system was designed by Fabrum Solutions, a local composite fabrication company. It involves bonding threaded fibreglass rods to each core sections so they can be pulled apart and held in position during testing. The advantage of this system is that it does not require any central hole in the transformer core as shown in Figure 7.10a. The disadvantage is that it requires detailed mechanical design and reduced portability because there cannot be more than two core sections.

The system used in this thesis involves a simpler method used by Bell [2009]. The core sections were built with a small hole in the center and separated by internal nylon spacers. A threaded axial clamping rod with polymer nuts clamps all the core sections together to minimise vibration. This method is less affected by magnetic forces but for safety reasons does not enable the PCRTX to be tuned on-line. A simple modification to enable on-line tuning involves using a threaded rod with opposing threads on either side of the axial center. The two central core sections would have threaded inserts bonded into their central holes as illustrated in Figure 7.10b.

7.5 FORMER

A G10 fibreglass former was used because of its relative strength, low weight and insulating properties. The former has to bond with the encapsulant to ensure there are no voids around the innermost winding layer. This also gives the windings added strength and prevents de-lamination of the insulation. The encapsulant used in this design is a proprietary infusion resin that bonds well with the G10 fibreglass former.

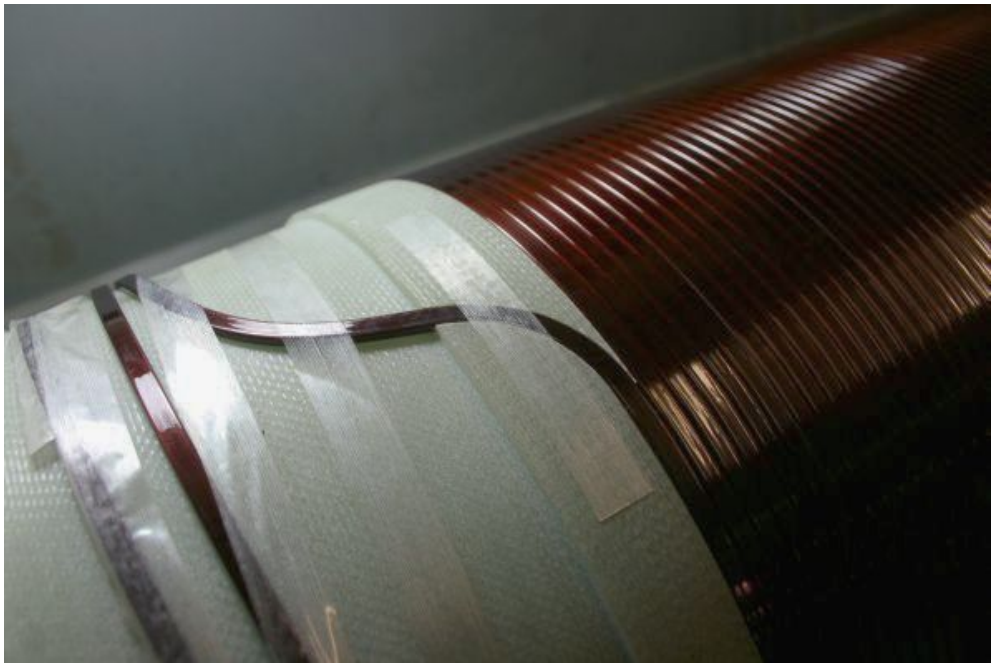

Figure 7.11 Fibreglass former with recessed tertiary winding and lead-out

The tertiary winding was wound first on the former. This winding has a shorter axial length than the secondary winding which was wound on top of it. To provide a solid surface on which to wind the secondary winding a small recess was cut into the former for the tertiary winding, leaving a flush surface for the secondary winding. The recess was cut using a five axis milling machine in the shape of the helical winding as shown in Figure 7.11. The recess provides additional axial support to the tertiary winding.

7.6 WINDINGS

Helical windings were chosen for this design due to their simplicity for winding without specialist machinery. The design parameters for the windings are listed in Table 7.3. The windings were wound with magnet wire on a speed controlled lathe machine with mass loaded tensioner. No additional insulation was used between turns because of the negligible inter turn voltage. Due to the generous secondary winding wire diameter of 1.6 mm the corresponding enamel insulation thickness was deemed enough to prevent turn to turn failures.

7.6.1 Wire joints

Due to the wire length of the secondary winding and the limited wire length of a standard roll of copper wire, multiple joins were required to achieve the desired number of turns. The joins had to be strong enough to hold the wire tension and insulated

Table 7.3 Transformer winding design parameters

Parameter	Primary	Secondary	Tertiary
Voltage Rating, V	400	33,000	400
Shape	Rectangular	Circular	Rectangular
Dimensions, mm	2.5 x 5	1.6 (D)	2.5 x 5
Wire insulation, mm	0.1	0.05	0.1
Axial length, mm	275.6	312.8	275.6
Radial thickness, mm	2.7	59.2	2.7
Turns	53	4416	53
Layers	1	24	1
Interlayer insulation, mm	-	0.8	-
Material	Aluminium	Copper	Aluminium
Wire length, m	41.6	4350	62.7
Weight, kg	1.4	78.3	2.12

adequately to prevent the formation of a void in the encapsulant or an inter turn failure. A simple rig was made to join the wires from two spools using two hollow stainless steel tubes. Both tubes were cut at an angle to increase the surface area of the join as shown in Figure 7.12. Silver solder was applied to the join assisted by capillary action from the tubes. The join was finally coated in multiple layers of enamel to match the insulation on the rest of the wire and placed within a strip of Nomex tape for extra inter turn insulation as shown in Figure 7.13.

Figure 7.12 Soldered secondary winding wire join

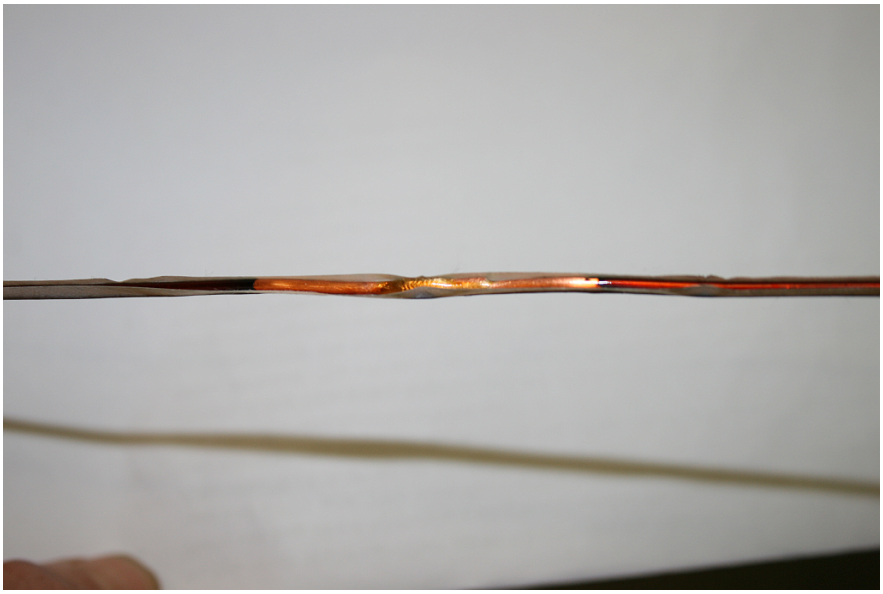

Figure 7.13 Enamel coated and Nomex tape wrapped secondary winding wire join

7.6.2 Lead-outs

The lead-outs were positioned to enable the HV end of the secondary to be connected to the tertiary winding using a linking bar. The location of this secondary HV connection was designed to be kept separate from the grounded side of the secondary winding as shown in Figure 7.14. The primary winding is wound on the outside of the secondary and the leads exit tangentially to the transformer. The primary lead-outs are well separated from the HV electrodes of the transformer.

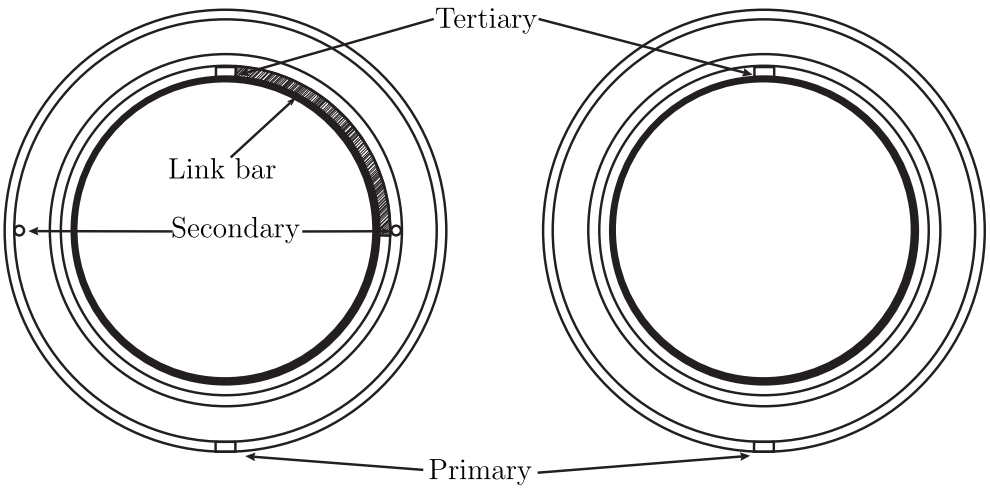

Figure 7.14 Diagram of transformer lead-outs

7.7 INSULATION SYSTEM

Transformers can be insulated using solid, liquid and gaseous insulation. Oil could not be used as an insulating material in this design due to the difficulty of transporting oil insulated transformers by plane. The extra material handling safety requirements make it impractical for use in portable test equipment. Transformers using gaseous insulation such as SF6 are gaining popularity worldwide due to their lower weight and fire risk. This was discounted because it requires additional design of a transformer tank that serves as a pressure vessel and additional facilities to fill and process the gas regularly. A solid insulation system was chosen for this design due to the ease of transportation and simplicity of construction.

7.7.1 Design

The design challenge presented by solid insulation involves finding the right combination of inter-winding insulation and encapsulant. The inter-winding insulation system needs to provide a rigid structure for the windings and also allow the encapsulant to flow throughout the winding layers without leaving any voids. The encapsulation system needs to bond with the interlayer insulation and impregnate it completely leaving a uniform insulating material between two winding layers.

Previous PCRTX designs have used sheets of Nomex-Mylar-Nomex for the interlayer insulation and an elastomeric polymer called Sylgard for encapsulation [Bell 2009]. The windings were encapsulated under vacuum to remove air voids. The problem with this design was that it was impossible to know for sure if voids had been adequately removed from the windings. On a failed transformer prototype it was found that the Sylgard had not completely penetrated axially between the secondary layers as shown in Figure 7.15.

Within PCRTXs the most likely location for these voids is between layers of windings. The lack of axial flow of the encapsulant creates small air voids between the interlayer insulation and the windings as shown in 7.16.

Recent research with superconducting partial core transformers resulted in a system to allow axial and radial flow of coolant [Lapthorn 2012]. This was composed of sheets of G10 fibreglass with grooved channels as shown in Figure 7.18. These grooves were machined using a CNC mill. The same system was used in a recent PCRTX design for a commercial client along with an infusion resin as the encapsulant. The advantage of this system is that it was able to guarantee a negligible number of voids in the winding insulation. The disadvantage was that it was expensive due to the large amount of CNC milling required to produce the insulating sheets.

The design used here trialled a simpler way to make slatted G10 sheets to allow resin

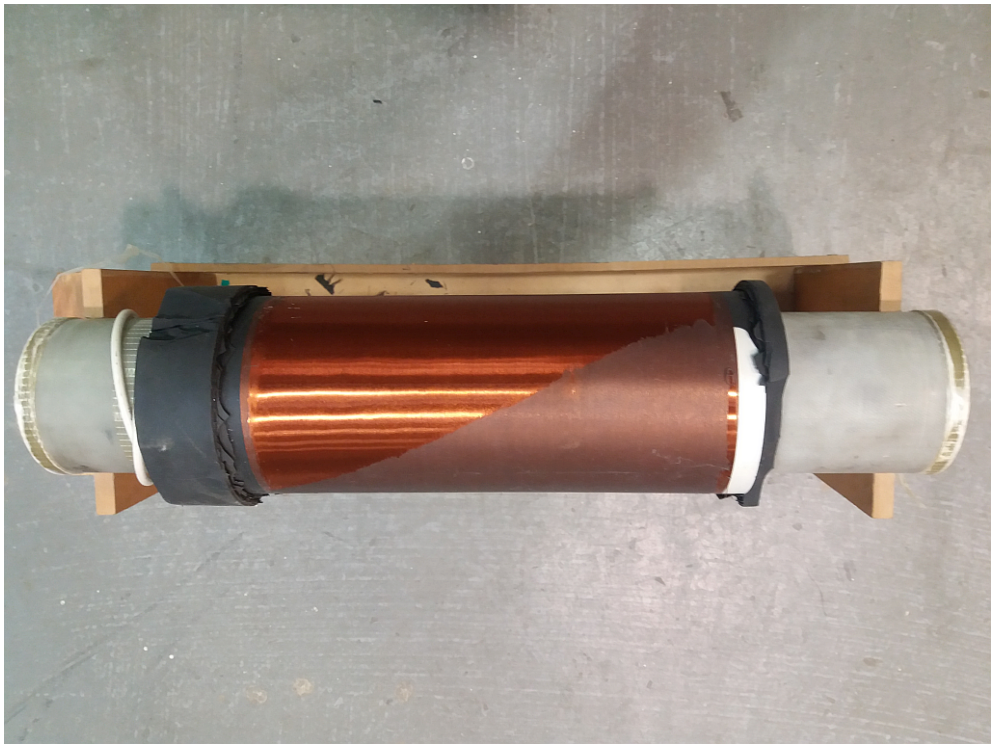

Figure 7.15 Incomplete penetration of interlayer encapsulant on a failed PCRTX

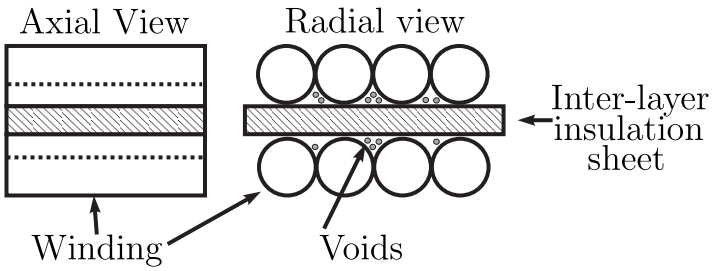

Figure 7.16 Void locations in inter-layer insulation

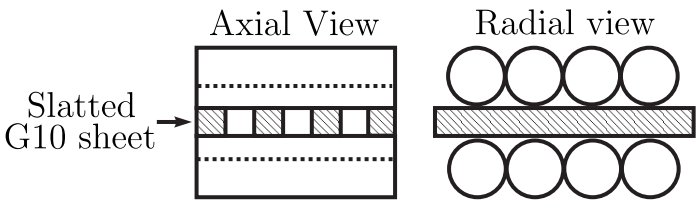

Figure 7.17 Axial channels to aid interlayer resin flow

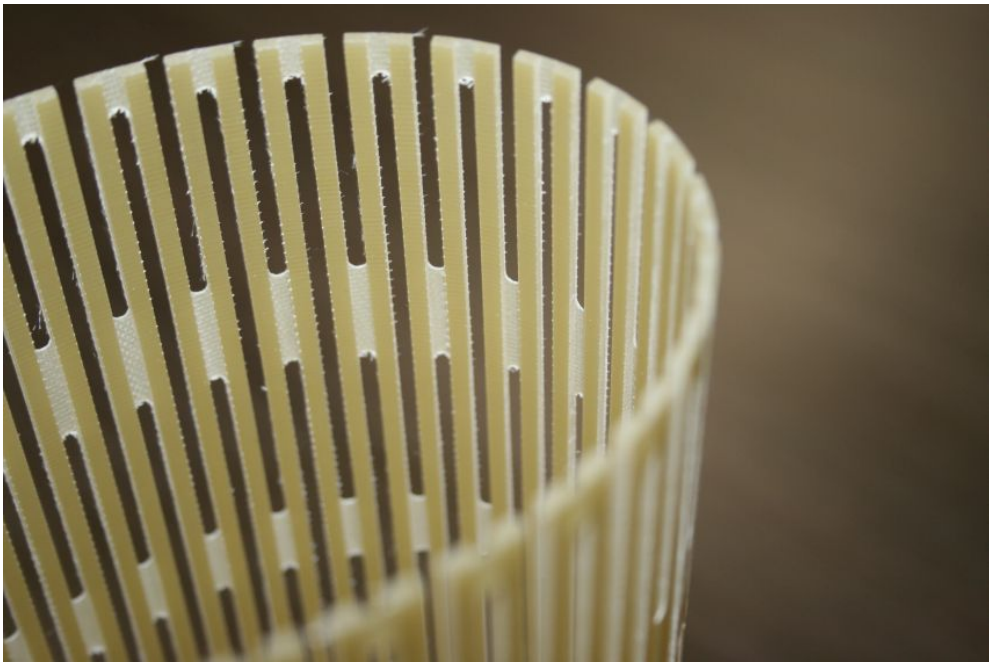

Figure 7.18 Milled G10 interlayer insulation sheets

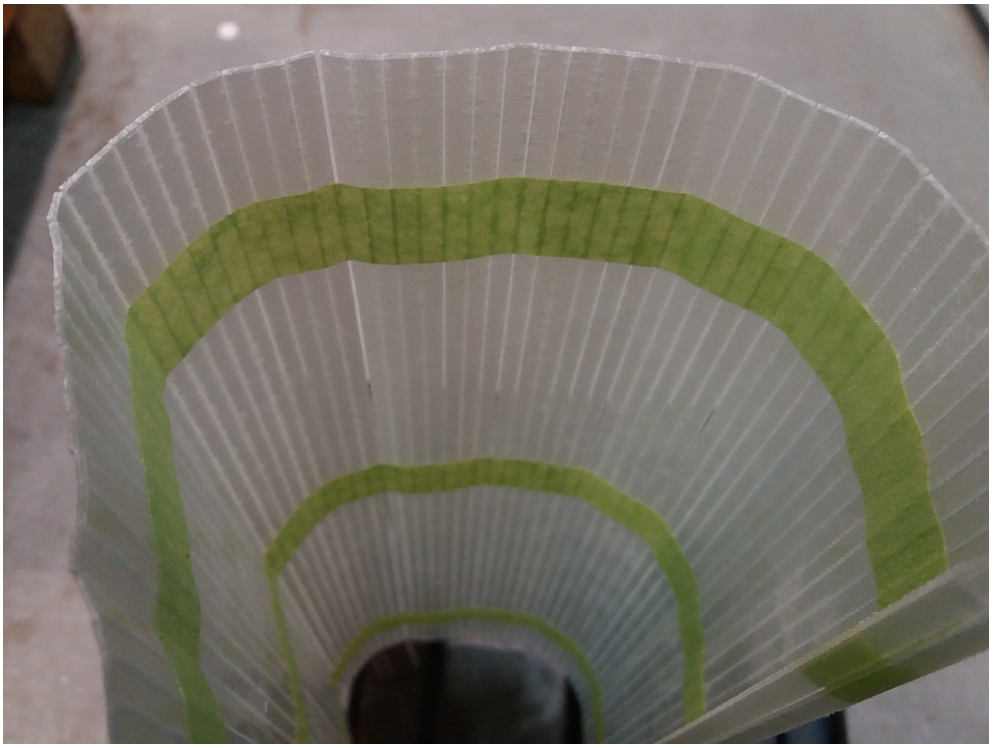

Figure 7.19 Water-jet cut G10 interlayer insulation sheets

to flow axially between winding layers. The G10 sheets were cut into small strips using a water jet instead of milling. These strips were then held together with Nomex tape leaving axial channels to aid resin flow as shown in Figure 7.17. The end result was a connected series of G10 strips separated by small gaps and held together by Nomex tape Figure 7.19. This reduced the manufacturing time and hence the cost of the interlayer insulation.

7.7.2 Construction

The finer details of the encapsulation process is the proprietary information of a local manufacturer. Generally it involved infusing the winding assembly with resin under a time varying profile of pressure and temperature. Before winding the coils, two end flanges were glued onto the former at either end of where the secondary winding would be wound. Figure 7.20 shows the G10 inter-layer insulation along with one of the end flanges. After the secondary winding was wound a fibreglass cylinder was fitted and glued around the entire winding assembly. At this stage the transformer itself functioned as a pressure vessel and dried for hours under cyclic heat and pressure before the resin was vacuum fed into the winding assembly. The resin was allowed to continuously run through the windings to ensure there were no voids present. Finally the encapsulated winding assembly was left to cure in an oven.

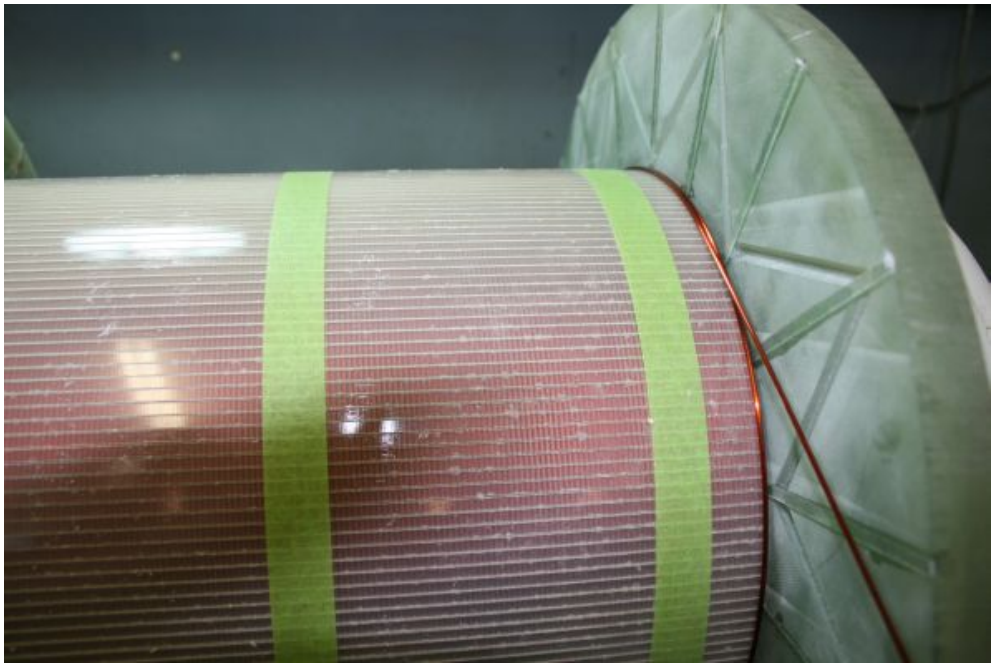

Figure 7.20 G10 interlayer insulation and end-flange

The end flanges had a series of holes and grooves carved into them to aid the flow of resin and allow the exit of the secondary and tertiary lead-outs. This method requires

a precise calculation of the axial winding length of the secondary and tertiary windings. This length defines where the flanges are fixed before the secondary winding is wound and also determines the size of the G10 sheets used for interlayer insulation. This distance was slightly miscalculated during design and as a result small strips of G10 had to be inserted radially around the end flanges to stop the end windings slipping onto the lower layer as shown in Figure 7.21. The two finished prototype stages are shown in Figure 7.22.

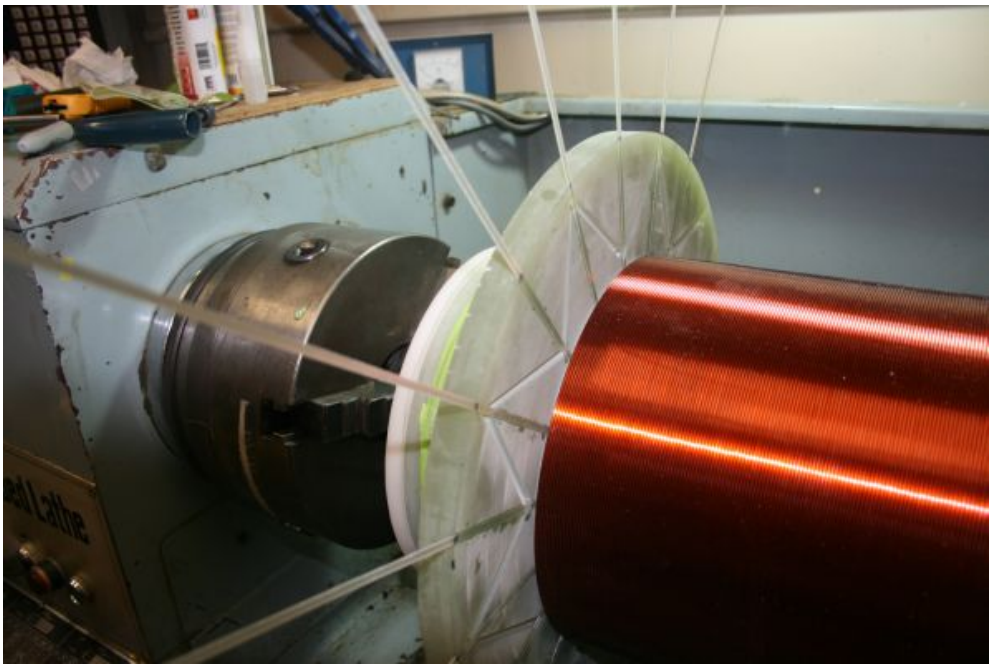

Figure 7.21 Radial G10 packing strips to secure end windings

7.7.3 Evaluation

While cheaper and less time consuming to implement, this insulation system posed problems during resin infusion. The interlayer insulation was designed to leave axial channels to aid resin flow through the windings. The infusion resin was coloured to highlight the presence of voids. The resin flow was not consistent across the outer layer of insulation as shown in Figure 7.23. This could be due to blockage of the axial channels cause by tension from overlapping winding coils. The blockages were not uniform around the circumference of the device resulting in resin flow short circuiting through some channels and bypassing others. Because of this, it could not be guaranteed that Unit 1's encapsulation was free of voids. On Unit 2, a lower viscosity resin was used and the infusion process was modified by the manufacturer to mitigate this risk. It is recommended that future designs should review the inter-layer insulation system with a view to cost effectively incorporate circumferential supports between axial channels.

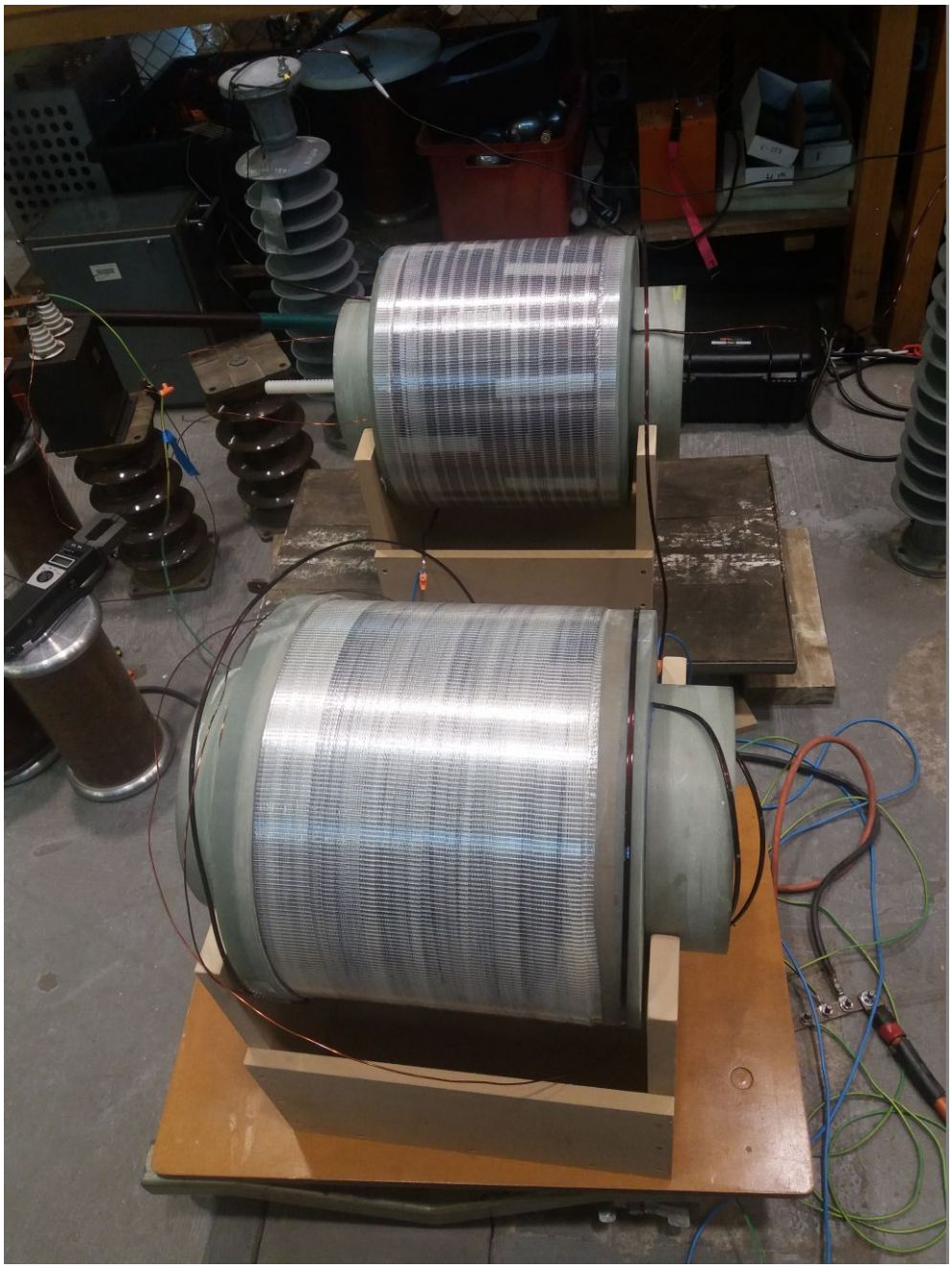

Figure 7.22 Finished two stage prototype cascaded PCRTXs

Figure 7.23 Voids in the outer layer of insulation on Unit 1

7.8 CONCLUSION

A two stage cascaded PCRTX was designed and built to energise load capacitances between 0.5 and 1 µF to test voltages of 66 kV. The cores were designed to have a mix of parallel and radial laminations to reduce losses due to radial flux. A new winding insulation system consisting of slatted sheets of G10 fibreglass vacuum infused with resin functioned as intended but could not guarantee an absence of interior voids. This is believed to be due to constrictions in axial channels between winding layers.

Chapter 8

PROTOTYPE TESTING

8.1 OVERVIEW

The cascaded PCRTX test kit was thoroughly tested in the laboratory. The aim was to determine the validity of the mathematical model, the electrical performance and evaluate the construction methods. Initially tests were conducted at low voltages to reduce the risk of inadvertent insulation damage before sufficient data was gathered. Test voltages were gradually increased to observe the test kit's performance under rated operating conditions. The newly built prototypes were tested individually, then as a two stage cascade and finally with an existing two winding PCRTX connected as a third stage. Power frequency AC tests were conducted to determine the open and short circuit performance of the individual devices. Repeated low voltage variable frequency tests were conducted across the tuning range to observe the test kit's performance at resonance. Single and multi-stage variable inductance tests were conducted by varying core gap/s and taking measurements of equivalent circuit component values and electrical characteristics. Loaded circuit testing was conducted at power frequency using capacitor banks as simulated high voltage insulation loads. A pre-existing PCRTX was added to the cascaded connection as a third stage to test the the operation of the test kit with non-identical stage transformers.

8.2 TEST EQUIPMENT

Power frequency tests were conducted using a variac to regulate the supply voltage. Variable frequency tests were conducted using an Ammetek MX Series programmable AC power supply shown in Figure 8.1a. Two *Fluke* 43B power quality analysers were used to measure current and voltage values on primary windings as shown in Figure 8.1c. High voltage measurements on secondary windings were measured with a *Fluke* 80K-40 HV high voltage probe and a *Keysight* multimeter. Winding self and mutual inductances were measured using a *National Instruments* AC impedance analyser. Winding resistance values were measured using a micro-ohm meter. Winding polarity was determined using

a multi-channel differential oscilloscope. Voltages above 40 kV were measured using an *Omicron* MCC 210 coupling capacitor shown in Figure 8.1b and an MPD 600 PD data acquisition unit. Infra red images were taken with an *EasyIR* thermal imaging camera and acoustic noise levels were measured using a *Brüel & Kjær* 2250 sound level meter.

8.3 INDIVIDUAL STAGE TESTING

Initially the individual circuit parameters were measured using the impedance analyser and micro-ohmeter. Open circuit tests were used to determine the core loss resistance. The results for Unit 1 are shown in Table 8.1 and they show adequate agreement with the model predictions. The largest measured error for both units is the core loss resistance. Apart from the core loss measurement, the percentage error between the model and measured values was less than 10%. This is comparable to results obtained by earlier PCRTX research using a similar model [Bell 2009]. The core losses of a PCRTX have not been adequately accounted for in any PCRTX model to date. The model used here does not account for the presence of two radially laminated core sections alongside two parallel laminated core sections.

Table 8.1 Unit 1 equivalent circuit parameter measurements with 2 parallel and 2 radial core sections

Parameter	Modelled	Measured	Max % Error
R_p, Ω	0.150	0.147	2.0
L_p, mH	1.72	1.86	8.1
R_s, Ω	37.2	37.1	0.27
L_s, H	10.4	10.1	2.9
R_t, mΩ	99.7	107	7.4
L_t, mH	1.81	1.82	0.55
R_c, Ω	22	27	33.1
M_{ps} mH	130	125	1.6
M_{pt} µH	1.52	1.37	3.5
M_{st} mH	137	130	1.6

On Unit 2 the tests were repeated with three different core configurations. The measured inductance values increased as more radially laminated core sections were used as shown in Table 8.2. This could be because the parallel laminated core sections have a slightly thicker layer of resin coating their surfaces compared to the radial core. This would decrease the inductance at zero core gap compared to radial cores but the effect should be negligible at large core gaps. The more likely cause is the anisotropic relative magnetic permeability of grain-oriented core steel. The design value relative permeability of 3000 used in the model is a compromise between the relative permeability in the

(a) Ammetek variable frequency source

(b) Omicron MCC 210 coupling capacitor

(c) Two stage cascade test setup and equipment layout

Figure 8.1 Photos of test equipment

rolling and transverse directions of the core laminations. In the direction normal to the lamination plane, the relative permeability can be less than 100 due to the inter lamination insulation [Pfutzner et al. 1994]. Radially laminated core sections present a lower reluctance path for radial flux and hence higher winding inductances were measured.

Table 8.2 Prototype cascade transformer Unit 2 measurements

Circuit Parameter	Model	Measured			Max % Error
		4 parallel cores	2 parallel 2 radial cores	4 radial cores	
L_p, mH	1.72	1.67	1.71	1.79	0.581
R_p, mΩ	150	152			1.33
L_s, H	10.3	9.7	9.77	10.1	5.33
R_s, Ω	37.2	37.1			0.269
L_t, mH	1.81	1.72	1.74	1.83	4.97
R_t, mΩ	90.7	104			3.88
R_c, Ω	20.3	25.1	28.7	30.4	49.8
M_{ps}, mH	122	125	125	130	4.97
M_{pt}, mH	1.42	1.32	1.35	1.41	7.04
M_{st}, mH	128	0.125	1.16	0.125	9.18

8.3.1 Variable inductance tests

The transformer tuning characteristic was determined by performing variable frequency tests on Unit 1 at different core gap spacings. The core was configured with two parallel laminated cores in the center and two radial cores at the ends. The secondary self inductance variation with core centre gap spacing is shown in Figure 8.2a. There is good agreement between the measured and modelled results.

The tuning characteristic of Unit 2 was obtained for different core configurations and the results are shown in Figure 8.3. Using all radially laminated core sections led to an increase in measured self inductance of approximately 5% throughout the tuning range compared to all parallel laminated core sections. At the larger core gaps this difference cannot be explained by thicker resin layers on the parallel laminated core sections. This further reinforces the finding that radially laminated cores present a lower reluctance to the radial flux and hence have a higher inductance than parallel cores at a range of core gaps.

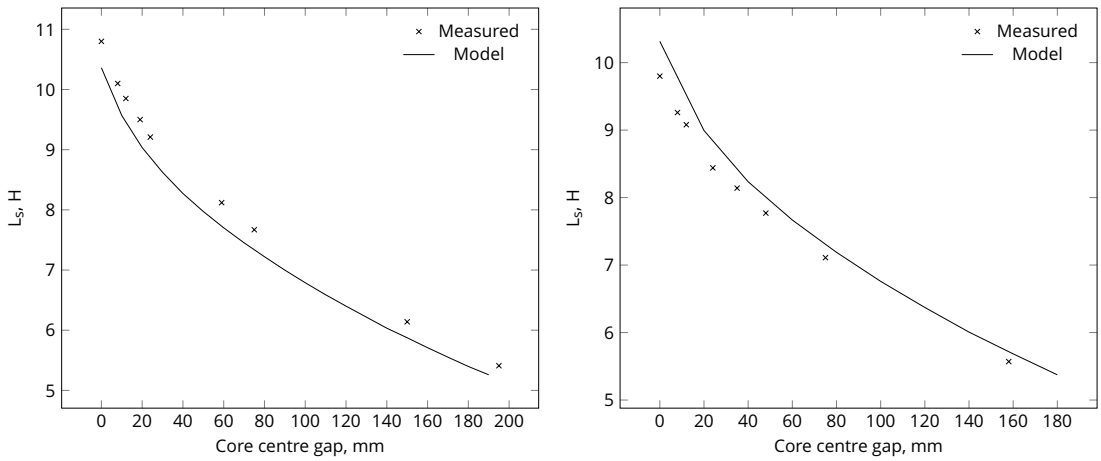

(a) Unit 1 (b) Unit 2

Figure 8.2 Single stage inductance variation with core centre gap

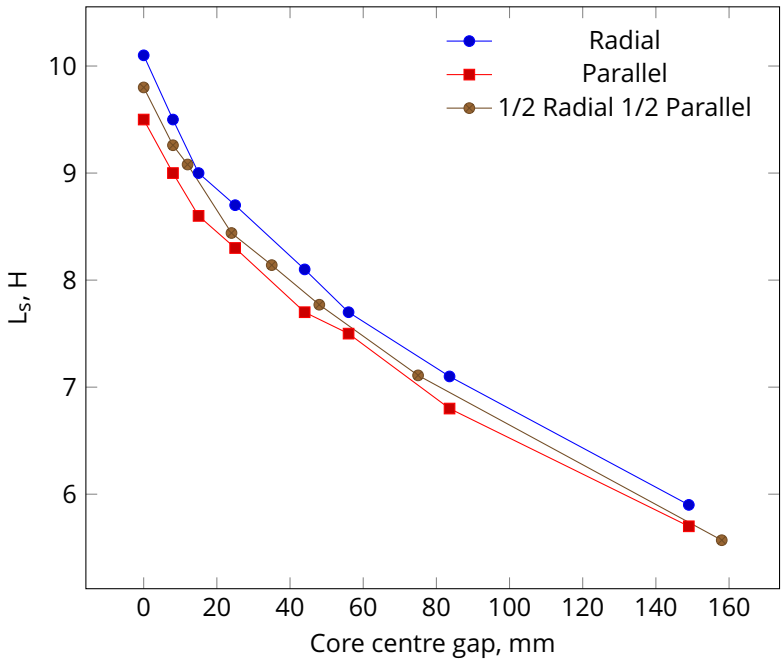

Figure 8.3 Unit 2 inductance variation with core gap for different core configurations

8.3.2 Variable frequency tests

The input impedance frequency response of both units is given in Figure 8.4. The modelled input impedance shows good agreement with the measured results. There is some discrepancy between the peak measured and modelled input impedance at resonance. This can be attributed to inaccuracies in the core loss model and possibly the significance of eddy current losses in the windings. At first each unit was tested with zero core gap using two radial and two parallel laminated core sections. A slightly different load capacitance was used when testing each stage as indicated in Figure 8.4. The load used to test Unit 1 was 10 nF larger than the load used for Unit 2, therefore Unit 1's resonant frequency is less than 50 Hz. This is also why the peak input impedance measured for Unit 1 was lower than Unit 2. For both stages the phase angle reaches zero at the same frequency as the peak input impedance, meaning that the unity power factor and maximum impedance resonant frequencies are indistinguishable.

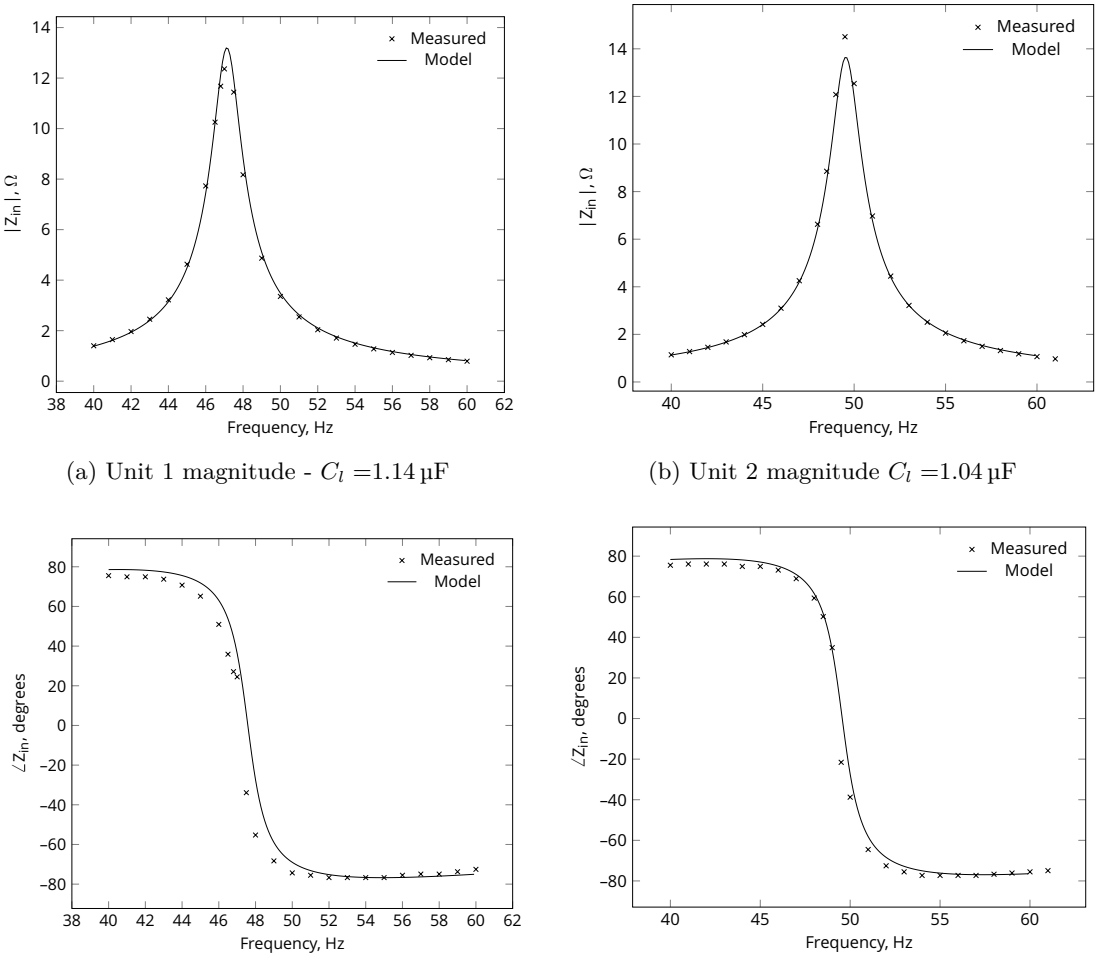

(a) Unit 1 magnitude - C_l =1.14 µF

(b) Unit 2 magnitude C_l =1.04 µF

(c) Unit 1 phase - C_l =1.14 µF

(d) Unit 2 phase - C_l =1.04 µF

Figure 8.4 Single stage frequency response

For Unit 2, the tests were repeated for three different core configurations. Four core

sections were used for each test consisting of entirely radially laminated sections, entirely parallel laminated sections and mixed with two of each. For the mixed core configuration, the parallel laminated cores were placed in the centre with the radial cores on the ends. The results are shown in Figure 8.5. The highest impedance at resonance was achieved using two parallel and two radial core sections. The resonant frequency when using all radial cores was lower due to the higher measured inductance. The lowest input impedance at resonance was achieved by the parallel laminated core.

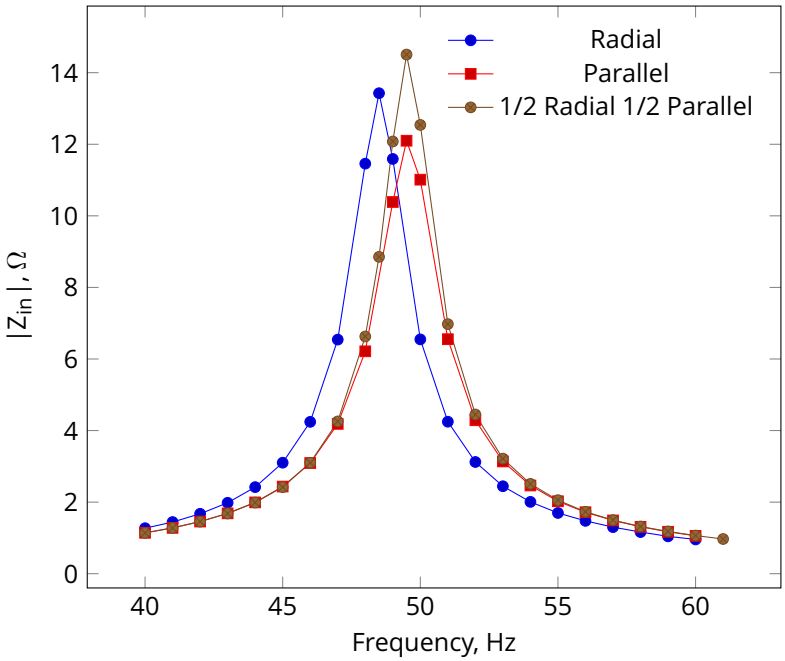

Figure 8.5 Unit 2 frequency response for different core configurations

8.3.3 Loaded circuit testing

Loaded circuit tests were conducted on each stage individually. The load consisted of 17x17.1 µF capacitors connected in series, giving a total load capacitance of 1.01 µF. Each capacitor was rated at 6.65 kV DC but operated at a nominal voltage of 1.9 kV AC during the test. The test was conducted up to the rated load voltage of 33 kV. The test voltage was held for less than 1 minute whilst measurements were taken. During the test, noise levels were monitored using an acoustic sensor and infra-red images were taken of the cores after the test.

The secondary voltage on both units increased linearly with the supply voltage as shown in Figure 8.6. This indicated there was no significant saturation of the core. This was the case for all three different core configurations.

Severe acoustic noise was heard at rated voltage when mixed core sections were used. Some of the visual indicators of magnetic forces included significant vibration of the

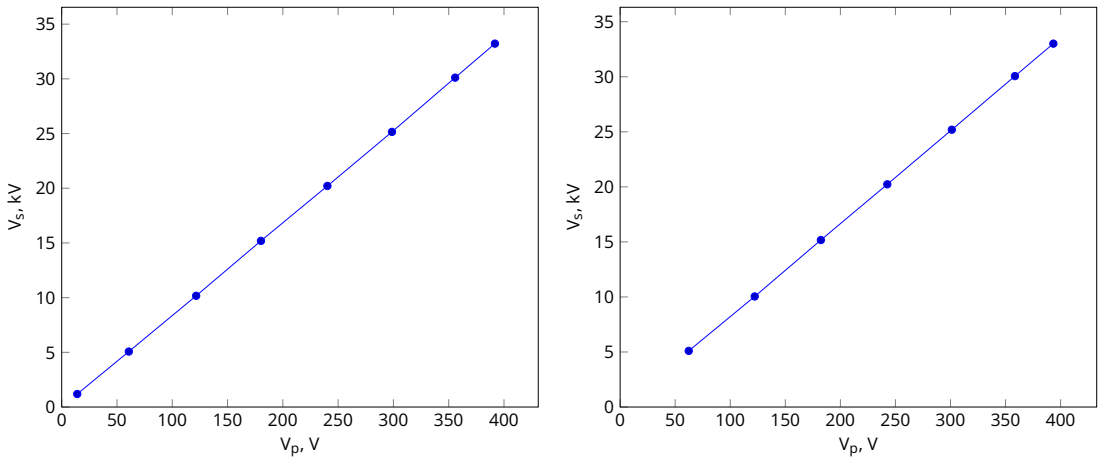

(a) Unit 1 (b) Unit 2

Figure 8.6 Single unit secondary voltage linearity

threaded clamping rod, rotation of outer radial core sections and unscrewing of the clamping nut. Some simple modifications were retrofitted to the core in order to dampen vibrations. These included wrapping the circumference of each core section in anti slip matting, sticking foam tape to the faces between core sections and placing two large nylon clamping washers over thick open cell foam padding between the clamping nuts and the outer core faces. These modifications caused a noticeable reduction in audible and visible vibration.

On Unit 2 the test was repeated with three core configurations using the retrofitted modifications outlined above. The average noise level was measured over ten seconds at each secondary voltage and the results are shown in Figure 8.7. The test with entirely radial core sections was the quietest with the least observed vibrations. At rated voltage, mixed cores had the highest level of measured noise followed closely by parallel cores. Mixed cores had the highest levels of observed vibrations.

After the test with mixed cores, the damage shown in Figure 8.9 was found. A section of one of the outer radially laminated core sections migrated axially outwards. The associated unscrewing of the clamping nut and movement of the clamping washer was observed at a voltage above 25 kV. This coincides with the increase in measured noise shown in Figure 8.7 for the mixed core configuration. Bands of de-bonded resin were observed on all core sections as shown in Figure 8.8. The outer laminations on one parallel laminated core section had separated from the rest of the core as shown in Figure 8.8c.

A brown mark was found on the interior of the former which corresponded to an abraded patch of resin on one of the exposed parallel core sections. This was caused by friction between the vibrating core section and former.

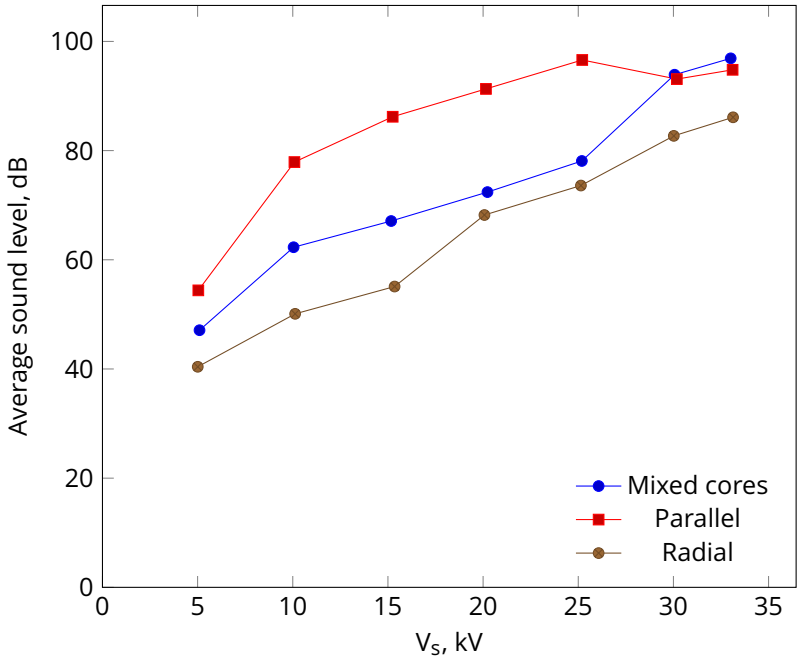

Figure 8.7 Unit 2 average sound level for different core configurations

Immediately following the loaded circuit test the core sections were individually photographed with an infra red thermal imaging camera. A peak temperature of 61 °C was observed on the outer laminations of the parallel core section as shown in Figure 8.10a. This exceeds the heat deflection temperature of the resin used to encapsulate the core sections which has a heat deflection temperature of 47.8 °C [West System 2014]. This is the most likely cause of the observed resin de-bonding and separation of laminations. The radial cores were significantly cooler, with the highest temperature shown in Figure 8.10b caused by the neighbouring parallel core section.

8.4 TWO STAGE CASCADE TESTING

8.4.1 Variable frequency tests

Variable frequency tests were conducted with the two stages connected together in cascade. The test load was halved in capacitance to 512 nF in order to resonate with the sum of both stage secondary inductances at approximately the same frequency with no core gap. As shown in Figure 8.11a the magnitude of the input impedance at resonance is approximately 6.7 Ω. This is lower than the value achieved with just one stage by approximately 50% due to the additional losses from the second stage. When the cascade set was tuned by increasing the core gap on both stages simultaneously, the frequency response in Figure 8.11b was obtained. The resonant frequency was closer to power frequency and the input impedance decreased slightly to 6.5 Ω.

(a) Migration of radial laminations

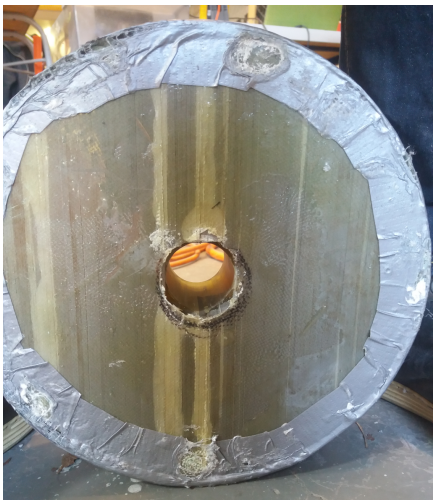

(b) Resin de-bonding

(c) Separation of parallel laminations

Figure 8.8 Damage caused by core vibration within former

(a) Brown mark on the former (b) Abraded patch on core section

Figure 8.9 Damage caused by core vibration within former

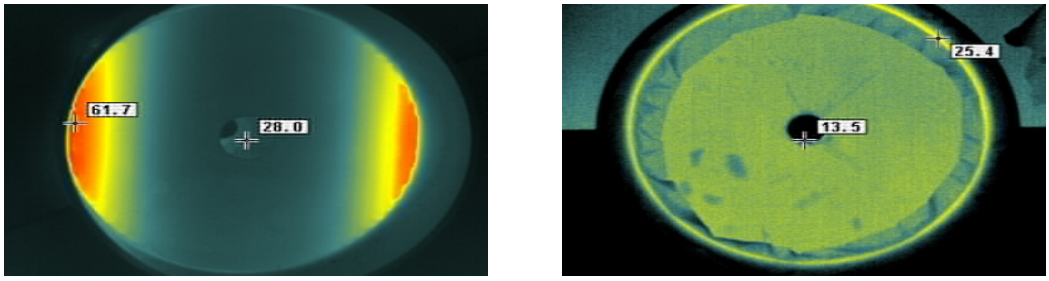

(a) Parallel core section (b) Radial core section

Figure 8.10 Infra red images of core sections after a short duration loaded circuit test at rated voltage 33 kV

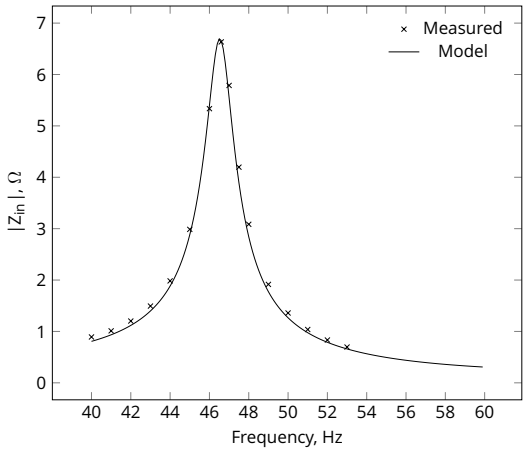

(a) No core gaps

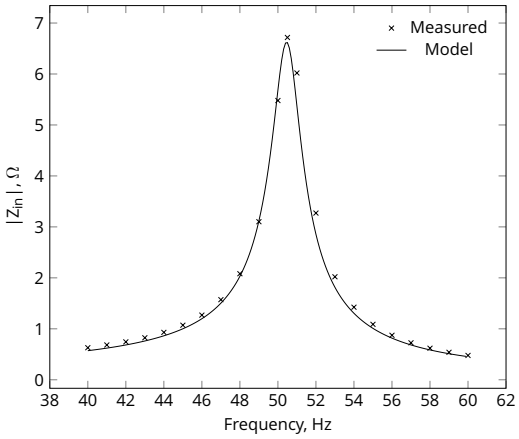

(b) Simultaneous tuning

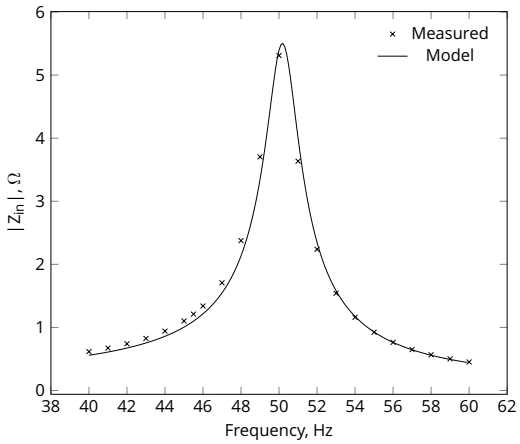

(c) First stage tuned

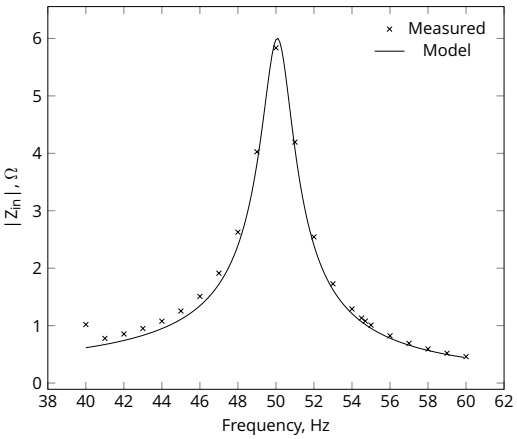

(d) Second stage tuned

Figure 8.11 Two stage cascade frequency response under different tuning

The test was repeated with only a single stage tuned and the resulting frequency responses are shown in Figures 8.11c and 8.11d. A low voltage variable frequency supply was used with an input voltage of around 1 V. This voltage was selected due to power supply limitations and to reduce the risk of damaging the device insulation before sufficient test data was gathered. Test results are likely to be less accurate at this voltage but are adequate for relative comparisons between tuning methods. Both tuning methods achieved the same resonant frequency but the peak input impedance under second stage tuning (6 Ω) was higher than when the first stage was tuned (5.5 Ω). First stage tuning drew 26% more supply current than simultaneous tuning whilst second stage tuning drew 15% more current.

As outlined in Section 4.5.2 tuning single stages to achieve resonance means higher losses are introduced into the circuit due to the increased magnetising current. If one stage is tuned, the inductance of all its windings decreases due to the larger core air gap. As a result the current drawn by the primary and tertiary windings increases. The secondary winding current of the tuned stage does not change noticeably because it is determined by the load and is the same for both stages. The increased primary and tertiary current on the tuned stage produces greater winding losses which limits the peak input impedance at resonance. The second stage tertiary winding is not loaded, so the increase in its losses are smaller. As a result the cascade set has a higher resonant input impedance during second stage tuning compared to first stage tuning.

The primary current distribution frequency response for the different tuning methods is shown in Figure 8.12. Both stages had different resonant frequencies, defined as the frequency where the impedance measured at the stage's primary winding reached a peak. In both cases where a single stage was tuned, the tuned stage had a higher resonant frequency due to its smaller secondary winding self inductance. With simultaneous tuning the first stage primary winding carries twice the current of the second stage primary at resonance which is expected for identical stages. The model predicts the measured current with good accuracy around resonance with a slightly greater deviation at higher and lower frequencies. This is possibly because higher frequencies alter the transformer losses which were not re-calculated at each frequency.

The secondary voltage distribution with frequency is shown in Figure 8.13. The tuning method determines the frequency at which a balanced voltage is achieved across both stage secondary windings. For simultaneous tuning this occurs at close to the design resonant frequency of 50 Hz. For first stage tuning this occurs at 48 Hz and for second stage tuning at 54 Hz. The tuned stage carries less of the load voltage across its secondary winding at resonance. This is because the load voltage is divided across two secondary windings connected in series. The winding with the larger inductance will have a greater voltage across its terminals. At higher frequencies the capacitive impedance of the load is lower, thus boosting the load voltage higher. It can be seen in the plots that the

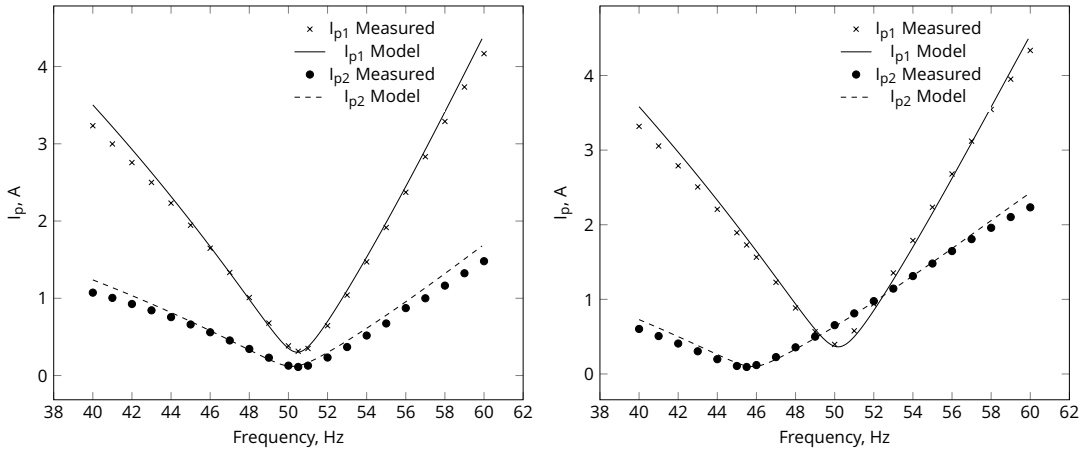

(a) Simultaneous tuning

(b) First stage tuned

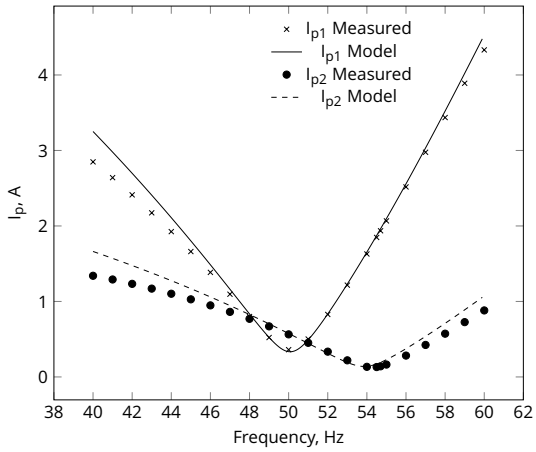

(c) Second stage tuned

Figure 8.12 Two stage cascade primary current frequency response

measured voltage values exhibit a larger reduction with higher frequencies than the model predicts. This is again probably due to the model underestimating the losses at higher frequencies.

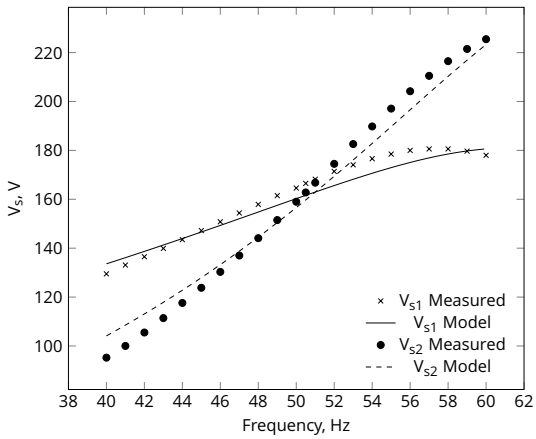

(a) Simultaneous tuning

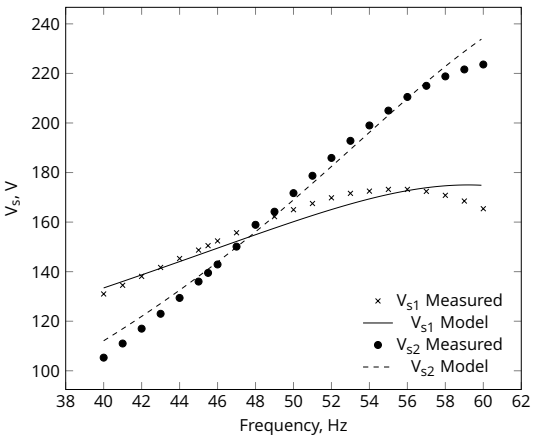

(b) First stage tuned

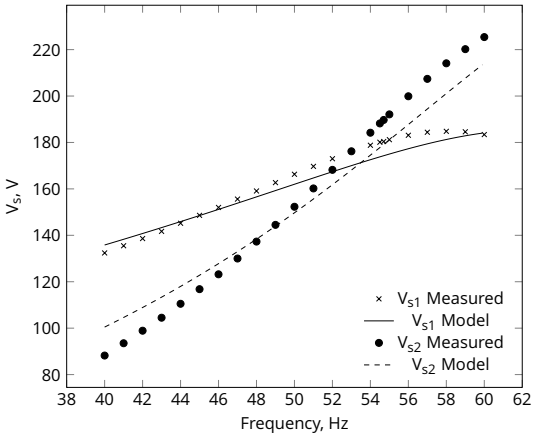

(c) Second stage tuned

Figure 8.13 Two stage cascade secondary voltage frequency response

8.4.2 Variable inductance tests

Variable inductance tests were conducted on the combined cascade set by varying the core gap with a fixed capacitive load. Tests were conducted using the three different tuning methods. The change in input impedance with frequency is shown in Figure 8.14. For both single stage tuning cases, resonance occurred at an air gap approximately three times larger than the air gap for simultaneous tuning. Tuning the second stage again produced a higher peak impedance than tuning the first stage. This is consistent with the variable frequency test results. This occurs because the tertiary winding on the second stage is not loaded and hence has less winding losses compared to the first stage.

The primary current distribution with core gap variation is shown in Figure 8.15. The

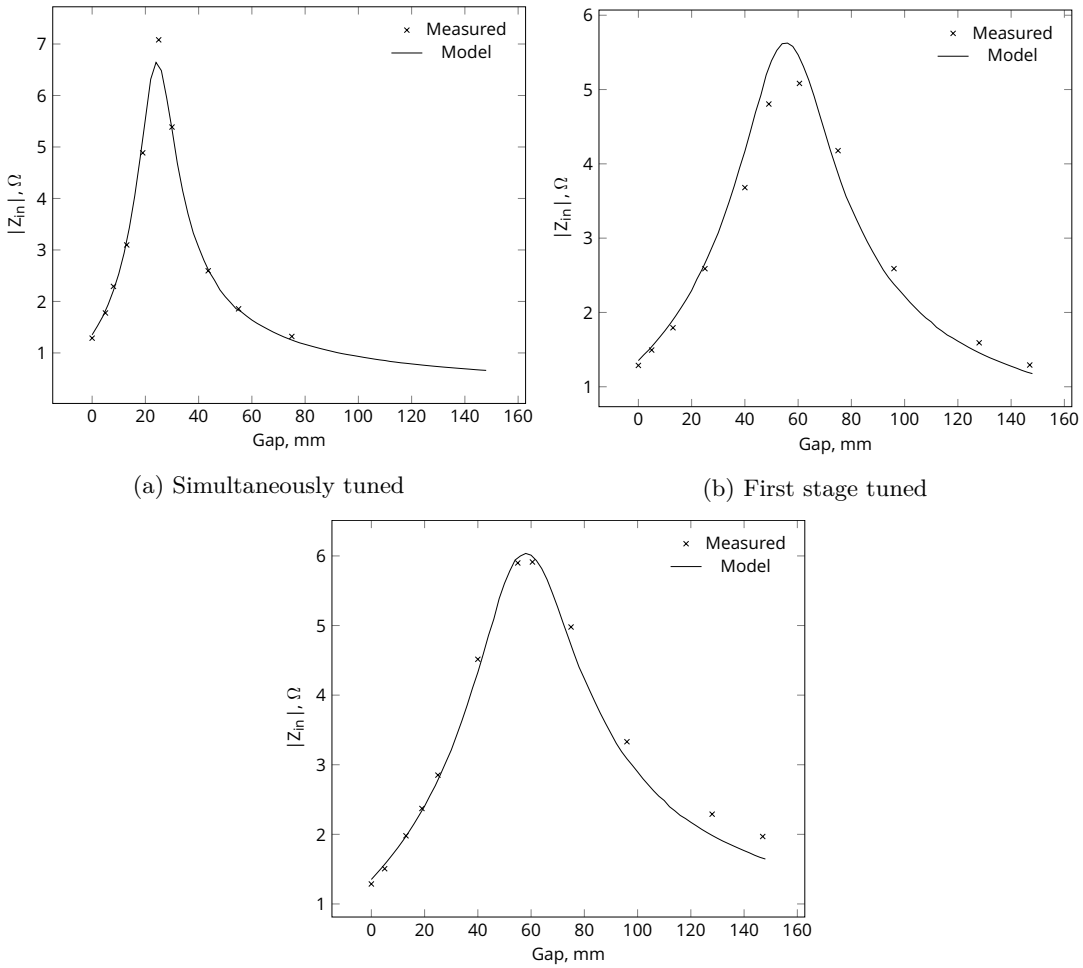

(a) Simultaneously tuned

(b) First stage tuned

(c) Second stage tuned

Figure 8.14 Two stage cascade impedance variation with core displacement under different tuning methods

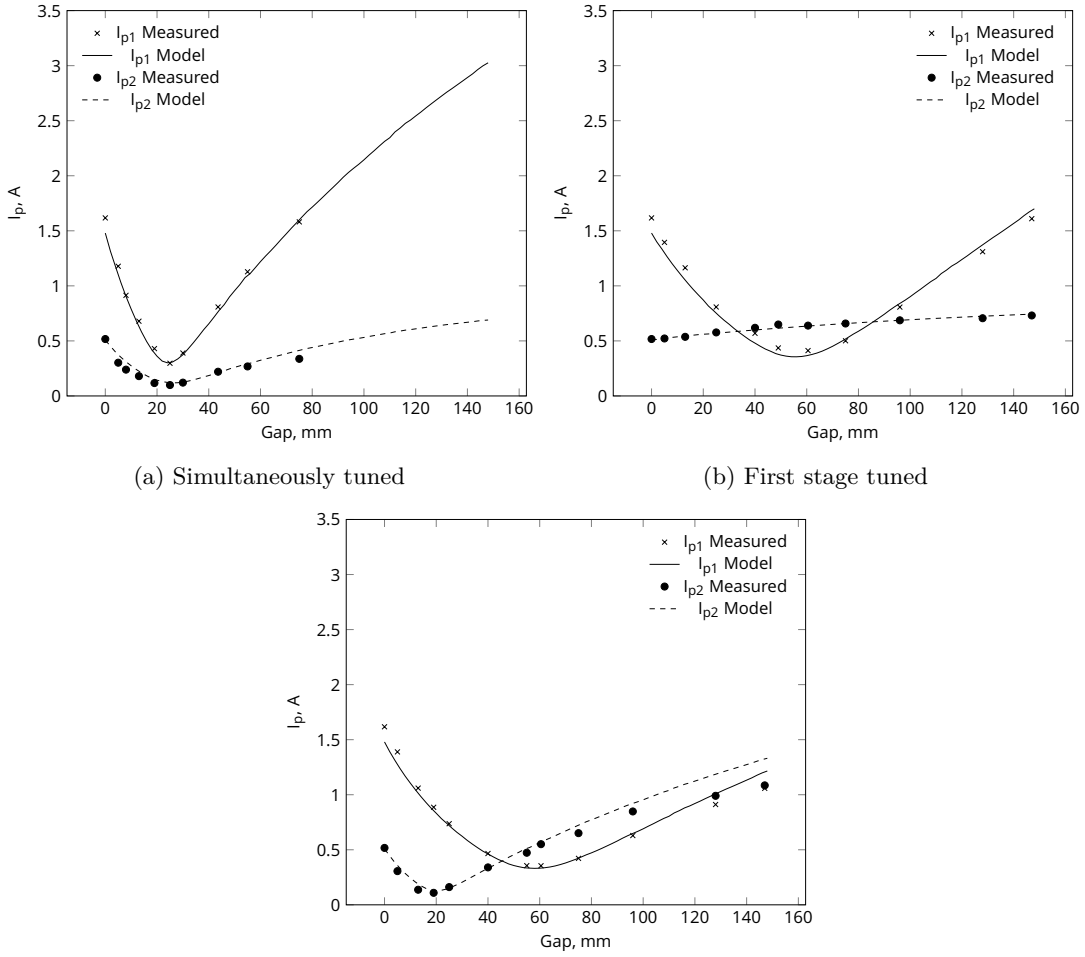

(a) Simultaneously tuned

(b) First stage tuned

(c) Second stage tuned

Figure 8.15 Two stage cascade primary current variation with core displacement under different tuning methods

model shows good agreement with the measured results at low core gaps and near the resonant point however greater error was observed at large core gaps when only the second stage was tuned as shown in Figure 8.15c. This could be due to an inaccuracy in the way losses are modelled at large core gaps. In the case when only the first stage is tuned the second stage primary current shows very little variation with the first stage core gap. Since the secondary inductance of the second stage was not varied there was no compensation of the secondary winding load capacitance from the second stage's frame of reference. This highlights the ability of the entire cascade to operate at resonance whilst one or more of its upper stages is not at resonance. There is very little difference between the resonant core gap of the second stage under simultaneous tuning and single stage tuning as shown in Figures 8.15a and 8.15c.

The voltage distribution across the secondary windings is not equal across the tuning range as shown in Figure 8.16. The second stage secondary voltage drops off as the core gap is increased with all the tuning methods. The model underestimates the steepness of the second stage secondary voltage decrease with an increased core gap. This is largely due to the accumulated error from two voltage ratio calculations in the three winding Steinmetz circuit model. The secondary voltage of the first stage is more accurately predicted by the model. Under second stage tuning the secondary voltage across the first stage increases with the core gap. This is due to the load voltage distributing itself across the higher secondary self inductance of the non tuned first stage.

8.4.3 Loaded circuit tests

The two stage cascaded test kit was connected to a capacitive load consisting of three 1.85 µF capacitors connected in series giving a capacitance of 615 nF and a load voltage rating of 41.7 kV. The stages had a standard core configuration of two parallel laminated and two radially laminated cores each. Voltage and current measurements were taken at all windings and the secondary voltages of each stage were measured to ground. The test kit was energised using a Variac powered from a 80 A three phase supply.

The first test was conducted up to a load voltage of 20 kV giving approximately 10 kV across each stage secondary winding. The test was repeated with different combinations of stage core gaps. One goal of this test was to determine if the theoretical optimal tuning point identified by the model could be practically realised. As outlined in Section 4.5.2 the model predicts a higher resonant impedance can be achieved when the second stage has a slightly higher core gap than the first. Compared to the gap settings for simultaneous tuning any increase in the second stage core gap would require a decrease in the first stage core gap to maintain the same resonant inductance. This is shown in Figure 8.17 where the simultaneously tuned case operated at a lagging power factor of 0.99 and an increase in only the second stage core gap made the power factor

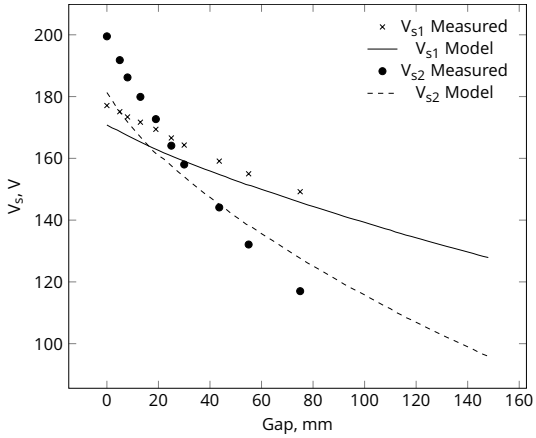

(a) Simultaneously tuned

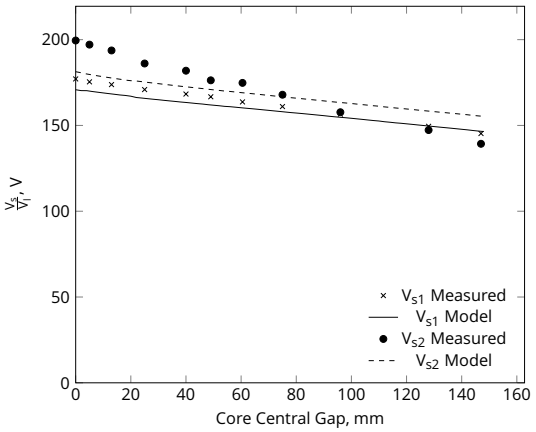

(b) First stage tuned

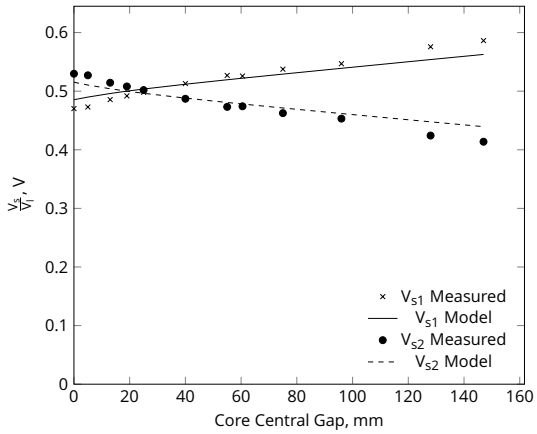

(c) Second stage tuned

Figure 8.16 Two stage cascade secondary voltage distribution with core displacement under different tuning methods

worse at 0.83 lagging.

The model predicts the required difference in first and second stage core gaps to achieve the highest input impedance is in the order of 5 to 10 mm. In practice it is difficult to achieve this accuracy of gap setting. This is due to uncertainties of a similar size introduced by magnetic forces shifting the core position during operation, and construction tolerances of the core sections and spacers. This is shown in Figure 8.17 where there is no identifiable difference in the measured primary current between simultaneous tuning and the case where the second stage is given a slightly larger core gap. For this reason it is recommended the stages are tuned simultaneously to achieve a high input impedance. The results for single stage tuning show a higher input current drawn than simultaneous tuning as expected with less current drawn during second stage tuning compared to first stage tuning.

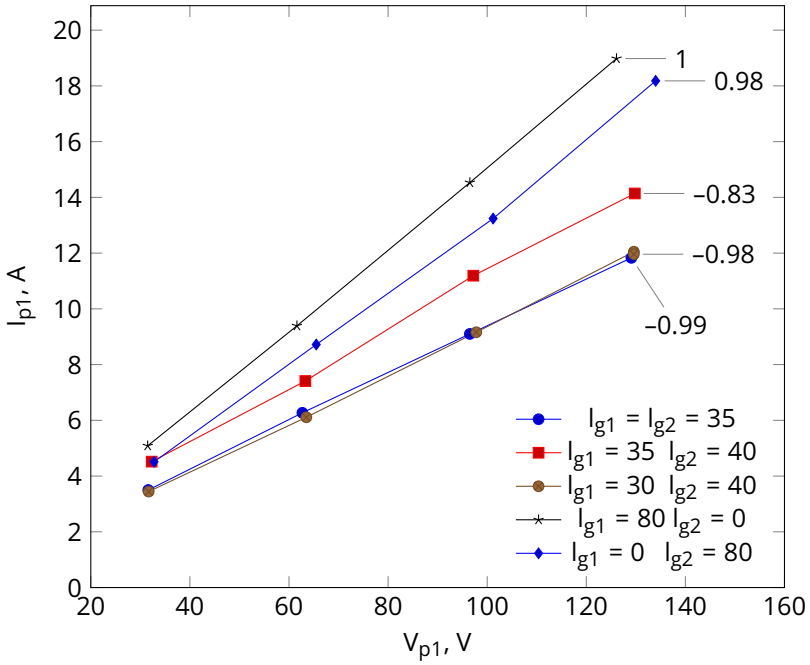

Figure 8.17 Two stage cascade loaded circuit primary current variation with input voltage for different core gap configurations. Labels indicate the peak measured power factor

Another two stage loaded circuit test was conducted up to the rated load voltage of 66 kV. The load in this test consisted of the same 17.1 µF capacitors used in Section 8.3.3 connected in series for an equivalent load capacitance of 515 nF. To further mitigate excessive vibrations and noise from the stages, stiff foam was inserted between each core section. The stages were not tuned and were left with no core gap. The load voltage and first stage tertiary (second stage primary) voltage increased linearly with the applied input voltage as shown in Figure 8.18. As with the single stage PCRTX, there was a noticeable increase in mechanical noise due to core vibration when the stage secondary voltages reached 10 kV. This was accompanied by a slight change in input

power factor indicating that the core sections had shifted due to magnetic forces.

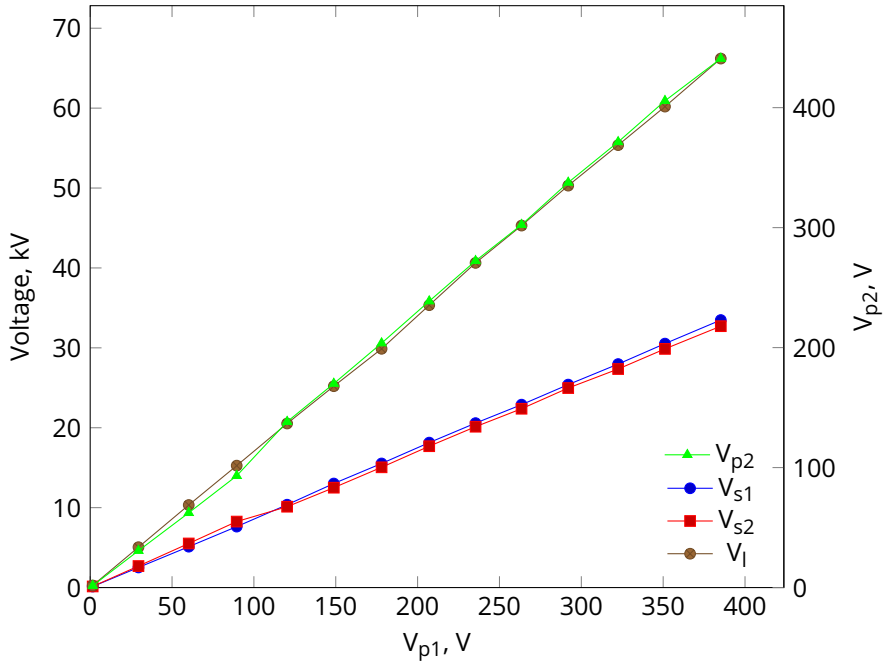

Figure 8.18 Two stage cascade loaded circuit voltage linearity

Unintended variation of tuning with increased test voltage has been observed in PCRTXs before. Along with magnetic forces, the input power factor can also become more leading as the test voltage rises due to increased corona discharge from the load. The variation in primary stage currents and input power factor is shown in Figure 8.19. As the voltage is increased, magnetic forces pull the core sections towards the axial centre of the windings increasing the winding inductance and decreasing the inductive current compensating the load. The input impedance dropped from 7 Ω at a load voltage of 5 kV to 6.1 Ω at 66 kV. As the voltage was raised further, magnetic forces further squashed the foam spacer between core sections, thus giving a more leading input power factor. The use of the foam spacer dramatically reduced vibrations and noise. It is recommended that a stiffer vibration absorbing material is used as a core gap spacer.

The percentage difference between the sum of each stage secondary voltage and the load voltage is defined as the residual voltage. This value is sensitive to the accuracy of the voltage measuring instrumentation. At rated voltage the residual voltage was determined to be 0.02 % of the load voltage, indicating that both stage secondary voltages added in phase. The primary current at the rated load voltage was 62.9 A which could be reduced with better tuning. The primary voltage required to reach the rated load voltage was 385.2 V which is lower than the design value of 400 V. This is because the required number of primary winding turns was rounded down to ensure the rated stage secondary voltage was reached.

These results were compared to the low voltage variable frequency test results to

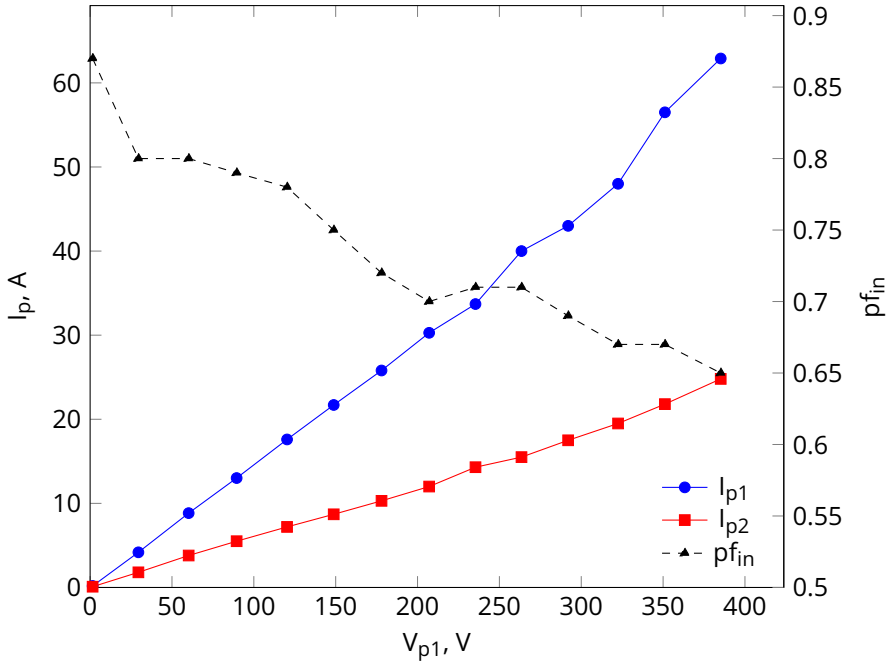

Figure 8.19 Two stage cascade loaded circuit input and impedance and power factor variation

determine the validity of testing the stage at low voltages. The core gaps required to tune the stages were the same for both tests. There was some discrepancy between the magnitudes of the peak resonant input impedance. Tests conducted at low voltages gave lower peak resonant input impedances than tests conducted at high voltages. This could be because the secondary winding was unable to provide enough ampere turns to magnetise the core into the linear region of its magnetisation curve at low voltages. Current measurements are also likely to be more accurate at higher current levels.

8.5 THREE STAGE CASCADE TESTING

A third two winding PCRTX was connected to the tertiary winding of the second stage to make a three stage cascaded PCRTX test kit as shown in Figure 8.20. This was the first test conducted using non-identical stages. The third stage transformer had double the inductance of the other two stages. It was designed to resonate with capacitive loads between 0.5 and 1 µF [Bell 2009] compared to the first two stages which were designed to resonate with loads between 1 and 1.5 µF. The third stage also used tapped winding sections for tuning. The second lowest number of winding sections were used on the third stage with no core gaps on any of the three stages. The load capacitance and voltage rating was reduced to 343 nF by combining 12 17.1 µF and 4 1.8 µF capacitors in series.

The test kit was tuned with an almost unity input power factor, the input impedance

Figure 8.20 Three stage cascaded PCRTXs

was 6.9 Ω at a load voltage of 100 kV. The distribution of secondary winding voltages is shown in Figure 8.21. The load voltage increase is linear and is shared almost equally amongst each stage secondary winding due to the simultaneous tuning. The residual voltage at 100 kV is approximately 10 % of load voltage indicating that the stage secondary voltages are not completely in phase.

The first stage primary winding current at rated voltage was measured at 60.6 A. As the stages were almost perfectly tuned, this is likely to be the lowest achievable input current for this arrangement. The second and third stage primary winding currents were higher than the first stage as shown in Figure 8.22. The current rise was slightly non-linear as the voltage increased due to minor changes in tuning caused by core movement.

The supply voltage required to reach the 100 kV load voltage was 419 V. This is possibly because winding sections had to be removed from the third stage for tuning purposes. The highest primary winding voltage was measured on the third stage at 431.7 V as shown in Figure 8.23.

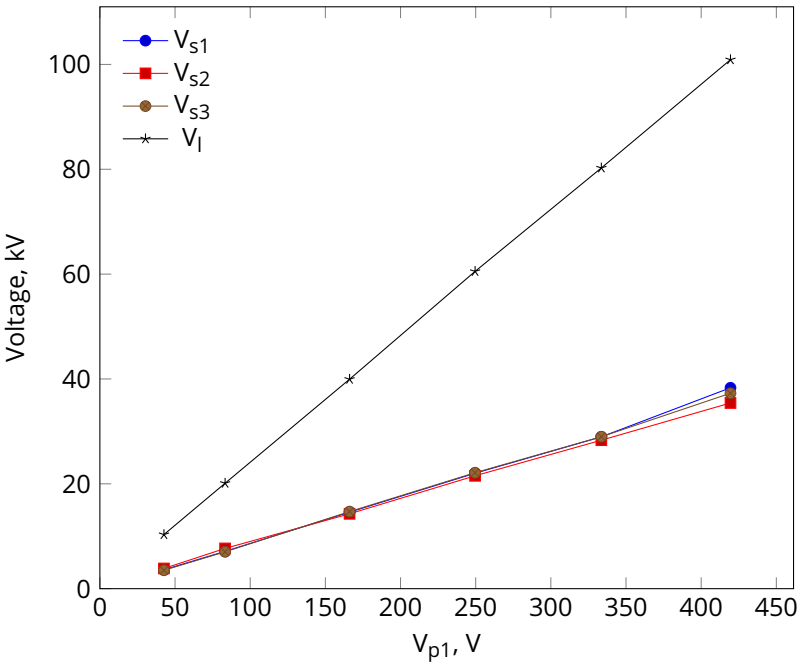

Figure 8.21 Three stage cascade loaded circuit secondary winding voltages

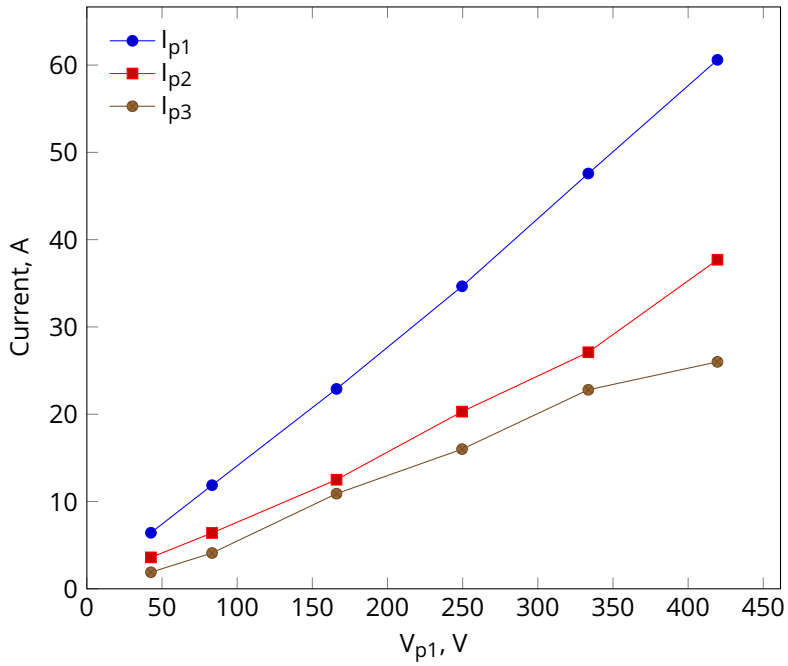

Figure 8.22 Three stage cascade loaded circuit primary winding currents

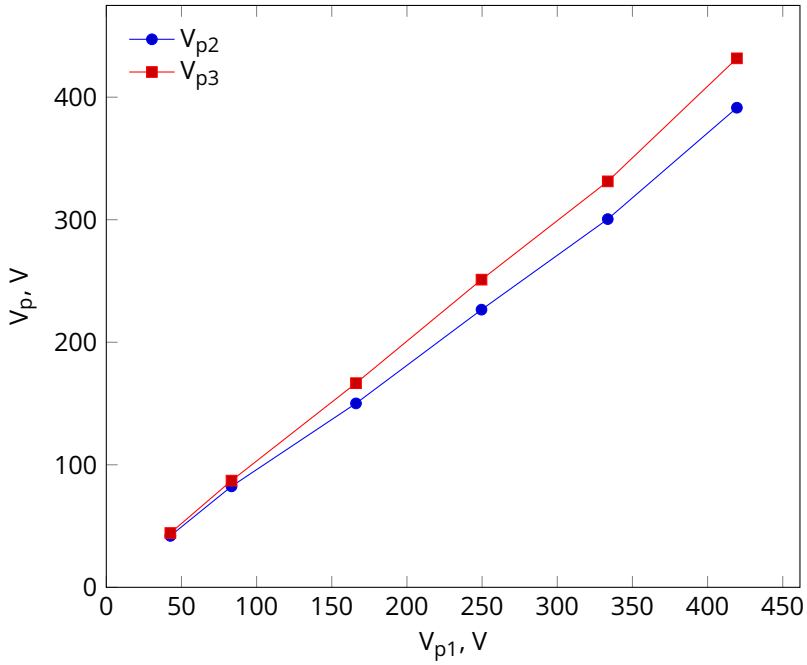

Figure 8.23 Three stage cascade loaded circuit primary winding voltages

8.6 DISCUSSION

The encapsulating core resin was not rated to withstand high operating temperatures. A high temperature resin should have been used. This is likely to require curing the core resin in an oven under an appropriate clamping pressure. Extra mechanical support should have been included in the core construction to better secure the laminations against magnetic forces.

The use of radially laminated core sections in PCRTXs proved to have numerous advantages. They were lighter than the parallel laminated cores and the procurement of core steel was cheaper due to the fewer lengths and quantity required. Assembling the steel laminations into wedges and stacking them was only slightly more time consuming than stacking the parallel core. For bespoke or small volume production the extra manufacturing time is not significant enough to be material.

Magnetically, radial cores present a higher relative permeability for radial flux which presents higher winding inductances even though the stacking factor is reduced. It is possible that the permeability could be increased further by cutting or slitting the core steel to line up the grain with the magnetic flux. This is likely to yield a small benefit as the relative permeability of steel in the rolling direction of the grain can be an order of magnitude higher than the value in the transverse direction. However this will have to be compared to the increased cost and wastage from slitting multiple lengths of steel.

The combination of radial and parallel cores gave the best electrical performance with

the highest input impedance at resonance. The radial core was not specifically modelled and hence its impact on the core losses was not fully explored. One disadvantage to using mixed parallel and radially laminated cores is the noticeable increase in audible noise and vibrations compared to cores constructed entirely from the same lamination style. Under long periods of operation this is likely to reduce the life of the test kit by vibrating the tensioned windings, thus wearing out the inter-turn insulation. The reason for this is unknown but the impact of flux passage through multiple lamination orientations should be further explored. Placing shock absorbing materials around the core sections noticeably reduced vibrations.

The new insulation system used to build the prototypes needs further refinement. A cheaper inter-layer insulation system is required, along with a way to keep fibreglass slats spaced uniformly around the circumference of the winding layer. The use of helical windings creates significant high voltage stress between end turns on neighbouring layers. The peak high voltage stress could be reduced using disc windings but will require industrial equipment to manufacture. Further detailed design is required on the high voltage lead-outs as they were identified as a significant source of audible corona discharge. A stress controlled transition away from the encapsulated winding would reduce the risk of surface tracking between the HV and LV windings.

The final rating of the test kit did not meet all intended design requirements as outlined in Table 8.3. The tuning range was achieved but the resonant input impedance at the maximum core gap was lower than required at 8 Ω. The required output voltage of 66 kV can be achieved using a slightly higher supply voltage than originally specified at 415 V. The rated operating time of the test kit is limited by the issues with core vibration and resin de-bonding. If the core is re-built using a high temperature resin and vibrations are reduced, the test kit should be able to achieve a rated operating time closer to the original specification of 30 mins. This means longer duration PD tests at the rated secondary voltage in accordance with IEEE Std 400.3 are not yet possible with this test kit. However short duration high voltage withstand tests as outlined in IEC 60060-1 and IEEE Std 400 are possible at the rated secondary voltage.

Table 8.3 Design requirements compared to final ratings

Parameter	Specified	Rated
$C_{l,min}$ @ $L_{s,max}$	500 nF @ 20.2 H	510 nF @ 19.9 H
$C_{l,max}$ @ $L_{s,min}$	1 µF @ 5.07 H	1.05 µF @ 4.82 H
$Z_{in,min}$	10 Ω	8 Ω
V_{in}	400 V	415 V
V_l	66 kV	66 kV
$I_{in,rated}$	50 A	50 A
t_{on}	30 mins	2 mins

The equivalent circuit model performed well for design purposes but needs a better

representation of the non-I^2R losses to enable prediction of the resonant input impedance. Based on results from Chapter 6, reducing material weight and cost reduces the maximum resonant input impedance achievable by the test kit. A better representation of this value could allow for further reductions in equipment size. It is possible that a significant amount of what is currently lumped into core loss is actually eddy current loss in the windings.

Tuning both stages simultaneously was clearly the best way to tune the cascaded set. If only a single stage could be tuned due to time constraints then it should be the second stage as this was found to achieve the next highest input impedance. The optimal tuning point predicted by the model was unachievable in practice due to the fine adjustment of the core gap required. The small differences in stage core gaps meant that optimal tuning was indistinguishable from simultaneous tuning. Simultaneous tuning also negates the need for concerns about the secondary voltage balance between stages as they were found to be almost equal.

At the moment the tuning process is difficult because the cores need to be removed and replaced along with a spacer. A tuning system like the one outlined in Section 7.4 would make this faster and enable on-line tuning of the device at low voltages. The Q factor of the input impedance frequency response is high and the device is sensitive to changes to the core gap at low gap settings. To achieve the best performance from this device, on-line tuning would be necessary for the weight to be reduced any further.

By adding the third stage the resonant capacitance was reduced as expected. The input impedance was lower than the two stage test kit would have been at the same power factor. However, it was still high enough to reach rated voltage without drawing more than 60.6 A from the supply.

8.7 CONCLUSION

The prototype cascaded test kit was thoroughly tested to validate mathematical design models and determine the device performance.

A mixed core consisting of centrally located parallel laminated sections and radially laminated sections at the core ends was found to give the highest resonant input impedance. Higher winding inductances were measured when using radially laminated cores despite their lower weight and stacking factor. A noted disadvantage of using mixed cores was the significant increase in device noise and vibration which was partially mitigated by covering core sections in shock absorbing foam.

The electrical performance of the cascaded 66 kV test kit showed good agreement with the model. The finite element model accurately predicted the measured equivalent circuit parameters. Simultaneous tuning of both stages was found to be the best method

of tuning the cascaded test kit yielding higher input impedances and better voltage balance between stages than individual stage tuning. A third non-identical stage was used to energise a 343 nF load to 100 kV whilst drawing only 60.6 A from the supply.

Chapter 9

FUTURE WORK

9.1 OVERVIEW

This chapter outlines a range of possible directions for future research in this subject. Preliminary investigations were conducted into some of the ideas and the outcomes are discussed but further work is required. For cascaded transformers future topics include inter stage coupling effects and a multi stage system consisting of non-identical stages. For single stage modelling, a better loss model is required. Certain design changes could allow for further reduction in weight. These include changes to the core shape to reduce the peak flux density and a cooling system allowing the use of smaller secondary winding wire.

9.2 INTER STAGE COUPLING

The impact of positioning the transformer in a cascaded connection was investigated. In commercially available cascaded transformers, individual stages have complete magnetic circuits in the form of a full core. As a result stage transformers have little influence on the magnetic behaviour of each other. The challenge with cascaded PCRTXs is stray magnetic flux due to the incomplete magnetic circuit on each stage. This manifests itself as coupling between windings of different stages and depending on the proximity of the stages, this can increase the self inductance of each winding.

To model this effect the existing cascaded transformer flux linkage matrix was expanded to include flux linkage between windings of different stages as shown in Equation (9.1). The notation follows the format where λ_{wjxk} is the flux linkage between the w winding (p for primary, s for secondary, t for tertiary) on the j^{th} stage and the x winding on the

k^{th} stage.

$$\left[\begin{array}{ccc|cc} \lambda_{p1p1} & \lambda_{p1s1} & \lambda_{p1t1} & \lambda_{p1p2} & \lambda_{p1s2} \\ \lambda_{s1p1} & \lambda_{s1s1} & \lambda_{s1t1} & \lambda_{s1p2} & \lambda_{s1s2} \\ \lambda_{t1p1} & \lambda_{t1s1} & \lambda_{t1t1} & \lambda_{t1p2} & \lambda_{t1s2} \\ \hline \lambda_{p2p1} & \lambda_{p2s1} & \lambda_{p2t1} & \lambda_{p2p2} & \lambda_{p2s2} \\ \lambda_{s2p1} & \lambda_{s2s1} & \lambda_{s2t1} & \lambda_{s2p2} & \lambda_{s2s2} \end{array}\right] \tag{9.1}$$

The matrix was determined for a two stage cascaded set of transformers using a finite element model that included both stages. Each winding was excited with unit ampere turns and the flux linkage between each combination of coils was extracted from the program. The corresponding permeance matrix P was calculated using the formula

$$P_{ij} = \frac{\lambda_i}{i_j} \tag{9.2}$$

where i_j is the current in amps exciting winding j.The corresponding inductance matrix is given by

$$L_{ij} = N_i N_j P_{ij} \tag{9.3}$$

This can be represented by the circuit diagram shown in Figure 9.1.

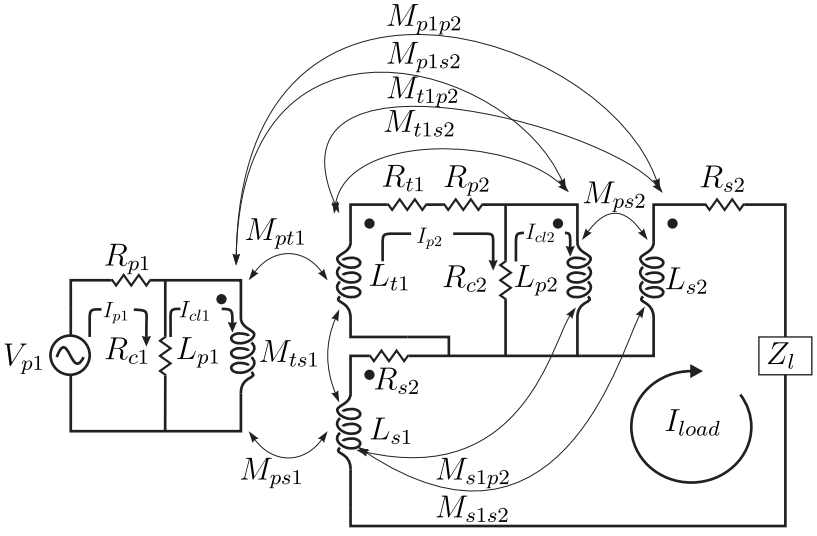

Figure 9.1 Cascaded PCRTX equivalent circuit with inter stage mutual inductances

The distance between the two simulated transformers was varied within the FEA model. It was assumed the cores had no central gap and were positioned on the axial center line of each stage transformer. At each distance the full flux linkage matrix was calculated and used to determine the self inductance of each winding and the mutual inductances between all the windings of all stages. The calculated change in the secondary winding

self inductances with increased spacing between the stages is shown in Figure 9.2.

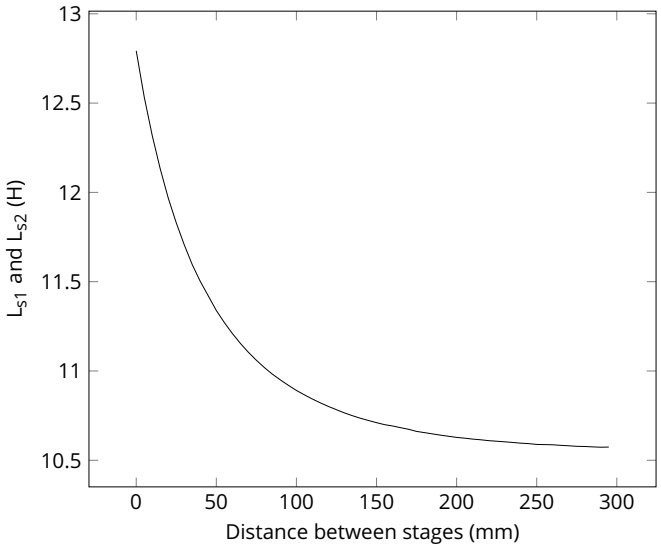

Figure 9.2 Secondary inductance variation as stages are moved further apart

The close proximity of stages causes an increase of up to 10% in the self inductance of the secondary windings. This decreased rapidly as the stages were moved further apart, to a point where the calculated self inductance matches the value determined by simulating each stage in isolation. In this case, that level was reached after the transformers were positioned approximately 200 mm apart.

The variation in inter stage coupling between windings is shown in Figure 9.3. Even at very close distances the peak coupling coefficient between windings of different stages was 0.45. This value dropped away quickly to below 0.1 as the stages were spaced further apart.

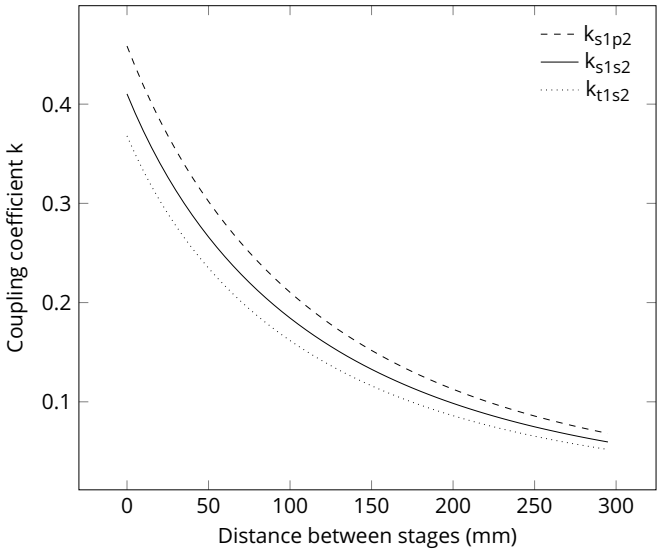

Figure 9.3 Inter stage coupling coefficient variation as stages are moved further apart

The coupling coefficients between windings of the same stage are only slightly affected by the proximity of the neighbouring stage when they are closely spaced. This becomes negligible after stages are spaced 100 mm apart as shown in Figure 9.4.

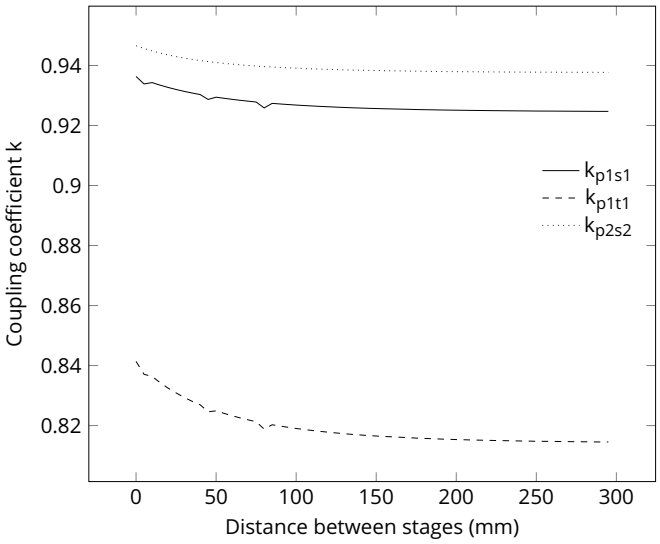

Figure 9.4 Intra stage coupling coefficient variation as stages are moved further apart

Under loaded circuit operation, closely spacing the stages can cause an imbalance in the magnetic flux density in both cores as shown in Figure 9.5. There is a significantly higher flux density in core regions located closest to the neighbouring stage. The imbalance drops away significantly as the stages are moved further apart.

This preliminary investigation was conducted by simulating axially separated stage transformers. This is how the design program models the transformers in FEA. A further investigation could be conducted on stages sitting side by side to see if similar results are obtained. This effect could be studied further to see if there is any benefit to sharing the flux between stages. The effects of inter stage magnetic coupling appear to become negligible once the transformers are separated by a short distance. This distance is smaller than the practical space between stages when they are connected under operating conditions.

9.3 LOSSES

9.3.1 Winding eddy current losses

A key constraint in the PCRTX optimisation routine is the minimum input impedance at resonance $Z_{in,min}$. This value is chosen based on the power supply specification. The losses in the transformer have a significant impact on $Z_{in,min}$. Existing algorithms aimed at optimising weight have yielded axially short windings and with shorter cores.

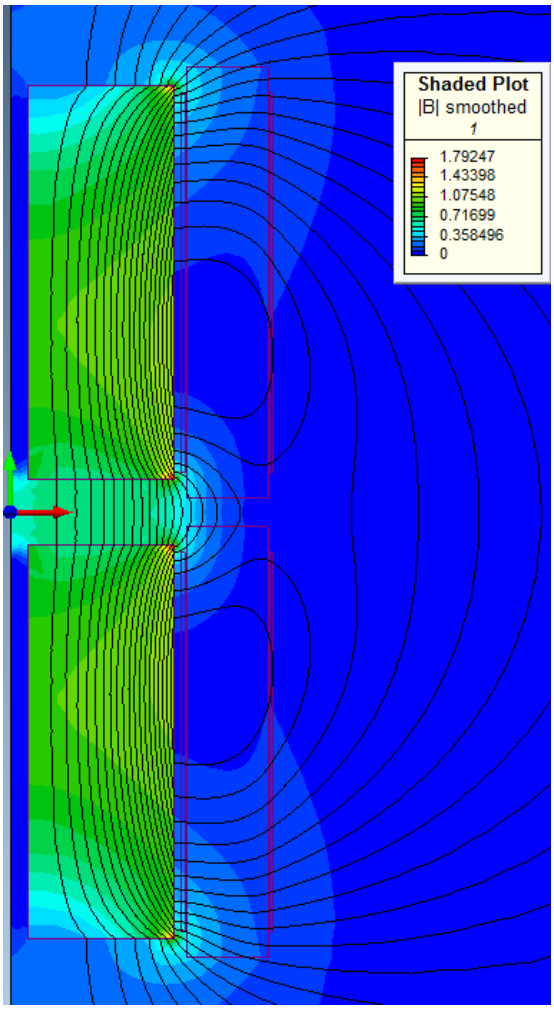

Figure 9.5 Finite element simulation of two stage cascaded PCRTXs under rated load and 20 mm apart.

This arrangement should theoretically increase radial flux cutting the axial ends of the windings. The associated eddy current losses in the windings will further reduce Z_{in} at resonance.

It is possible that a proportion of the modelled losses currently attributed to the core could be due to eddy current loss in the windings. A model should be developed for these losses and and included in the transformer design program. The optimisation routine should be repeated using this model. It is possible that consideration of winding eddy current losses could produce optimised designs with different core and winding dimensions to meet the $Z_{in,min}$ constraint.

9.3.2 Core losses

Core losses in partial core transformers are dependent on the anisotropic nature of the magnetic flux flowing through the core. Losses need to be considered in all three directions from the frame of reference of a steel lamination. These are the rolling, transverse and normal directions. Radially laminated cores would significantly reduce the losses from planar eddy currents induced by lines of flux oriented normal to the laminations. Losses from flux travelling in the transverse and rolling directions need to be considered.

9.4 PARTIAL DISCHARGE MEASUREMENTS

Sometimes high voltage testing can be accompanied by partial discharge measurements. High frequency partial discharge signals are susceptible to interference. This can be from noise, radio signals and other sources of PD apart from the equipment under test. Modern PD measuring equipment has the ability to block interfering PD signals with proper calibration, filtering and active cancellation. However none of these methods are perfect, and a PD free PCRTX would reduce the burden on the instrumentation to provide good data.

An attempt was made to measure the PD from the PCRTXs built as part of this work. This proved unsuccessful due to limitations of the available test equipment. The PD signature of the PCRTXs should be measured and compared with previous designs to determine the effectiveness of the new insulation system at minimising voids.

9.5 CORE SHAPE

With an incomplete magnetic flux path, partial core transformers have non-uniform distributions of core flux density. There is a significant amount of radial flux spilling from the top and bottom of the core. This leads to a high flux density in the middle and at any sharp corners of the core. This can cause localised saturation, leading to a reduction in Z_{in}, localised heating and greater device noise. This is illustrated in Figure 9.6.

As an attempt to avoid this effect, the core radius was simply increased as part of the optimisation process. When optimising a design for weight this is unfavourable. An investigation should be conducted into whether changing the core shape can reduce these concentrations of high flux densities. One possible solution is to round the corners of the core to smooth the flux field gradient at the top. When the simulation was repeated with the corners of the core rounded with a radius of 20 mm the peak flux

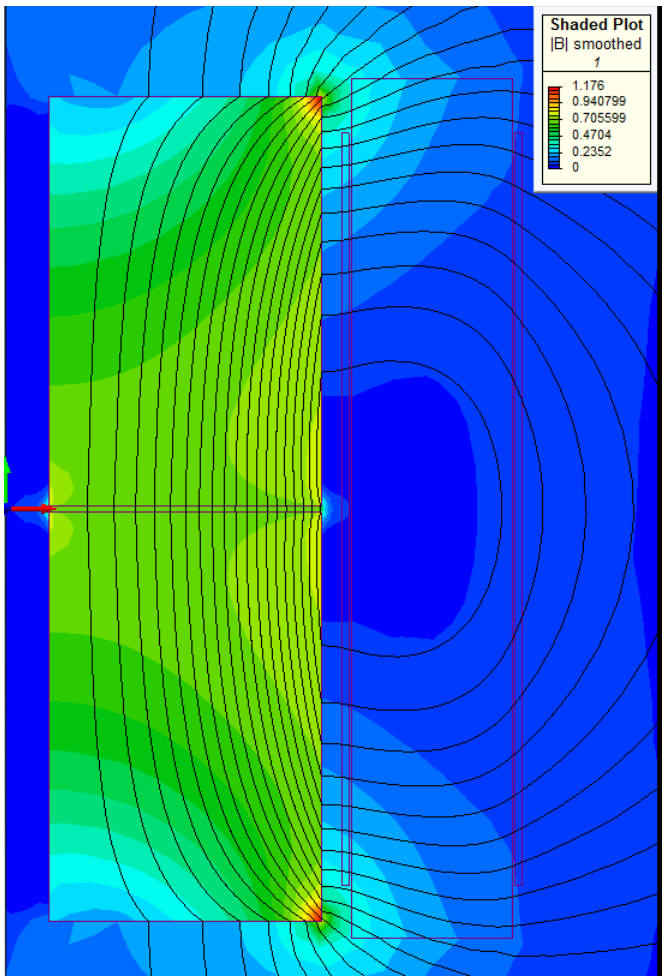

Figure 9.6 FEA field plot of PCRTX under loaded circuit conditions with zero gap and 1 µF load

density at the corners reduced from 1.175 T to 0.933 T as shown in figure 9.7. There was no significant increase in flux density in the rest of the core.

Sharp corners in finite element models are prone to increased error. In this case the magnitude of the error around the corners is not enough to account for the observed difference in flux density. Other changes to the core shape could be investigated with the aim of reducing the peak core flux density thus allowing the radius to be made smaller.

9.6 COOLING SYSTEMS

An important parameter for reducing the device weight is the secondary winding wire diameter. Due to the large number of secondary winding turns, any reduction in cross sectional area significantly reduces the weight. It is also likely that winding eddy current losses could be reduced and primary-tertiary coupling increased with a lower secondary winding thickness.

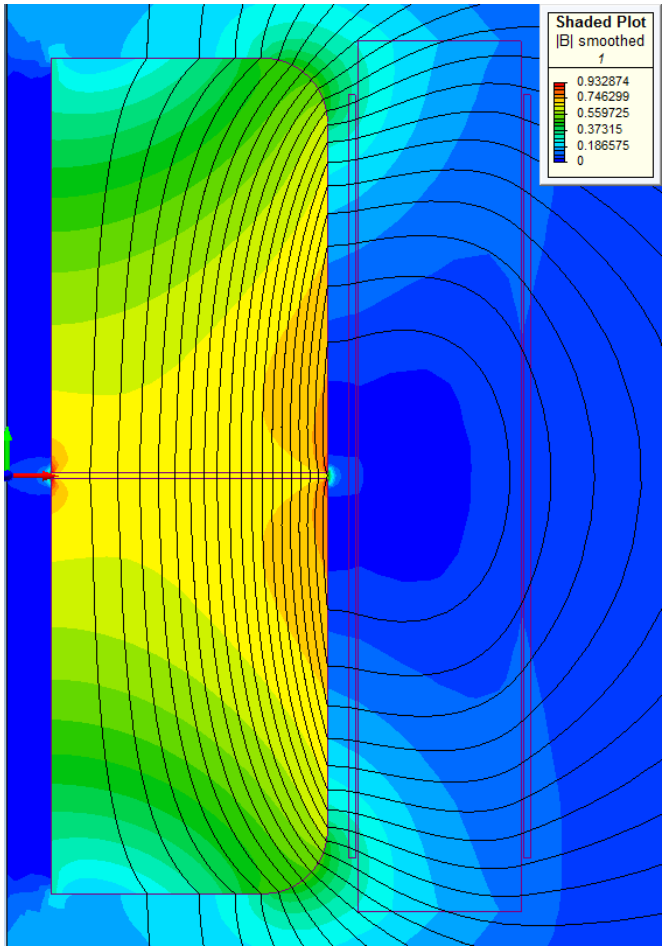

Figure 9.7 FEA field plot of a PCRTX under loaded circuit conditions with the core rounded

The present motivator for a large secondary winding wire diameter is to reduce the current density in the winding, allowing it operate at higher currents for longer. The benefits of a simple cooling system to remove the excess heat could be investigated. This would allow the winding current density to be increased due to heat removal by the cooling medium.

One simple way to achieve this could be passing chilled water through cooling channels machined into the former. This would also remove the heat from the core. A similar set of channels placed between one pair of secondary winding layers could remove more waste heat. The key benefit would be lighter and smaller windings. The cooling system might not be necessary for all types of testing and a modular cooling system could be attached only for long duration, high load tests.

9.7 VIBRATION REDUCTION

Further work could be done on alternative means to reduce device noise and vibration. Currently the method of preventing excessive device noise is to reduce the constraint on the peak core flux density B_{pk} to 1.2 T. This is below the saturation flux density of the steel. Higher values of B_{pk} would allow smaller and lighter weight cores to be used which in turn would reduce winding length and hence weight.

The rigid materials used to construct PCRTXs provide minimal damping to the forces generated by vibrating cores. It is likely over time that excessive vibrations will reduce the life of the PCRTX. One method of reducing the impact of vibrations could be to incorporate an elastomer in the core encapsulation instead of a solid resin. Another solution could be changing the material used for the radial spacers. During testing a piece of closed cell foam was inserted as a spacer between core sections. This noticeably reduced the device noise heard at similar voltages.

9.8 NON-IDENTICAL STAGES

The prototypes designed as part of this thesis have identical stages just like commercially available cascaded transformers. This simplifies the design, manufacturing and tuning process. It also reduces flexibility due to the identical tuning range of each stage. A cascaded test kit consisting of different stages and different tuning ranges would be able to test a wider range of loads.

A three stage test kit could be designed to individually tune to a different range of load capacitances. If a tertiary winding is provided with each stage they can also be connected in cascade. This provides more options for connecting stages in different configurations. Higher voltages can be produced with more stages but it is harder to tune to larger capacitances due to more series connected secondary inductances. Single or double stage connections could tune to higher capacitances if a higher test voltage is not required.

Chapter 10

CONCLUSION

This thesis began by introducing partial core resonant transformers and the concept of connecting them in cascade. The context of the application was outlined by reviewing related developments in high voltage field testing, laboratory testing and transformer design. A new equivalent circuit model of a three winding partial core resonant transformer was presented and validated by testing on existing prototype transformers.

Existing research into cascaded transformers was reviewed and presented. A new equivalent circuit model based on tunable coupled inductors was detailed. A new analytical matrix formulation was developed to enable performance parameters such as the input impedance and stage current distribution to be calculated. A phasor analysis was presented highlighting the small voltage and current phase shifts within cascaded transformers. The new model was used to explore the current and voltage distribution between stages and the change in electrical performance with inductive tuning. It was found that under normal conditions higher stages carried a larger proportion of the load voltage. Simultaneously tuning all stages produced the best electrical performance with high input impedance and balanced stage secondary voltages. The limitations of adding further cascaded stages was explored. It was found that adding more stages reduced the peak input impedance at resonance and reduced the stage weight. Nevertheless it was found that the weight savings diminished after two or three stages especially given that the cost of building multiple stages is almost always higher than building a single stage.

A set of modelling and design tools for cascaded PCRTXs was developed using the *Python* programming language. This consisted of an integrated finite element model, object oriented class structure and a library of functions to perform a range of simulations. The programme could be operated using a custom built GUI or scripted commands.

A new optimisation routine for cascaded PCRTXs was developed. This was aimed at enabling comparisons between optimal designs using different numbers of stages to meet the same design specification. The routine used an adapted version of the particle swarm optimisation algorithm with a constraint handling mechanism to rank potential solutions based on their feasibility before optimising for weight. Simulations

were conducted on designs constrained to between one and three stages using the same design specification. Even though the total weight increased with more stages it was found that the stage weight decreased by 43% when using two stages compared to a single stage. The optimum weight of a single stage converged to 517 kg compared to 262 kg per stage for a four stage cascade using the same specification.

The optimised model was used to design and build a new two stage cascaded transformer test kit. A number of new construction methods and designs were trialled to investigate possible cost savings and better performance. A new insulation system was trialled using slatted G10 fibreglass sheets and an infusion resin. On each stage half the core was constructed using radially oriented core laminations and the other half used standard parallel laminations. During testing the radially laminated cores resulted in higher inductance values for less weight than parallel laminated cores.

The cascade stages were tested thoroughly and the the mathematical models showed good agreement with the measured results. During loaded circuit tests each 33 kV stage was tested individually and in cascade to generate a load voltage of 66 kV. An existing two winding PCRTX was used as a third stage to energise a 343 nF load to 100 kV whilst drawing 60.7 A from the supply.

A few ideas for future research in this area were presented.

REFERENCES

Anis, H., Trinh, N. and Train, D. (1975), 'Generation of switching impulses using high voltage testing transformers', *IEEE Transactions on Power Apparatus and Systems*, Vol. 94, No. 2.

Arora, R. and Mosch, W. (2011), *High voltage and electrical insulation engineering*, John Wiley and Sons.

Asztalos, P. (1985), 'Centenary of the transformer', *Periodica Polytechnica Electrical Engineering*, Vol. 30, No. 1, pp. 3–16.

Bagheri, P., Xu, W. and Freitas, W. (2012), 'A resonant tertiary winding-based novel air-core transformer concept', *IEEE Transactions on Power Delivery*, Vol. 27, No. 3, pp. 1519–1528.

Bell, S. (2009), *High Voltage Partial Core Resonant Transformers*, PhD thesis, Department of Electrical and Computer Engineering, University of Canterbury, Christchurch, New Zealand.

Bell, S.C. and Bodger, P.S. (2008a), 'Inductive reactance component model for high-voltage partial-core resonant transformers', *IET Electric Power Applications*, Vol. 2, No. 5, pp. 288–297.

Bell, S.C. and Bodger, P.S. (2008b), 'Equivalent circuit for high-voltage partial-core resonant transformers', *IET Electric Power Applications*, Vol. 2, No. 3, pp. 155–163.

Bendre, V., Bodger, P.P. and Wood, A. (2008), 'Towards a practical partial core transformer - compensation of reactive power requirements with a VSC', In *Proceedings of the Second IASTED Africa Conference Power and Energy Systems*, .

Bertotti, G. (1988), 'General properties of power losses in soft ferromagnetic materials', *IEEE Transactions on Magnetics*, Vol. 24, No. 1, pp. 621–630.

Bertotti, G., Fiorillo, F. and Mazzetti, P. (1992), 'Basic principles of magnetization processes and origin of losses in soft magnetic materials', *Journal of Magnetism and Magnetic Materials*, Vol. 112, pp. 146–149.

Blalock, T.J. (1997), 'Transformers at pittsfield', Available at http://http://ethw.org/Archives:Transformers_at_Pittsfield,part_1, Accessed: 2015-03-07.

Bodger, P. and Enright, W. (2004), 'A resonant transformer for high voltage testing of generator stators', *Australian Journal of Electrical and Electronics Engineering*, Vol. 1.

Boglietti, A., Cavagnino, A., Lazzari, M. and Pastorelli, M. (2003), 'Predicting iron losses in soft magnetic materials with arbitrary voltage supply: An engineering approach', *IEEE Transactions on Magnetics*, Vol. 39, No. 2 II, pp. 981–989.

Booker, J.R., Nichols, D.K. and Larzelere, W. (1983), 'Design of a Modular UHV AC Outdoor Test System', *IEEE Transactions on Power Apparatus and Systems*, Vol. PAS-102, No. 8, p. 2501.

Boyajian, A. (1925), 'Resolution of Transformer Reactance Into Primary and Secondary Reactances', *Transactions of the American Institute of Electrical Engineers*, , No. June, pp. 805–820.

Bratton, D. and Kennedy, J. (2007), 'Defining a standard for particle swarm optimization', *Proceedings of the IEEE Swarm Intelligence Symposium*, , No. Sis, pp. 120–127.

Cavallini, A. and Montanari, G. (2006), 'Effect of supply voltage frequency on testing of insulation system', *IEEE Transactions on Dielectrics and Electrical Insulation*, Vol. 13, No. 1, pp. 111–121.

Clerc, M. and Kennedy, J. (2002), 'The particle swarm - explosion, stability, and convergence in a multidimensional complex space', *IEEE Transactions on Evolutionary Computation*, Vol. 6, No. 1, pp. 58–73.

Coello, C.A.C. (2002), 'Theoretical and numerical constraint-handling techniques used with evolutionary algorithms: a survey of the state of the art', *Computer Methods in Applied Mechanics and Engineering*, Vol. 191, No. 11-12, pp. 1245–1287.

Coello, C.A.C. and Pulido, G.T. (2005), 'Multiobjective Optimization using a Micro-Genetic Algorithm', *Structural and Multidisciplinary Optimization*, Vol. 30, No. 5, pp. 388–403.

Davies, J. (1990), *Conduction and Induction Heating*, IET, London, UK.

Dawes, C.L. and Hoover, P.L. (1926), 'Ionization Studies in Paper-Insulated Cables—I', *Transactions of the American Institute of Electrical Engineers*, Vol. XLV, pp. 141–164.

Eager, G., Katz, C., Fryszczyn, B., Densley, J. and Bernstein, B. (1997), 'High voltage VLF testing of power cables', *IEEE Transactions on Power Delivery*, Vol. 12, No. 2, pp. 565–570.

El-Hamamsy, S.A. and Chang, E.I. (1989), 'Magnetics modeling for computer aided design of power electronic circuits', In *20th Annual IEEE Power Electronics Specialists Conference*, Vol. 2, pp. 635–645.

Fuentes Cabrera, J. and Coello Coello, C. (2007), 'Handling constraints in particle swarm optimization using a small population size', *MICAI 2007: Advances in Artificial Intelligence*, Vol. 4827, pp. 41–51.

Gaulard, L. (1886), 'System of electrical distribution', US Patent 351589 A.

Gemant, A. and Philippoff, W.V. (1932), 'Die funkenstrecke mit vorkondensator', *Z. Tech. Phys.*, Vol. 13, pp. 425–430.

Gerlach, H., Ag, K. and Derendingen, C. (1991), 'Resonant power supply kit system for high voltage testing', *IEEE Transactions on Power Delivery*, Vol. 6, No. 1, pp. 1–7.

Goodlet, B.L. (1937), 'The Impedance of Transformers Connected in Cascade', *Journal of the ICE*, Vol. 4, No. 3, pp. 475–482.

Graham, C.D. (1982), 'Physical origin of losses in conducting ferromagnetic materials', *Journal of Applied Physics*, Vol. 53, No. 11, p. 8276.

Haefely Hipotronics (2015), 'ACS/PSZ AC Test System - Cylinder Type Transformers', Available at http://www.haefely-hipotronics.com/wp-content/uploads/2015/12/LL_ACS-PSZ_151130.pdf, Accessed: 2015-09-03.

Hayes, J.G., O'Donovan, N., Egan, M.G. and O'Donnell, T. (2003), 'Inductance characterization of high-leakage transformers', In *Applied Power Electronics Conference and Exposition, 2003. APEC '03. Eighteenth Annual IEEE*, Vol. 2, pp. 1150–1156.

Hayt, W.H., Kemmerly, J.E. and Durbin, S.M. (2007), *Engineering Circuit Analysis*, McGraw-Hill, 7th ed.

Horeth, A. (2012), 'New approaches for transformer testing on site and in the factory based on static frequency converters', In *10th International Conference on the Properties and Applications of Dielectric Materials*, IEEE.

Huo, X.T. (2009), *New model of eddy current loss calculation and applications for partial core transformers*, Master's thesis, Department of Electrical and Computer Engineering, University of Canterbury, Christchurch, New Zealand.

IEC 60034-1 (2010), 'Rotating electrical machines - Part 1: Rating and performance', .

IEC 60060-1 (2010), 'High voltage test techniques', .

IEC 60076-3 (2003), 'Power transformers - Part 3: Insulation levels, dielectric tests and external clearances in air', .

IEC 60404-2 (2008), 'Magnetic materials - Part 2: Methods of measurement of the magnetic properties of electrical steel strip and sheet by means of an Epstein frame', .

IEC 62271-203 (2003), 'Gas-insulated metal-enclosed switchgear for rated voltages above 52 kV', .

IEEE Std 286 (2000), 'IEEE Recommended Practice for Measurement of Power Factor Tip-Up of Electric Machinery Stator Coil Insulation', .

IEEE Std 400 (2012), *IEEE Guide for Field Testing and Evaluation of the Insulation of Shielded Power Cable Systems Rated 5 kV and Above*, Vol. 2012.

IEEE Std 400.3 (2006), 'IEEE Guide for Partial Dirscharge Testing of Shielded Shielded Power Cable Systems in a Field Environment', .

IEEE Std 400.4 (2015), 'IEEE Guide for Field Testing of Shielded Power Cable Systems Rated 5 kV and Above with Damped Alternating Current (DAC) Voltage', .

Irani, Y., Lapthorn, A. and Bodger, P. (2013), 'A Comparison of VLF and 50 Hz Field Testing of Medium Voltage Cables', In *Electricity Engineers Association Conference Auckland New Zealand*, pp. 19–21.

Jayaram, B.N. (1958), 'A Study On Cascade Connected Transformers', *Journal of the Indian Institute Of Science*, Vol. 40, No. 2, pp. 87–96.

Jayaram, B.N. and Badkas, D.J. (1960), 'A Study of Cascade Connected Transformer Ratio Characteristics', *The Institution of Engineers (India)*.

Jayaram, B.N. and Badkas, D.J. (1962), 'Determination of Output Voltage in Cascade-Connected Transformers', *Part III Power Apparatus and Systems Transactions of the American Institute of Electrical Engineers*, Vol. 81, No. 3, pp. 936–938.

Kennedy, J. and Eberhart, R. (1995), 'Particle swarm optimization', In *Proceedings of ICNN'95 - International Conference on Neural Networks*, Vol. 4, IEEE, pp. 1942–1948.

Kennedy, J. and Mendes, R. (2002), 'Population structure and particle swarm performance.pdf', *Proceedings of the 2002 Congress on Evolutionary Computation, CEC 2002*, pp. 1671–1676.

Kuffel, E., Zaengl, W.S. and Kuffel, J. (2000), *High Voltage Engineering Fundamentals*, Newnes, 2nd ed.

Lapthorn, A. (2012), *High Temperature Superconducting Partial Core Transformers*, PhD thesis, Department of Electrical and Computer Engineering, University of Canterbury, Christchurch, New Zealand.

Lapthorn, A., Bodger, P. and Enright, W. (2013), 'A 15-kVA High-Temperature Superconducting Partial-Core Transformer - Part 1 : Transformer Modeling', *IEEE Transactions on Power Delivery*, Vol. 28, No. 1, pp. 245–252.

Lapthorn, A., Irani, Y., Race, P., Schicker, K. and McDonald, C. (2016), 'Three phase partial discharge investigation of a 108 mw hydro stator', In *EEA Conference & Exhibition*, Wellington.

Lee, R. (1933), 'A practical analysis of parallel resonance', *Proceedings of the Institute of Radio Engineers*, Vol. 21, No. 2, pp. 271–281.

Liew, M.C. (2001), *Reverse Design Transformer Modelling Technique with Particular Application to Partial Core Transformers*, PhD thesis, Department of Electrical and Computer Engineering, University of Canterbury, Christchurch, New Zealand.

Ludwig, G. and El-Hamamsy, S. (1991), 'Coupled inductance and reluctance models of magnetic components', *IEEE Transactions on Power Electronics*, Vol. 6, No. 2, pp. 240–250.

Margueron, X. and Keradec, J.p. (2007), 'Design of Equivalent Circuits and Characterization Strategy for n -Input Coupled Inductors', *IEEE Transactions on industry applications*, Vol. 43, No. 1, pp. 14–22.

Meder, R. (2011), 'Cascade Partial Core Resonant Transformer', Final year project, Department of Electrical and Computer Engineering, University of Canterbury, Christchurch, New Zealand.

Megger (2017), 'Portable oil test sets', Available at http://en.megger.com/portable-oil-test-sets-ots80pb-and-ots60pb, Accessed: 2017/02/19.

Mendes, R., Kennedy, J. and Neves, J. (2004), 'The fully informed particle swarm: Simpler, maybe better', *IEEE Transactions on Evolutionary Computation*, Vol. 8, No. 3, pp. 204–210.

Mohseni, H., Jadidian, J., Shayegani-akmal, a., Hashemi, E., Naieny, a. and Agheb, E. (2008), 'In-situ insulation test of 400 kV GIS', *IEEE Transactions on Dielectrics and Electrical Insulation*, Vol. 15, No. 5, pp. 1449–1455.

NengLing, T. and Yan, D. (2005), 'Stator ground fault protection based on phase angle differential of delta third harmonic voltages', *Electric Power Systems Research*, Vol. 74, pp. 203–209.

Norris, E.T. and Taylor, F.W. (1931), 'High-voltage testing equipments', *Journal of the Institution of Electrical Engineers*, Vol. 69, No. 414, pp. 673–694.

Okabe, S., Takami, J., Tsuboi, T., Ueta, G., Ametani, A. and Hidaka, K. (2013), 'Discussion on standard waveform in the lightning impulse voltage test', *IEEE Transactions on Dielectrics and Electrical Insulation*, Vol. 20, No. 1, pp. 147–156.

Olivier, G., Bouchard, R.P., Gervais, Y. and Mukhedkar, D. (1980), 'Frequency Response of HV Test Transformers and the Associated Measurement Problems', *IEEE Transactions on Power Apparatus and Systems*, Vol. PAS-99, No. 1, pp. 141–146.

Olivier, G., Roy, G., Bouchard, R. and Gervais, Y. (1984), 'Analytical model of hv cascade connected test transformers', In H. Buyse and J. Robert (editors), *Proceedings of the IMACS International Symposium*, Elsevier Science Publishers B.V. (North-Holland), pp. 185–191.

Omicron (2013), 'CP RC Resonance circuit for GIS testing: A new approach to testing gas-insulated switchgear', Available at https://www.omicronenergy.com/en/products/all/primary-testing-monitoring/cp-rc/#Documents, Accessed: 2016-11-10.

Parsopoulos, K.E. and Vrahatis, M.N. (2011), 'Particle Swarm Optimization Method for Constrained Optimization Problems', *Optimization*, Vol. 181, No. 6, pp. 1153–1163.

Pfutzner, H., Bengtsson, C., Booth, T., Loffler, F. and Gramm, K. (1994), 'Three-dimensional flux distributions in transformer cores as a function of package design', *IEEE Transactions on Magnetics*, Vol. 30, No. 5, pp. 2713–2727.

Phenix Technologies (2013), 'Phenix Technologies Resonant Test Systems', Available at http://www.phenixtech.com/resonant.html, Accessed: 2013-07-02.

Ping Tian, D. (2013), 'A Review of Convergence Analysis of Particle Swarm Optimization', *International Journal of Grid and Distributed Computing*, Vol. 6, No. 6, pp. 117–128.

Pinto, C. (1991), 'An improved method of detecting contamination of HV stator windings in the field', In *Proceedings of the 20th Electrical Electronics Insulation Conference*, IEEE, pp. 55–59.

Preis, K., Biro, O., Friedrich, M., Gottvald, A. and Magele, C. (1991), 'Comparison of different optimization strategies in the design of electromagnetic devices', *IEEE Transactions on Magnetics*, Vol. 27, No. 5, pp. 4154–4157.

Pry, R.H. and Bean, C.P. (1958), 'Calculation of the energy loss in magnetic sheet materials using a domain model', *Journal of Applied Physics*, Vol. 29, No. 1958, pp. 532–533.

Pulido, G.T. and Coello, C.A.C. (2004), 'A constraint-handling mechanism for particle swarm optimization', *Proceedings of the 2004 Congress on Evolutionary Computation, CEC2004*, Vol. 2, No. 4, pp. 1396–1403.

Reinert, J., Brockmeyer, A. and De Doncker, R.W.a.a. (2001), 'Calculation of losses in ferro- and ferrimagnetic materials based on the modified Steinmetz equation', *IEEE Transactions on Industry Applications*, Vol. 37, No. 4, pp. 1055–1061.

Rickmann, J. and Kremer, D. (2012), 'Use of static inverters for performing field testing on HVAC cables', *2012 IEEE International Symposium on Electrical Insulation*, pp. 255–260.

Rogers, T.H. (1955), 'Industrial Applications of X-Ray Techniques', *IRE Transactions on Industrial Electronics*, pp. 20–26.

Schaffer, H. (1960), 'A Method of Calculating the Voltage Distribution of Cascade-Connected Testing Transrormers', *IEEE Transactions on Power Apparatus and Systems*, pp. 771–776.

Schikarski, P., Gamlin, M. and Rickmann, J. (1999), 'Two years of experience with a mobile resonant test system for testing of installed medium-and high voltage power cables', In *11th International Symposium on High-Voltage Engineering*, Vol. 5, IEE, p. 236.

Schufft, W. (1999), 'Frequency-tuned resonant test systems for on-site testing and diagnostics of extruded cables', In *11th International Symposium on High-Voltage Engineering (ISH 99)*, Vol. 1999, IEE, pp. v5–335–v5–335.

Shahzad, F., Baig, A.R., Masood, S., Kamran, M. and Naveed, N. (2009), 'Opposition-based particle swarm optimization with velocity clamping (ovcpso)', In *Advances in Computational Intelligence*, pp. 339–348, Springer, Berlin, Heidelberg.

Slemon, G.R. (1966), *Magnetoelectric devices: transducers, transformers, and machines*, John Wiley and Sons, USA, 1st ed.

Srinivas, N. (1993), 'EPRI Report TR-101245. Effect of DC Testing on Extruded Cross-Linked Polyethylene Insulated Cables', Tech. rep., Detroit Edison Co.

Steinmetz, C.P. (1895), 'Theory of the General Alternating Current Transformer', *Transactions of the American Institute of Electrical Engineers*, Vol. XII, pp. 245–256.

Tanaka, T., Fukuda, T. and Suzuki, S. (1976), 'Water tree formation and lifetime estimation in 3.3 kV and 6.6 kV XLPE and PE power cables', *IEEE Transactions on Power Apparatus and Systems*, Vol. 95, No. 6, pp. 1892–1900.

Train, D. and Vohl, P.E. (1976), 'Determination of ratio characteristics of cascade connected transformers', *IEEE Transactions on Power Apparatus and Systems*, Vol. 95, No. 6, pp. 1911–1918.

van Bolhuis, J., Gulski, E. and Smit, J. (2002), 'Monitoring and diagnostic of transformer solid insulation', *IEEE Transactions on Power Delivery*, Vol. 17, No. 2, pp. 528–536.

Velluppillai, S. (2010), 'Partial Core Resonant Testing Transformer', Final year project, Department of Electrical and Computer Engineering, University of Canterbury, Christchurch, New Zealand.

Voith Hydro (2013), 'Micalastic insulation for high voltage hydro generators', Technical brocure, Heidenheim, Germany.

Wardman, J.B. (2013), *Vulnerability of Electric Power Systems to Volcanic Ashfall Hazards*, PhD thesis, Department of Geological Sciences, University of Canterbury, Christchurch, New Zealand.

West System (2014), '105 epoxy resin / 205 fast hardener', Technical datasheed, Gougeon Brothers, Inc.

Yuan, J.J., ZHOU, J., Chen, B., Song, J., Yu, Z., Lei, Y. and Yuan, J.J. (2015), 'A Novel Compact High-Voltage Test System Based on a Magnetically Controlled Resonant Transformer', *IEEE Transactions on Magnetics*, Vol. PP, No. 99, p. 1.